Strategies to Improve Efficiency and Emissions in Spark Ignition Engines

by

Taehoon Han

A dissertation submitted in partial fulfillment
of the requirements for the degree of
Doctor of Philosophy
(Mechanical Engineering)
in the University of Michigan
2019

Doctoral Committee:

Professor André L. Boehman, Chair
Research Scientist George A. Lavoie
Professor Venkat Raman
Professor Margaret S. Wooldridge

Taehoon Han
taehoonh@umich.edu
ORCID iD: 0000-0003-2030-5891

Dedication

“To my beloved parents; Sangwon and Younsoon.”

Acknowledgments

Looking back on my graduate studies at the University of Michigan, I have had lots of good memories thanks to many people. My doctoral journey would not have been possible without these special people acknowledged below.

Above all, I would like to sincerely thank my advisor professor André Boehman, who gave me limitless support and opportunities on valuable projects. He always believed in me, and whenever I got overwhelmed or couldn't find solutions for research and graduate student life, he always encouraged and showed me how to deal with it and waited for me to be grown up and find it myself. You are my best role model not only as a researcher but also as a leader and an educator in my life.

Besides, I would like to thank my wonderful co-advisors and committees who provided dedicated guidance for the completion of this study: Dr. George Lavoie, for his mentorship in encouraging me to confidently evolve to a researcher with fruitful guidance and friendly discussions; Professor. Margaret Wooldridge, for her mentorship and various opportunities while working on our best research team; Professor Venkat Raman, for a supportive committee member. In addition, I would like to appreciate my earlier doctoral study co-advisor Mr. John Hoard for his mentorship and intensive coaching on the find details of the research.

The financial support for my doctoral study including the U.S. Department of Energy, the Ford Motor Company, and the University of Michigan Rackham Graduate School: without these financial and intellectual supports from sponsors, my graduate works would have not been possible. First, I am very grateful to Dr. James Anderson and Dr. M. Matti Maricq at Ford for their unconditional supports, and Dr. Steven Wooldridge and Mark Meinhart for allowing me to extend my knowledge in practical automotive fields. Also, I would like to express my gratitude to Daniel Styles and Dr. Chih-Kuang Kuan at Ford for allowing me to take the first step for being a researcher in my graduate study.

Many thanks to the technicians of W.E Lay Automotive Laboratory, in particular James Elkins who always encourages and provides me a lot of positive thinking as a mentor and offers me fantastic technical supports, and the machine shop "magicians" William Kirkpatrick and Kent Pruss for their manufacturing supports, fuel storage management, and valuable technical advices. Also, I would like to thank Chuck Solbrig for his supports on engine experiments.

My senior and fellow students have been an amazing support for me throughout my doctoral studies at Michigan. I would like to thank Dr. Stefan Klinkert and Dr. Vasileios Triantopoulos for enormous support for Hydra engine installation and meaningful discussions. And, I would like to send special thanks to Dr. Ripudaman Singh who shared many things on our co-growing step as being a doctor. Also, I want to send many thanks to Dr. Doohyun Kim for providing me lots of theoretical engine fundamentals with in-depth discussions.

A large number of undergraduate and masters intern students who supported my experiments and experimental setup, I cannot imagine finishing my doctoral journey without you guys; Hyunki Sul, Nyinyi Gwa, Michael Adams, Iljin Eum, Asit Kumar, Evan Harris, Sumanth Mamidanna, Gaurav Handa, Ashwin Ramesh, Apoorv Vishneek, and Jeremy Babinet.

Thanks to my past lab mates, who supported me to be a better engineer with valuable discussions and technical advice: Dr. Dongil Kang, Dr. Eduardo Barrientos, Dr. Vickey Kalaskar, Dr. Chenxi Sun, Michael Mayo, Dr. Jordan Easter, Dr. Yan Chang, and Dr. Jeongyong Choi. Also, many thanks to my present lab folks, (soon to be Drs.) Jonathan Martin, Justin Koczak, Kwanghee Yoo, Shuqi Cheng, and Andrew Di Mauro, Erick Garcia, Taemin Kim, and Kaustav Bhadra for friendship and discussions.

Most importantly, I would like to thank my family, especially my parents, Sangwon and Younsoon, who always embraced and believed in me, and encouraged me in best environments. Also, I would like to thank my older brother Taeyong, his wife Yunjeong, and my adorable nephew Seungyun.

Table of Contents

List of Figures

List of Tables

List of Appendices

List of Abbreviations

A/F	Air to Fuel ratio
CA0005	Crank Angle difference between time of spark and 5% mass fraction burned
CA0550	Crank Angle difference between 5% and 50% mass fraction burned
CA5090	Crank Angle difference between 50% and 90% mass fraction burned
CA1090	Crank Angle between 10% and 90% mass fraction burned
CA50	Crank Angle at 50% mass fraction burned
CAD	Crank Angle Degree
CFD	Computational Fluid Dynamics
CoD	Coefficient of Determination
CoV	Coefficient of Variation
DI	Direct Injection
DISI	Direct Injection Spark Ignition
DMF	2,5-dimethylfuran

EGR	Exhaust Gas Recirculation
ETOH	Ethanol
EVC	Exhaust Valve Close
EVO	Exhaust Valve Open
FFT	Fast Fourier Transformation
FPGA	Field Programmable Gate Array
GCI	Gasoline Compression Ignition
IBOH	Isobutanol
IMEP	Indicated Mean Effective Pressure
IMEPg	Gross Indicated Mean Effective Pressure
IMEPn	Net Indicated Mean Effective Pressure
ITE	Indicated Thermal Efficiency
ITEg	Gross Indicated Thermal Efficiency
ITEn	Net Indicated Thermal Efficiency
IVC	Intake Valve Close
IVO	Intake Valve Open
KI	Knock Intensity
KI 20	Knock Index during 20 crank angle degrees

$KI_{\text{peak to peak}}$	Knock Index peak to peak (difference between maximum and minimum of filtered cylinder pressure)
KL	Knock Limit
KO	Knock Onset
KLSA	Knock Limited Spark Advance
LAS	Laser Absorption Scattering
LHV	Lower Heating Value
LIF	Laser Induced Fluorescence
MAPO	Maximum Amplitude Pressure Oscillation
MBT	Maximum Break Torque
NO_x	Nitrogen Oxides (in emissions)
OS	Octane Sensitivity
PAHs	Polycyclic Aromatic Hydrocarbons
PFI	Port Fuel Injection
PIV	Particle Image Velocimetry
PM	Particulate Matter
PMI	Particulate Matter Index
PN	Particle Number

PROCO	Programmed Combustion
PSD	Power Spectral Density
SCXI	Signal Conditioning Extension for Instrumentation
SEPO	Signal Energy of Pressure Oscillation
SI	Spark Ignition
slpm	Standard Liter Per Minute
SOI	Start of Injection
TCP	Texaco Combustion Process
TDC	Top Dead Center
aTDC	After Top Dead Center
bTDC	Before Top Dead Center
TDC_{ign}	ignition Top Dead Center
TEM	Transmission Electron Microscopy
THC	Total Hydrocarbon (in emissions)
WOT	Wide Open Throttle
λ	Air to Fuel equivalence ratio
ϕ	Fuel to Air equivalence ratio

S_L	Laminar flame speed
$S_{L,0}$	Laminar flame speed constant for a certain fuel
T_u	Unburned mixture temperature
Q_{LHV}	Lower heating value
Q_{LHVi}	Lower heating value of each species
η_c	Combustion efficiency
$\eta_{t,i}$	Indicated thermal efficiency
$\dot{m}_a$	Air mass flow rate
$\dot{m}_f$	Fuel mass flow rate
τ_{id}	Ignition delay

Abstract

Downsized boosted spark ignition (SI) engines offer considerable thermal efficiency improvements compared to conventional naturally aspirated SI engines. However, the increase in boost level severely increases knock propensity, and knock tends to decrease the potential gains of thermal efficiency and increase pollutant emissions. Hence, engine knocking should be controlled at all running conditions, and research on knock mitigation strategies is essential to improve both performance and emissions.

This research investigates the knock mitigation strategies and their experimental validation for improving performance and emissions with three different engine parameters: (i) Fuels (oxygenated fuel gasoline blends and syngas addition); (ii) Mixture dilution (EGR and Lean dilution); (iii) Injection strategies (DI and PFI combined dual fuel injection and multiple injections). Besides, a newly discovered unique relation between knocking and particulate matter emissions is examined in the last part with several conceptual models for better understanding of this phenomenon.

The first part of this dissertation is about the effects of three oxygenated fuels (2,5-dimethylfuran, ethanol, and isobutanol) blended in gasoline on general engine combustion, knock, and particulate matter emissions. Furan functional group is a novel candidate for oxygenated fuels as gasoline additives, and one of the most promising furan fuels, 2,5-

dimethylfuran gasoline blends, is experimentally compared with two common alcohol-type oxygenates, ethanol and iso-butanol. Three major parameters are varied for the examination of oxygenates: fuel type, blend ratio, and boost level. The blend ratios are swept from 0 to 30 volume basis percentage, and all fuels are tested from throttled 0.8 bar to boosted 1.4 bar intake pressure to identify the knock limits along with spark timing sweep. The results show that the 2,5-dimethyl furan blends have the ability to extend knock limits as much as ethanol, but with relatively higher particulate matter emissions.

As a second fuel study, syngas (hydrogen and carbon monoxide) aided engine combustion is experimentally investigated under EGR diluted and lean conditions by focusing on knock propensity, thermal efficiency, and emissions. Syngas amount is controlled on an energy basis from 0% to 15% to compare the difference between EGR and air dilution. Knocking tendencies with respect to the frequency, combustion phasing, and burn duration are analyzed, and the thermal efficiency and emissions difference are discussed as well. The results show that with increasing the syngas addition, knocking is strongly suppressed, and the effect is more beneficial with EGR dilution than with air dilution.

For the study of fuel injection strategies, two concepts of injection strategies are introduced and experimentally investigated. The first injection strategy is combined direct and port fuel injection to extend knock and EGR dilution limits using gasoline and ethanol fuels. Test conditions are divided into dual injection and direct injection for accurate comparison. For the dual injection tests, gasoline, representing 80% by volume of the total fuel, is injected using the direct injector, and ethanol, representing 20% by volume of the total fuel, is injected using the port fuel injector. For the direct injection tests, a splash blended E20 (20% ethanol by volume) fuel is used for comparing with dual injection. EGR mass fraction was varied from 0% to 21%,

under boosted intake air pressure of 1.25 bar for both injection strategies. The results showed that dual injection was beneficial to shorten the burn duration and improve combustion stability, but dual injection is slightly more sensitive to knock than direct injection primarily due to increased unburned gas temperature. The particulate matter emissions from dual injection were slightly lower, and the gaseous emissions showed lower total hydrocarbons and similar nitrogen oxides compared with only using direct injection of E20 fuel.

The second fuel injection strategy involves multiple direct injections, which inject fuel multiple times in a cycle. This study explores the effect of multiple injections on knock, engine performance, particulate matter and gaseous emissions in direct injection spark ignition engines. Two aspects of multiple injection strategies are experimentally investigated: the number of injections (up to five times in a cycle); and the timing of injections (classified relative to the timings of intake valve opening and closing). The results from thermodynamic process analysis confirm that multiple injection maintains torque and combustion stability compared to single injection but increases knock limits and thermal efficiency due to improved heat release phasing, especially with an additional late injection during the intake valve closed (compression stroke) period. The gaseous pollutant emissions including nitrogen oxides and unburned hydrocarbons are significantly reduced with multiple injection particularly with compression stroke injection. In contrast, carbon monoxide emissions are increased. Particulate matter emissions are not directly related to the injection period, but the number of injections significantly reduces particulate matter emissions.

Finally, a unique phenomenon of a relation between knock and particulate matter emissions is analyzed and explained with conceptual models for spark ignition engines. In general, particulate matter emissions are rapidly increased after the onset of knock as the spark

advances, and the increased amount of particulate matter emissions are proportionate to the knock intensity. This phenomenon is a novel observation, and there is very limited understanding of this phenomenon and the relationship between knocking and PM emissions. So, phenomenological analyses are introduced using several experimental data, and three theories to explain this phenomenon are proposed along with conceptual models.

Through the studies presented in this thesis, several potential contributions for higher efficiency and lower emissions spark ignition engine have been obtained with strategies using three major parameters. By utilizing proper fuel properties, injection type, and dilution strategies, the knocking and combustion stability could be significantly improved, so that the engine performance, gaseous pollutant emissions, and particulate matter emissions could be improved. In addition, as a result of detailed strategic research in this study, it is expected that the spark ignition engine could achieve a higher boost pressure and compression ratio by avoiding spark knock.

Chapter 1

Introduction

1.1 Motivation

Vehicle efficiency and emissions targets are ever increasing challenges as automakers pursue meeting rigorous fuel economy standards, emission regulations, and customer demand for higher mileage vehicles. Figure 1.1 describes an example of strengthening emissions regulation, particulate matter and nitrogen oxides from the EU emissions standards from first to the sixth stage [1], and Figure 1.2 shows the history of increasing average fuel economy from 2000 to 2017 and enacted targets up to 2030 for passenger cars by country in miles per gallon, normalized to The U.S. Corporate Average Fuel Economy (CAFE) standards [2]. Previous work has shown that one of the most promising strategies to improve engine thermal efficiency is turbocharging with engine downsizing [3,4]. Downsized boosted spark ignition (SI) engines offer considerable thermal efficiency improvements compared to conventional naturally aspirated SI engines, however, knocking is a major concern under boosted conditions [5,6]. Engine knocking is an abnormal combustion phenomenon in SI engines in which the end-gas

auto-ignites before it is consumed by the flame front. This phenomenon causes strong pressure waves and severe noise and thereby can damage engines. Also, it has been shown, in this work, that knock promotes engine-out particulate matter emissions. Hence, engine knocking should be controlled and avoided at all engine running conditions especially under boosted charge or higher compression ratio.

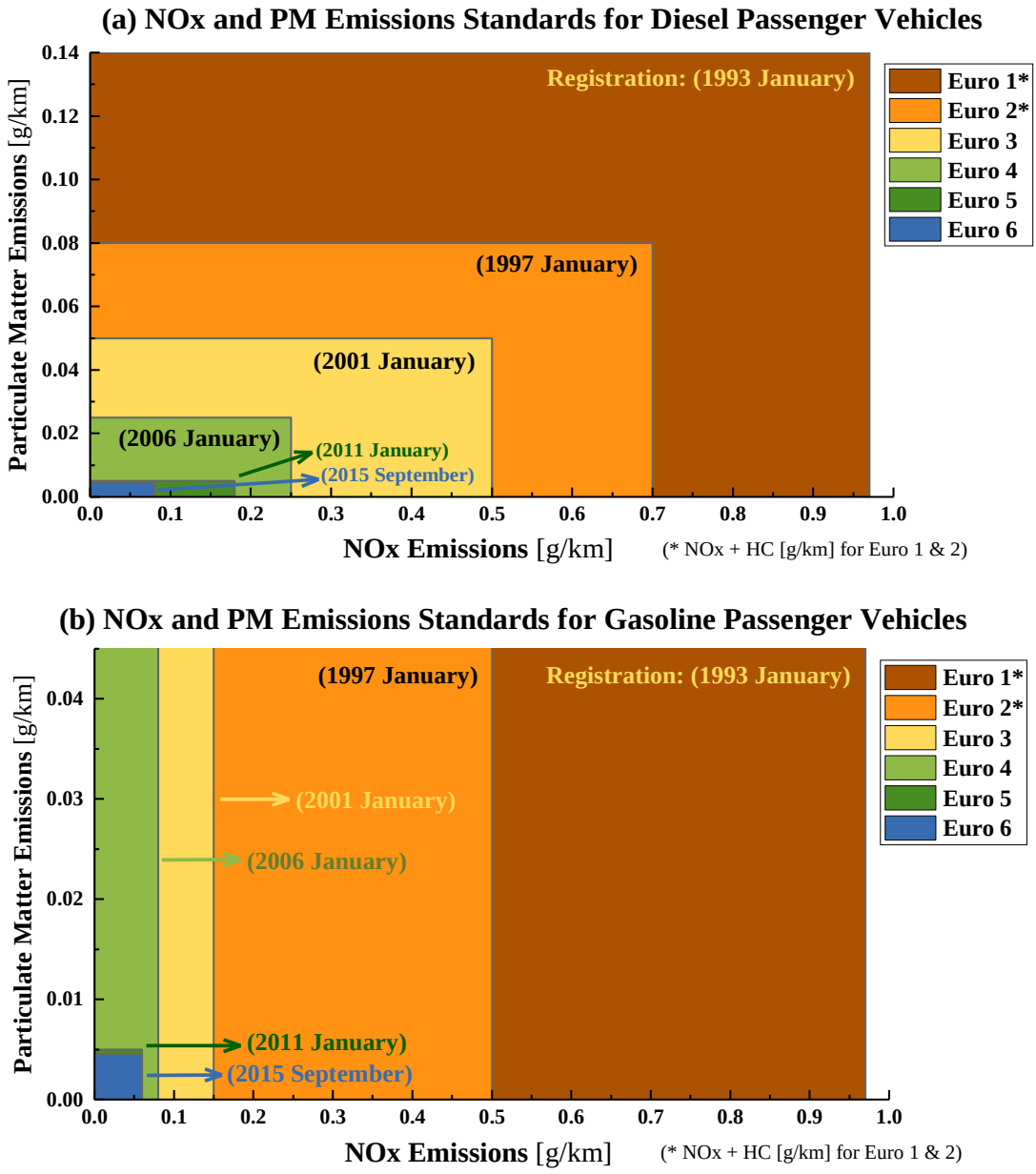

Figure 1.1 EU Emissions standards history for passenger vehicles (Euro 1 ~ 6: PM and NO_x) [1]: (a) Diesel, (b) Gasoline

There are several conventional ways to prevent knock, such as retarding a spark timing or strengthening the mixture with additives or fuel rich conditions. These methods, however, rather reduce engine efficiency and increase undesirable unburned hydrocarbons and carbon monoxide emissions [7], so fundamental and sustainable knock mitigation strategies are needed for improving efficiency and emissions.

Therefore, this dissertation focuses on the knock mitigation strategies and its effects on engine performance and emissions with fuels, mixture dilution, and injection strategies.

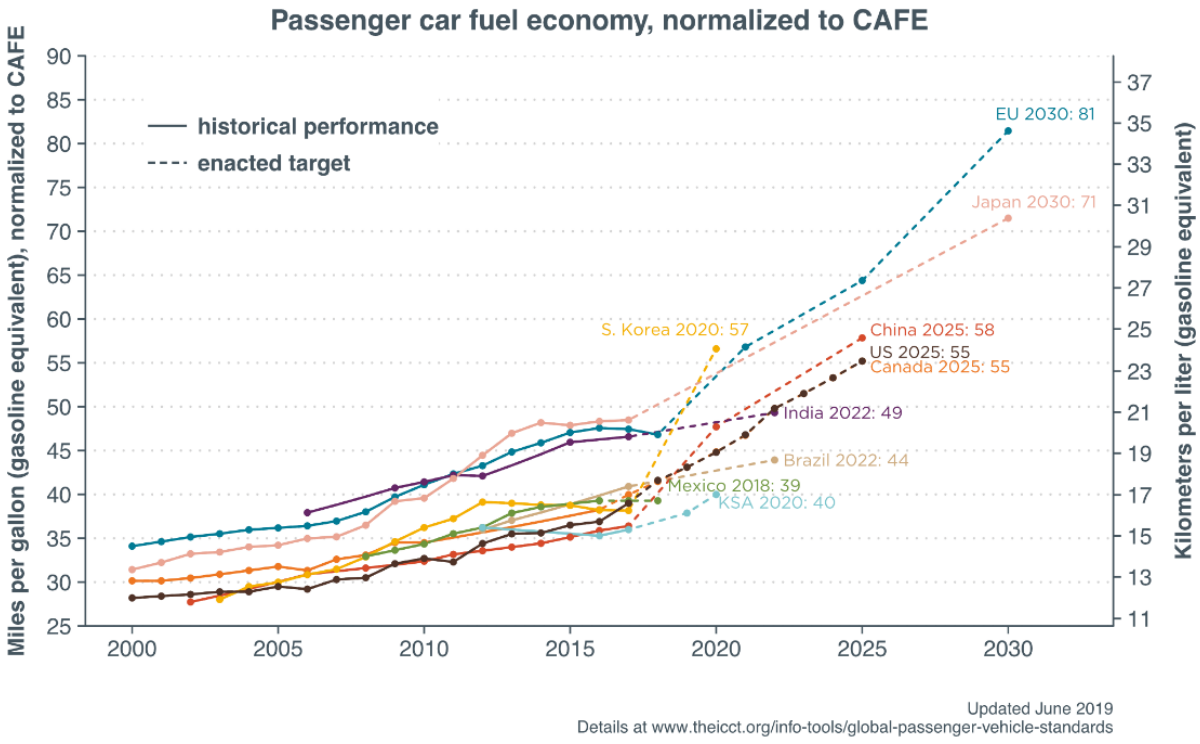

Figure 1.2 Normalized passenger car fuel economy history and enacted targets by region [2]

1.2 Objectives

The goal of this dissertation is to demonstrate the combination of fuel selection, fuel injection strategy, and mixture preparation that enable meeting the worldwide efficiency targets along with the global emissions targets in spark ignition engines through knock limit extension. All strategies are experimentally validated using a single cylinder research engine, and a detailed dissertation storyline is shown in Figure 1.3. As shown in Figure 1.3, the effects of three main strategic parameters, (*i*) Fuels (oxygenated fuel gasoline blends and syngas addition); (*ii*) Mixture dilution (EGR and Lean dilution); (*iii*) Injection strategies (DI and PFI combined dual fuel injection and multiple injections), on knock limit extension are investigated with binary parameter combinations, and ultimately engine performance and emissions results are validated as well. In addition, an exploratory study about the unique relationship between knocking and particulate matter emissions is examined to better understand an important impact of the knocking phenomenon in the last section of the thesis, using several conceptual models.

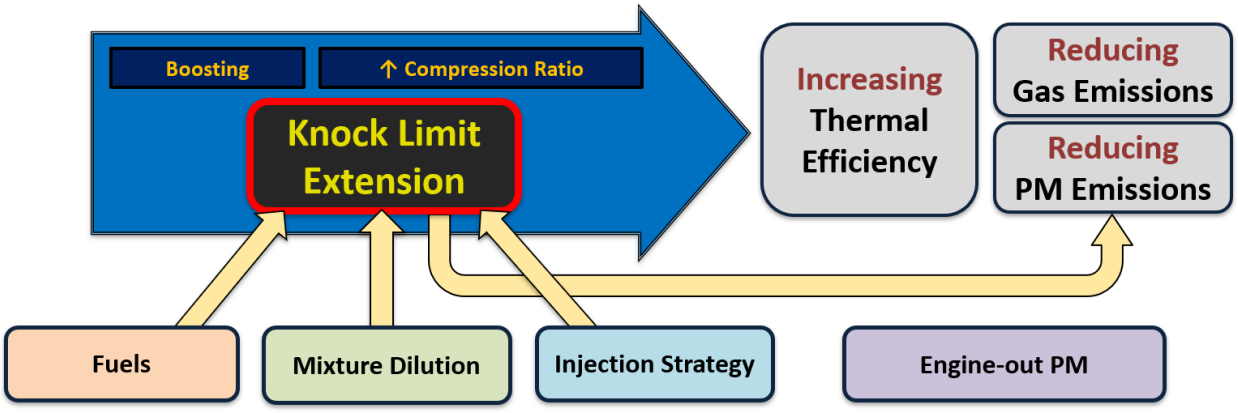

Figure 1.3 Dissertation storyline schematic for improving efficiency and emissions

1.3 Chapters Overview

The present dissertation is organized as follows. In Chapter 1, the motivation and dissertation storyline of knock limit extension are discussed, and Chapter 2 provides a brief background for the dissertation, and surveys experimental equipment and data processing details.

The following five chapters describe the strategies and experimental results of the three main parameters and an exploratory study of particulate matter and knock relation with literature reviews in each chapter.

The first strategy, utilizing high knock resistant fuel, is divided into two chapters, and the first fuel study regarding blends of different oxygenated fuel in gasoline are introduced in Chapter 3. The second fuel research study involves syngas, which is comprised of hydrogen and carbon monoxide, and is presented in Chapter 4.

The next strategy, mixture dilution, is covered in Chapters 4 and 5. In Chapter 4, two dilution features (EGR and Lean dilution) are compared in conjunction with syngas addition, and the effects of two different approaches to charge dilution on knocking and emissions are introduced. Chapter 5 compares the EGR steps from 0 to 21% with 7% discrepancy with dual fuel injection research. An analysis of efficiency benefits and knock limit extension with EGR dilution is presented in Chapter 5, as well.

The third strategy for knock limit extension, involving fuel injection strategies, is investigated in Chapters 5 and 6. The first injection study shown in Chapter 5 concerns the dual fuel injection, which combines a direct fuel injection and a port fuel injection using oxygen free gasoline and pure ethanol injection under four steps of EGR dilution. Chapter 6 covers the multiple injection strategy, in which direct inject fuel occurs multiple times (up to five separate

injection) in a cycle. The combustion characteristics and engine out harmful emissions improvement are analyzed in Chapter 6.

Chapter 7 introduces an exploratory study of the relationship between knock and particulate matter emissions and along with analysis using several conceptual models. This phenomenological relationship between knock and particulate matter emissions is a novel observation from the present work, so the phenomenon is analyzed first and then possible reasons for this relationship are introduced in this chapter.

Chapter 8 gives a summary of the work accomplished in this dissertation, conclusions from each chapter, and suggestions for future work.

Chapter 2

Background

2.1 Knocking in Spark Ignition Engines

Knocking in spark ignition engines is the name given to the noise which is delivered through the engine structure because of in-cylinder abnormal combustion. There are several types of abnormal combustion in spark ignition engines such as spark knock, hot spot or chamber deposit induced surface ignition, and low speed preignition, but the most problematic abnormal combustion under boosted condition is spark knock. There have been many studies to understand the knocking phenomenon over the decades, and the most convincing reason for spark knock is the end-gas auto-ignition caused by increased in-cylinder pressure and temperature [7]. Figure 2.1 provides a visualized example of end-gas auto-ignition in a knocking cycle using an optical engine via laser-induced fluorescence (LIF) imaging [8]. As the captions describe on the left-hand side of Figure 2.1, several near-wall spots in the end-gas region start to auto-ignite before it is consumed by the spark induced regular flame during the knocking cycle.

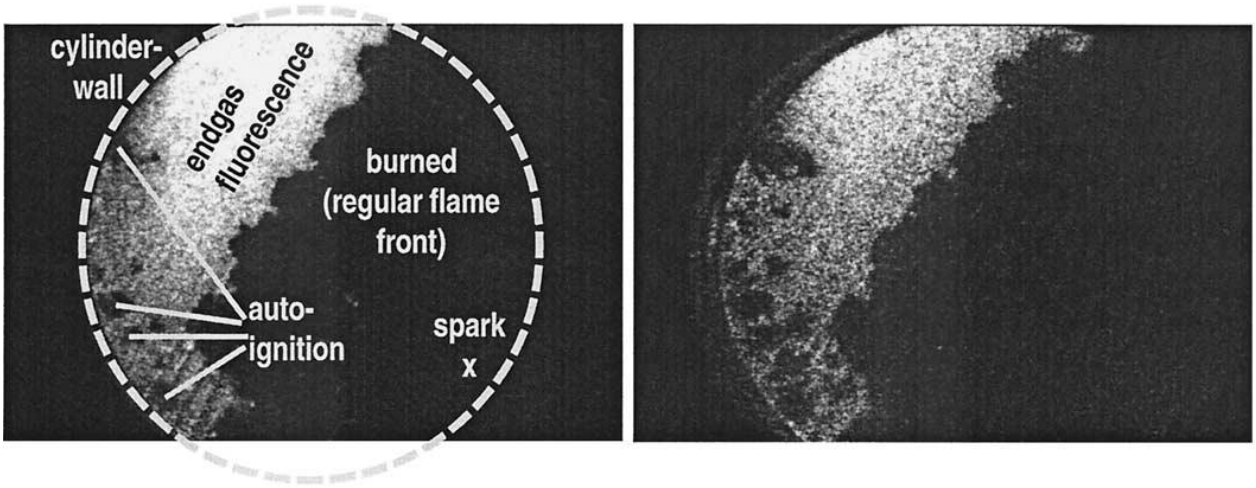

Figure 2.1 A knocking cycle example: Optical engine LIF image (Schießl and Maas [8])

In order to suppress this spark knock phenomenon, various studies have been conducted as well [9–11], and the most effective methods known so far can be summarized as follows.

- Enhancing fuel knock resistance: high octane fuel, additives, oxygenated fuels.
- Increasing the inert gas portion in the mixture: cooled EGR.
- Reducing total combustion duration in a cycle: fast flame speed via in-cylinder conditions or selection of fuel chemical structure.
- Increasing turbulence intensity: swirl, tumble by engine geometry, injection strategy.
- Reducing end-gas temperature: maximizing charge cooling effect using direct injection, making end-gas mixture rich.

These methods, however, are closely related and have trade-off relationships with each other, so rigorously developed strategies are essential to utilizing these methods to improve the spark knock phenomenon. In addition, these methods significantly affect engine-out pollutant emissions, so even more sophisticated strategies are needed. Therefore, this dissertation studies various strategies for knock limit extension using experimental validation of the methods above.

2.2 Particulate Matter Emissions in Spark Ignition Engines

It is known that spark ignition engines emit less mass of particulate matter compared to compression ignition engines. But, in recent years, boosted spark ignition engines have become more common in the automotive industry, and the particulate matter emissions from these boosted DI gasoline engines are becoming a growing concern. The direct injection systems for reducing in-cylinder temperature under boosted conditions tend to produce more soot due to less mixing time and more possibilities for fuel impingement on the piston and the cylinder walls. In contrast, SI engines with port fuel injection systems emit much less particulate matter compared to engines with direct fuel injection systems due to pool fires under boosted conditions. Also, spark ignition engines tend to produce a greater number density of ultra-fine nanoscale particles compared to compression ignition engines. As a consequence, additional research on particulate matter emissions for boosted DI gasoline engines is needed. In response to this need, this dissertation focuses on the effects of fuel injection strategies on particulate matter emissions, and the trade-off relationship between spark knock and soot is discussed, as well.

2.3 Equipment

2.3.1 Engine Facility

A boosted Ricardo Hydra single cylinder research engine is used to perform all of the experimental research in this dissertation. This engine has three types of fuel injection systems which are direct injector, port fuel injector, and gaseous fuel injector, and two types of engine cylinder head, which include one cylinder head with a centrally mounted spark plug and another

cylinder head with a side mounted spark plug. Figure 2.2 shows a schematic of the boosted Hydra single cylinder research engine and supporting facilities. Three yellow circles indicate the injector locations, and the head type shown in Figure 2.2 is for the direct fuel injection mode. The gaseous fuel injector is located in the front side of the intake runner, and the injector tip is made of a porous sintered metal to evenly fumigate the gaseous fuels.

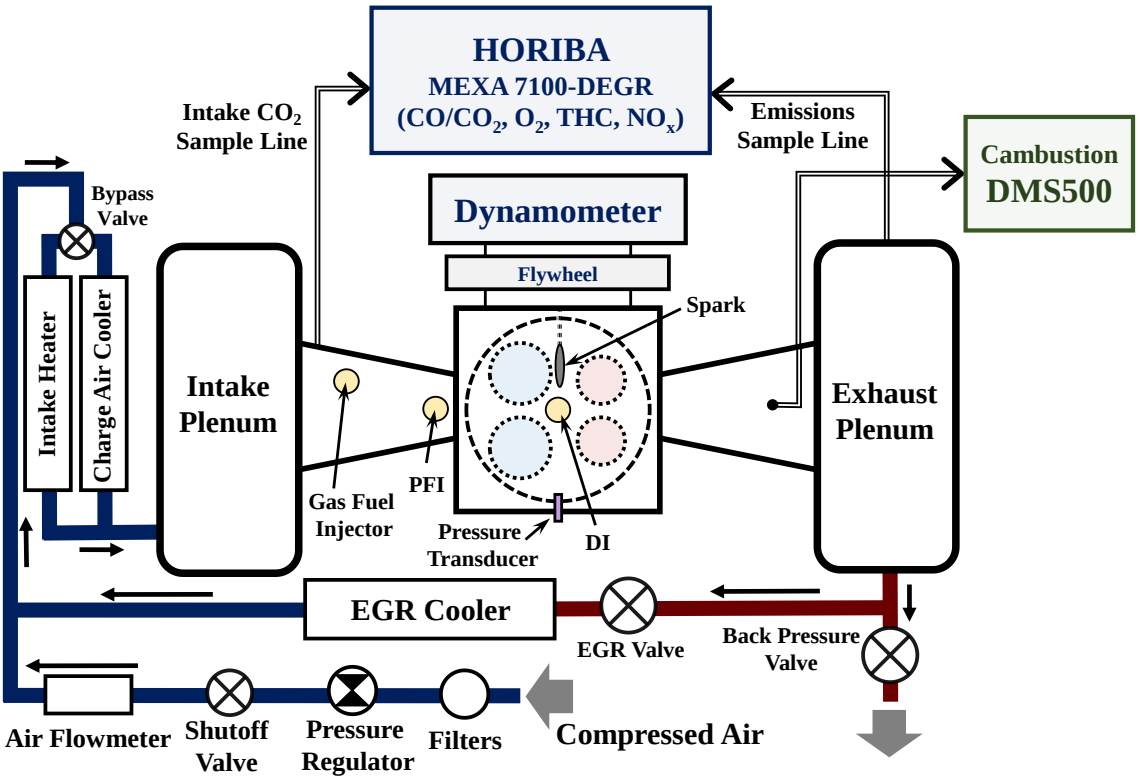

Figure 2.2 A schematic overview of Hydra single cylinder research engine facility

Figure 2.3 describes the two types of engine cylinder head. The pent-roof design cylinder head can be divided into two modes of operation. The first mode is centrally mounted spark plug type for port fuel injection mode which is depicted in Figure 2.3 (a), and the second mode is side mounted spark plug type for direct injection or dual injection modes shown in Figure 2.3 (b). The

centrally mounted direct injector (Bosch HDEV4) in Figure 2.3 (b) is a piezoelectric injector and produces a hollow cone spray with a maximum of 30mm penetration length. The cylinder head for the centrally mounted spark (port injection) mode is used for Chapter 3 and 4 in this dissertation, and the cylinder head for the side mounted spark (direct or dual injection) mode is used for Chapter 5, 6, and 7. A detailed facility setup is described in each chapter.

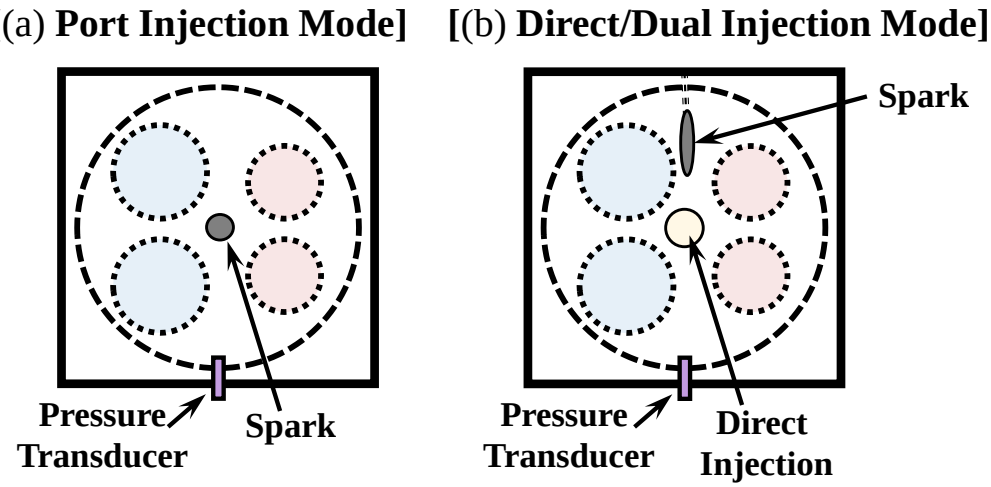

Figure 2.3 A schematic of engine cylinder head: (a) Port Fuel Injection Mode; (b) Direct Injection or Dual Injection Mode

As shown in the Figure 2.2, intake air is compressed and filtered, and the pressure is regulated using a pneumatic valve downstream of the air filters to maintain the target intake pressure at the intake plenum. The air supply system to the engine intake includes a bypass heater and cooler located upstream of the intake plenum to maintain constant intake air temperature. Engine oil and coolant are conditioned by external systems to maintain constant temperature, and an oil filter is located in the oil conditioning system.

The fuel supply system for direct injection has a fuel flow meter to calculate the air-fuel equivalence ratio in conjunction with an air mass flow meter (Fox Instruments FT2). The air to

fuel equivalence ratio was confirmed by the measured gaseous emissions using an emissions bench (Horiba MEXA-7100DEGR) and a lambda meter (ETAS LA4) with a lambda sensor (Bosch LSU 4.9) in the exhaust runner. The fuel supply system for port injection also has a fuel flow meter, and the fuel flow is controlled by injection duration with constant fuel rail pressure.

The compression ratio of the engine is 10.5:1 with 0.5-liter displacement volume. The valve timing is fixed for all experimental conditions, and the valve opening duration is 226 crank angle degrees for both the intake and exhaust valves based on 0.5mm valve lift. Additional specifications are summarized in Table 2.1.

Table 2.1 General Engine Geometry and Specifications

Parameter	**Value**
Displaced Volume	500 cm^3
Bore / Stroke	86 mm / 86 mm
Connecting Rod	143 mm
Compression Ratio	10.5 : 1
Intake Valve Timing	IVO 362 / IVC 136 bTDCign
Exhaust Valve Timing	EVO 138 / EVC 364 aTDCign
Head Design	Pent-roof
Number of Valves	4
Spark Plug	Centrally mounted / Side mounted
Port Fuel Injector	Bosch port fuel injector (280-150-15)
Direct Injector	Bosch HDEV4 piezoelectric spray guided injector Hollow-cone spray (85° ± 5° spray angle)

The engine operating parameters were controlled using an in-house developed National Instruments (NI) Labview FPGA (Field-Programmable Gate Array) and real-time programs. The hardware was accompanied by eight digital and analog input and output modules in a compact real-time controller (cRIO). The in-house developed engine operating program allows for control over the spark timing, fuel injection timing, and fuel injection duration for the direct injector. The low-speed data including temperature, pressure, air and fuel flows, etc., are measured using NI modules and SCXI (Signal Conditioning Extension for Instrumentation) systems.

2.3.2 Gaseous Emissions Measurements

Exhaust gaseous emissions are measured using Horiba MEXA 7100-DEGR emissions bench. As presented in Figure 2.2, exhaust gases are sampled from the center top of the exhaust plenum through a perforated stainless tube and goes to the analyzers through heated filters and lines. Also, the intake air carbon dioxide concentration is measured using Teflon tubing and a separate analyzer. The temperature of all filters and line for exhaust gases is set to 191.15°C to avoid measuring species condensation, and the five analyzers and their operating principle are summarized in Table 2.2 and described below.

The emissions bench measures a total of five species which are CO_2, CO, O_2, Total hydrocarbon (THC), and NO_x. The CO_2 and CO analyzers are combined in one analyzer instrument for the exhaust gas measurements, and a separate instruments measures CO_2 exclusively in the intake runner to calculate EGR rate. Both CO_2 and CO absorb light in the infrared spectrum as a consequence of their molecular structures, so these species are measured by the non-dispersive infrared (NDIR) analyzer, which measures the absorption of infrared

radiation emissions at a certain frequency correlated to CO and CO_2 (2.5 ~ 8μm) to determine the concentration by relating the amount of absorption compared to a calibration gas.

Table 2.2 Emissions bench measuring species and operating principle

Measuring Species	**Operating Principle**
O_2	Paramagnetic
CO_2 (Intake/Exhaust)	Non-dispersive infrared (NDIR)
CO	Non-dispersive infrared (NDIR)
THC (Total Hydrocarbon)	Flame ionization detector (FID)
NO_x	Chemiluminescence

Total hydrocarbon (THC) emissions are measured using the FID (flame ionization detector). The FID determines the carbon mass in the gas sample and converts it into a hydrocarbon mass by assuming a specific carbon to hydrogen ratio. The FID measures the ions released from combustion on a burner fueled by a mixture of helium and hydrogen. The sample hydrocarbon containing exhaust flow is premixed with the hydrogen and increases the ion counts, which can be correlated to the concentration of hydrocarbons.

Oxygen concentration is evaluated by a paramagnetic analyzer that takes advantage of the phenomenon that oxygen uniquely has a much higher magnetic susceptibility than most other gases. As the concentration of oxygen in the analyzer, which is surrounded by a non-uniform magnetic field, changes, a rotational force is imparted on a suspended test body. The voltage required to keep the test body from rotating is proportional to the sample oxygen concentration.

Nitrogen oxides (NO_x) emissions are measured by two chemiluminescence analyzers, one is for high concentration and the other one is for low concentration. The chemiluminescence analyzer utilizes ozone (O_3) to oxidize NO to NO_2 upon which light is released, whose intensity correlates to the NO concentration. Any NO_2 in the exhaust is converted to NO prior to passing through the ozone stage, so that both NO and NO_2 commonly referred to as NO_x are measured.

Furthermore, the air to fuel equivalence ratio (λ) of emission bench is calculated from the measured emissions using Brett/Spindt equation [12,13].

2.3.3 Particulate Matter Emissions Measurements

A Cambustion DMS500 (Differential Mobility Spectrometer) is used to measure exhaust particulate matter emissions, specifically the particle size distribution. As Figure 2.2 shows, the particulate matter samples are collected at the end of exhaust runner with a quarter inch outer diameter stainless steel tubing with insulation, and for some of the experiments in Chapter 7, particulate matter is collected from the exhaust plenum. The measurement range for particle size is from 5 to 1000 nm (1 μm) with two stage dilution, and the exhaust sample flow pass through a cyclone separator on the first stage to filters large particles over 1 μm using heated first dilution air. The filtered sample flow is passed through a corona discharge where a charge is applied on the entrained particles, and then the flow travels to a classifier column with a high voltage electrode in the center. The particles get deflected towards the walls of the classifier rings according to their charge to drag ratio and deposit their charge on highly sensitive current pickups. Particles with a high charge/low drag ratio are deflected more and detected earlier in the classifier column and vice versa. A schematic of the classifier column is shown in Figure 2.4.

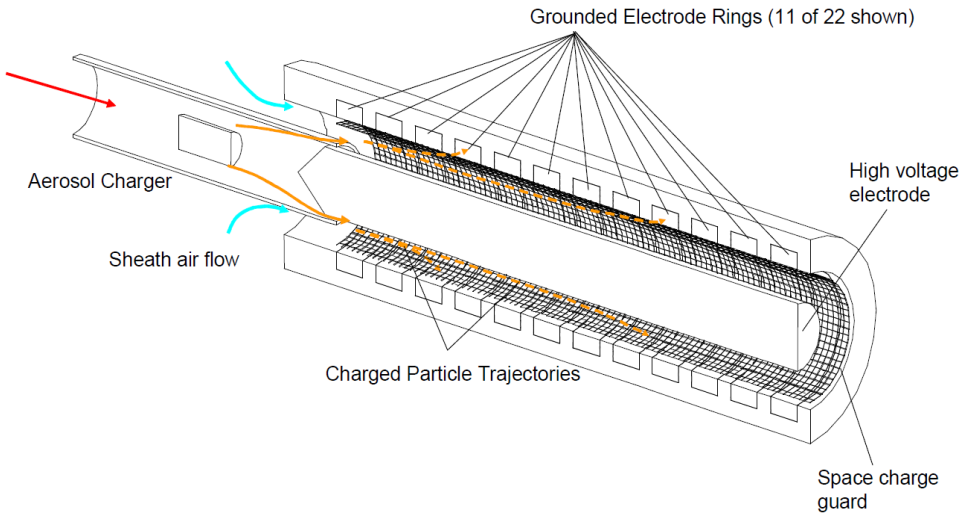

Figure 2.4 A schematic of DMS500 classifier [14]

2.4 Knock Quantification Method

There are several techniques to characterize engine knock such as cylinder pressure trace, audible knock, engine block vibration measurement, and intermediate radical species detection, and each method has specific objectives. Because the focus of this study is in-cylinder physical knock, the cylinder pressure and audible knock measuring methods are used to detect and quantify the engine knock. (This section is an extracted and modified from Han et al. [15], which is the same as Chapter 4.)

2.4.1 Filtering Cylinder Pressure

In order to obtain knock measurements from the raw in-cylinder pressure trace, an appropriate filtering process is essential. The most commonly used pressure-rectifying method, Fast Fourier Transformation (FFT), is used in this study. The process of FFT based filtering

involves converting raw pressure signals from the time to the frequency domain based on the Equation 2.1 and applying a high pass filter with a certain cut-off frequency, and then inverting the data from the frequency to the time domain. In Equation 2.1, the ‘t’ and ‘ω’ indicate the time and frequency variables, respectively.

$$\hat{p}(\omega) = \frac{1}{\sqrt{2\pi}} \int_{-\infty}^{\infty} p(t)\, e^{-i\omega t}\, dt \qquad (2.1)$$

Figure 2.5 shows the converted frequency domain cylinder pressure data from motoring to heavy knock for the baseline condition. Normally, lower frequencies represent the signal associated with compression and the standard flame propagation heat release, so a high pass filter is generally used to filter the knocking data. The cut-off frequency of the high pass filter is selected by comparing the knocking and non-knocking frequency domains. As the amplitudes of motoring, normal, and light knock signals illustrate in Figure 2.5, most of the normal combustion frequency is located under 3 to 4 kHz. So, the cut-off frequency for this study is chosen to be 3500 Hz as illustrated by the dashed line in Figure 2.5. An example of the inverted signal from high pass filtered pressure is shown in Figure 2.6.

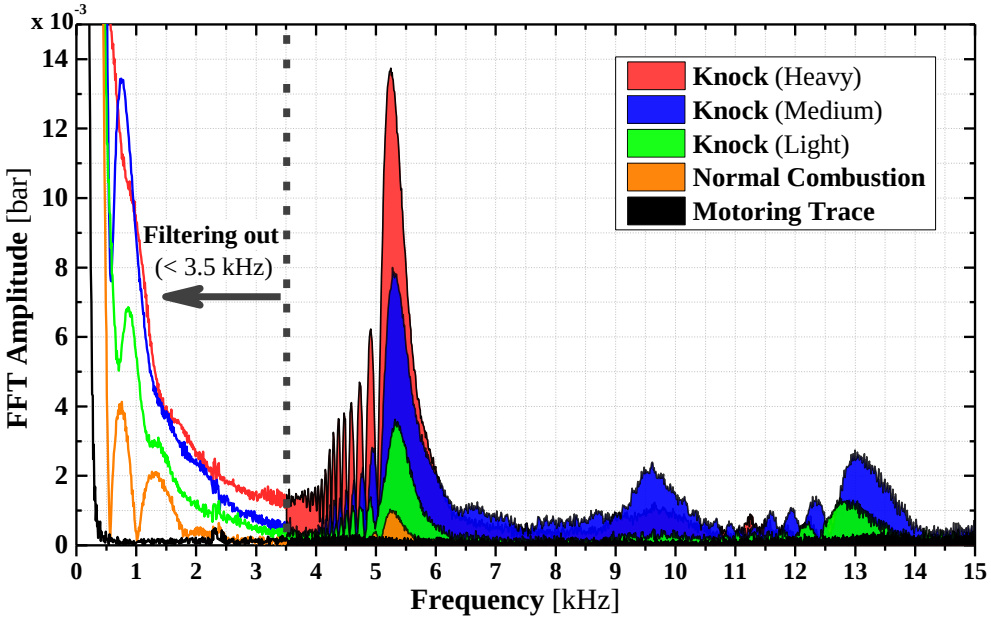

Figure 2.5 FFT amplitude and cut-off frequency: various cycles from motoring to heavy knock. (Gasoline only, λ=1.00, intake pressure = 1.2 bar, varied spark timing)

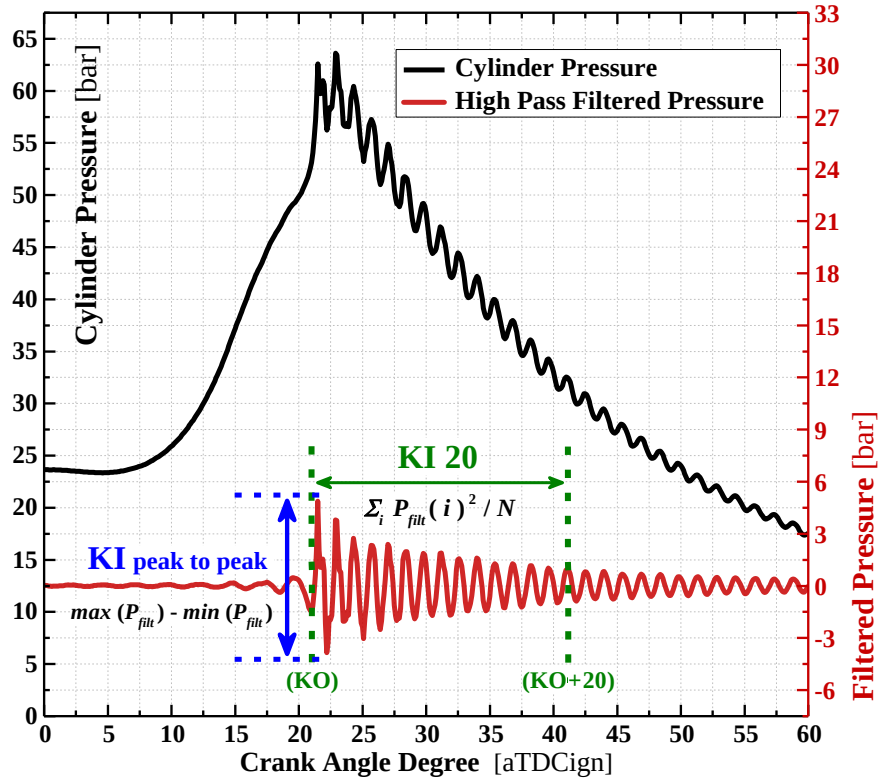

Figure 2.6 Heavy knock cylinder pressure (top, black line) and filtered pressure (bottom, red line). (Gasoline only, λ=1.00, intake pressure = 1.2 bar, spark timing 13º bTDC)

2.4.2 Knock Index (KI)

Knock intensity characterization methods are various and there is no conventional guideline to measure knock. The most commonly used methods are categorized by the domains of FFT: time and frequency. Time domain based intensity can be divided into peak basis single intensity and peak and duration integrated intensity. Also, the frequency domain based intensity is normally linearly matched to the time domain based intensity, but it has an additional benefit which is the ability to find a dominant frequency range on the frequency domain [10,16]. The time domain basis peak and energy index and frequency domain basis PSD (Power Spectral Density) analysis are described below. (Data processing MATLAB code is attached in **Appendix A. Data Processing** (MATLAB Script for Knock Intensity Calculation: 'KI 20' and 'KI $_{\text{peak to peak}}$'))

2.4.2.1 Peak Basis Index

Among the peak intensity measuring methods, two indices are commonly used: MAPO (Maximum Amplitude of Pressure Oscillations) and KI peak to peak (pressure difference between maximum peak and minimum peak of the filtered pressure). The MAPO index involves the absolute value of filtered pressure data and choosing the peak value in a knock occurring window [17,18]. In contrast, the KI peak to peak is the difference between maximum peak and minimum peak values.

In this study, KI peak to peak is used for the peak basis intensity calculation. As shown by the vertical blue arrow in Figure 2.6, the difference from the maximum to minimum peak of filtered pressure is calculated using Equation 2.2.

$$\mathbf{KI}_{\mathbf{peak\ to\ peak}} = |\,(\,\boldsymbol{max}\,\{\,\boldsymbol{p(i)}\,\}\,) - (\,\boldsymbol{min}\,\{\,\boldsymbol{p(i)}\,\}\,)\,| \qquad (2.2)$$

In Equation 2.2, *p(i)* indicates the filtered pressure and the '*i* ' is crank angle degree value. The range of '*i* ' is set from -20 TDCign to +70 TDCign, this is to avoid noise from other sources such as intake and exhaust valve closing signals; signal oscillation caused by the valve closing is occasionally higher than knocking oscillation in lower knocking cycle cases.

2.4.2.2 Energy Basis Index

The peak basis intensity above is simple to calculate, but there is a drawback that such measurements could be affected by external noise. To address this concern, the signal energy basis intensity is also used to measure knock [19,20]. The common name of the energy basis intensity is SEPO (Signal Energy of Pressure Oscillations), and the SEPO method takes the average value of the square of the filtered pressure from the onset of knock to a given point of crank angle degree. The range of crank angle degree used by researchers varies, but a typical range is from 5 to over 20 crank angle degrees.

Konig et al. [21] suggested an energy basis knock intensity method which is measured over a 20 crank angle degree range, which is called 'KI 20'. The KI 20 measurement is adopted in this study, and the detailed calculation is shown in Equation 2.3, and illustrated in Figure 2.6.

$$\mathbf{KI\ 20} = \frac{1}{N_{samp}} \sum_{i=1}^{N_{samp}} (P(i) - P_{mean})^2 \qquad (2.3)$$

In Equation 2.3, P_{mean} is the average pressure value – zero level of the high-pass filtered data and N_{samp} is the number of pressure samples within the 20 degree crank angle range following the offset of the first pressure pulse. The pressure data are measured per 0.1 crank

angle degree, so there are 200 data points for every 20 crank angle degrees, and N_{samp} is 200 in this experiment.

2.4.2.3 Power Spectral Density Analysis

The frequency domain can be also used to measure knock intensity. Two most commonly used methods are FFT amplitude spectrum analysis, shown in Figure 2.5, and PSD analysis. The advantage of the frequency domain analysis is the ability to find the peak frequency. The benefit of the PSD method is the ability to make an overall intensity comparison, regardless of the signal frequency.

2.4.3 Relation between Peak and Energy Index

Both the peak and energy basis indices are calculated and compared in order to determine a proper knock quantification index. First, the comparison between EGR and air dilution is carried out. Figure 2.7 demonstrates the relation between peak basis intensity (KI peak to peak) and energy basis intensity (KI 20). The green round symbols are air dilution data while the blue diamond symbols indicate EGR dilution, and the dilution cases show no noticeable difference.

To examine the relation between the two knock indices, a regression equation is performed based on the combined air and EGR dilution data. When the polynomial regression is obtained without restrictions, the KI 20 is linear to 2.14th order of KI peak to peak, and the origin of KI peak to peak corresponds to a negative value of KI 20 (-0.0046 bar^2). But considering the meaning and units of each knock index (bar and bar^2), the equation form is set to a second order polynomial equation and forced to pass through the origin (0, 0).

$$\boldsymbol{KI\ 20} = 0.0285 \times \left(\boldsymbol{KI_{peak\ to\ peak}}\right)^2 \ ; \ R^2 = 0.9643 \tag{2.4}$$

Equation 2.4 is the result of the final regression equation between KI 20 and KI peak to peak, with proper restrictions. The coefficient of determination (CoD, denoted by R^2) of the KI peak to peak basis KI 20 regression is 0.9643. Meanwhile, the CoD of KI 20 basis KI peak to peak intensity is 0.843.

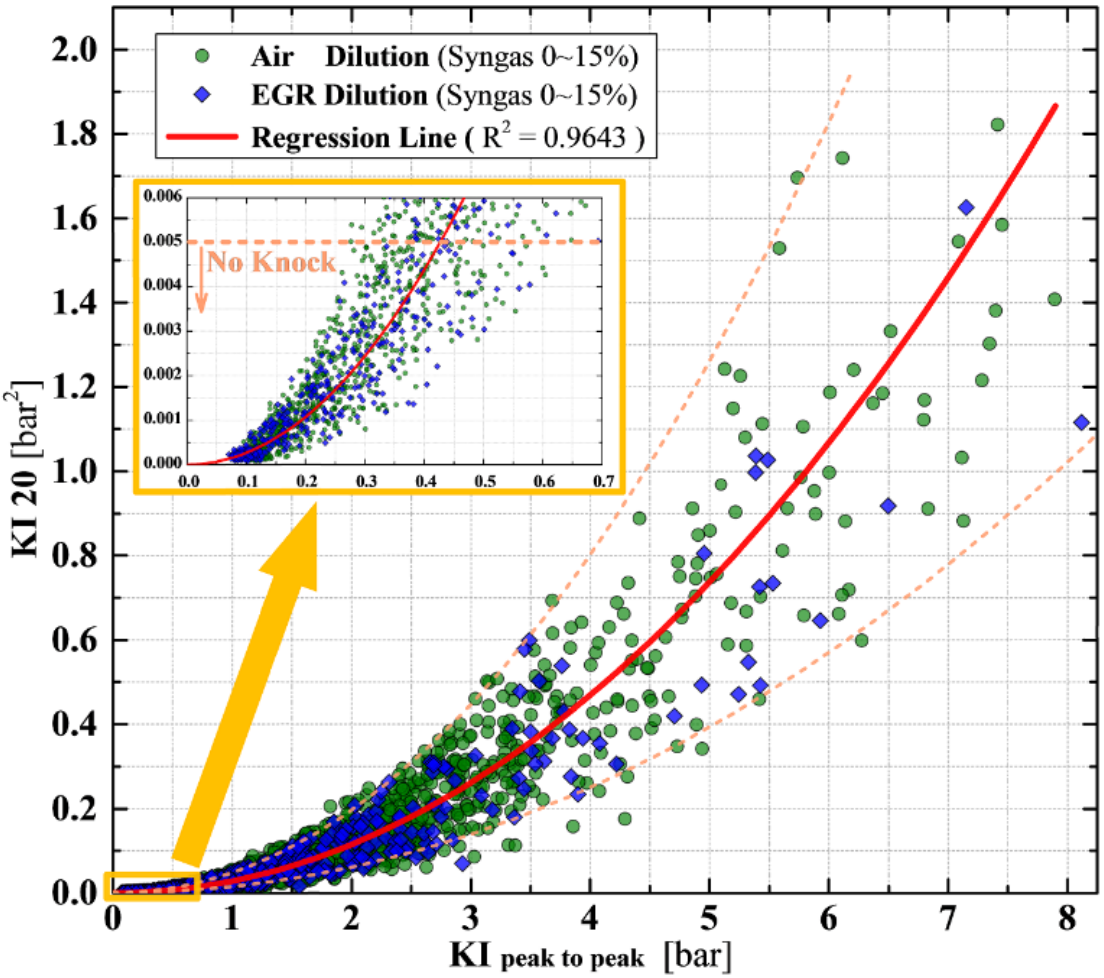

Figure 2.7 The relation between peak intensity (KI peak to peak) and energy intensity (KI 20) under lean air and EGR dilution conditions.

Due to the advantage of using KI 20, which is less vulnerable to external noise and has higher predictability based on the higher CoD, the KI 20 method is chosen for knock quantification. Although the values of these indices that represent knock onset vary, the most frequently used knock onset guidelines are between 0.4 and 0.5 bar for KI peak to peak and between 10^{-3} and 10^{-2} for KI 20. From these ranges of values and the filtered data from the engine, the knock intensity guideline is set to 0.005 bar^2 of KI 20. In the magnified view of Figure 2.7, the points below the dashed line are considered non-knocking points.

In addition, the upper and lower dashed lines are the maximum and minimum trend lines with only changes to the coefficient of $KI_{peak\ to\ peak}^2$ of Equation 2.4. The coefficient for the maximum line is 0.048, and for the minimum is 0.005. For a constant value of $KI_{peak\ to\ peak}$, variation of KI 20 suggests the duration of the pressure oscillations is varying [16]. In other words, as KI 20 increases, the duration of pressure oscillation is longer. So, comparing points in Figure 2.7 along a vertical path (constant KI peak to peak), KI 20 varies substantially, where a higher value of KI 20 indicates less rapid decay of the pressure oscillations and a lower value indicates a more rapid decay of the pressure oscillations.

2.5 Heat Release Analysis

Heat release analysis is the most important data processing strategy for understanding the in-cylinder combustion process during operation of internal combustion engines. This study used two types of heat release analysis programs separately: The first one is a commercialized fast response combustion analysis tool named Indicom by AVL List GmbH [22], and the other one is an in-house code called ACE-HRA (Advanced Combustion Engine – Heat Release Analysis) [23] which is used for detailed post processing. Both analysis tools use similar principles (in-

cylinder pressure data and various assumptions) and equations based on the first law of thermodynamics, but the two codes differ with regard to several details regarding assumptions.

2.5.1 Instant Processing (AVL Indicom)

The AVL IndiCom software [22] uses the first law of thermodynamics for calculating the heat release rate in real time with several preset parameters as provided in Equation 2.5.

$$Q_i = \frac{K}{\kappa - 1}\{\kappa \times p_i \times (V_{i+n} - V_{i-n}) + V_i \times (p_{i+n} - p_{i-n})\} \quad (2.5)$$

n	Interval (1 crank angle degree)
κ	Polytropic coefficient
p	Cylinder pressure
V	Volume
K	Constant (for unit conversion)

The polytropic coefficient (κ) is constant which is specified in the engine parameters. Since the polytropic coefficient depends on temperature, the software uses a second coefficient for the calculation range after TDC. By setting the second coefficient to a value which is slightly smaller than the one used before TDC (which is transferred from the engine parameters), the heat release integral does not rise further after the end of combustion. This allows for a more accurate calculation of the end of combustion. For the polytropic coefficients for compression and expansion, the port fuel injection mode uses 1.32 (Compression) and 1.27 (Expansion), and the dual and direct injection modes employ 1.35 (Compression) and 1.30 (Expansion).

2.5.2 Post Processing (ACE-HRA)

The ACE-HRA in-house MATLAB code developed by Ortiz-Soto et al. [23] also uses the first law of thermodynamics equation to calculate the rate of heat release profile. The gross chemical heat release rate calculation is shown in Equation 2.6.

$$\frac{dQ_{hr,ch}}{dt} = mc_v \frac{dT}{dt} + P\frac{dV}{dt} + \dot{Q}_{wall} \qquad (2.6)$$

In the Equation 2.6, C_v, m, T, are estimated mass, constant volume specific heat, mass, and gas mixture bulk temperature respectively, and P and V are the measured cylinder pressure data and calculated cylinder volume based on the engine geometry. The left-side term in Equation 2.6 is the net apparent heat release rate, and the right-side terms are the change in sensible internal energy, engine piston work, and cylinder wall heat transfer rate, respectively.

The mass fraction burned x_b is calculated by normalizing the left-side term with respect to the cumulative value from the start to end of combustion which are defined as the crank angle location of the minimum and maximum values. The heat release rate is obtained by differentiation of the cumulative gross heat release with respect to crank angle. The gas mixture bulk temperature is calculated from the ideal gas state equation shown in Equation 2.7.

$$T = \frac{PV}{mR} \qquad (2.7)$$

In the Equation 2.7, P and V are the instantaneous cylinder pressure and volume, and m is total mass of the entrained mixture. The specific gas constant, R, is defined by the mean composition of the charged in-cylinder mixture which is changed based on the composition changes during combustion process.

2.6 Uncertainty Analysis

Uncertainty analyses were performed to determine the precision and repeatability of the experimental results, for example, combustion phasing, efficiencies, and emissions based on the square root of the variance method introduced by Moffat [24], which is explained in Equation 2.8.

$$\delta \boldsymbol{R} = \sqrt{\sum_{i=1}^{N} \left(\frac{\partial \boldsymbol{R}}{\partial \boldsymbol{X}_i} \, \delta \boldsymbol{X}_i \right)^2} \tag{2.8}$$

Each individual term in the parenthesis is combined by a root sum square method, and it represents the contribution made by the uncertainty in one variable, δX_i, to the overall uncertainty in the result δR. Each term has the same form: the partial derivative of R with respect to X_i multiplied by the uncertainty interval for the variables. For the data analysis in this dissertation, the number N for is 200 for high speed data such as in-cylinder pressure basis combustion data, and 5 for gaseous emissions with 5 seconds interval, and 6 for particulate matter emissions with 10 seconds interval.

Chapter 3

Combustion Characteristics of Oxygenated Fuel (2,5-Dimethylfuran, Ethanol, and Isobutanol) Gasoline Blends in a Boosted SI Engine

3.1 Preface

This chapter is dealing with the first strategic parameter about the effect of oxygenated fuel blending on knock, engine combustion, and emissions. Three fuels (2,5-dimethylfuran, ethanol, and isobutanol) are selected for this oxygenated fuel study and the abstract for this chapter is attached below.

Along with alcohol-based fuels such as ethanol and isobutanol, fuels with furan functional groups are of increasing interest for gasoline blends in boosted spark ignition (SI) engines due to their high knock resistance. Among various furan group fuels, 2,5-dimethyl furan is one of the most promising oxygenated fuel candidates owing to its higher energy density, water insolubility, accessible manufacturing process, and other desirable properties. This study investigates the effects of three different oxygenated fuels (2,5-dimethylfuran, ethanol, and isobutanol) in blends with gasoline on knocking engine combustion and particulate matter emissions in a boosted SI engine. The experimental results for the 2,5-dimethylfuran blends are compared with these two common alcohol fuels, ethanol and isobutanol. In the engine

experimental study, three major parameters are varied for the examination of the oxygenates: fuel type, blend ratio, and boost level. The blend ratios are swept from 0 to 30 volume percent, and all fuels are tested from throttled 0.8 bar to boosted 1.4 bar intake pressure to identify the knock limits along with spark timing sweep. Comparison these fuels at 20 volume percent blending ratio, the knock limit of the 2,5-dimethylfuran blend shows similar a result as the ethanol blend, and particulate number emissions of 2,5-dimethylfuran lie between that for ethanol and isobutanol. But, large diameter particles in the accumulation mode range are higher for 2,5-dimethyl furan than for the alcohol blends, and the size distribution range is wider than for the alcohol blends.

3.2 Introduction

Boosted spark ignition (SI) engines offer considerable thermal efficiency benefit compared to naturally aspired SI engines, but the increase in boost level increases knock propensity and knock tend to reduce the potential gains of efficiency. Therefore, many knock mitigation studies are conducted for boosted SI engines, and one of the most effective knock mitigation methods is blending high octane oxygenated fuels into gasoline [7,25].

There are several high octane oxygenated fuel candidates, and the most common oxygenated fuel is ethanol. Ethanol is well known to have knock suppressing properties compared to gasoline, including high heat of vaporization. Also, ethanol is currently produced in large volumes via multiple second generation bio-fuel pathways, which can lower the dependency on fossil fuels. However, several challenges must be overcome including engine cold starts caused by low vapor pressure, lower energy density, higher aldehyde emissions, and so on. To overcome the drawbacks of alcohol fuels as gasoline additives, recently furan

functional group fuels have been suggested as high octane oxygenated fuels. Among several furan group fuel candidates, 2,5-dimethyl furan is considered to be one of the most promising furan fuel candidates because of its higher energy density, water insolubility, accessible manufacturing process [26], and so on. But, there are not many experimental engine studies with 2,5-dimethylfuran blends in gasoline.

Therefore, the focus of this study is to experimentally validate the knock related engine combustion and particulate matter emissions of 2,5-dimethylfuran gasoline blends, and to compare 2,5-dimethylfuran with two common alcohol fuels, ethanol and isobutanol, under boosted conditions.

3.3 Experimental Details

3.3.1 Engine and Fuel Specifications

A boosted Ricardo Hydra single cylinder research engine is used for studying the three oxygenated fuels. As described in Chapter 2, a cylinder head configured for port fuel injection mode engine head with a pent-roof design and with a central mount spark plug, is used in this study. The cylinder pressure transducer (Kistler 6125A piezoelectric transducer) is located on the side of the head, and the compression ratio is 10.5:1 with 0.5-liter displacement volume. All gasoline-oxygenated fuel blends are premixed and injected by port fuel injector with 550 kPa (= 5.5 bar) rail pressure. Additional engine specifications and operating conditions for Chapter 3 studies are provided in Table 3.1.

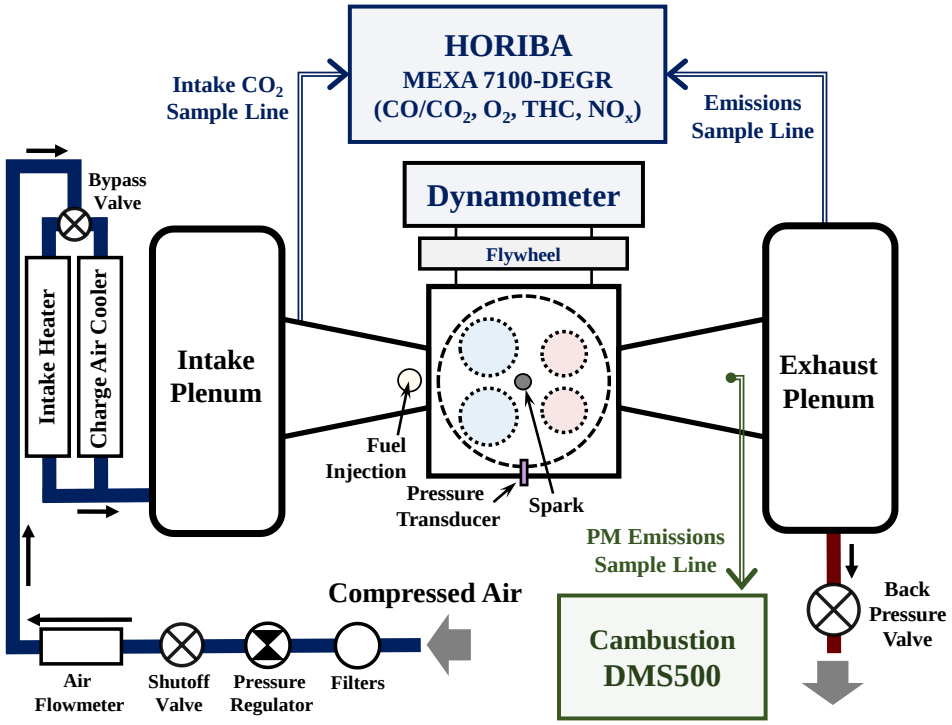

Figure 3.1 A schematic of boosted Hydra single cylinder research engine for Chapter 3

The schematic in the Figure 3.1 shows the air flow path and key components of the boosted engine. Compressed air is filtered, and the incoming pressure is regulated to maintain the target intake pressure. The air mass flow is measured by thermal mass flowmeter (Fox Instruments FT2), and the engine includes a by-pass heater and cooler located in front of the intake plenum for maintaining consistent intake air temperature. The engine is controlled with a National Instruments compact real-time controller (cRIO) and digital and analogue modules provided by Drivven hardware. The modules are accompanied by a piece of software that was used to implement the engine controller software within NI Labview. The in-house developed engine controller program permits the control of spark timing, port fuel injection timing and port fuel injection duration. The low-speed data acquisition system is based on the National Instrument modules and a SCXI system, and the high-speed data acquisition system is based on the AVL indiset modules.

Table 3.1 Engine specifications and operating conditions for Chapter 3

Displaced Volume	0.5 L
Bore / Stroke	86 mm / 86 mm
Compression Ratio	10.5 : 1
Intake Valve Timing	IVO: 362 $bTDC_{ign}$ / IVC: 136 $bTDC_{ign}$
Exhaust Valve Timing	EVO: 138 $aTDC_{ign}$ / EVC: 364 $aTDC_{ign}$
Head Design	Pent-roof / 4-valves / Central Spark
Engine Speed	1500 rpm
PFI Fuel Rail Pressure	5.5 bar (abs.)
Intake Air Temperature	26.7 °C ± 0.8 °C
Coolant / Oil Temperature	85 °C / 85 °C

Gaseous emissions including CO/CO_2, O_2, THC (Total Hydrocarbon), and NO_x are measured using the Horiba MEXA 7100-DEGR as described in Chapter 2. A Bosch LA4 wide range oxygen sensor, which is mounted in the exhaust runner, is used to determine the air to fuel equivalence ratio, and the values are matched to the lambda value of Horiba MEXA emissions bench for all experimental sets in real-time.

Particle size distribution and particle number concentration are measured using a Cambustion DMS500 (Differential Mobility Spectrometer) mk2 fast particulate analyzer. As Figure 3.1 shows, the exhaust samples are collected on the exhaust side runner with 0.25-inch diameter stainless steel tubes and the captured samples are diluted with heated dry air in the first stage with a dilution ratio of 6:1 to prevent water and hydrocarbons from condensing onto the instrument and to avoid significant particle agglomeration. The diluted samples on the first stage are passed through a heated line maintained at 150°C and are diluted with dry air (dew point -62°C) at a dilution ratio of 1:1 (0.8, 0.9, and 1.0 bar intake pressure conditions) and 12:1

(boosted intake pressure 1.1, 1.2, 1.3, and 1.4 bar conditions). All collected data are at a sampling rate of 10 Hz for 60 seconds and consequently averaged.

Table 3.2 Properties of gasoline and blended oxygenated fuels (Ethanol, Isobutanol, and 2,5-dimethylfuran)

	Gasoline [a]	**Ethanol**	**Isobutanol**	**2,5-Dimethylfuran**
Chemical Formula	-	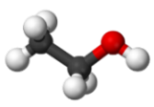	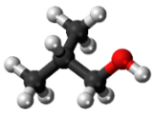	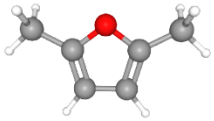
	C_2-C_{15}	**C_2H_6O**	**$C_4H_{10}O$**	**C_6H_8O**
H/C ratio (mole basis)	1.910	3	2.5	1.333
O/C ratio (mole basis)	0.0	0.5	0.25	0.167
MW [g/mole]	97.34 (calculated)	46.07	74.12	96.13
RON	91.5	109 [b]	105 [b]	119 [b] / 101.3 [c]
MON	83.4	90 [b]	90 [b]	N/A [b] / 88.1 [c]
Sensitivity (R-M)	8.1	19	15	13.2 [c]
LHV [MJ/kg]	43.6	26.8 [b]	33.1 [b]	33.8 [b]

[a] Analysis Result from Gage Products Company, Ferndale, MI, USA. (2016);

[b] Yanowitz. et al. Utilization of renewable oxygenates as gasoline blending components. No. NREL/TP-5400-50791. National Renewable Energy Laboratory (NREL), Golden, CO., (2011) [27];

[c] API Research Project (1956) [28];

The baseline gasoline fuel used in this study is oxygenate free, research grade gasoline provided by Gage Products Company. The research octane number is 91.5 and motor octane

number is 83.4 (sensitivity of 8.1). The ethanol used in this study is 200-proof anhydrous provided by the Deacon labs Inc., and the Isobutanol is a fuel grade 96~99% purity isobutyl alcohol from bio-feedstock provided by the Gevo Inc. The 2,5-dimethylfuran is from Acros Organics with 99% purity.

3.3.2 Knock Intensity and Combustion Analysis

In order to determine the knock limit, two types of methods are used in this study. The first one is audible knock which is measured during the experiment with a microphone and speakers, and the second method uses the filtered cylinder pressure profile in the post processing step. To determine the knock intensity for the second method, two calculation approaches are used in this study: $KI_{\text{peak to peak}}$ (Equation 3.1) and KI 20 (Equation 3.2), which are described in Chapter 2. Both knock intensities are used for determining the knock limit, but the $KI_{\text{peak to peak}}$ equation is given priority for plotting in Chapter 3. Heat release analyses including burn duration and mean effective pressure calculations are processed by Indicom commercial software which is described in Chapter 2.

$$\mathbf{KI}_{\mathbf{peak\ to\ peak}} = \left| \left(\boldsymbol{max} \{ \boldsymbol{p(i)} \} \right) - \left(\boldsymbol{min} \{ \boldsymbol{p(i)} \} \right) \right| \tag{3.1}$$

$$\mathbf{KI\ 20} = \frac{1}{N_{samp}} \sum_{i=1}^{N_{samp}} (P(i) - P_{mean})^2 \tag{3.2}$$

3.3.3 Experimental Conditions

The investigated fuel blends are shown in the Table 3.3. Tested fuel blends include a total of 9 sets. Pure gasoline was tested twice under the same conditions (E0, IB0, DMF0) to check baseline repeatability. Ethanol and Isobutanol are blended up to 30 % by volume in 10 percent increments, and 2,5-dimethylfuran blends are two cases, 10 and 20 by volume blended in gasoline.

Table 3.3 List of gasoline-oxygenated fuel blends investigated

Oxygenated Fuel	Abbreviation	Abbreviation for blends	Blends (v/v%)
Ethanol	ETOH	E	E0, E10, E20, E30
Isobutanol	IBOH	IB	IB0, IB10, IB20, IB30
2,5-Dimethylfuran	DMF	DMF	DMF0, DMF10, DMF20

Engine experiments were conducted with three types of parameters for studying knocking related combustion, gaseous emissions, and particulate matter emissions. The first parameter is fuel blending ratio, which is up to 30 volume percent for ETOH and IBOH and up to 20 volume percent for DMF. The second parameter is a comparison of fuel molecular structure using gasoline and 20 volume percent blends of each of the three oxygenated fuels. The last parameter is intake pressure, which is swept from 0.8 bar to boosted condition up to 1.4 bar for each fuel set, demonstrating the each blend's effects. Injection timing is 400 bTDC (closed valve injection), and injection duration is varied by intake pressure. The exhaust pressure is maintained

at 0.98 bar to avoid internal EGR (exhaust gas recirculation) effect in all cases, and the air to fuel ratio was maintained at 1.00 in all fuel cases.

3.4 Engine Combustion and Knock

3.4.1 Combustion Phasing and Knock Intensity

In order to investigate the effects of these three parameters (fuel molecular structure, blend ratio, and intake pressure) on knock intensity, spark timing sweeps at 1 or 2 crank angle degree intervals are performed to find the maximum brake torque (MBT) or knock limit (KL) points. Figures 3.2 to 3.4 show the relationship between the three parameters and knock intensity as a function of combustion phasing.

For the comparison of fuel molecular structure, the knock intensity of gasoline and 20 volume percent oxygenated fuel blends are plotted in Figure 3.2 as a function of combustion phasing under four intake pressure conditions from 0.8 to 1.4 bar. The MBT region, which is between 7 and 10 crank angle degrees, is indicated in each plot from 0.8 to 1.2 bar conditions. As the combustion phasing advances, knock intensity starts to rise, and the increasing slopes are pretty similar for all fuel cases except 0.8 bar throttled condition. In the 0.8 bar throttled condition shown in Figure 3.2 (a), E20 fuel does not show any knocking points over the MBT timing, and DMF20 and IB20 also show the knocking points after the MBT timing. So, only gasoline showed a knocking phenomenon under 0.8 bar throttled condition.

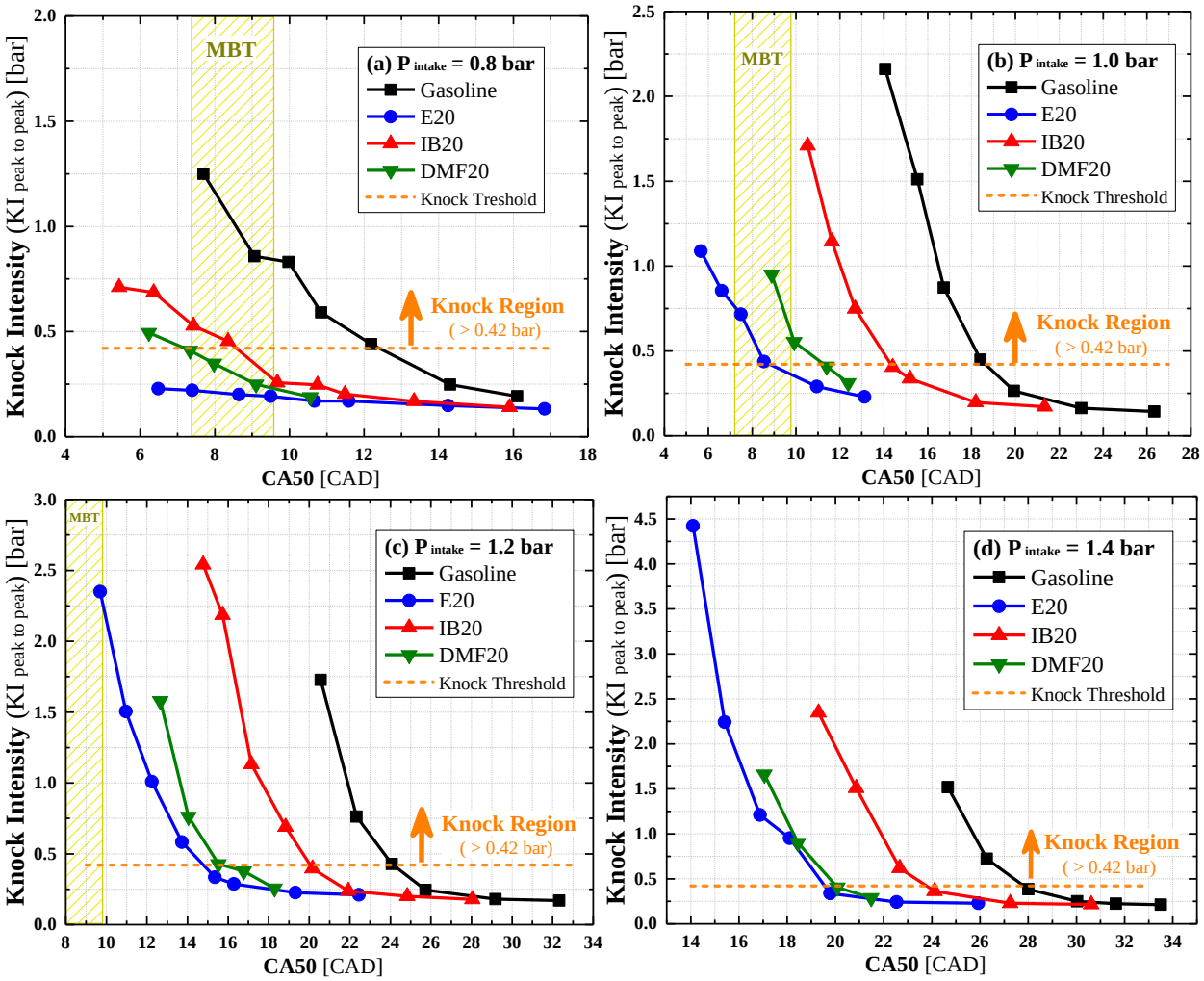

Figure 3.2 Knock intensity ($KI_{peak\ to\ peak}$) as a function of combustion phasing (CA50) of gasoline and 20 percent blend sets; (a) 0.8 bar, (b) 1.0 bar, (c) 1.2 bar, and (d) 1.4 bar intake pressure.

In the wide open throttle (WOT) condition shown in Figure 3.2 (b), E20 also showed MBT before knocking, and all three other fuel sets show knocking prior to reaching MBT timing, and all fuel sets under boosted conditions (1.2 and 1.4 bar) show knocking before reaching MBT, as shown in Figures 3.2 (c) and (d). The order of knock onset timing is the same for all the fuels, regardless of the intake pressure: gasoline (earliest), isobutanol, 2,5-dimethylfuran, and ethanol (latest). This order agrees with the order of both research and or motored octane numbers (RON / MON) for gasoline (91.5 / 83.4), isobutanol (105 / 90), and

ethanol (109 / 90) in Table 3.2, but the 2,5-dimethylfuran did not agree with any of the published research octane numbers (119 [27] and 101.3 [28]), which should be between 105 and 109 based on this experimental result. There could be several possibilities for this mismatch with research octane numbers compared to these engine experimental data. The first possibility could be different blending effects on octane number between the furan and the alcohol functional groups. For instance, Anderson et al. [29] studied the blending ratio effects on octane number in detail using gasoline and ethanol, and observed a non-linear relationship with volumetric ethanol concentration and different gasoline compositions of various blendstocks. Considering their blending study, 2,5-dimethylfuran (or furan functional group) could have significantly different characteristics of the relationship between blending rate and octane number compared to the alcohol group. Another possibility could be octane sensitivity (OS) [30–32] (which is closely related to knock resistance at boosted high load conditions) differences of 2,5-dimethylfuran gasoline blends. In detail, furan blends are less sensitive to high pressure due to the stable chemical structure, and this agrees with an auto-ignition research of 2,5-dimethylfuran as a diesel additive using motored CFR engine [33]. As comparing DMF20 knock intensity sets with other fuels in Figure 3.2 (a) to (d), the onset of knocking point of DMF20 gradually reaches out to ethanol knock onset points. So, this possibility is pretty persuasive. The other possibility could be due to the less accurate octane number measurements in the referenced studies as discussed in the Introduction of this chapter of the thesis. Since 2,5-dimethylfuran came to be an oxygenated fuel candidate quite recently, there are not many octane related studies and octane rating results. So, more 2,5-dimethylfuran studies need to be conducted regarding blending octane number and knocking.

Figure 3.3 is the same knock intensity data set as Figure 3.2, but categorized by fuels under different intake pressure conditions. The cross-sectional points between the graph and the orange dashed line indicate knock onset points in each figure, and the amount of knock limit extension is consistent for all fuels.

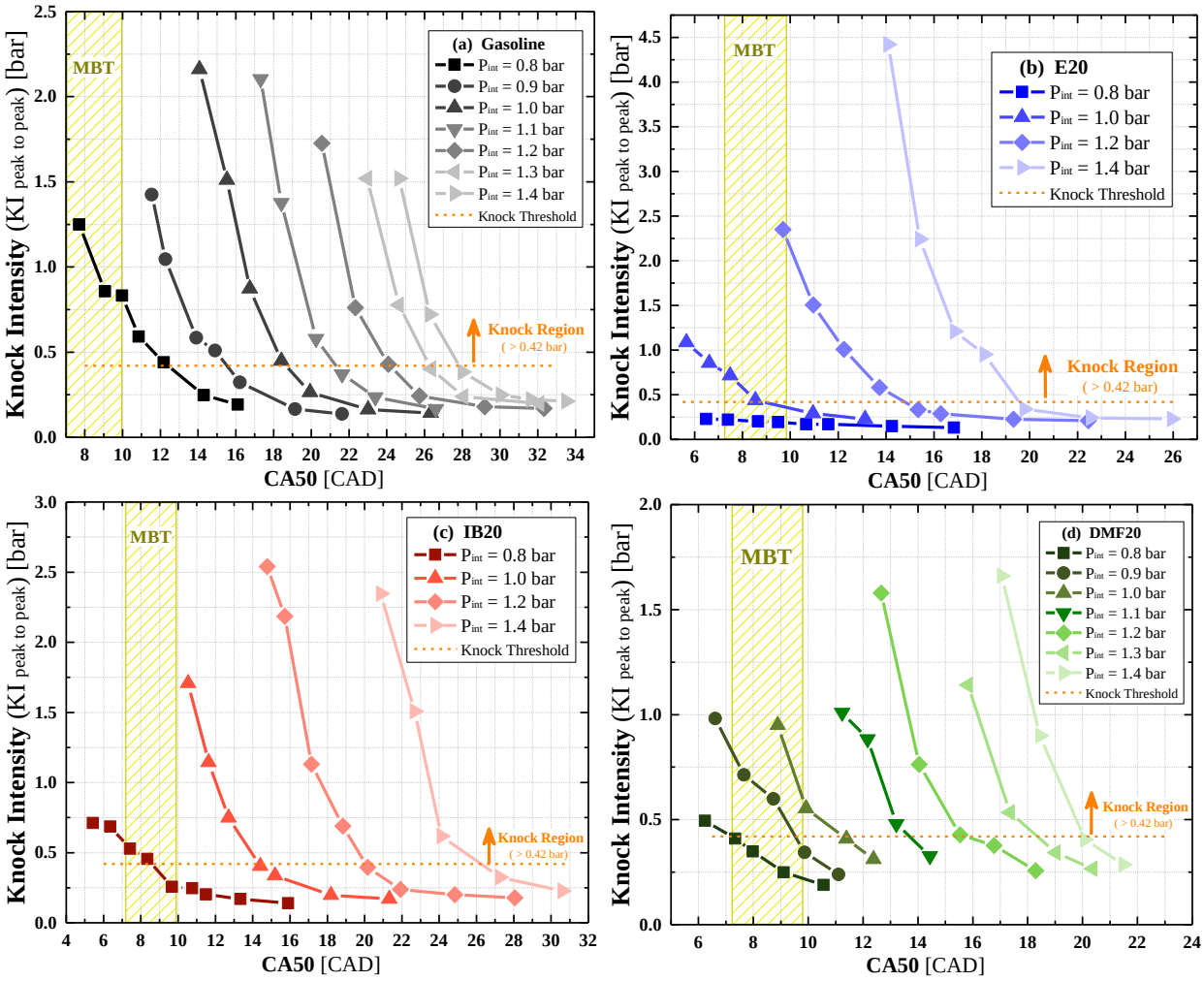

Figure 3.3 Knock intensity ($KI_{peak\ to\ peak}$) as a function of combustion phasing (CA50) of different intake pressure; (a) gasoline, (b) E20, (c) IB20, and (d) DMF20.

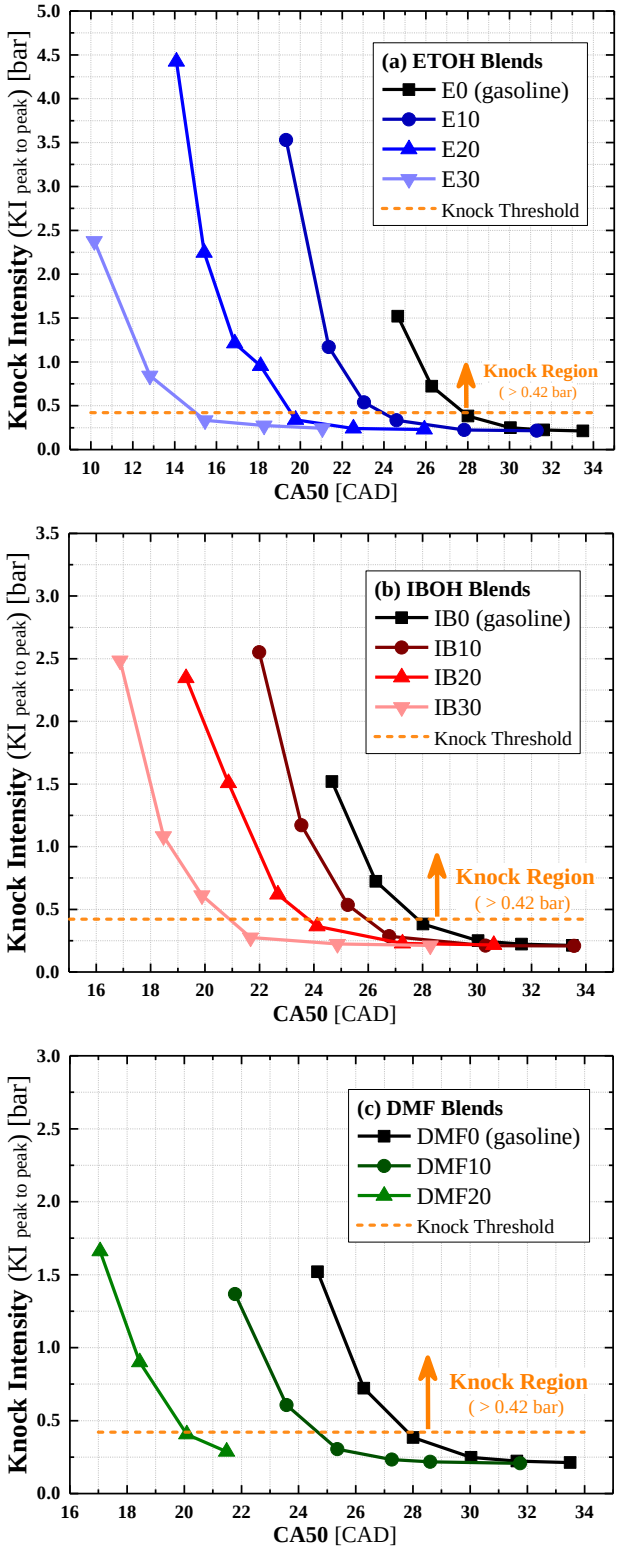

Figure 3.4 Knock intensity ($KI_{peak\ to\ peak}$) as a function of combustion phasing (CA50) of blend ratio sets under 1.4 bar boosted condition; (a) ETOH blends, (b) IBOH blends, and (c) DMF blends.

The effect of the third parameter (blend ratio) on knock intensity is plotted in Figure 3.4. This graph is the highest boosting pressure data set (1.4 bar intake pressure), and three other cases are attached in **Appendix B. Supplemental Material for Combustion Characteristics of Oxygenated Fuel Gasoline Blends** (Chapter 3). Gasoline is shown in the black color line, which is same as E0, IB0, and DMF0 for all plots.

3.4.2 Combustion Phasing and Knock Limit

Figure 3.5 shows the maximum brake torque or knock limited combustion phasing (CA50) as a function of load (IMEPg). The knock limited (KL) points are indicated by filled symbols and maximum brake torque (MBT) points are indicated by empty symbols in Figure 3.5.

Figure 3.5 (a) is a summary graph for the 20 percent oxygenated fuel blends, and Figures 3.5 (b) to (d) are blend ratio differences of ethanol, isobutanol, and 2,5-dimethylfuran respectively. The advance of knock limited combustion phasing with increasing blend ratio for the three fuels is consistent, and the amount advance in combustion phasing for isobutanol is less than for the other two oxygenated fuels as shown in the knock intensity graphs in Figure 3.4. The amount of advance of knock limited combustion phasing for E20 and DMF20 are twice as high as for IB20, as shown in Figure 3.5 (a).

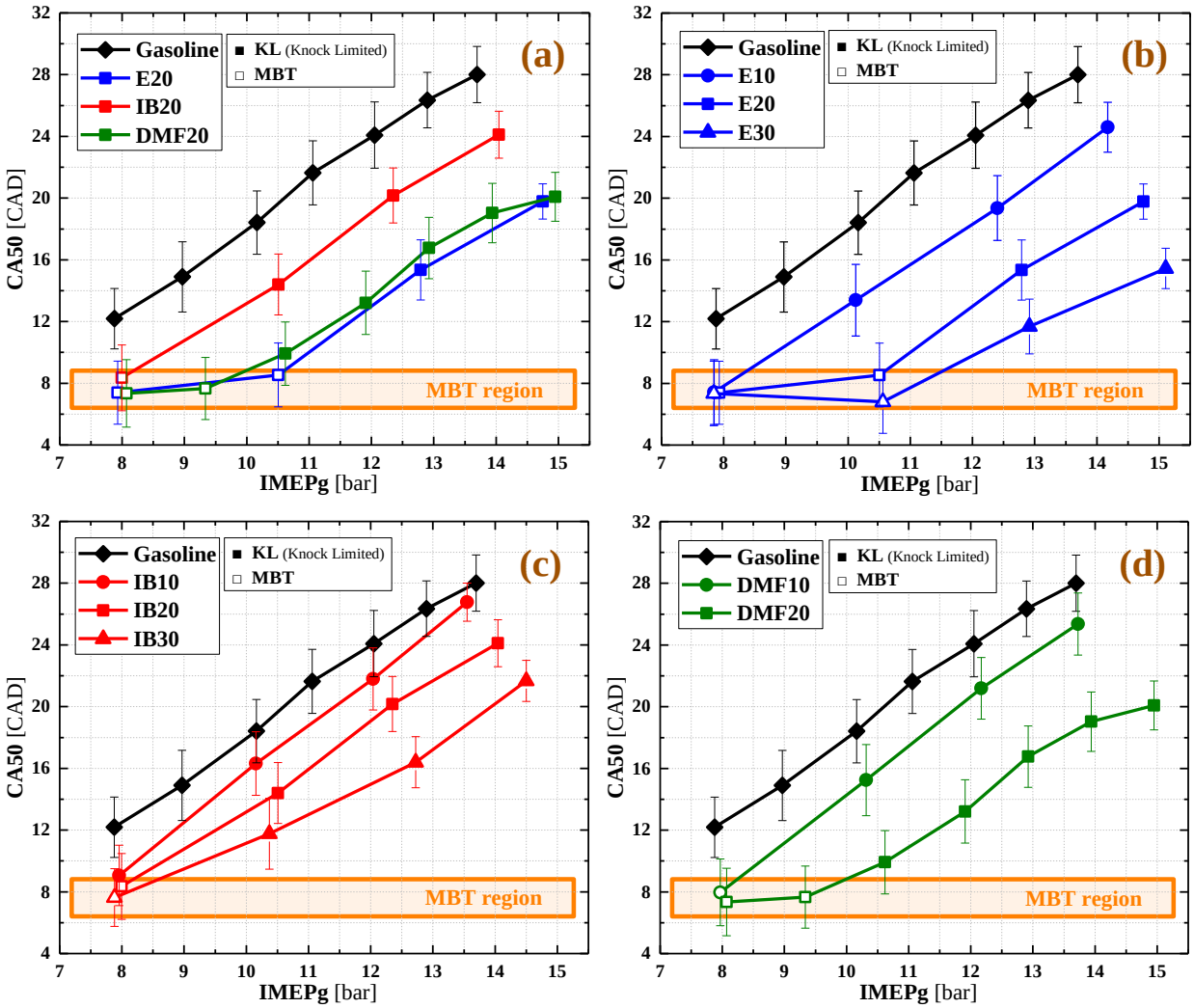

Figure 3.5 Maximum Break Torque (MBT) and Knock Limited (KL) combustion phasing (CA50) based on the load (gross IMEP); (a) 20% blend sets comparison, (b) ethanol blend sets comparison, (c) iso-butanol blend sets comparison, and (d) 2,5-dimethylfuran blend sets.

3.4.3 Burn Duration and Knock Limit

Burn duration (CA1090), crank angle between 10 and 90 percent mass fraction burned, for all intake pressures for gasoline is plotted in Figure 3.6 as a function of combustion phasing (CA50). With increasing intake pressure, the burn duration line gradually moves to right hand

side, and burn duration at the same combustion phasing is shortened along with intake pressure, shown by the green vertical line. But, the knock limited burn duration is increased with increasing boost pressure, shown with an orange arrow (1.3 crank angle degrees increased from 0.8 bar to 1.4 bar intake pressure). The effect of retarded spark timing under boosted conditions, follows the same trend for each 20-volume percent fuel blend, as shown in Figure 3.7.

Figure 3.8 is a summary graph of the burn duration of the knock limited points under different boost pressure. This trend agrees with the knock limited combustion phasing as a function of load (IMEPg), as shown in Figure 3.5 (a).

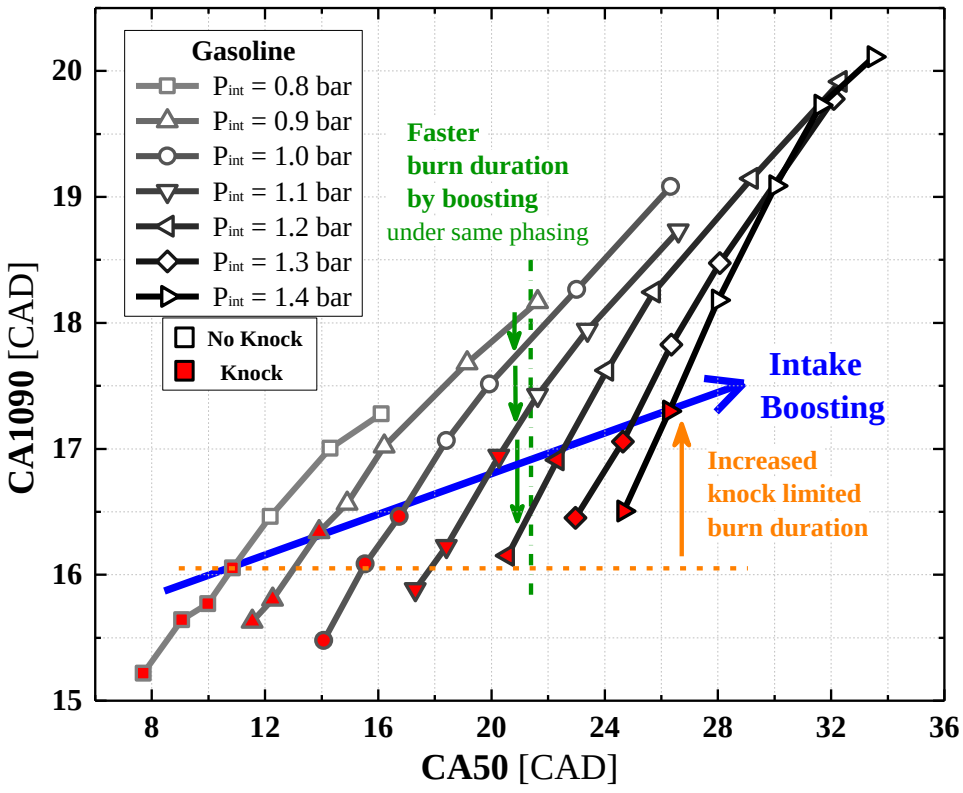

Figure 3.6 Averaged burn duration (CA1090) for gasoline as a function of combustion phasing (CA50) from 0.8 bar to 1.4 bar intake pressure.

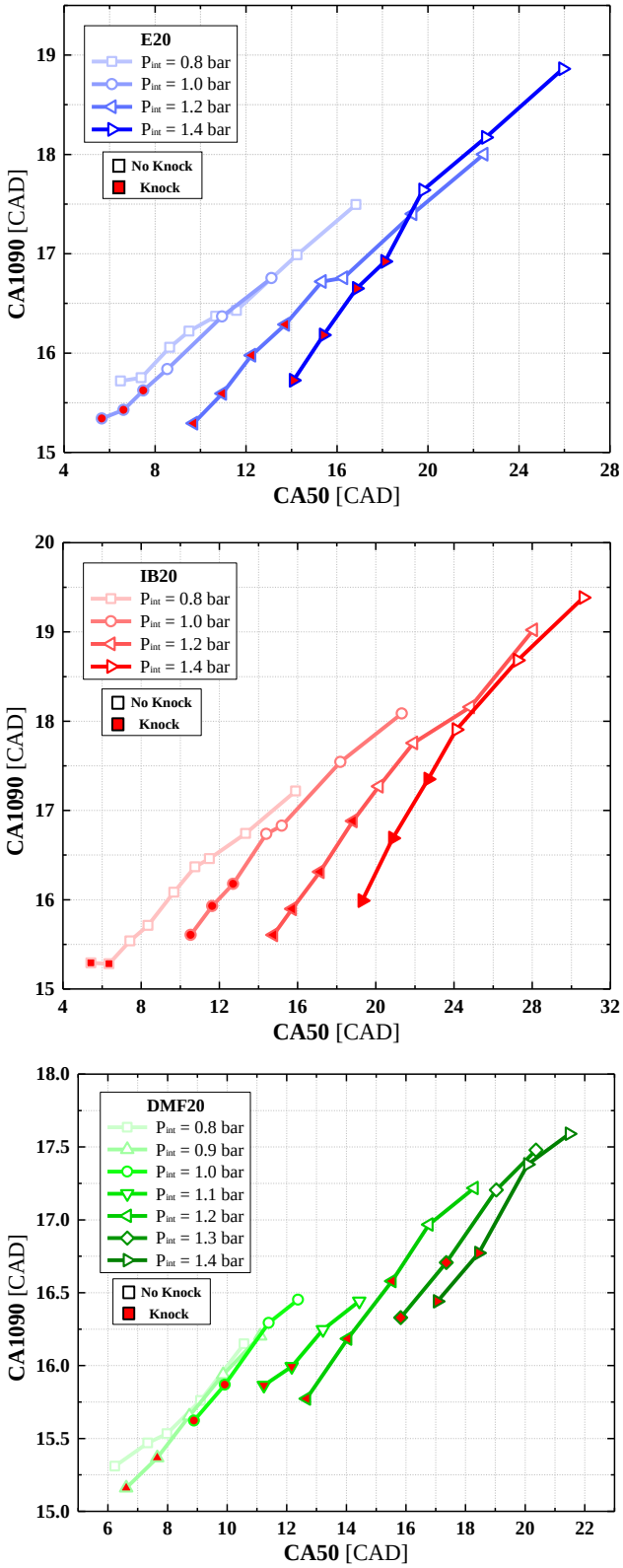

Figure 3.7 Averaged burn duration (CA1090) of 20 volume percent blends as a function of combustion phasing (CA50) from 0.8 bar to 1.4 bar intake pressure

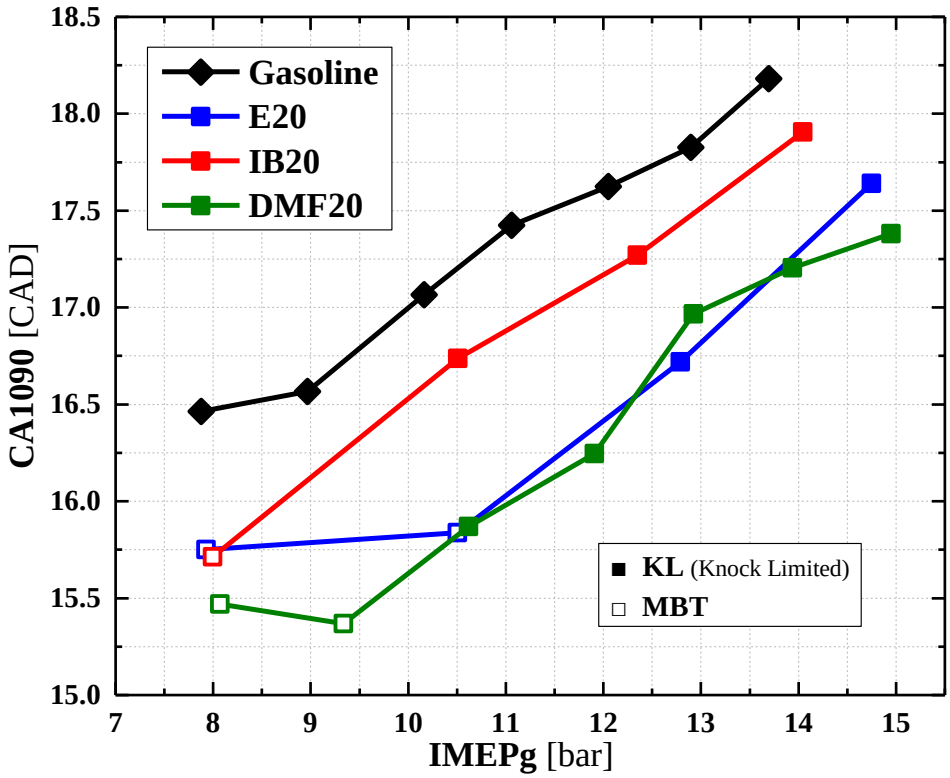

Figure 3.8 Averaged burn duration (CA1090) for gasoline and 20 volume percent blends as a function of load (IMEPg)

3.4.4 Indicated Thermal Efficiency

Consistent with the knock limit extension with the addition of the oxygenated fuels, the thermal efficiency is improved under boosted conditions. Figure 3.9 depicts the gross indicated thermal efficiency (ITEg) for gasoline and 20 volume percent oxygenated fuel blends, with error bars, as a function of the load (IMEPg). As shown for the 0.8 bar throttled condition near 8 bar of IMEPg, thermal efficiencies for all fuels are almost identical regardless of whether they are knock limited or maximum brake torque conditions (filled symbols are knock limited and open symbols indicate MBT timing). But the thermal efficiency for gasoline gradually decreases with

increasing the boost level due to the retarded knock limit under boosted conditions. The IB20 fuel blend shows better thermal efficiency than gasoline under boosted conditions, and the improvement increases with increasing boost level. The E20 and DMF20 cases show the highest efficiency among the four sets of experiments, and the amount of efficiency improvement is higher with increasing boosting level, as well. The order of thermal efficiency improvement under boosted pressure is same as the knock limited phasing. Knock limited phasing for DMF 20 is slightly earlier than for E20 as Figure 3.2 shows, but the effect of knock limited phasing difference on thermal efficiency appears negligible. While in some cases the thermal efficiency for DMF20 is slightly higher than E20, the differences are not statistically significant.

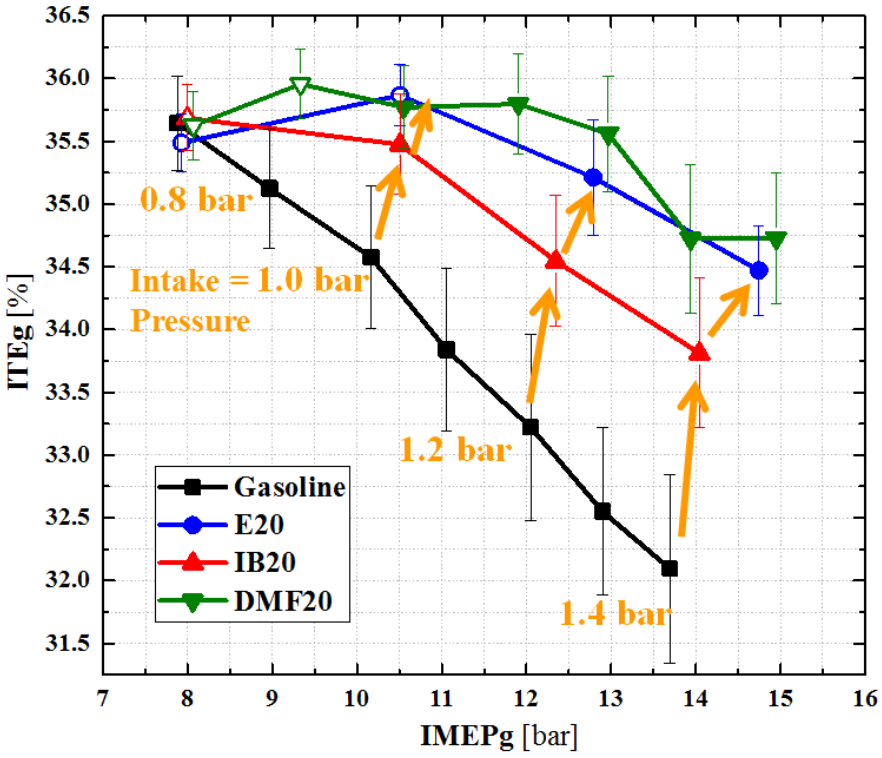

Figure 3.9 Gross indicated thermal efficiency (ITEg) for gasoline and 20 volume percent blends as a function of load (IMEPg)

3.4.5 Combustion Stability

Combustion stability differences, which is calculated from the coefficient of variation (CoV) of the load (IMEPg), are shown in Figure 3.10. Gasoline shows the most unstable combustion compared to the other fuels, but all CoV values are in an acceptable range (less than 3%). The reason of higher CoV value for gasoline is because of early knock limited condition. In general, as spark timing advances, CoV values are gradually decreased, so the CoV of gasoline under higher load could be due to earlier knock limited phasing. The order of combustion stability also agrees with the order of knock limited phasing.

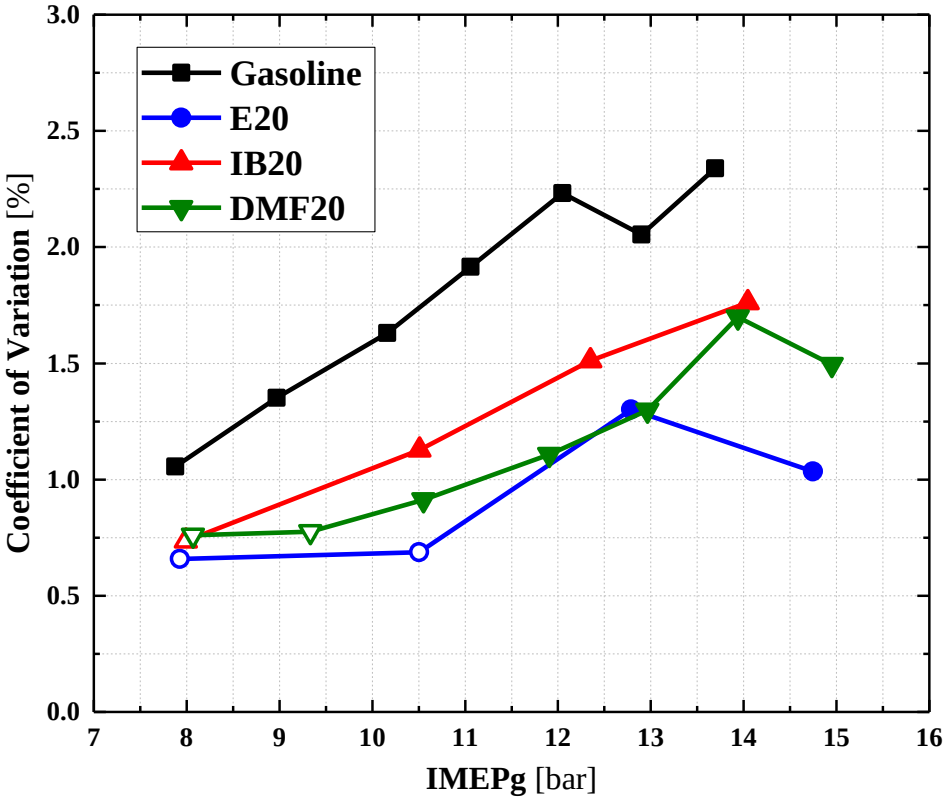

Figure 3.10 Coefficient of Variance (CoV) of IMEPg for gasoline and 20 volume percent blends as a function of load (IMEPg)

3.5 Gaseous Emissions

3.5.1 Total Unburned Hydrocarbon (THC) Emissions

Figure 3.11 shows total unburned hydrocarbon (THC) emissions at knock limited points as a function of the load. All emissions values are converted into indicated specific values using 'ppmC_1' basis. Unburned hydrocarbon emissions are generally related to combustion quality (i.e., combustion efficiency). THC emissions for gasoline are higher than the other fuel blends, and this could be due to excessive spark retard due to knocking. Three other blends (E20, IB20, and DMF20) show very similar THC emissions levels.

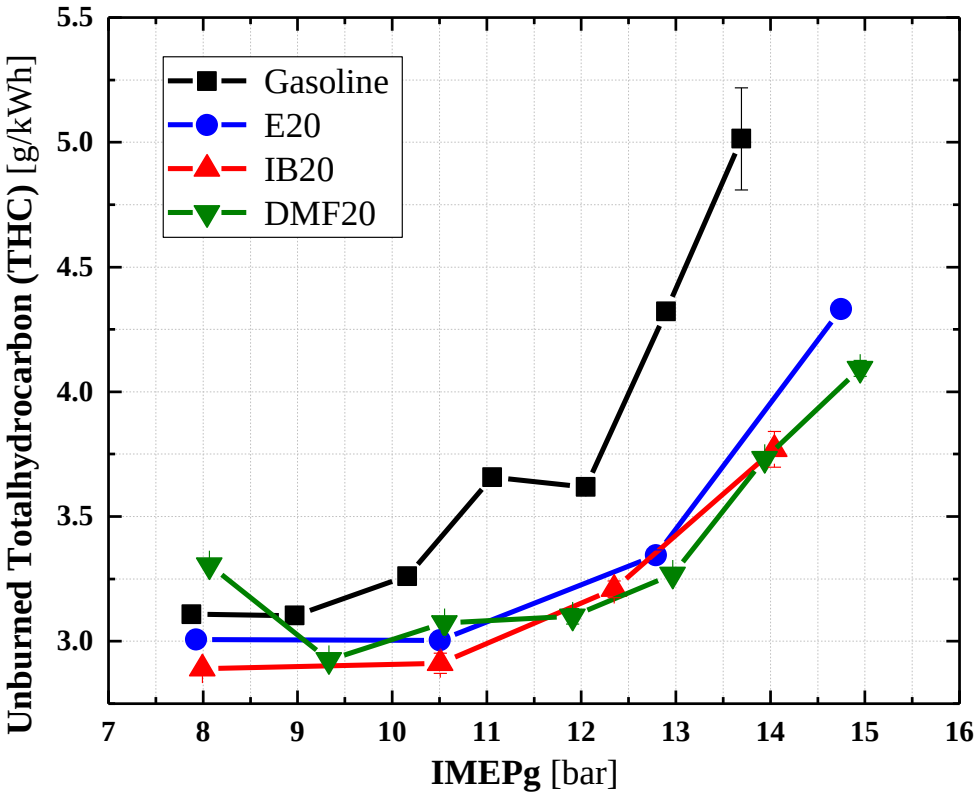

Figure 3.11 Indicated specific total unburned hydrocarbon (THC) emissions of knock limited points as a function of load (IMEPg).

One noticeable phenomenon in Figure 3.11 is the gradually increase of THC emissions with increasing boost level. The unburned hydrocarbon emissions are not changed much by fuel blends, but all fuels show significantly increased THC emissions by increased intake pressure. This could be an important signal of general combustion quality, for example, insufficient mixing rate or in-cylinder pool fires. This is a port fuel injection mode configuration (not a direct injection system), so the mixing rate might not be a problem for this study. The most likely reason for the higher unburned hydrocarbon is the in-cylinder pool fire. With increasing boost level, more fuel is needed to maintain 1.00 of air to fuel equivalence ratio. For instance, around 2 times more fuel is injected under 1.4 bar boosted condition compared to 0.8 bar throttled condition, in the case of gasoline. If there is a pool fire, generally more particulate matter is emitted, which is observed in the particulate matter emissions results, as discussed in the next section.

3.5.2 Carbon Monoxide (CO) Emissions

Figure 3.12 depicts carbon monoxide (CO) emissions results for gasoline and 20 volume percent blends as a function of load (IMEPg). Carbon monoxide emissions are generally affected by lambda value and combustion quality, as well. The air to fuel equivalence ratio (λ) is kept at 1.00 for all experiments, so combustion quality could be the reason for different carbon monoxide emissions. Carbon monoxide emissions for gasoline and the three oxygenated blend sets are relatively comparable to each other, but the order of carbon monoxide emissions are DMF20, IB20, gasoline, and E20. The higher carbon monoxide value for DMF20 could be because more time is needed for chain branching of the furan structure compared to alcohol

structure [34] due to the more stable structure of DMF. Also, CO emissions for all cases gradually decreased with increasing intake pressure. This is possibly due to the increased cylinder temperature, which promotes more complete combustion, under boosted conditions.

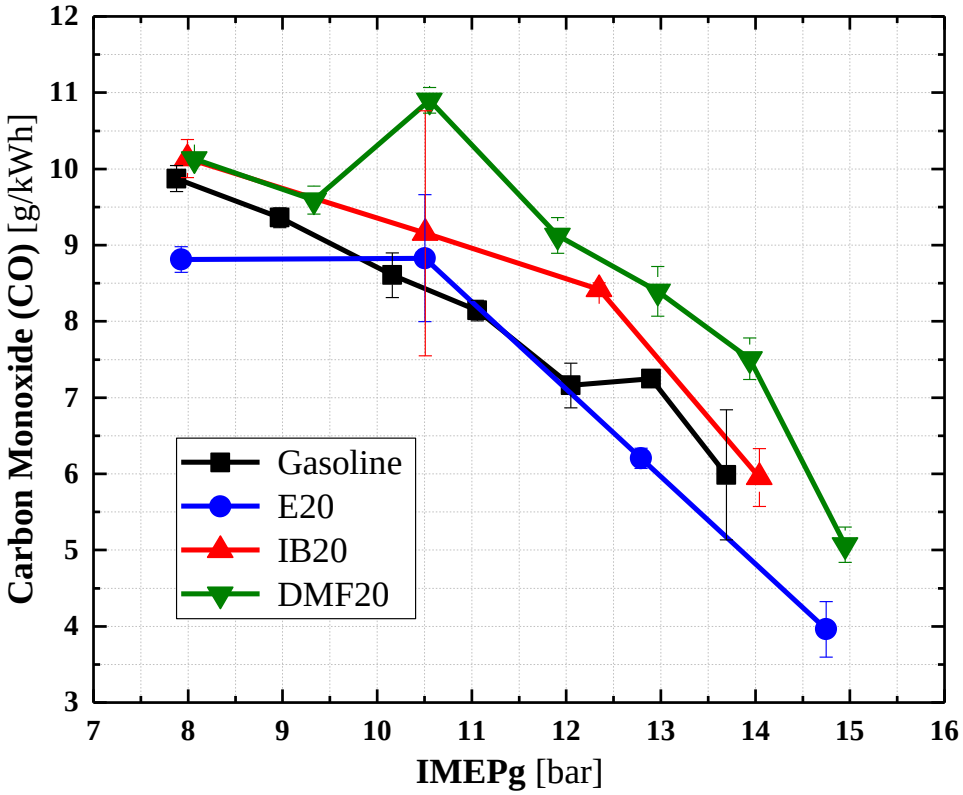

Figure 3.12 Indicated specific carbon monoxide (CO) emissions for knock limited points as a function of load (IMEPg)

3.5.3 Nitrogen Oxides (NO_x) Emissions

Nitrogen oxides (NO_x) emissions for gasoline and 20 volume percent blends are shown in Figure 3.13 as a function of load. The level of nitrogen oxides emissions is strongly related to the in-cylinder peak temperature [35,36]. Considering the higher heat of vaporization values for the

oxygenated fuels, the higher nitrogen oxides emissions value for gasoline are reasonable. Lower nitrogen oxides emissions for IB20 and DMF20 could be due to retarded spark timing compared to E20 fuel under boosted conditions, and higher NO_x emissions for DMF20 under throttled condition appears to be because of more advanced combustion phasing (near 7 crank angle degree of CA50) compared to the other fuels (after 10 crank angle degree of CA50) under non-knocking condition as shown in Figure 3.2 (a).

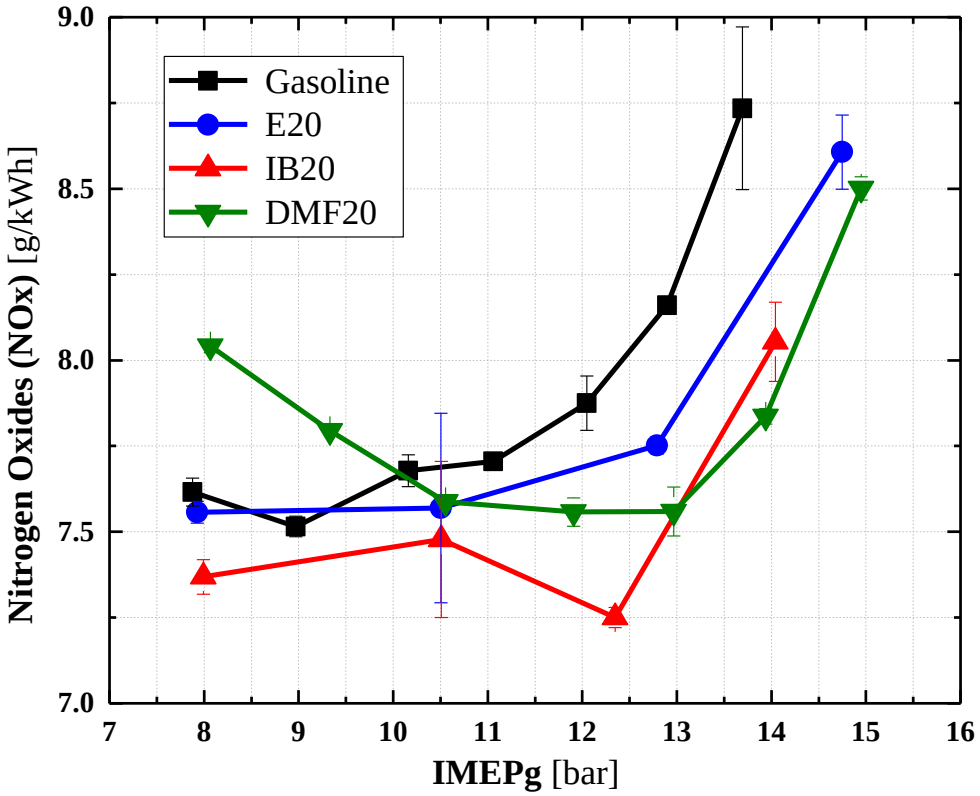

Figure 3.13 Indicated specific nitrogen oxides (NO_x) emissions of knock limited points as a function of load (IMEPg)

3.6 Particulate Matter Emissions

Particulate matter (PM) emissions results are divided into three sections: Intake pressure, Blend ratio, and Knock limited conditions.

3.6.1 Particulate Matter Emissions by Intake Pressure

Figure 3.14 shows the particulate matter size distributions and numbers for gasoline and the 20 volume percent blends at knock limited or maximum brake torque points under four different intake pressure conditions from 0.8 to 1.4 bar. The scale of the vertical axis is set to the same value in all pressure conditions for comparing the effect of intake pressure on particulate matter emissions. Unlike direct injection system, the port fuel injection system has enough time for fuel evaporation and mixing before combustion starts, so as the 0.8 bar throttled condition data shows, very low particulate emissions are produced with port fuel injection, regardless of the fuel. With increasing intake boost level, particulate matter emissions gradually increase under knock limited points. Particulate matter emissions under wide open throttle (1.0 bar intake) conditions are slightly increased compared to the 0.8 bar condition for the 20 volume percent blends, but for gasoline PM emissions start to increase significantly. The PM emissions for the three 20 volume percent oxygenated fuel blends start to significantly increase from 1.2 bar, and continue to increase under 1.4 bar boost. The order of particulate matter emissions under knock limited operation is generally the same as the order of knock onset timing shown in Figure 3.2.

Figure 3.15 indicates calculated accumulation mode particles (growth of nucleation mode particles normally between 23 nm and 1 μm diameter [37]) under 1.4 bar boosted condition. One observation from the accumulation mode particle results is that DMF20 blend set shows wide soot distribution range compared to the other fuel sets. This wide distribution can be found in the

1.2 bar condition of Figure 3.14, as well. The reasons for a wide soot distribution could be due to the furan structural effects on sooting tendency, and this wide distribution phenomenon agrees with several particulate matter results from other research [38–40].

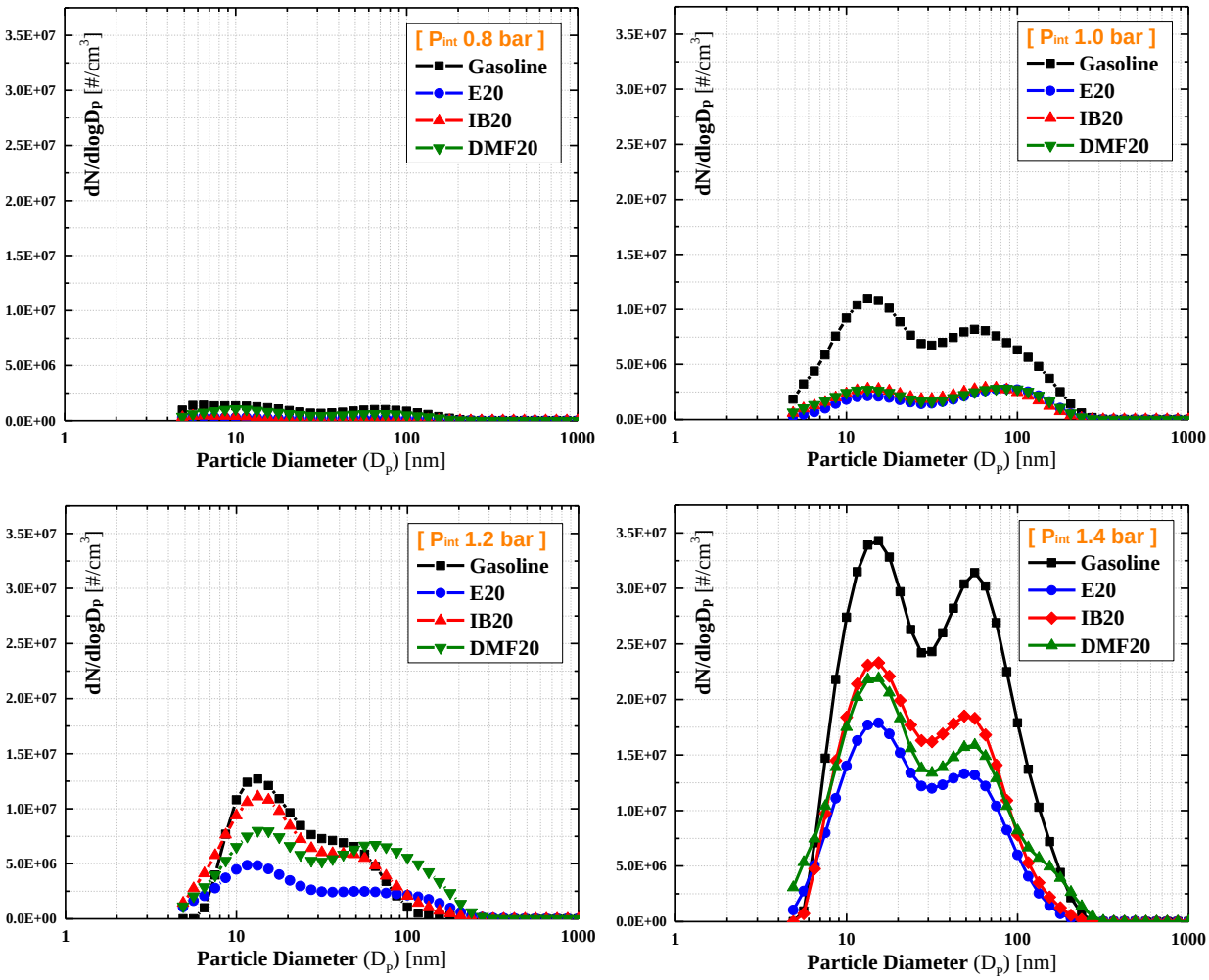

Figure 3.14 Particulate matter emissions size distribution and total number for gasoline and 20 volume percent blends at knock limited points; Intake pressure 0.8, 1.0, 1.2, and 1.4 bar.

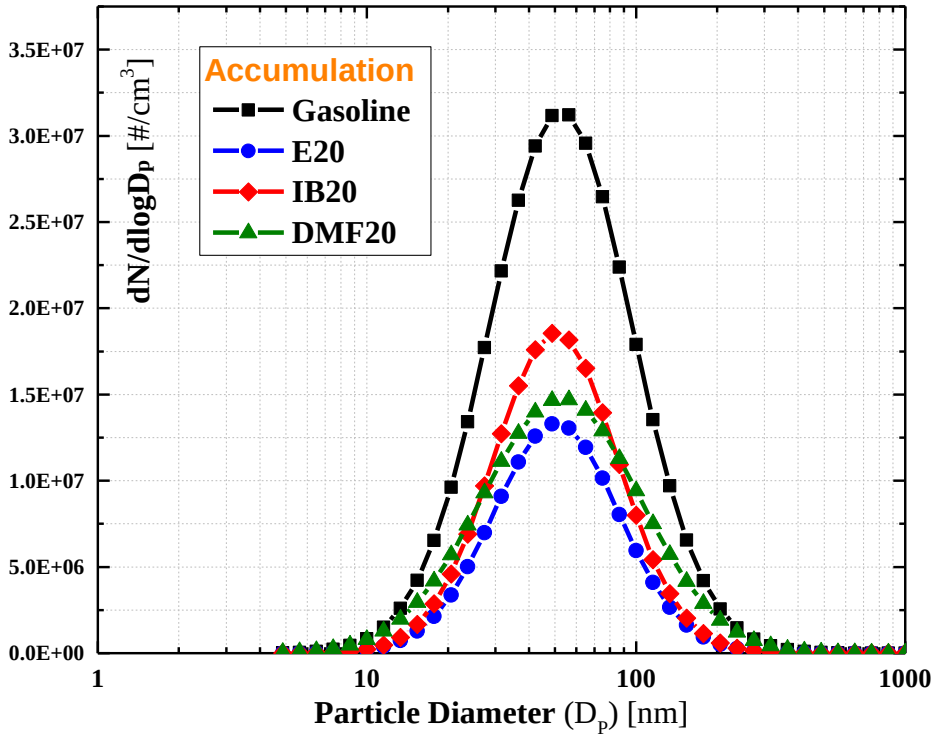

Figure 3.15 Accumulation mode size distribution for gasoline and 20 volume percent blends at knock limited points under 1.4 bar boosted condition.

3.6.2 Particulate Matter Emissions by Blending Ratio

Figures 3.16 and 3.17 shows blend ratio effects on accumulation mode particulate matter emissions at knock limited points under boosted conditions, and the points are shown in Figure 3.4 (a) and (b) in detail. The accumulation mode particles are gradually decreased with oxygenated fuel addition to gasoline for both isobutanol and ethanol. There could be several possible reasons for the reduced particulate matter emissions. One possible reason is that the addition of oxygenated fuel to gasoline reduces the aromatic content in the gasoline mixture. Accumulation mode particle emissions vary linearly with polycyclic aromatic hydrocarbons (PAHs) in the fuel, and the decreasing amount of accumulation mode particles shows a linear

trend as well. The other reason could be increased oxygen content. Increased oxygen in fuel helps to a lower the formation rate of soot and yields a higher soot oxidation rate, in general. And, this trend agrees with a diesel engine particulate matter emissions results by Song et al. [41]

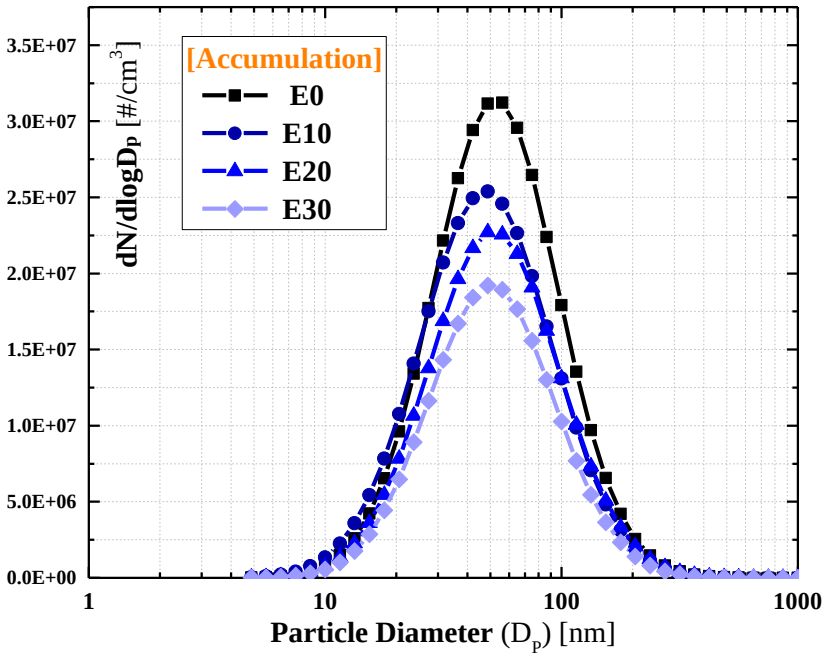

Figure 3.16 Accumulation mode size distribution of ethanol blend sets at knock limited point

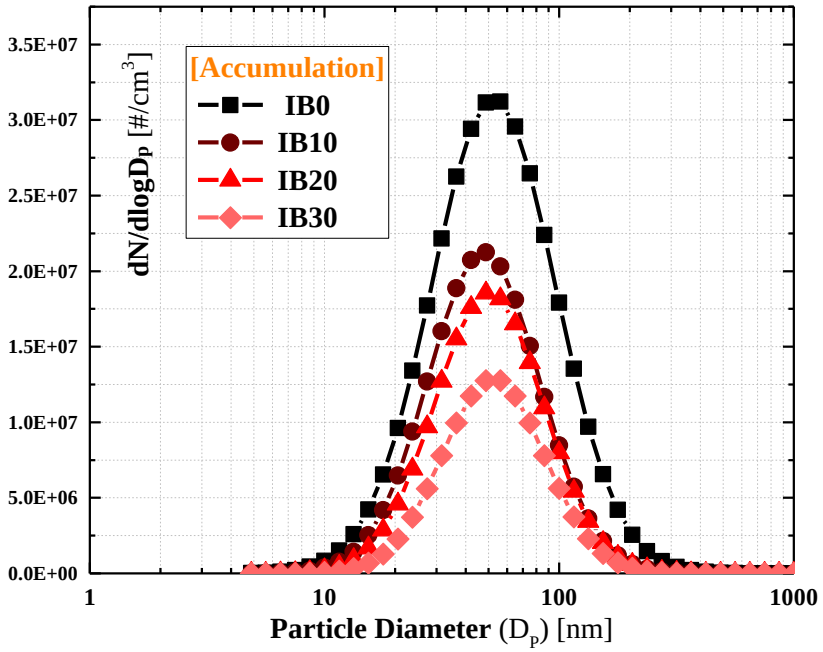

Figure 3.17 Accumulation mode size distribution of isobutanol blend sets at knock limited point

3.6.3 Particulate Matter Emissions by Knock Limits

In general, particulate matter emissions gradually increased with advancing spark timing mainly due to reduced oxidation time, as much as the advanced combustion phasing. However, the particulate matter emissions near knocking condition show a somewhat different trend from normal engine combustion. Figure 3.18 shows the particulate matter emissions trend near knock limited conditions and the size distributions for gasoline and 20 volume percent blends. The top left figure shows total particulate numbers as a function of combustion phasing. The filled symbols are knocking points and the empty symbols are non-knocking points. Figure 3.18 is clearly shown that the slope of total numbers is instantly increased after the onset of knock for all cases. For a better understanding of the increased total particle number emissions, the size distributions for all four fuels are plotted in the lower four figures. All fuels show very similar trends, in that nucleation mode particles are not changed much even under knocking conditions, but the accumulation mode particles are dramatically increased after the onset of knock. As the total number graph shows, the extent of increase of particulate number emissions is fairly consistent. There could be several reasons for the increased particulate matter emissions after the onset of knock, and these concepts are discussed in Chapter 7. The DMF20 blend set shows wide distributions under knock limited conditions as shown in the right bottom plot in Figure 3.18.

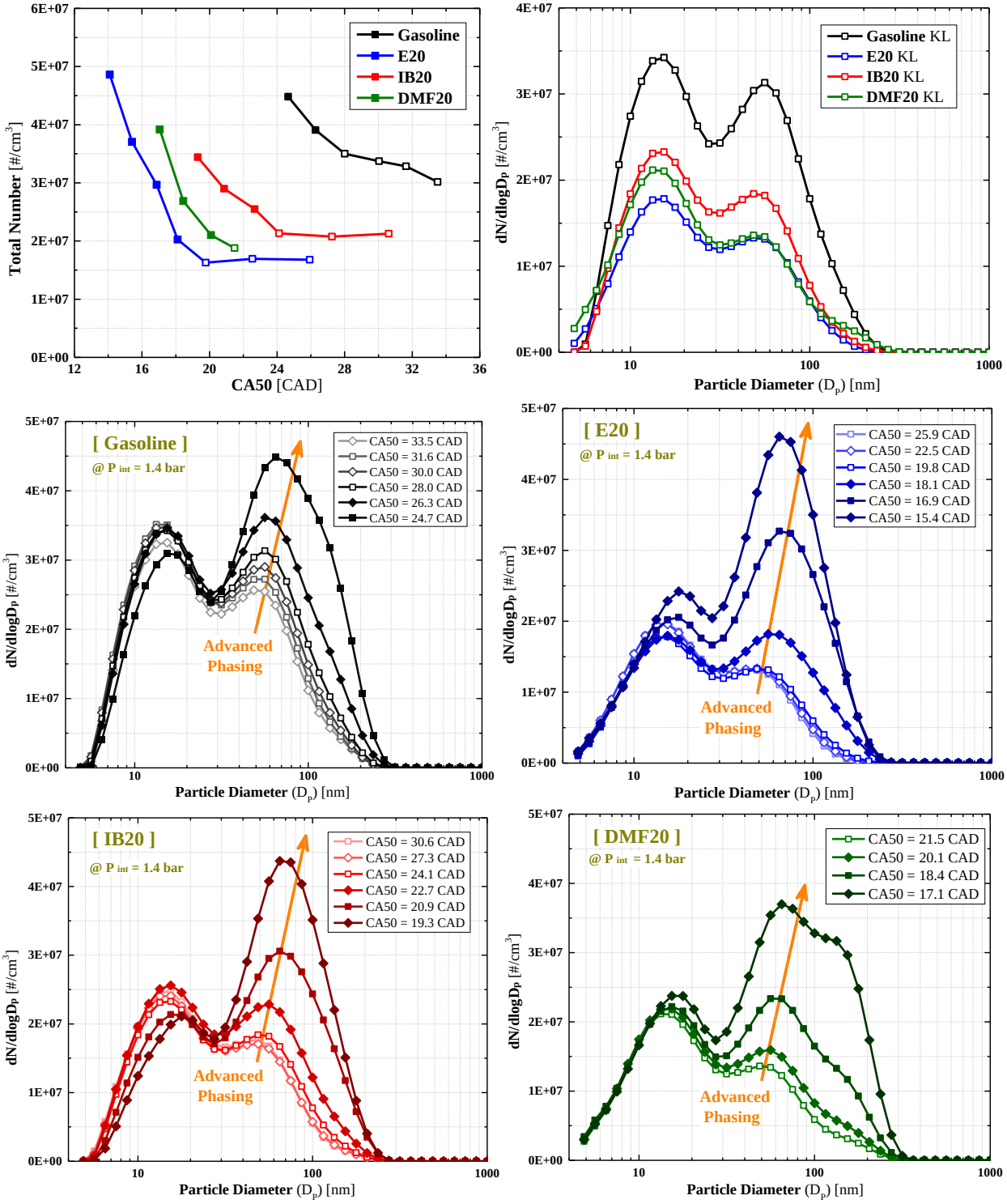

Figure 3.18 Total numbers as a function of combustion phasing (top left), and particulate matter size distributions for gasoline and three oxygenated fuels at knock limited point (top right) and various combustion phasing (the others) under 1.4 bar boosted condition. The filled symbols denote knocking conditions.

3.7 Conclusions and Summary

The effect of three parameters (fuel type, blend ratio, and boost level) on combustion characteristics and emissions has been experimentally explored using three oxygenated fuels (2,5-dimethylfuran, ethanol, and isobutanol) in blends with gasoline. The following conclusions are derived from the experimental results and analyses:

(1) Engine Combustion and Knock

- By adding 20 percent of the oxygenated fuels into gasoline, knock limits are extended based on combustion phasing (CA50), and the order of knock limit extension is Gasoline < Isobutanol < Dimethylfuran ≤ Ethanol.
- Thermal efficiency is improved due to extended knock limits, especially under boosted condition with oxygenated fuels. The order of thermal efficiency improvement is the same as the knock limit extension.
- Combustion stability is improved with oxygenated fuel blends by reasons of advanced spark timing compared to gasoline.
- Unburned hydrocarbon (THC) emissions are significantly increased with boosting, and this could be due to lower combustion quality, such as due to pool fires.
- Nitrogen oxides (NO_x) emissions are slightly increased with the fuel blends under boosted conditions.

(2) Particulate Matter Emissions

- Overall PM and PN trends for all fuel blends were similar regardless of the intake pressure.
- Particulate numbers are gradually decreased with oxygenated fuel blends

- The order of particulate number emissions for 20 percent volume blends is Gasoline >> IB20 > DMF20 > E20 under knock limited condition.
- Addition of 2,5-dimethylfuran generally yields a wide soot distribution range compared to the alcohol group fuels.

Chapter 4

Effect of Syngas (H_2/CO) on SI Engine Knock under Boosted EGR and Lean Conditions

This chapter was published as *Han, T., Lavoie, G., Wooldridge, M., and Boehman, A., "Effect of Syngas (H_2/CO) on SI Engine Knock under Boosted EGR and Lean Conditions", SAE International Journal of Engines 10(3):959-969, 2017.* [15] *(doi:* https://doi.org/10.4271/2017-01-0670*).*

4.1 Preface

This chapter is about the first and second strategic parameters about the gaseous fuel and the mixture dilution. Syngas, which is comprised of hydrogen and carbon monoxide, is selected for gaseous fuel study, and both EGR (Exhaust Gas Recirculation) dilution and lean combustion are compared in detail. The abstract for this chapter is attached below.

Syngas (synthesis gas) aided combustion from various fuel reforming strategies is of increasing interest in boosted lean burn SI engines due to its impact on dilution tolerance and knock resistance. Due to the interest in reformed fuels, more concrete understanding of how to leverage syngas supplementation under various lean conditions is essential to optimize engine

performance and derive the most benefit from the availability of syngas in the combustion process. While the impact of syngas supplementation on combustion stability has been studied adequately, detailed understanding of the impact of syngas on knocking is still limited. Hence, this study investigates the effect of syngas (H_2/CO) addition on knock tendency under boosted EGR (Exhaust Gas Recirculation) and air diluted conditions. Syngas amount is controlled on an energy basis from 0% to 15% to compare the difference between EGR and air dilution. At first, several knock quantification methods are compared, and a suitable knock index and guideline are selected. Knocking tendencies with respect to the frequency, combustion phasing, and burn duration are analyzed based on observed engine knock. Also, the thermal efficiency and emissions difference are discussed as well. The results show that with increasing the syngas supplementation ratio, knocking is strongly suppressed, and the effect is more beneficial with EGR dilution than with air dilution.

4.2 Introduction

Boosted EGR (Exhaust Gas Recirculation) or air diluted lean burn SI (Spark Ignition) engines offer considerable thermal efficiency benefits compared to naturally aspirated SI engines [5,6,42]. By increasing boost level, thermal efficiency increases due to the rise in volumetric efficiency and reductions in pumping and friction losses. Additionally, with higher dilution levels, efficiency is improved as a result of lowered peak cylinder temperature and increased specific heat ratio (γ) of the working fluid [7]. However, with increasing boost level and dilution ratio, combustion instability and engine knock are severely increased due to mixture and cylinder conditions.

To counteract the stability and knocking problems of SI combustion under boosted lean conditions, synthesis gas, which is generally comprised of hydrogen and carbon monoxide, supplemented combustion is one of the most promising methods in the advanced combustion field due to its impact on dilution tolerance and knock resistance [43–45]. Hydrogen has faster flame speed as well as higher octane number, so it helps to improve combustion stability and knock mitigation. Carbon monoxide also has relatively high-octane number, so it helps to reduce knocking tendency as well. In addition, it is known that when carbon monoxide oxidizes in the presence of water vapor, such as with EGR or water injection, the knocking tendency is decreased due to inhibition of auto-ignition because CO is less likely to react with oxygen as a result of the speed of the $CO + OH\cdot \rightarrow CO_2 + H\cdot$ reaction [25].

The most practical way to supply syngas to an engine is through fuel reformation. As a consequence, a variety of on-board fuel reforming systems have been developed such as in-cylinder reformation [46–49], plasmatron [50], solid oxide fuel cell [51], endothermic catalytic reformer using exhaust waste heat [52,53], etc. However, the reforming capacities and product compositions of these systems are diverse, so adequate guidelines and concrete understanding of how to leverage syngas addition are essential to optimize engine performance based on the flammability and knock limits of lean boosted condition.

Up to the present, many studies have considered the effect of hydrogen or syngas addition on combustion stability in boosted lean burn SI engines [54–56]. Studies on the effect of syngas on engine knock, however, are still limited, and the relation between the addition of syngas and knock mitigation varies depending on operating conditions. Shinagawa et al. [57] demonstrated that hydrogen addition decreases engine knocking tendency due to reduced burn duration and inhibition of fuel decomposition and radical production under rich conditions. Gerty

et al. [58] conducted a reformate fuel addition experiment under stoichiometric conditions, and results showed that 30% reformate addition decreases the required octane number by more than 10, and the change in required octane number is affected by fuel composition. Topinka et al. [45] described that 15% of fuel reformation increases by 10 the octane number of a fuel mixture under air diluted lean conditions mainly due to slowing the ignition of the end-gas. However, with increasing air-fuel ratio at constant fuel mass and intake air boosting, knock tendency increases as a result of peak pressure and temperature rise. In contrast, Chen et al. [59,60] asserted that knocking is increased with hydrogen addition under lean conditions. Therefore, a clear explanation of knock and lean combustion is essential.

The focus of this study is to examine and compare the knock trends between boosted EGR and air diluted lean conditions with varied syngas addition amount. First, multiple knock indices are applied, and the propensity of knock under EGR and lean conditions is discussed. In addition, combustion and knock are examined with respect to the combustion phasing, burn duration, efficiency, and emissions.

4.3 Experimental Setup

4.3.1 Engine and Fuel Specifications

All experimental data presented in this study were obtained with a boosted Ricardo Hydra single cylinder research engine at the W.E. Lay Automotive Laboratory at the University of Michigan. Two fuel injection systems were used in this experiment; one is port fuel injection for gasoline and the other one is a gaseous fuel fumigation system for syngas supplementation.

Both fuel systems have fuel flow meters to enable calculation of the air-fuel ratio independently from the exhaust lambda meter and the emission bench air-fuel ratio calculation.

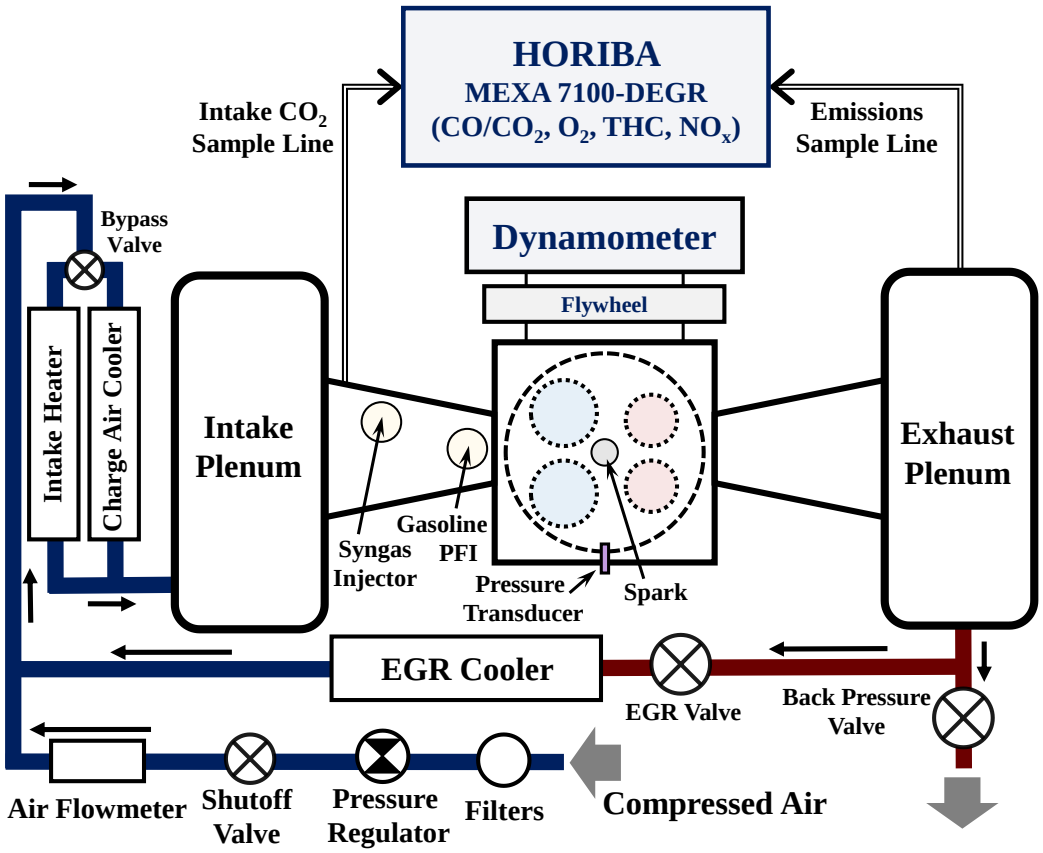

Figure 4.1 A schematic of boosted Hydra single cylinder research engine for Chapter 4

The engine includes an external cooled EGR loop controlled by back pressure and EGR valves. The intake air temperature is regulated with a by-pass heater and a cooler located in front of the intake plenum. The schematic in Figure 4.1 shows the air flow path and major components of this engine. The engine has a compression ratio of 10.5:1 and the cylinder pressure transducer (Kistler 6125A piezoelectric transducer) is 4mm in diameter and is located on the side of the head. The transducer is used for the in-cylinder pressure measurement, and the signal is

amplified (AVL IFEM) and recorded (AVL Indiset module) with a crank angle encoder signal (AVL 365C01).

Table 4.1 Boosted Hydra single cylinder research engine specifications and operating conditions for Chapter 4

Displaced volume	0.5 L
Bore / Stroke	86 mm / 86 mm
Compression Ratio	10.5 : 1
Intake Valve Timing	IVO: 362 bTDCign / IVC: 136 bTDCign
Exhaust Valve Timing	EVO: 138 aTDCign / EVC: 364 aTDCign
Head Design	Pent-roof / 4 Valve / Central Spark
Engine Speed	1500 rpm
Intake Air Temperature	26.5 ºC ± 0.75 ºC
Coolant Temperature	85 ºC
Oil Temperature	85 ºC

The gasoline fuel used in this study is HF0072 research grade gasoline provided by Haltermann Solutions Ltd. The research octane number is 91.1 and motor octane number is 83.0 (sensitivity of 8.1). Syngas composition is 43.97 mole% of hydrogen and 56.03 mole% of carbon monoxide using bottled gas provided by Airgas. The composition of syngas is motivated by the plasmatron reformate fraction [45].

Table 4.2 Fuel (Gasoline, Syngas) specifications

	Gasoline (HF0072)	**Syngas** [45,61]	
		H_2 (44%mol)	**CO** (56%mol)
Research Octane Number	91.1	> 130	106
Lower Heating Value [MJ/kg]	43.1287	120	10.1
Stoichiometric A/F ratio	14.52	34.2	2.47
Hydrogen / Carbon ratio (mole basis)	1.8805	-	-
Oxygen / Carbon ratio (mole basis)	0.0	-	1.0

4.3.2 Experimental Condition

To explore the effects of the synthesis gas supplementation on knocking under different dilution conditions, both stoichiometric and EGR / Air diluted experimental conditions were considered. Prior to the comparison experiments at diluted conditions, stoichiometric experiments were performed with gasoline only and with syngas supplement on a 10% energy basis to find MBT (Maximum Brake Torque) and knock limited points. The intake pressure was varied from 0.4 to 1.6 bar with 0.1 bar intervals and spark sweep was done in each intake pressure case. The engine speed for all experiments is controlled to 1500rpm.

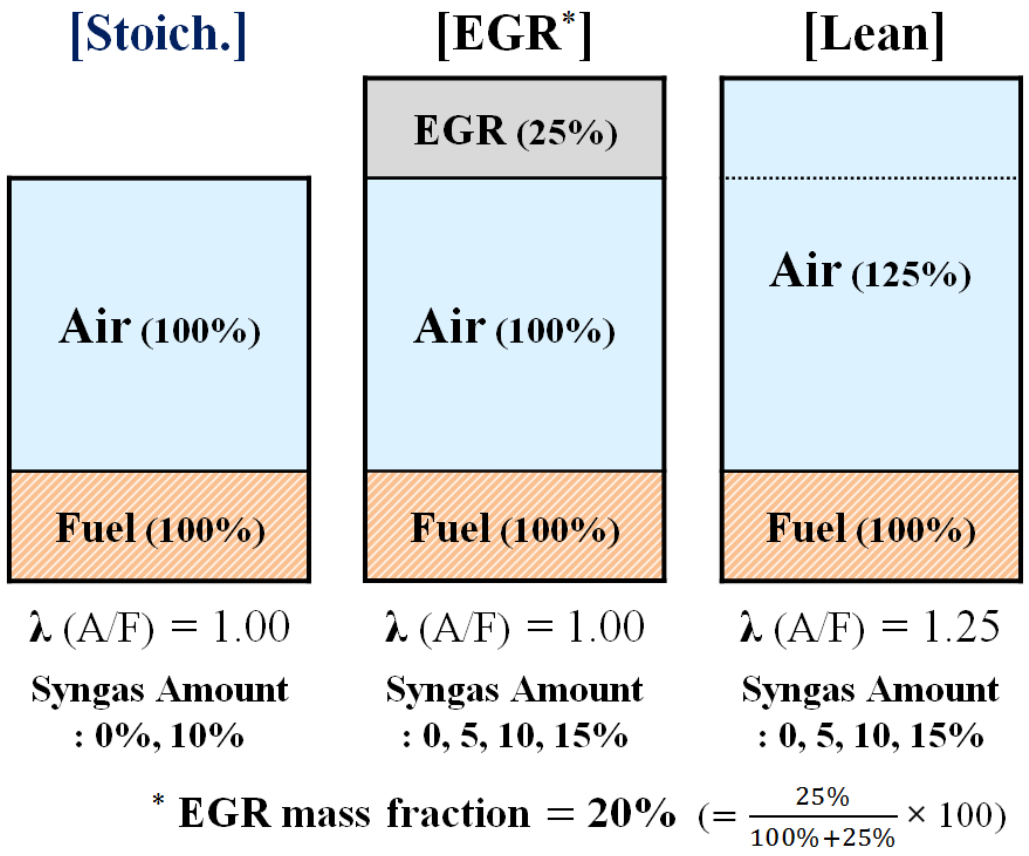

Figure 4.2 Air to fuel ratio and experimental conditions (Stoichiometry, EGR, and Lean conditions)

For the comparison experiments between EGR and lean conditions, the intake and exhaust pressures are fixed to 1.20 and 1.40 bar respectively, and a schematic of EGR and air diluted conditions is shown in Figure 4.2. Based on the stoichiometric air mass, additional 25% of EGR and air is added in cylinder. Thus, the EGR mass fraction of the charge is controlled to 20% with lambda value of 1.00, and the lambda value of the lean condition is 1.25. The intake and exhaust pressures are kept constant in all comparison tests to avoid the possibilities of internal EGR effects. The fuel energy is kept constant in all identical intake pressure conditions, and the syngas amount is controlled on an energy basis from 0% to 15% in 5% intervals.

Since the knock behavior is very sensitive to day-to-day changes in ambient conditions, each comparison experiment is performed on the same day, and identical sets are repeated for a total of three times on different days to test repeatability.

4.3.3 Air Fuel Ratio and EGR Measurement

To measure and control the air fuel ratio in real time, both the ETAS LA4 lambda meter and the Horiba MEXA 7100-DEGR emissions bench are used. Lambda meter has a faster response than the emissions bench, so all data recording is done after stabilization and matching of these two air-fuel ratio values. In addition, recorded fuel and air flow based calculations are analyzed as a post processing step to check the air-fuel ratio values again.

$$\boldsymbol{EGR_{ratio}}\ [\%] = \frac{CO_{2\ (intake)} - CO_{2\ (ambient)}}{CO_{2\ (exhaust)} - CO_{2\ (ambient)}} \times 100 \qquad (4.1)$$

EGR ratio is controlled based on the emissions bench measured value using Equation 4.1.

4.4 Knock Propensity and Frequency

4.4.1 Cylinder Pressure and Knock Trend

To directly compare the difference of pressure traces and knock trends among varied syngas ratios for the two dilution conditions, cylinder pressures and filtered pressures are plotted at the same spark timing conditions. Figure 4.3 shows the normal and filtered pressure traces for the two dilution conditions. In each dilution case, the spark timing was fixed while the syngas

amount varied. The spark timings for EGR dilution and for air dilution were different. Selected cylinder pressure traces are the closest traces to each average value of cylinder pressure, onset of knock, and KI 20 among the recorded 200 cycles.

As shown in the pressure traces presented in the upper panels of Figure 4.3, combustion is advanced with increased syngas amount due to the faster flame speed of the hydrogen in the syngas. The lower panels in Figure 4.3 show the filtered knocking cycles using a FFT high pass filter with a 3.5 kHz cut-off frequency. The oscillations of all cases look similar, but the onset of knock is advanced with increasing amounts of syngas. This trend agrees with similar knocking cycle comparisons for neat gasoline and for neat hydrogen conducted by Szwaja et al [62].

4.4.2 Power Spectral Density Analysis

The PSD analysis is a tool for observing peak frequency ranges and signal intensity regardless of which frequency is dominant. Figure 4.4 shows the PSD analysis for various syngas amounts for EGR dilution (upper panel) and air dilution (lower panel). The dominant frequencies denoted by R1 through R5 in Figure 4.4 are similar for all of the syngas cases and for both EGR and air dilution. The dominant frequencies are unaffected by syngas amount or method of dilution.

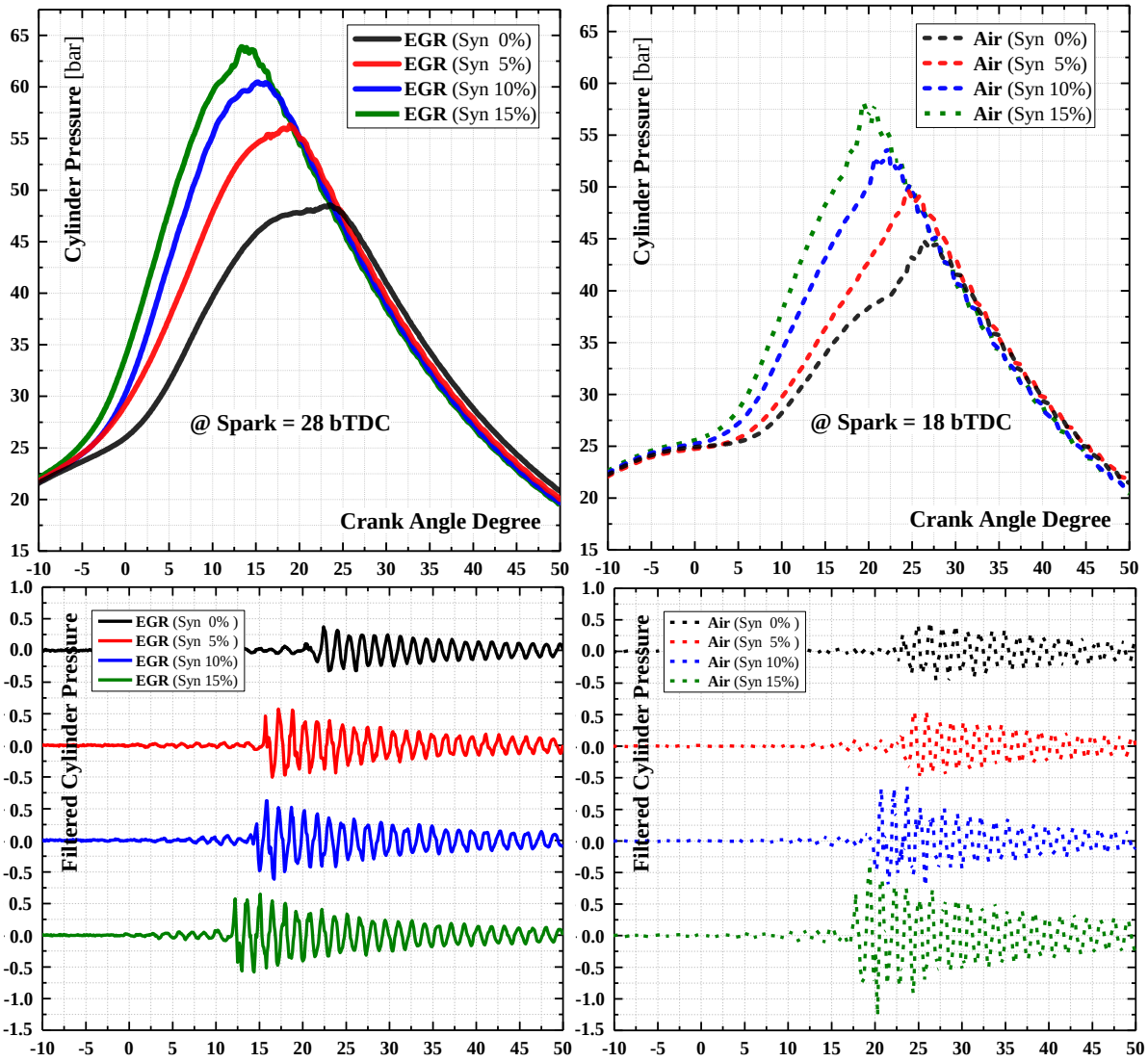

Figure 4.3 Pressure traces and rectified pressure signals; EGR dilution at 28 bTDC spark, P_{int} = 1.2bar (left) and Air dilution at 18 bTDC spark, P_{int} = 1.2bar (right)

Figure 4.3 suggests that for fixed spark timing, syngas addition increases knocking intensity. In contrast, Figure 4.4 indicates that at the same CA50 value, syngas addition decreases knock intensity.

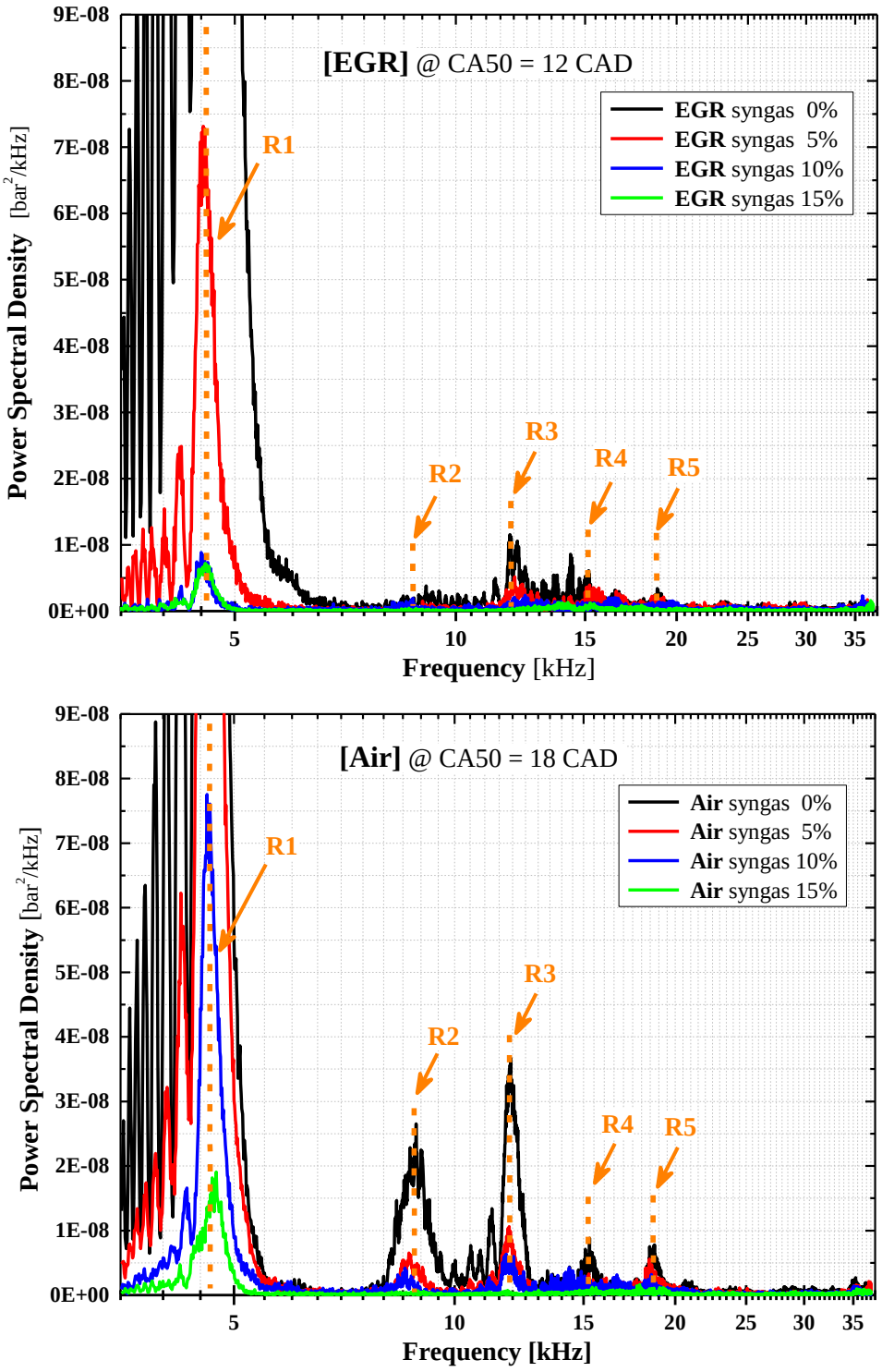

Figure 4.4 PSD analysis results of same CA50 points; EGR at 12 CAD, P_{int} = 1.2 bar (top), Air at 18 CAD, P_{int} = 1.2 bar (bottom)

4.5 Engine Combustion Results

4.5.1 Combustion Phasing and Knock

A spark timing sweep at 1 crank angle degree interval is performed to find the knock limit for each dilution condition while varying the amount of syngas. Figure 4.5 indicates the spark timing versus combustion phasing (CA50), and the audible knock points are indicated by the filled symbols in the figure. CA50 is clearly decreasing as spark timing advances, and it is clear that by increasing the syngas ratio, the knock limit approaches MBT (between 7 and 10 crank angle degrees) timing.

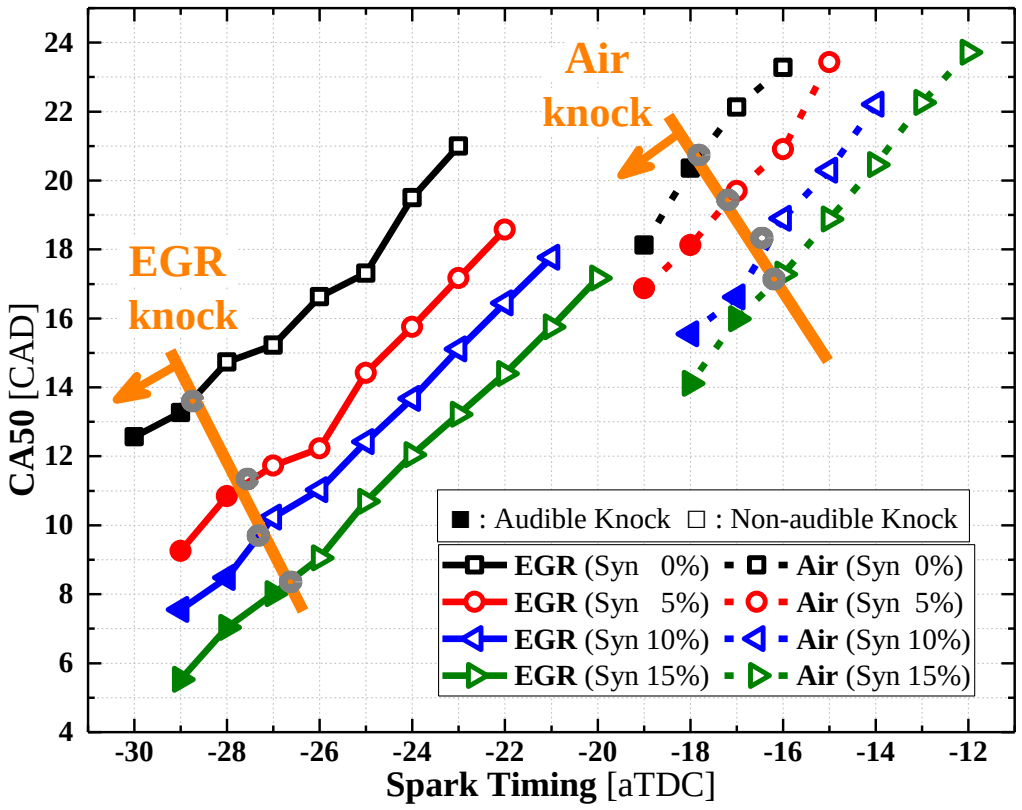

Figure 4.5 Relation between spark timing and average CA50. The filled symbols denote audible knock.

For fixed spark timing, more knock occurs with increased syngas energy ratio, for instance, the spark timing regions of -26 ~ -28 aTDC for EGR and -16 ~ -17 aTDC for air dilution. This trend is seen more clearly in Figure 4.3, which presents pressure trace and filtered knock graphs. However, for fixed CA50, knocking decreases with increased syngas addition. The audible knock method, however, is only able to detect general knock occurrence, so the more accurate knock index, KI 20, is applied to the experimental data.

Figure 4.6 shows the knock intensity (natural log of KI 20 value) versus CA50 along with regression lines. The top and middle graphs show scatter plots of all knocking cycles under air dilution and EGR dilution, respectively. The knocking guideline is set to -5.298 (= ln (0.005)) based on the guideline of KI 20 (0.005 bar^2), and linear regression lines are extracted from the scatter points for each syngas amount. The bottom graph indicates the combined regression lines of both diluting conditions with error bars indicating the standard deviation. For advancing CA50, knock intensity linearly increases and the slope is similar for all cases.

Using the intersection of the regression lines and KI 20 knock guideline, the CA50 values at knock onset can be extracted (grey circles in Figure 4.5, 4.6, and 4.7). The CA50 values of knock onset are 13.4, 11.4, 9.6, and 8.4 at 0%, 5%, 10%, and 15% of syngas addition, respectively under EGR condition, and 20.7, 19.5, 18.3, and 17.2 at 0%, 5%, 10%, and 15% of syngas addition, respectively, under air dilution. From these CA50 numbers, it is more clear that syngas addition is beneficial to knock mitigation based on combustion phasing.

In case of knock occurrence, for the comparison between EGR dilution and air dilution, the effect of syngas addition is represented by the CA50 of knock onset. For EGR dilution, the difference between syngas addition levels of 0% and 15% is 5.0 crank angle degrees, and for air dilution the difference is 3.5 crank angle degrees. Therefore, EGR dilution is almost 1.5 times

more effective than air dilution for knock mitigation with syngas based on CA50 under boosted conditions.

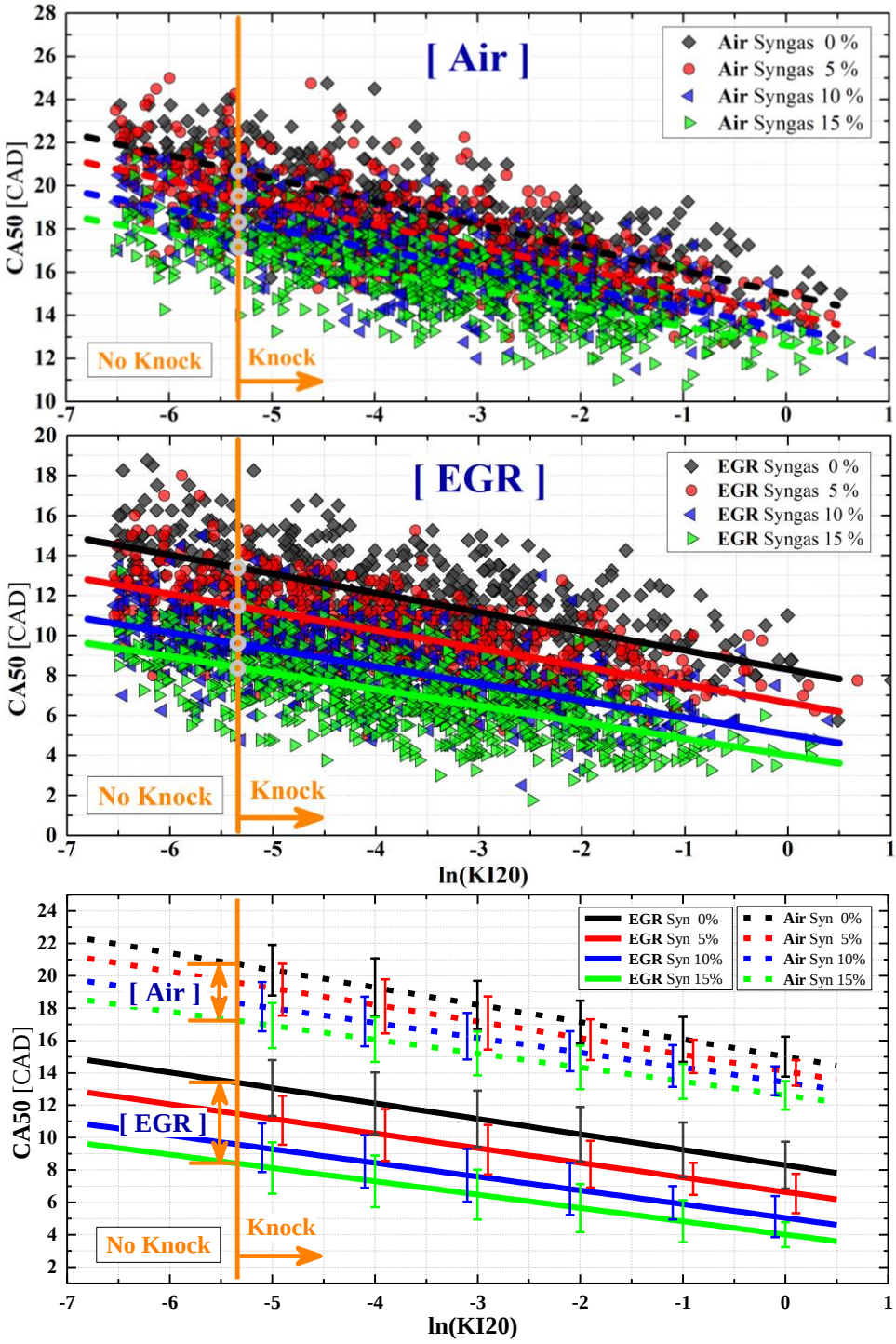

Figure 4.6 Knock intensity (natural log of KI 20) and CA50 of knock cycles. (Air / EGR / Combined regression)

Figure 4.7 indicates another criterion of knock, which is knock cycle percentage. This criterion is obtained by counting the knock cycle numbers over 200 cycles at the same test condition, and the knock guideline is set to 0.005 bar^2 of KI 20, as well. The knock cycle percentage proportionally increases with overall knock intensity. Based on the knock onset conditions identified from Figure 4.6, knock limited cycle percentage range is higher than nearly 65% and which is consistent with other engine studies [63].

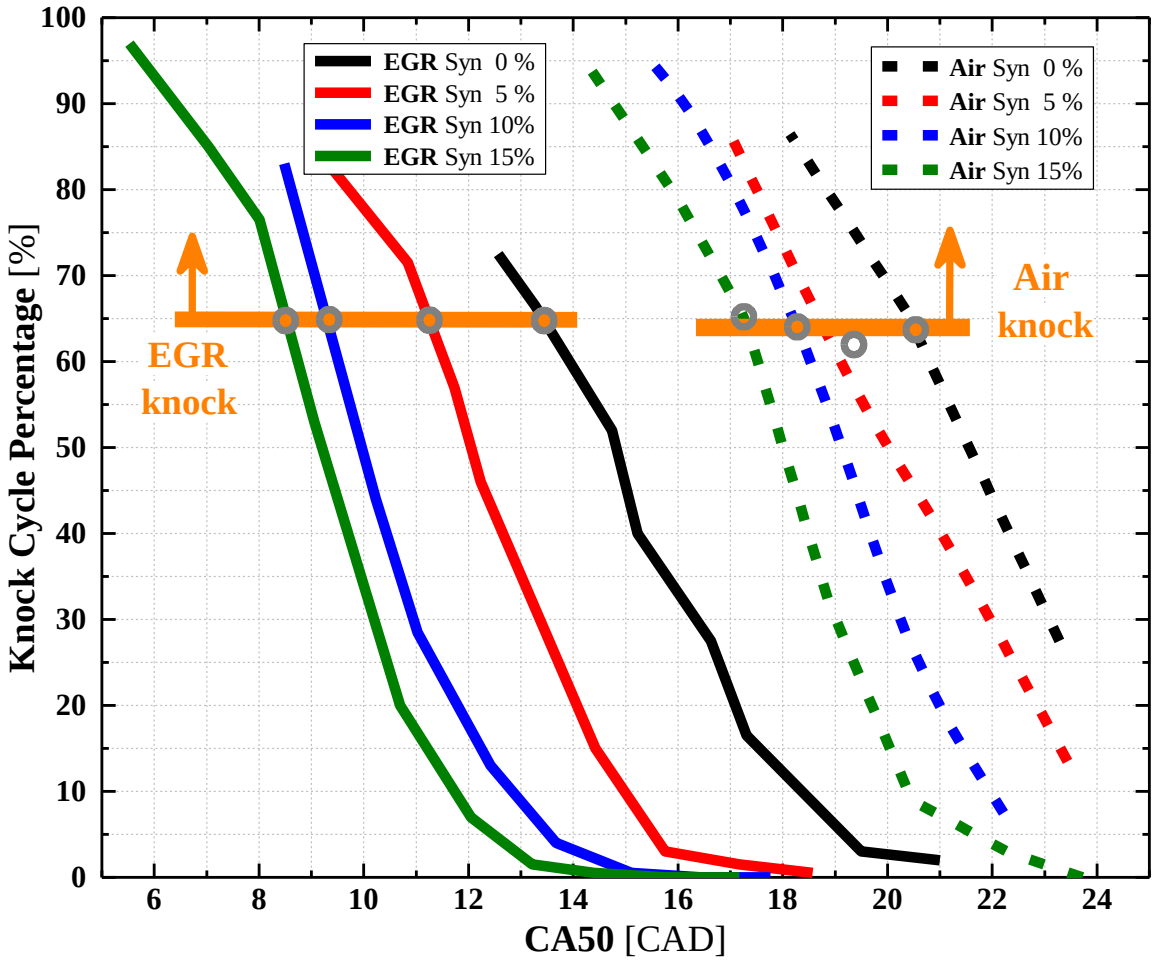

Figure 4.7 Relation between average CA50 and knocking cycle percentage

4.5.2 Burn Duration and Knock

Engine knock is generally affected by both in-cylinder physical factors (in-cylinder pressure, temperature, mixture conditions and so on) and fuel chemistry factors (properties of fuels).

First, the burn duration is calculated to explore the impact of the fuel factors (syngas addition) in both dilution cases. Figure 4.8 presents the burn duration (CA1090) on a spark timing basis. By increasing the ratio of syngas supplementation, burn duration is substantially shortened for the same spark timing. As much as the shortened burn duration time, the delay time before end-gas auto ignition is improved as well. Consequently, the knocking tendency is able to be decreased due to the effects of adding syngas to the fuel, but from the perspective of the physical factors, the in-cylinder condition becomes more vulnerable to knocking because of the increased peak pressure and temperature, using the same spark timing. The pressure traces in Figure 4.3 show this trend well. The knocking tendency result can be identified through comparison of data along a vertical line (same spark timing) in Figure 4.8. For example, more knock occurs with syngas supplementation in the case of -28 bTDC spark timing with EGR. This result suggests that the physical factor is more dominant with fixed spark timing, and this tendency is the same for the air dilution condition as well as EGR dilution.

Although the knocking tendency is increased with fixed spark timing due to dominant physical factors, the physical factors help the combustion phasing. Therefore, as discussed in the section on combustion phasing, knock on the basis of CA50 is decreased. Figure 4.9 shows the burn duration on the basis of combustion phasing. In comparing with the trends on the spark timing basis, the burn duration trend is similar between 0 to 15 percent syngas addition. This

means that combustion can be readily controlled regardless of the physical factors associated with syngas addition.

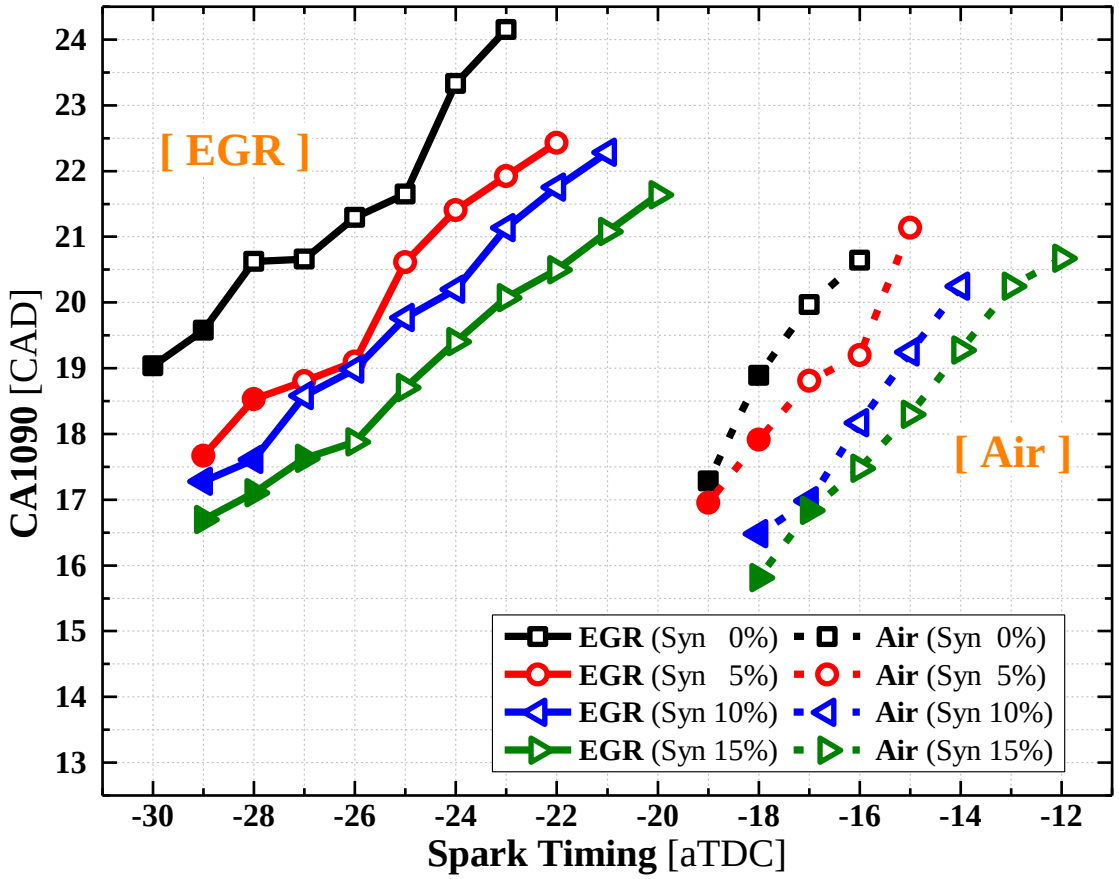

Figure 4.8 Relation between spark timing and average burn duration (CA1090)

In addition, burn duration provides another metric for comparison between the impacts of EGR dilution and of air dilution. As shown in Figure 4.9, the burn duration with air dilution is much faster than with EGR dilution. Nevertheless, the knock limit with air dilution is more severe than with EGR dilution. One can deduce that the severe knock with air dilution is caused by other physical factors such as the thermal properties of the cylinder charge, e.g. changes in the pressure and temperature due to changes in the ratio of specific heats.

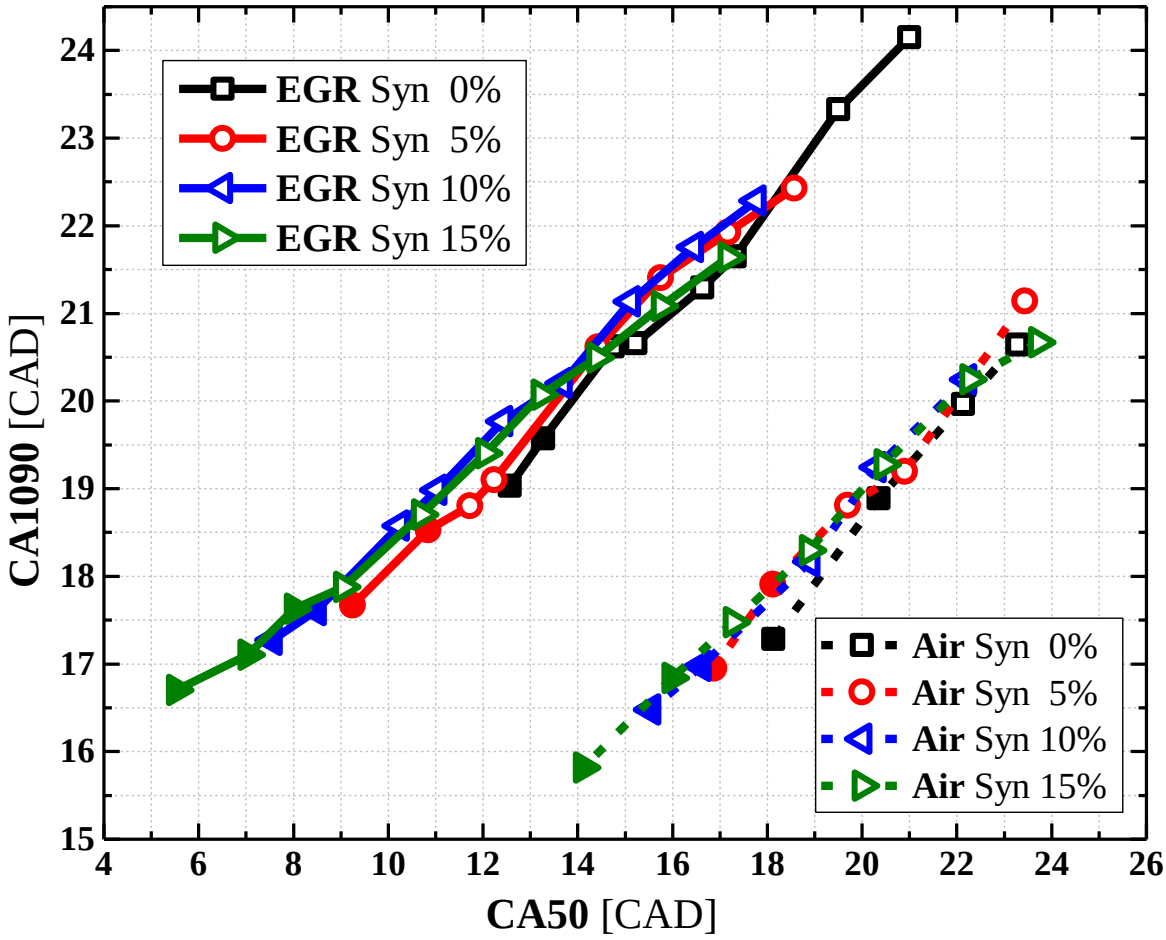

Figure 4.9 Average CA50 versus average burn duration (CA1090)

One more reason for the knock vulnerability with air dilution relates to the ignition delay difference caused by the fuel to charge equivalence ratio and oxygen mole fraction of the mixture. Equation 4.2 presents an ignition delay correlation for iso-octane and syngas [64,65]. All five coefficients are positive numbers and summarized in Table 4.3. For a simple comparison, considering the $\emptyset$ and $x(O_2)$ terms, the difference between lean air dilution and EGR dilution for this experiment can be represented by using values of $\emptyset = 1.00$ and $x(O_2) = 0.8$ for EGR dilution and 0.80 and 1.0 for lean air dilution, respectively. C_3 is less than 1 and C_4 is

greater than 1, so the ignition delay time with EGR dilution should be always longer than with lean air dilution.

$$\boldsymbol{\tau_{id}}\ [\text{ms}] = C_1 \times P^{-C_2} \times \emptyset^{-C_3} \times \boldsymbol{x_{O_2}}^{-C_4} \times exp\left(\frac{C_5}{T}\right) = \boldsymbol{f}(\emptyset, \boldsymbol{x_{O_2}}) \quad (4.2)$$

Table 4.3 Coefficients of ignition delay in Equation 4.2

	C_1	C_2	C_3	C_4	C_5
Iso-octane [64]	1.3 x 10^{-4}	1.05	0.77	1.41	33700/R
Syngas [65]	3.7 x 10^{-6}	0.5	0.4	5.4	12500/R

From the perspective of burn duration and ignition delay, EGR dilution shows more benefits than air dilution with regard to knock limited combustion.

4.5.3 Thermal Efficiency and Combustion Stability

Regardless of the knock limit, the overall thermal efficiency is higher with air dilution due to the higher ratio of specific heats than with EGR dilution. This trend is seen in Figure 4.10 over the 14 crank angle degrees of the CA50 overlap range. Ivanič et al. [66] also showed the same trend under low load condition at 3.5 bar of IMEPn (net Indicated Mean Effective Pressure). However, under knock limited boosted conditions, the thermal efficiency is higher with EGR dilution due to the extended knock limit. The range of IMEPg (gross Indicated Mean

Effective Pressure) in this study is 10.0 bar ± 0.1 bar with the same energy input and different combustion phasing. As shown in the upper graph of Figure 4.11, the overall gross indicated thermal efficiency difference between EGR dilution and air dilution is 1.0 % on average at each level of syngas addition.

The thermal efficiency benefit of varied syngas addition is higher than the dilution benefit in the 0 to 15% syngas addition range. As shown in the upper graph of Figure 4.11, the gross indicated thermal efficiency consistently increases with increasing syngas amount, and the difference is 1.84% and 1.90% under EGR dilution and air dilution conditions, respectively. In addition, the thermal efficiency benefit compared to the baseline of stoichiometric condition is 1.92% and 1.09% (gasoline only), and 2.97% and 1.78% (10% syngas) under EGR dilution and air dilution conditions, respectively.

The effect of syngas addition on combustion stability is noticeably higher in both dilution cases. The lower graph of Figure 4.11 shows the coefficient of variance of IMEPg for EGR and air dilution. Without syngas addition, the combustion instability with EGR dilution is much higher than with air dilution, but with increasing syngas addition, the stability is improved for EGR dilution. For 15% syngas addition, the CoV of IMEPg with EGR dilution follows the same trend as CoV of IMEPg with air dilution. Thus, the benefits of syngas addition on combustion stability are more pronounced with EGR dilution than with air dilution.

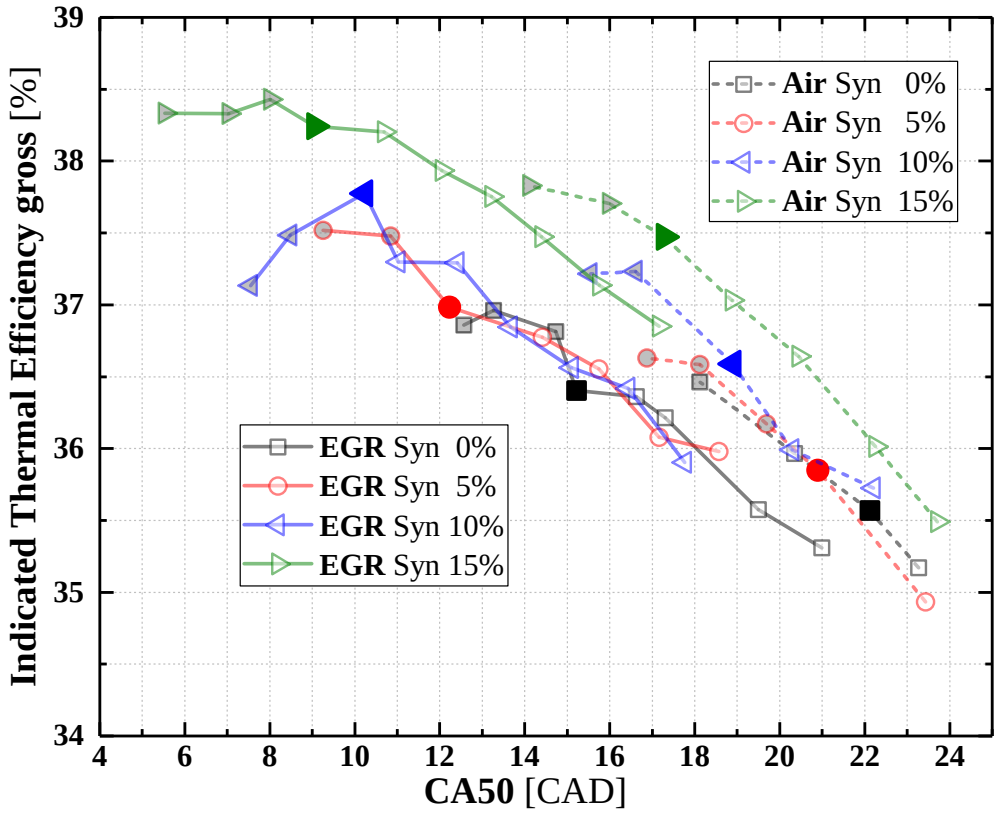

Figure 4.10 Combustion phasing (CA50) basis Gross Indicated Thermal Efficiency. (Emphasized symbols are MBT or knock limited thermal efficiency, same as upper figure of figure 4.11)

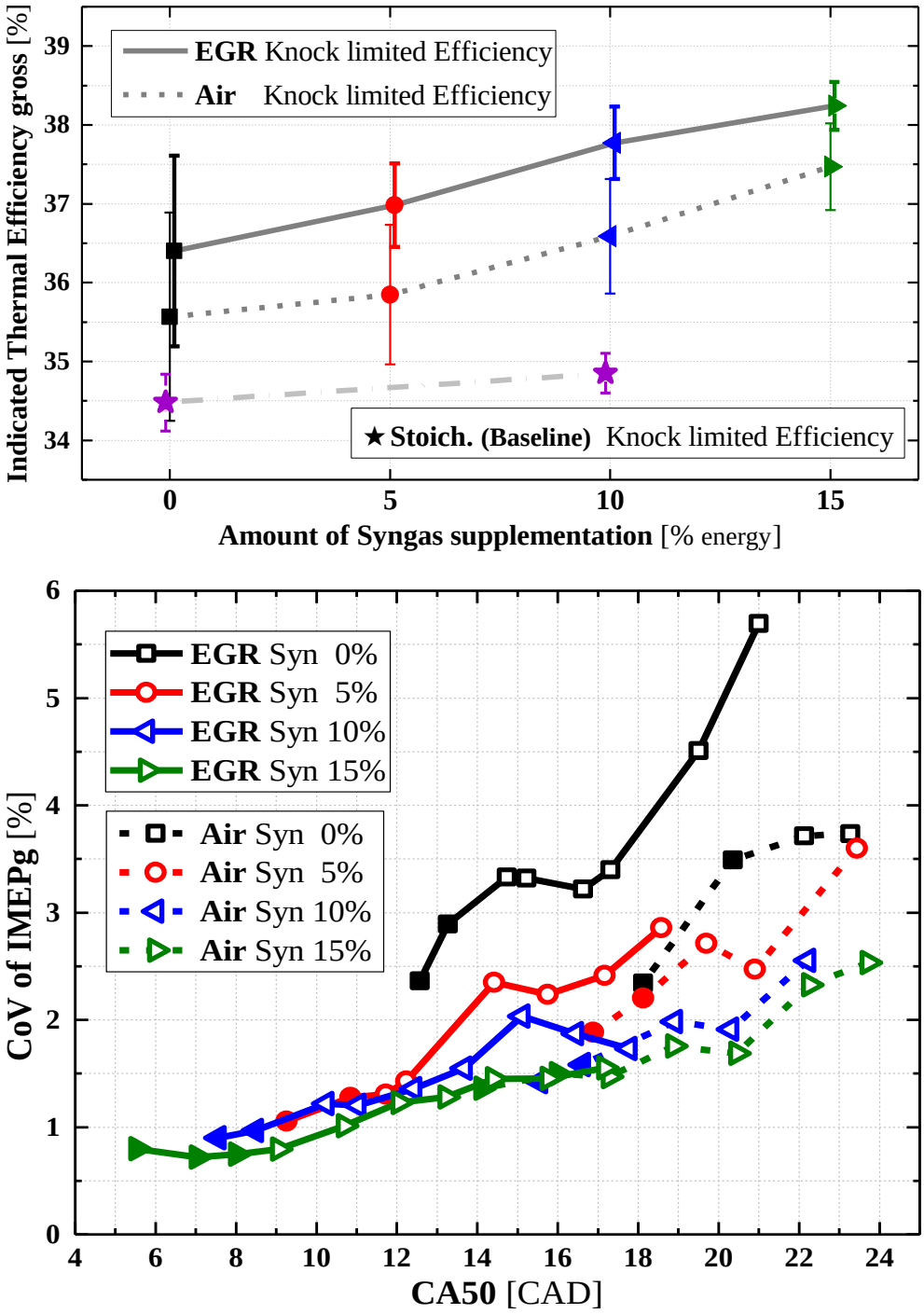

Figure 4.11 Gross Indicated Thermal Efficiency (ITEg) of knock limited points (upper) and Coefficient of Variance (CoV) of IMEPg (lower)

4.5.4 Emissions

The overall emissions including total hydrocarbons are not much different regardless of the syngas amount or the type of dilution, except for emissions of nitrogen oxides and carbon monoxide. Figures 4.12 and 4.13 show the NO_x and CO emissions, respectively for the EGR dilution and air dilution cases. The emissions are measured 5 times at each condition at 5 second intervals, and the error bars indicate the standard deviation. The NO_x reduction was significant with EGR dilution. With increasing the syngas amount, the nitric oxides increase slightly under air dilution. The NO_x emission is well known to vary with the peak cylinder temperature linearly, so this trend also agrees with the discussion regarding lengthened ignition delay with reduced peak temperature under EGR condition.

On the other hand, carbon monoxide emissions showed the opposite trends. The CO emissions for EGR dilution are higher than for air dilution, which agrees with the typical trend of carbon monoxide emissions with lambda (the lambda value of EGR is 1.00 and air dilution is 1.25). Relatively higher error bar for carbon monoxide with EGR dilution is caused by the emission bench system variation due to measurement of high levels of CO. Nonetheless, the CO trend of EGR is considered to be consistent and reasonable.

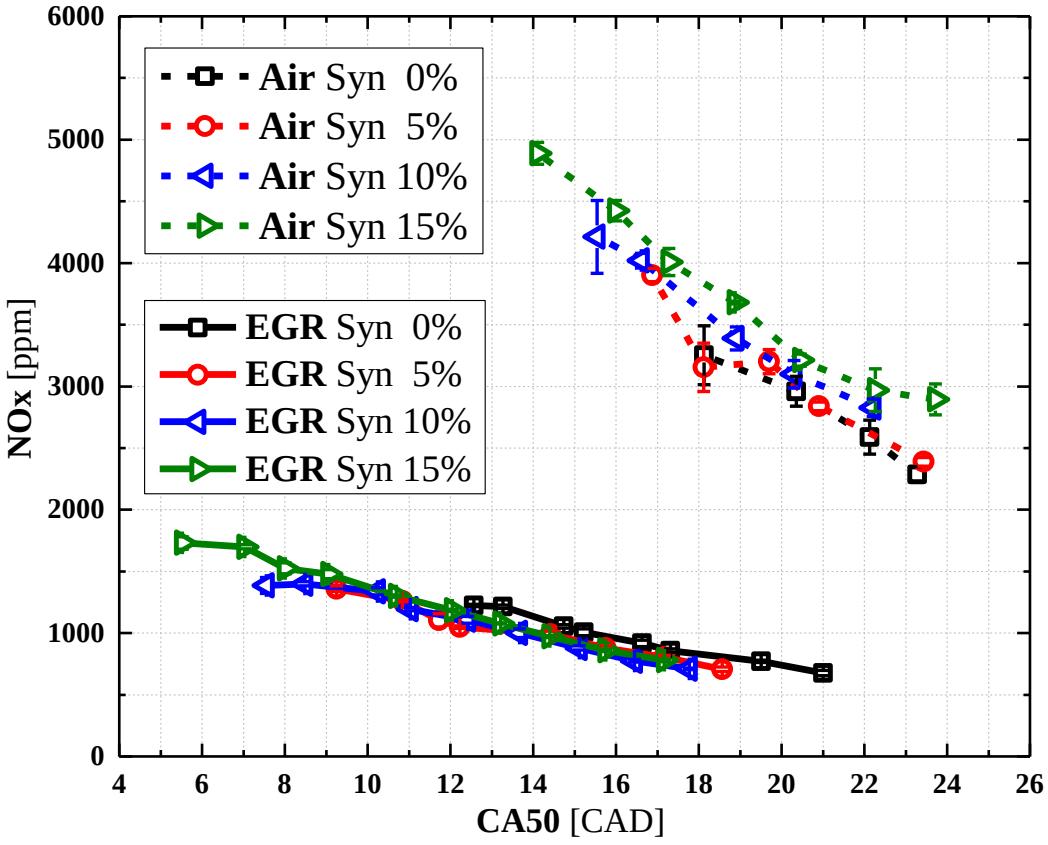

Figure 4.12 CA50 basis NO_x emissions. (EGR: full line, Air: dashed line)

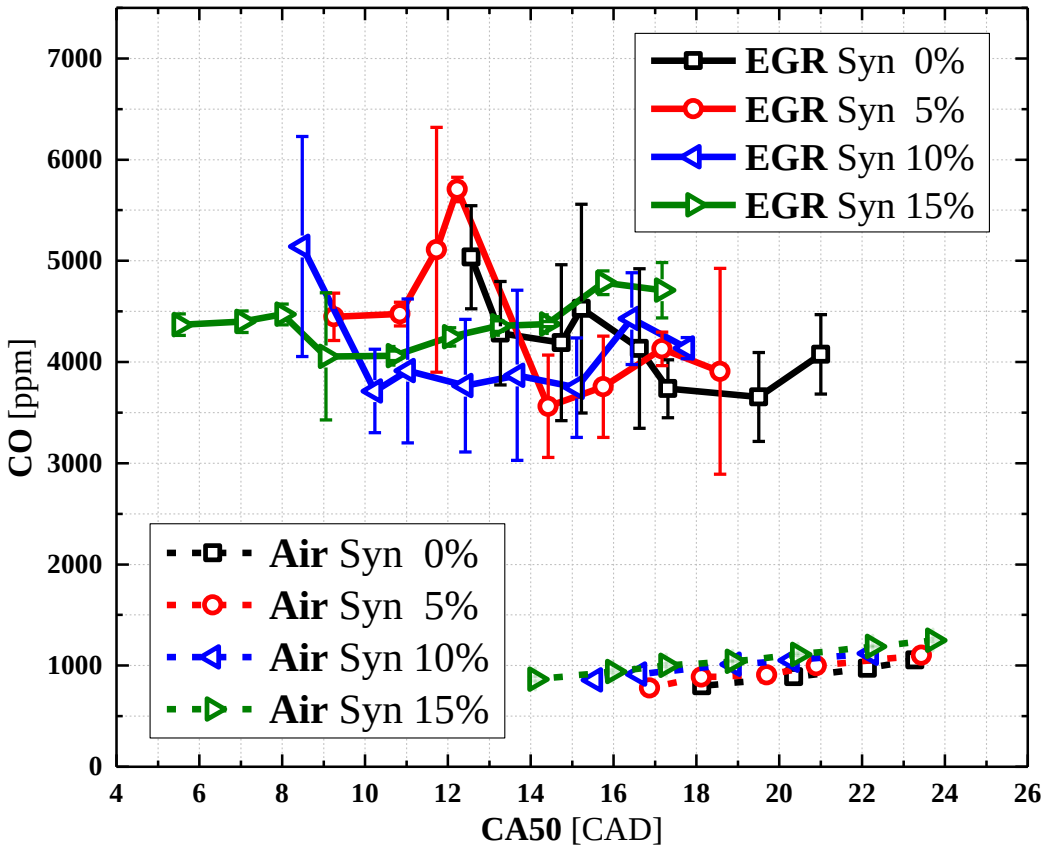

Figure 4.13 CA50 basis CO emissions. (EGR: full line, Air: dashed line)

4.6 Conclusions and Summary

Experiments with syngas supplementation under EGR dilution and air dilution demonstrated that syngas addition efficiently mitigates engine knock under both boosted and diluted conditions. In addition, supplementing syngas is more beneficial under EGR dilution than

under air dilution, from the perspective of not only knock mitigation but also thermal efficiency and emissions of nitrogen oxides.

Based on the experimental results and analyses, the following conclusions are drawn:

- The two most commonly used knock indices (peak basis '$KI_{peak\ to\ peak}$' and energy basis 'KI 20') show strong correlation with each other, and KI 20 is proportional to the square of KI peak to peak regardless of dilution type (EGR or air).
- KI 20 is selected as the best metric for investigating knock due to its statistical significance and lower noise vulnerability. Moreover, the knock guideline was chosen to be 0.005 bar^2 of KI 20.
- The frequency of knock was constant whether adding syngas or diluting with EGR or air. It is inferred that the frequency is not directly related to air-fuel mixture conditions but is influenced by other factors such as cylinder and engine block geometry.
- For a given spark timing, engine knock is increased with increasing syngas amount in both EGR dilution and air dilution cases.
- When combustion phasing is fixed, engine knock is decreased with increased amount of syngas supplementation in both EGR dilution and air dilution cases. And, the knock mitigation effect of syngas is stronger under EGR dilution than air dilution, based on combustion phasing.
- In both dilution cases, burn durations on a combustion phasing basis for varied syngas amounts are not noticeably different, and estimated end-gas ignition delay difference is higher under EGR dilution. One can infer that the end-gas ignition delay is more the dominant factor for knock mitigation than burn duration.

- EGR dilution is more beneficial than air dilution with regard to improving thermal efficiency, due to more optimal combustion phasing with extended knock limit.
- The impact of syngas addition on combustion stability is more pronounced for EGR dilution than for air dilution under boosted conditions.
- The differences in engine out emissions between EGR dilution and air dilution are not significant except for carbon monoxide and NO_x.
- NO_x emissions are significantly reduced with EGR dilution, but the carbon monoxide emissions are higher under EGR rather than air dilution.

Chapter 5

Dual Fuel Injection (DI + PFI) for Knock and EGR Dilution Limit Extension in a Boosted SI Engine

This chapter was published as *Han, T., Lavoie, G., Wooldridge, M., and Boehman, A., "Dual Fuel Injection (DI + PFI) for Knock and EGR Dilution Limit Extension in a Boosted SI Engine", SAE Technical Paper 2018-01-1735, 2018.* [67] *(doi: https://doi.org/10.4271/2018-01-1735)*

5.1 Preface

This chapter is about the second and third strategic parameter about the EGR (Exhaust Gas Recirculation) and dual injection strategy. Gasoline and ethanol fuels are used to figure out the effect of dual fuel injection strategy and EGR dilution on engine combustion and emissions. The abstract for this chapter is attached below.

Combined direct and port fuel injection (i.e., dual injection) in spark ignition engines is of increasing interest due to the advantages for fuel flexibility and the individual merits of each system for improving engine performance and reducing engine-out emissions. Greater understanding of the impact of dual injection will enable deriving the maximum benefit from the two injection systems. This study investigates the effects of dual injection on combustion,

especially knock propensity and tolerance to exhaust gas recirculation (EGR) dilution at different levels of EGR. A baseline for comparison with dual injection results was made using direct injection fueling only. A splash blended E20 fuel was used for the direct injection only tests. For the dual injection tests, gasoline, representing 80% by volume of the total fuel, was injected using the direct injector, and ethanol, representing 20% by volume of the total fuel, was injected using the port fuel injector. EGR mass fraction was varied from 0% to 21%, under boosted intake air pressure of 1.25 bar for both injection strategies. The results showed dual injection was beneficial to shorten the burn duration and improve combustion stability. Dual injection was more sensitive to knock than direct injection primarily due to increased unburned gas temperature. The overall thermal efficiency for the two injection types was comparable. The particulate matter emissions from dual injection showed slightly lower values, and the gaseous emissions showed lower total hydrocarbons and similar nitrogen oxides compared with only using direct injection of E20.

5.2 Introduction

Engine efficiency and emissions targets are ever increasing in pursuit of rigorous fuel economy standards, emission regulations, and customer demand for higher mileage vehicles. Previous work has shown one of the most promising strategies to improve thermal efficiency and reduce engine-out emissions of SI engines is using a downsized boosted engine with fuel/air mixture dilution [5,42]. By increasing boost level, thermal efficiency increases due to the rise in volumetric efficiency and reduction of pumping loss. Also, with increasing dilution ratio, efficiency is improved due to the lower peak cylinder temperature and increased specific heat

ratio (γ) of the working fluid. However, with increasing boost and dilution levels, engine knock and combustion instability are severely increased due to in-cylinder mixture conditions [7].

There are several ways to mitigate spark ignition (SI) engine knocking. One of the general methods is to use high octane oxygenated fuels such as ethanol and using direct injection. Such fuels can have longer ignition delay and higher heat of vaporization than gasoline, so in-cylinder temperatures can be significantly reduced with alcohol fuels. Also, direct injection can maximize the benefits of the oxygenated fuels by enhanced charge cooling and volumetric efficiency, especially with a stratified injection strategy. Globally stoichiometric stratified direct injection, however, has several drawbacks such as complicated load dependent injection control, higher particulate matter emissions caused by locally fuel rich zones, and lower combustion efficiency and stability [68,69]. In addition, the combustion stability is usually worse with exhaust gas recirculation (EGR) [70].

Dual injection, which separates the fuels into two injection systems; port fuel injection (PFI) for homogeneous charge formation and direct injection (DI) for stratified charge formation, has been proposed to counteract the problems of knock and combustion instability associated with stratified direct injection. More specifically, this study focuses on dual fuel injection which uses gasoline in the stratified direct injection event and high-octane oxygenated fuels in the homogeneous port fuel injection event. This injection strategy has been developed to make the end-gas less likely to auto-ignite.

To date, several experimental studies have been conducted with DI and PFI dual injection in SI engines. Zhu et al. [71,72] conducted studies of dual injection using gasoline and E85 in a single cylinder engine. They compared combustion characteristics for three injection modes: gasoline for both PFI and DI; gasoline PFI and E85 DI; and E85 PFI and gasoline DI with

varying fueling ratios for the two injectors under light load and wide-open throttle conditions. The results showed only a minor increase in efficiency for the gasoline PFI and ethanol DI case under the light load condition, and combustion stability was higher when gasoline was used in DI than when ethanol was. Daniel et al. and Wu et al. [73–76] expanded the oxygenated fuels to consider methanol and 2,5-dimethylfuran using a dual injection system and reported an improvement in thermal efficiency and emissions under different fuel blending ratios under throttled, low- and medium-load conditions with gasoline in PFI and oxygenated fuels in DI. Zhuang et al. [77–80] conducted dual injection studies under three medium load conditions using gasoline in PFI and ethanol in DI with varied direct injection timing and ethanol ratio, and they observed that late direct injection timing reduces thermal efficiency and knock limit, possibly due to lower mixing rate caused by stratified late injection. Cho et al. and Kim et al. [81,82] investigated a PFI injection strategy with ethanol in a gasoline direct injection engine, and showed improved thermal efficiency with ethanol PFI regardless of compression ratio. Liu et al. and Wang et al. [83–85] also compared gasoline DI with alcohol PFI, as well as, alcohol DI with gasoline PFI. The results showed better anti knock in the alcohol DI case. Catapano et al. [86,87] studied gasoline PFI and ethanol DI experiments under higher engine speed, and concluded that the effect of ethanol on particulate matter reduction is improved under higher speed condition.

The previous studies are limited to a small range of load conditions, and there are few results relating to the effects of dual injection strategies on knocking phenomena. Also, combustion stability at EGR dilute conditions has not been studied in depth for dual injection. Consequently, the objective of this study is to experimentally verify the effects of dual injection on combustion performance including knock propensity, thermal efficiency, and EGR dilution

tolerance at boosted EGR dilute conditions. The impact of dual injection on particulate matter and gaseous emissions is also explored.

5.3 Experimental Setup

5.3.1 Engine and Fuel Specifications

The experimental study was conducted using a boosted Ricardo Hydra single cylinder research engine. The pent-roof cylinder head has a centrally mounted direct injector (Bosch HDEV4), side mounted spark, and four valves. Two fuel injection systems were used in the experiments. The direct injector is a piezoelectric injector and produces a hollow cone spray, and the other is a conventional port fuel injector. Each fuel system has a fuel flow meter to calculate the air-fuel equivalence ratio in conjunction with an air mass flow meter (Fox Instruments FT2). The air-fuel equivalence ratio was confirmed by the measured values from an emissions bench (Horiba MEXA-7100DEGR) and a lambda meter (ETAS LA4) with a lambda sensor (Bosch LSU 4.9) in the exhaust runner.

Figure 5.1 shows a schematic of the boosted Hydra single cylinder research engine and supporting facilities. Intake air is compressed and filtered, and the pressure is regulated using a pneumatic valve after air filters to maintain the target intake pressure at the intake plenum. The engine intake air system includes a by-pass heater and cooler located upstream of the intake plenum to maintain constant intake air temperature. The engine includes a cooled EGR loop, and the EGR ratio is controlled by back pressure and an EGR valve. Engine oil and coolant are

conditioned by external systems to maintain constant temperatures, and an oil filter is located in the conditioning system.

The compression ratio of the engine is 10.5:1 with 0.5-liter displacement volume. The valve timing is fixed for all experimental conditions, and the valve opening duration is 226 crank angle degrees for both the intake and exhaust valves, based on 0.5mm valve lift with 6 crank angle degrees of valve overlap. Additional specifications are provided in Table 5.1.

The engine operating parameters were controlled with National Instruments (NI) Labview based in-house FPGA (Field-Programmable Gate Array) and real-time programs. The hardware was accompanied by eight digital and analog input and output modules in a compact real-time controller (cRIO). The in-house developed engine operating program allows for control over the spark timing, fuel injection timing, and fuel injection duration for both the direct injector and port fuel injector. The low-speed data including temperature, pressure, air and fuel flows, etc., are measured using NI modules and SCXI (Signal Conditioning Extension for Instrumentation) systems. The high-speed data are measured using an AVL Indiset module and calculated using IndiCom software.

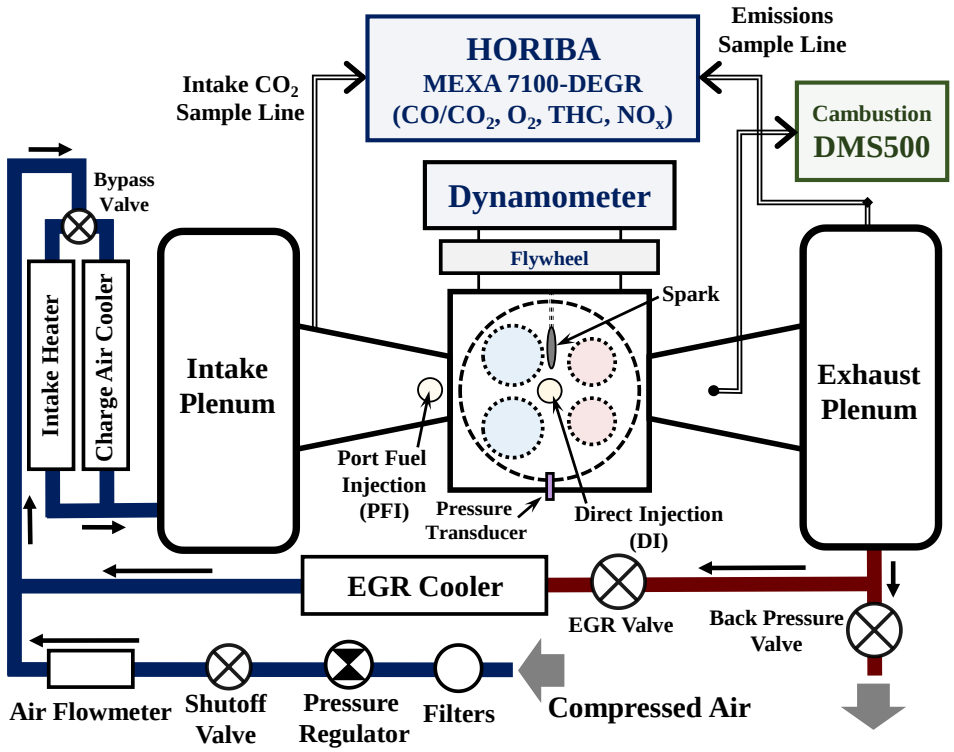

Figure 5.1 Schematic of the boosted Hydra single cylinder research engine for Chapter 5

Table 5.1 Boosted Hydra single cylinder research engine specifications for Chapter 5

Displaced volume	0.5 liter
Bore / Stroke	86 mm / 86 mm
Compression Ratio	10.5 : 1
Intake Valve Timing	IVO: 362 bTDCign / IVC: 136 bTDCign
Exhaust Valve Timing	EVO: 138 aTDCign / EVC: 364 aTDCign
Head Design	Pent-roof / 4 valve / side mounted spark
Direct Injector	HDEV4 piezoelectric spray-guided injector, Hollow-cone spray (85° ± 5° spray angle), Penetration length (< 30 mm).
EGR System	Cooled external EGR

The cylinder pressure is measured using a cylinder pressure transducer (Kistler 6125A piezoelectric transducer) which is 4mm in diameter and is located on the side of the cylinder head. The pressure signal is amplified (AVL IFEM) and recorded (AVL Indiset module) using a crank angle encoder signal (AVL 365C01). Knocking calculations are based on the pressure data from each cycle and knock detection during the test was via audible knock using a microphone and speaker in the control room.

Particulate matter emissions including particle number concentration and size distribution were measured using a fast particulate analyzer [Cambustion DMS500 (Differential Mobility Spectrometer) mk2]. The measurement range for particle size is from 5 nm to 1000 nm (1 µm) with two-stage dilution. For all engine conditions, the samples are diluted with 150 °C of heated dry air in the first stage with 6:1 dilution ratio to prevent condensation of hydrocarbons, water, and significant particle agglomeration. The samples are diluted with dry air at the second dilution stage of 1:1 ratio. The first stage inlet flow is regulated to 8 liter per minute with a 0.90 mm size orifice to prevent over-flow caused by higher back pressure conditions (1.40 bar – 1.00 mm orifice is used for ambient pressure). Exhaust samples are collected from the exhaust side runner with a 0.25-inch (6.35 mm) diameter stainless steel tubing with insulation. All data were collected at a sampling rate of 10 Hz for 45 seconds and subsequently averaged, and the standard deviation calculated.

A Horiba MEXA-7100DEGR was used to measure the gaseous emissions. The bench measures CO_2, CO, total hydrocarbon (THC), O_2, and NO_x emissions and calculates lambda and EGR ratio. Exhaust gases were sampled from the center of the exhaust plenum through a perforated tube and transferred to the emission analyzers using a heated filter and sample line.

The gasoline used in the study was oxygenate-free research grade gasoline provided by Gage Products Company. The research octane number was 90.9 and motor octane number was 83.4 (sensitivity of 7.5). The ethanol was 200-proof anhydrous (Purity > 99.5%, H_2O < 0.005%) ethyl alcohol provided by Deacon Labs, Inc. Gasoline and ethanol were used separately for the dual injection experiments, and splash blended E20 (20% ethanol and 80% gasoline, volume basis) was used for the direct injection only experiments. The fuel properties are summarized in Table 5.2.

Table 5.2 Fuel (Gasoline, Ethanol, E20) specifications

	Gasoline [a]	**Ethanol** [b]	**E20** [c]
Research Octane Number	90.9	109	97.4
Motor Octane Number	83.4	90	85.8
Octane Sensitivity	7.5	19	11.6
Hydrogen / Carbon Mole Ratio	1.920	3.0	2.061
Oxygen / Carbon Mole Ratio	0.000	0.5	0.069
Lower Heating Value [MJ/kg]	43.6	26.9*	40.7

[a] Analysis Result of Gage Products Company, Ferndale, MI, USA (2017)

[b] Hunwartzen, I. [88] (* Heywood, J. [7])

[c] Calculated values based on Anderson et al. [29]

5.3.2 Dual Injection Concept and Injection Timing

In order to investigate the effects of the different types of injection strategy (direct only or dual injection) on engine performance, the fuel composition was kept globally consistent, and the composition was a splash blended E20 fuel blend (volume basis). The dual injection method followed the concept illustrated on the left side of Figure 5.2. Gasoline, representing 80% by volume of the total fuel, was injected using a centrally mounted direct injector, and ethanol, representing 20% by volume of the total fuel, was injected using a port fuel injector installed upstream of the intake valve. The splash blended E20 fuel was used in the direct injection only condition, which is described on the right side of Figure 5.2. More fuel was required for the direct injector in the DI only condition due to without PFI, and the amount of fuel was controlled by the injection duration. The effect of longer injection duration for the DI only condition is illustrated by the longer spray plume in Figure 5.2, where the plume length indicates the amount of injection mass, not the spray penetration length.

A split injection strategy was adopted for the direct injector to increase the stable stratified combustion for both the DI-only and the dual injection experiments. The initial fueling strategy was split injection with 50% of the fuel mass injected at 280° bTDC, and 50% injected at 120° bTDC. However, that fuel injection strategy led to incomplete combustion with >1% (by volume) carbon monoxide and oxygen emissions. Consequently, tests varying the timing of the second injection event from 220 to 45° before top dead center (bTDC) were conducted while fixing the first injection event at 280° bTDC. The results showed an optimum for combustion efficiency at 200° bTDC, so the second injection timing was then set to 200° bTDC for both the DI-only and the dual-injection experiments. Figure 5.3 illustrates the valve timing superimposed with the split injection timing used for the direct injection.

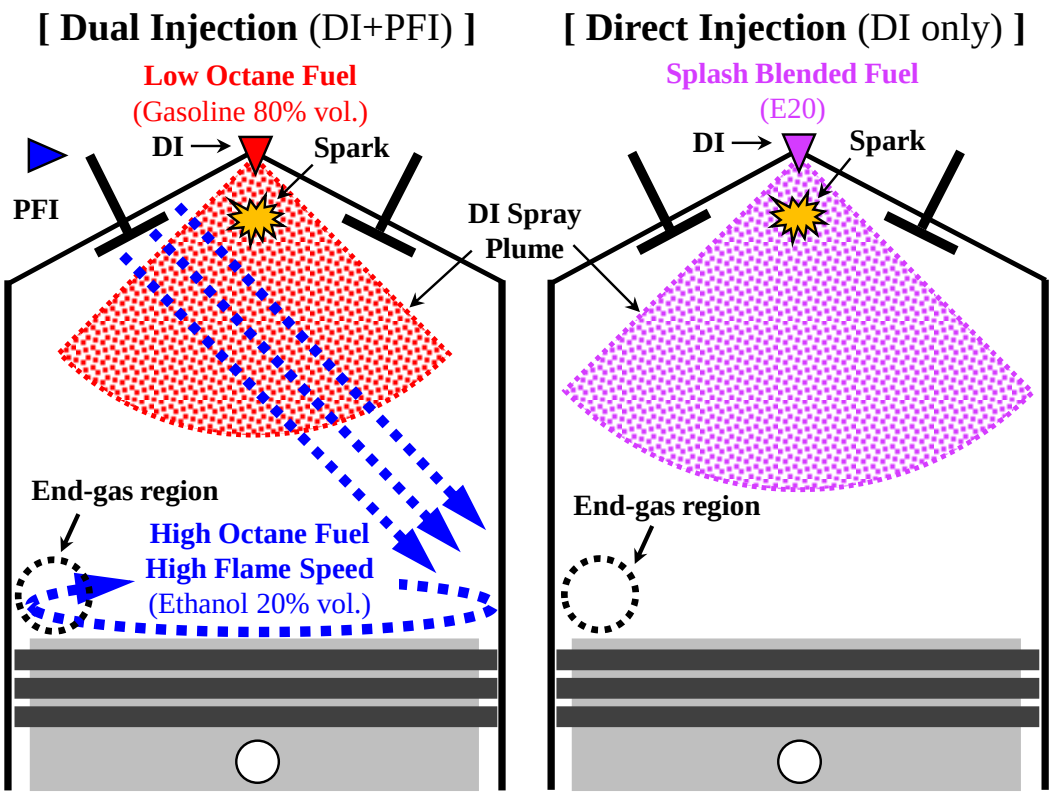

Figure 5.2 Fuel injection concepts for the dual (left) and direct injection (right) conditions

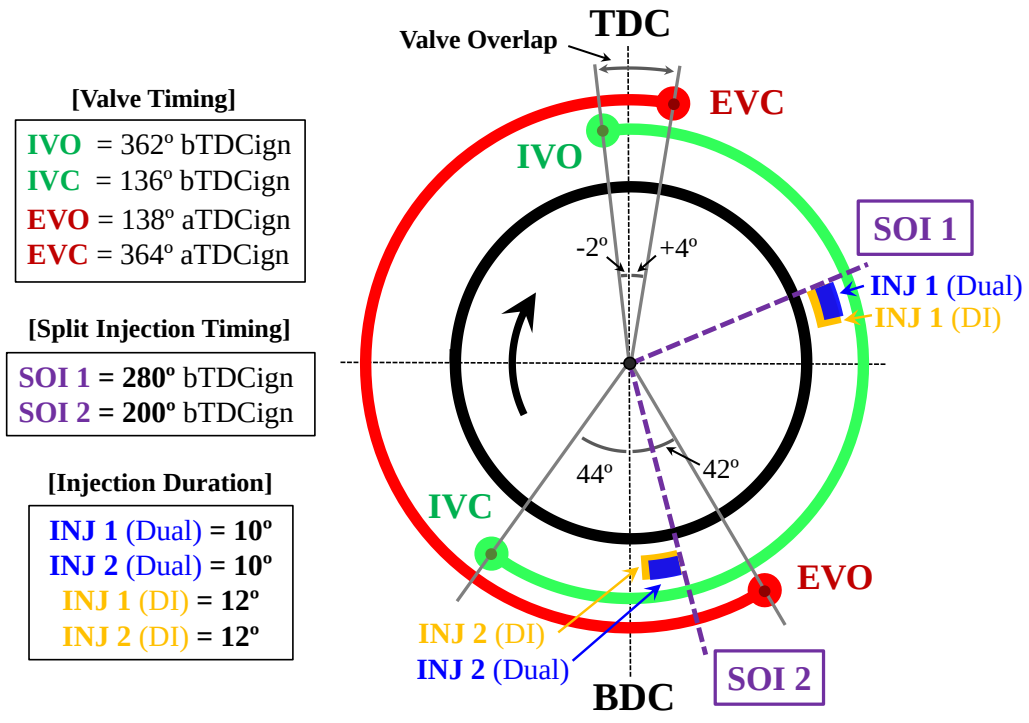

Figure 5.3 Diagram of the valve timing and the timing and duration used for the two direct injection events

5.3.3 Engine Experimental Condition

To explore the effects of the injection type and fuel separation on dilution tolerance, four levels of EGR mass fraction were considered: 0%, 7%, 14%, and 21% for both dual and direct injection only experiments. In all tests, the global air to fuel equivalence ratio was maintained at 1.00, and the amount of fuel injected was controlled by monitoring the values of the lambda meter and the emissions bench. The lambda meter has a faster time response than the emissions bench, so all data recording was conducted after stabilizing and matching the two values. The EGR mass fraction was controlled based on the emissions data, where the EGR mass fraction was calculated using the Equation 5.1.

$$\boldsymbol{EGR_{ratio}}\,[\%] = \frac{CO_{2\,(intake)} - CO_{2\,(ambient)}}{CO_{2\,(exhaust)} - CO_{2\,(ambient)}} \times 100 \qquad (5.1)$$

Spark dwell time was held constant at 2.22 ms which is equivalent to a 20-crank angle degree duration at an engine speed of 1500 rpm with constant ignition energy. Port fuel injector rail pressure was maintained at 5.2 bar with an external fuel pressure pump and pressure regulator, and direct injector rail pressure was held at 200 bar with an external high-pressure nitrogen cylinder and an accumulator. The intake pressure was set to 1.25 bar boosted condition, and the exhaust pressure was 1.40 bar to enable the smooth external EGR flow with a back-pressure control valve. Both pressures were kept constant to avoid different internal EGR ratio. The operating conditions are summarized in Table 5.3.

Table 5.3 Boosted Hydra single cylinder research engine operating conditions for Chapter 5

Engine Speed	1500 rpm
DI Split Injection Timing	280 bTDC (50%) + 200 bTDC (50%)
DI Rail Pressure	200 bar
PFI Rail Pressure	5.2 bar
Air/Fuel Equivalence Ratio (λ)	1.00 (Stoichiometric)
Spark Dwell Time	2.22 ms (20 CAD @1500 rpm)
Intake / Exhaust Pressure	1.25 bar / 1.40 bar
Intake Air Temperature	25.0 ºC ± 0.75 ºC
Coolant Temperature	85 ºC
Oil Temperature	85 ºC

Knocking and combustion stability results are sensitive to the surrounding environment, so each set of experiments was repeated three times on different days. Knock was measured two ways: the first using audible knock during the experiments; and the second using knock intensity calculations based on the in-cylinder pressure data.

Two calculation methods were used for the knock quantification: an energy basis method 'KI 20' and the peak basis method '$KI_{peak\ to\ peak}$'. The two knock intensity methods showed similar trends, and the KI 20 values were prioritized in case the threshold values were different. Equations 5.2 and 5.3 are used to compute KI 20 and KI peak to peak. The detailed calculation including FFT filtering guideline is described in a previous study by Han et al. [15]. The knock threshold value of KI 20 was set at 0.005 bar^2 and is equivalent to 0.42 bar of $KI_{peak\ to\ peak}$.

$$\mathbf{KI\ 20} = \frac{1}{N_{samp}} \sum_{i=1}^{N_{samp}} (P(i) - P_{mean})^2 \qquad (5.2)$$

In Equation 5.2, P_{mean} is the average pressure data and N_{samp} is the number of pressure samples within the 20-degree crank angle range following the offset of the first pressure pulse. The pressure data are measured per 0.1 crank angle degree. So, there are 200 data points for every 20 crank angle degrees, and N_{samp} is 200 in this experiment.

$$\mathbf{KI}_{\mathbf{peak\ to\ peak}} = |\,(\,\boldsymbol{max}\{\,\boldsymbol{p(i)}\,\}\,) - (\,\boldsymbol{min}\{\,\boldsymbol{p(i)}\,\})\,| \qquad (5.3)$$

In Equation 5.3, *p(i)* indicates the filtered pressure and '*i* ' is the crank angle degree. The range of '*i* ' is set from -20 TDC_{ign} to +70 TDC_{ign}, to avoid noise from other sources such as intake and exhaust valve closing signals. Signal oscillation caused by the valve closing is occasionally higher than the knocking oscillation in lower knocking cycle cases.

5.4 Engine Combustion and Knock

5.4.1 Combustion Phasing and Knock

A range of spark timings was explored to determine the knock limited combustion phasing and maximum brake torque conditions. Figure 5.4 shows the effects of spark timing and EGR dilution level on combustion phasing (CA50), and the red symbols indicate the knock limited conditions. The solid lines with filled symbols are the dual injection (PFI + DI) conditions and the dashed lines with open symbols are the direct injection only conditions. The

error bar is the standard deviation for 200 cycles, and all graphs in this paper follow the same formatting guidelines. All eight cases showed knock limited combustion phasing at the intake air pressure of 1.25 bar boost, but the onset of knock for the 21% EGR was after the maximum brake torque (MBT) for both dual and direct injection only strategies. The combustion phasing for dual injection generally showed slightly advanced phasing before the knock limits, but all conditions were within the error bars. So, the combustion phasing difference between dual and direct injection was small and for fixed spark timing.

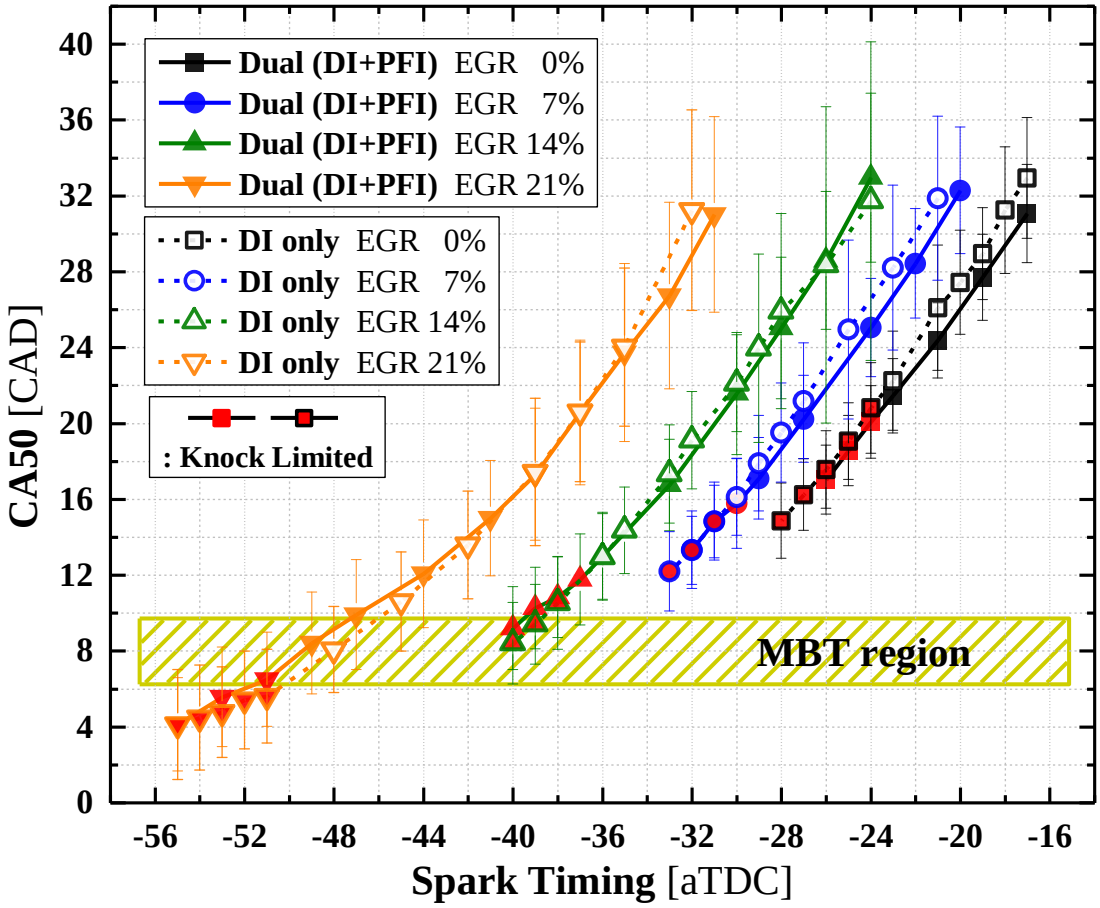

Figure 5.4 Effects of spark timing and EGR dilution levels on combustion phasing (CA50). (Error bars are standard deviation of 200 cycles). The red open and filled symbols denote knocking conditions.

Figure 5.5 illustrates the calculated knock intensity (KI 20) from the in-cylinder pressure data based on the average combustion phasing (CA50). KI 20 values are dramatically increased after the onset of knock, so the vertical axis is presented as the natural log of KI 20. As described previously, the knock threshold of KI 20 was set to 0.005 bar^2 (natural log of KI 20 is -5.298), which is equivalent to 0.42 bar $KI_{peak\ to\ peak}$, and it is indicated by the red horizontal line in Figure 5.5. With increasing EGR mass fraction, knock intensity is decreased regardless of the combustion phasing. While the knock intensity differences among EGR dilution steps below the knock threshold look large, the actual difference on a natural log scale under this threshold is quite small, so the difference are considered negligible.

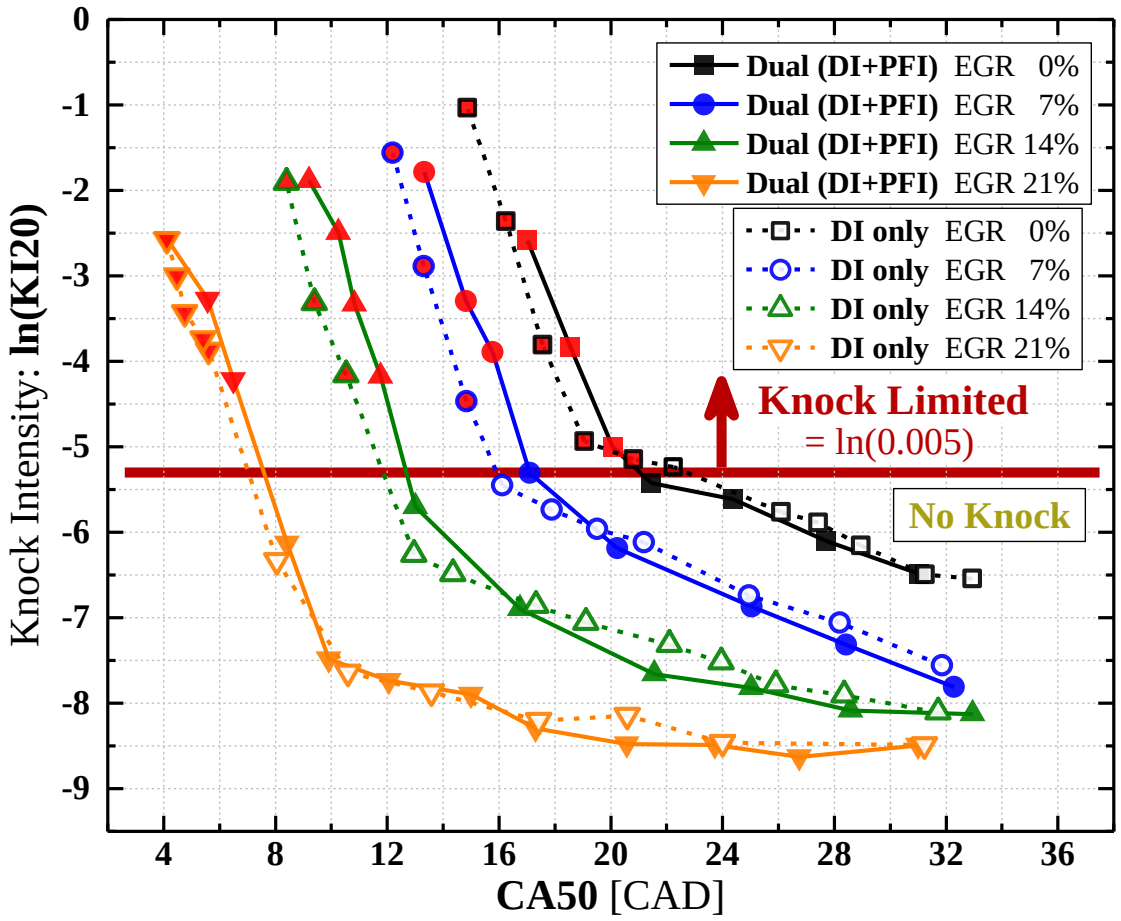

Figure 5.5 Effects of combustion phasing (CA50) and EGR dilution levels on knock intensity (natural log of KI20). The red open and filled symbols denote knocking conditions.

The knock limited combustion phasing difference between dual and direct injection is less than 1 crank angle degree in all EGR dilution cases. Although the difference in phasing at the knock limit is marginal, the intensity above the knock threshold shows clear differences. The slope of the intensity is almost the same, and the dual injection lines are consistently shifted to later phasing. Because the slope of the knock intensity is steep, the knock intensity difference at the same phasing is fairly large for all EGR dilution conditions, especially considering the natural log scale. Figure 5.6 shows an example of the intensity difference at the same combustion phasing. The top graph presents the cylinder pressure traces for the dual and direct injection conditions using 7% EGR. The combustion phasing for both injection strategies are the same (14.8 aTDC), and the plotted traces are selected from the recorded 200 cycles under the same condition with guidelines. Selection guidelines are the closest traces to each average value of cylinder pressure and KI 20 value with the same phasing. There are no significant differences between the in-cylinder pressure data from the two injections, but the direct injection data shows marginally higher pressure after actual combustion and longer burn duration. This trend was observed for all EGR dilution levels. The bottom panel in Figure 5.6 shows filtered cylinder pressures data for the two injection strategies. A Fast Fourier Transform with 3.5 kHz high pass filter was used for this filtering. The dual injection results show earlier knock onset and higher intensity than direct injection at the same combustion phasing. Both filtered traces show pre-oscillation between TDC and the crank angle timing of peak knock intensity, and this could be caused by the location of the spark plug and the cylinder geometry. So, the onset of knock was defined as the peak of absolute oscillation. In addition, the $KI_{peak\ to\ peak}$ values are shown in the filtered traces and used as a secondary metric in this study.

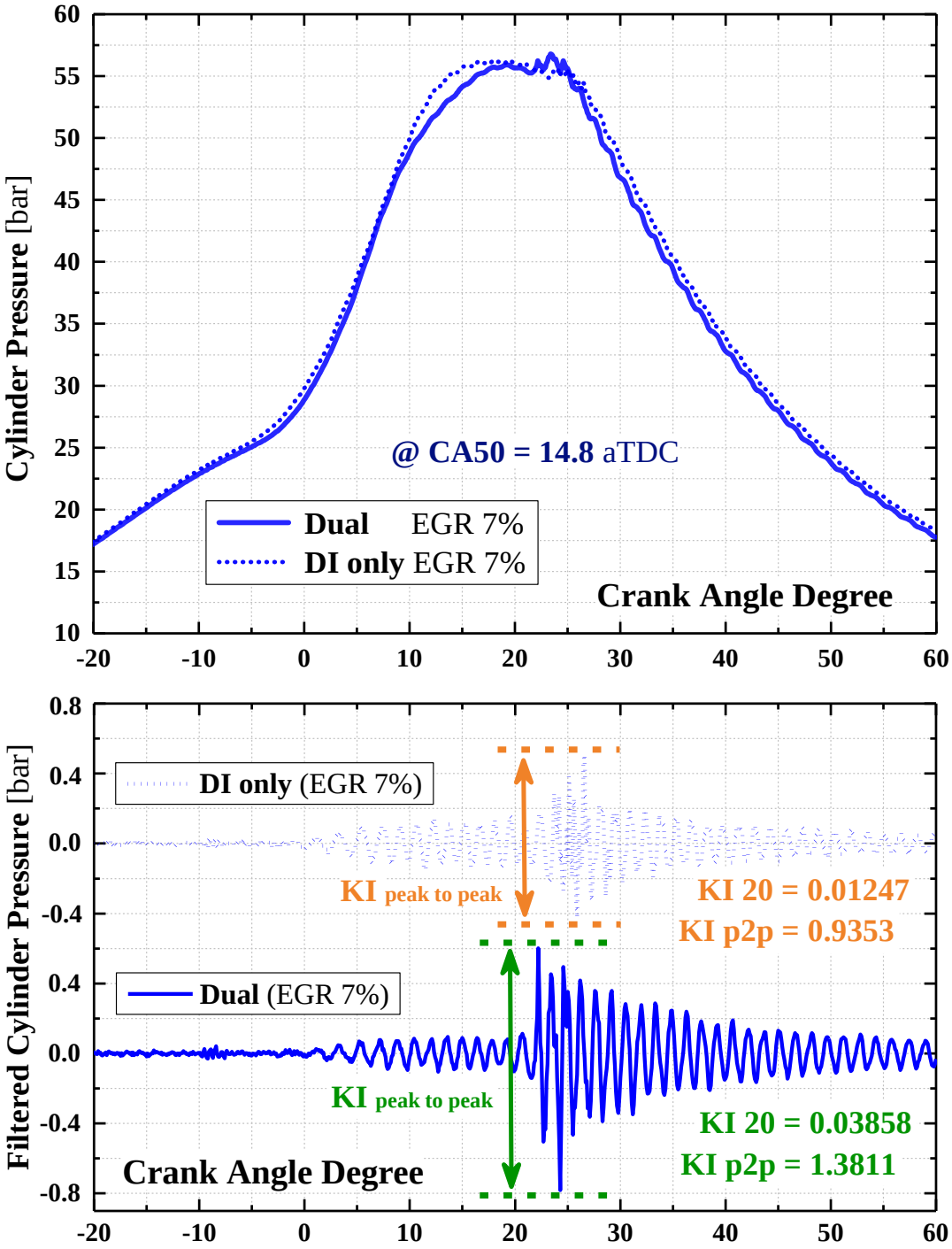

Figure 5.6 Cylinder pressure and filtered pressure trace comparisons between two injections under same combustion phasing (CA50 = 14.8 aTDC, 7% EGR case)

The initial hypothesis was that dual injection would extend the knock limit compared with direct injection only, but the results show the dual injection was slightly more likely to knock, based on combustion phasing. There are several possible reasons which are discussed in the following two sections.

5.4.2 Burn Duration and Knock

Engine knock is generally affected by two major combustion factors: one is burn duration; and the other is ignition delay time of the mixture in the end-gas region. Figure 5.7 shows the difference in burn duration (CA1090) as a function of combustion phasing for dual and direct injection and the four levels of EGR dilution. With increasing EGR mass fraction, overall burn duration lengthened, and as combustion phasing was advanced, the burn duration was shortened in all cases. The reduction of burn duration is proportional to the level of EGR dilution. The burn duration for 21% EGR dilution was nearly 1.5 times longer than with no EGR dilution. The changes in the value of burn duration are consistent with the flame speed simulation study of Middleton et al. [89] who found the flame speed decreased by a factor of two with 20% EGR dilution. Comparison of the injection strategies shows the burn duration for dual injection is faster than with direct injection. As the schematic diagrams of Figure 5.2 illustrate, the biggest difference with injection strategies is the local fuel distribution. In other words, the distribution of the ethanol and gasoline in cylinder is different but globally has the same composition. Hence, the most likely reason for the faster burn duration with dual injection is the creation of locally ethanol rich regions which burn faster, i.e., with higher flame speeds. More details will be discussed in the EGR dilution tolerance section.

From the viewpoint of the combustion factors that tend to induce knock, dual injection with its faster flame speed should have improved the knock limit by leaving less time for end-gas auto-ignition. But the knocking result is opposite. Thus, we can suspect that the environment of the end-gas region is more likely to auto-ignite due to higher temperature or pressure. As the pressure trace in Figure 5.6 shows, the difference in overall cylinder pressure is minimal, so the local pressure in the end-gas region should be similar for both injection conditions. But the temperature of the end-gas region could be quite different. To verify the difference of unburned charge temperature with the two injection strategies, volumetric air flow and load (gross IMEP) are discussed in the next section.

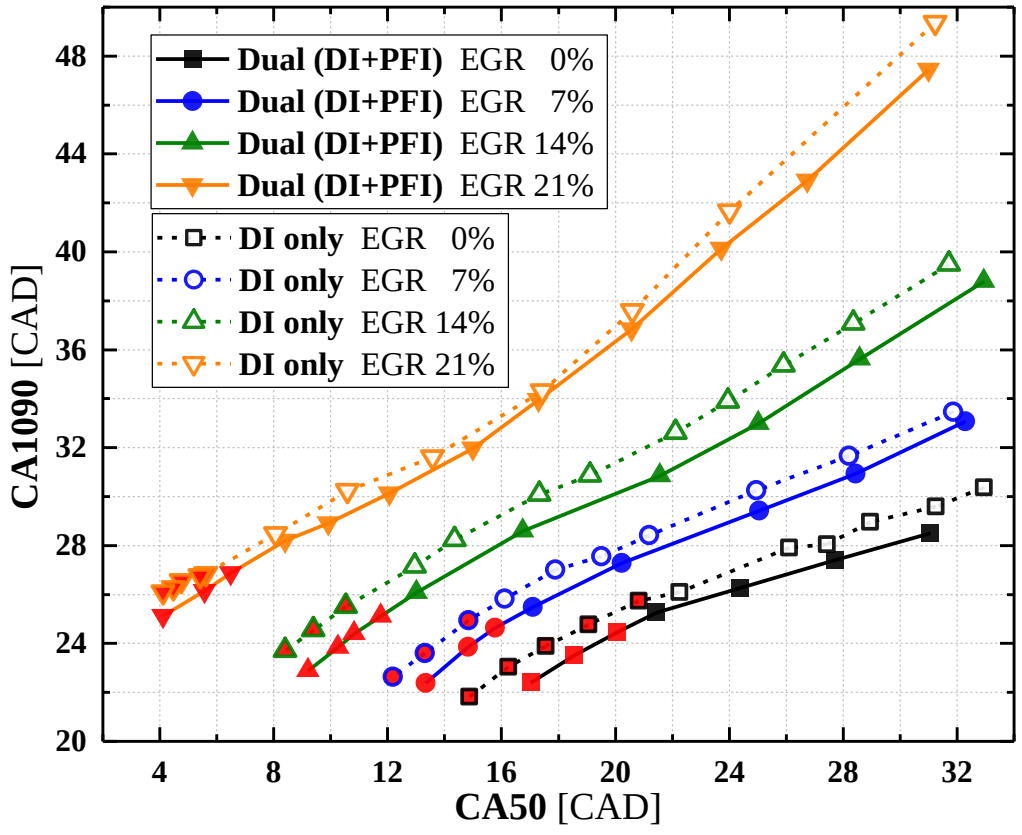

Figure 5.7 Effects of fuel injection strategy and EGR levels on averaged burn duration (CA1090) as a function of combustion phasing (CA50). The red open and filled symbols denote knocking conditions.

5.4.3 Volumetric Efficiency, IMEPg, and Knock

To investigate the volumetric efficiency difference between the two injection strategies, the measured fresh air flow rate is presented in Figure 8. All measured values in slpm (standard liter per minute) are normalized by the maximum flow rate (394 slpm) from the no EGR condition. Increasing EGR mass fraction leads to lower volumetric air flow rates, and the amount is fairly consistent with the EGR ratio. Also, notable in Figure 8 is the difference in air flow rates between dual and direct injection. The percentage values in the figure denote the relative loss in volumetric air flow rate of the dual strategy compared to the DI fueling strategy. All conditions show more than two percent of volumetric air flow rate decrease, and the difference is lower with higher EGR dilution.

The reasons for the air flow rate difference, despite the controlled intake temperature and pressure, are attributed to differences in charge cooling caused by direct injection and fresh air displacement of evaporated fuel using the port fuel injector. The charge cooling effect is maximized when fuel with a higher latent heat of vaporization (i.e., ethanol) is injected through the direct injector, so dual injection should have lower volumetric efficiency in consideration of the reduced amount of fuel injected and having pure gasoline in the direct injector.

Returning to the discussion of the unburned gas temperature in the end-gas region, the temperature can be compared using an ideal gas calculation with a given relative pressure and volume. Assuming the fuel is all in the vapor phase, the air to fuel equivalence ratio is 1.00, the mixture composition is globally homogeneous, and using the isentropic ideal gas law equation (Equation 5.4), the temperature can be calculated. Dual injection has 5% less fuel/air mixture based on the results presented in Figure 8, but the fuel/air compositions are the same (i.e. stoichiometric), so the end-gas temperature is estimated to be around 15 ºC higher than for direct

injection. While the difference in temperature is estimated to be small, the effects on knock limits are amplified due to the dependence on the ignition delay time which is considered with the effects on gross IMEP.

$$\frac{T_{isen,unburned}}{T_{IVC}} = \left(\frac{P_{cyl}}{P_{IVC}}\right)^{\frac{\gamma-1}{\gamma}} \tag{5.4}$$

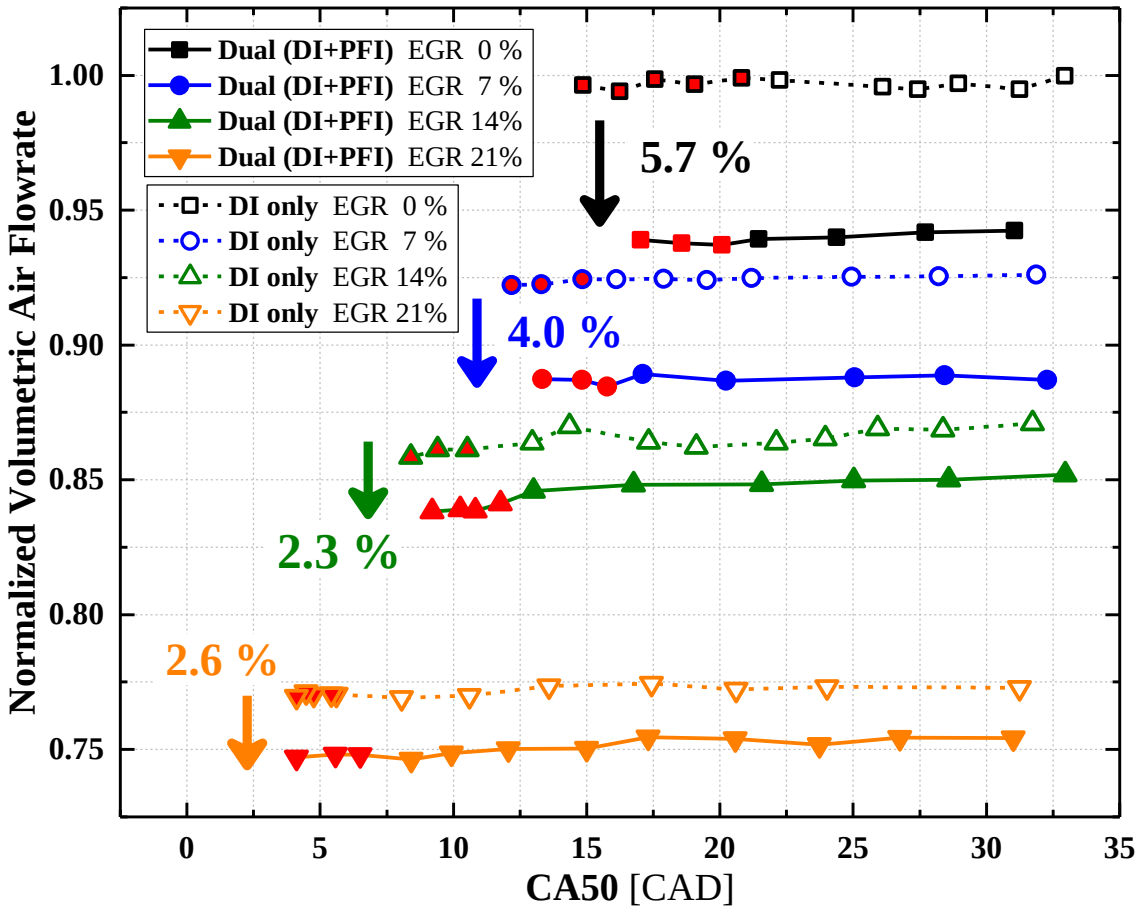

Figure 5.8 Effects of fuel injection strategy and EGR levels on normalized volumetric air flow rate as a function of combustion phasing (CA50). The red open and filled symbols denote knocking conditions.

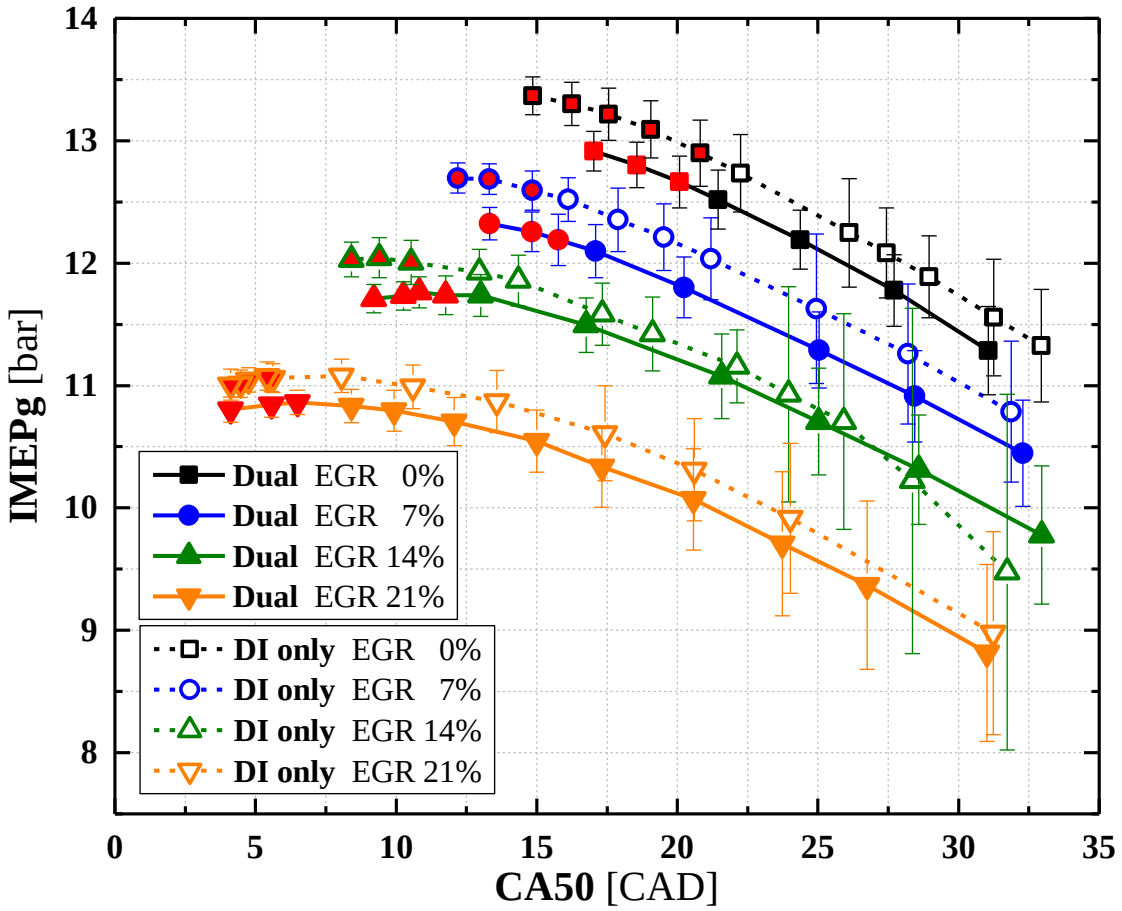

Figure 5.9 Effects of fuel injection strategy and EGR levels on gross indicated mean effective pressure (IMEPg) as a function of combustion phasing (CA50). The red open and filled symbols denote knocking conditions.

Figure 5.9 shows the gross indicated mean effective pressure for the two injection strategies and the different EGR mass fractions. Recall that the exhaust side lambda and volumetric ratio of fuel flow were fixed for all experiments. The results show the IMEPg was systematically lower with dual injection compared with the direct injection. The decrease in IMEPg was very close to the difference in air flow rate. For instance, the knock limited IMEPg for dual injection was 5% lower than for direct injection at the no-dilution, which is close to the air flowrate reduction.

Using the dual injection and direct injection only combustion data, the knock intensity difference between the two fuel injection strategies in Figures 5.5 and 5.6 can be inferred from a knock intensity correlation equation. McKenzie et al. [90,91] formulated Equation 5.5 based on engine physical properties, an ignition delay time equation, and empirical data. The knock intensity value is a function of the gross IMEP, dilution ratio, and the ignition delay time of the unburned mixture.

$$\left[\frac{\mathbf{KI\ mean}}{\mathbf{IMEPg}}\right] = C_1 \times exp\left(-\frac{C_2 \times \boldsymbol{\tau_{id}}(t^*)}{(1-EGR) \times \boldsymbol{IMEPg}^{C3}}\right) \qquad (5.5)$$

In the Equation 5.5, C_1 and C_2 are constants with values greater than 1, and C_3 is expected to very small number such as 0.12 in the original work by McKenzie et al. [90,91]. Considering the ignition delay equations are typically exponential with temperature and proportional to the power of pressure [64,65], it can be inferred that the ignition delay term is the most critical element in the equation. From the perspective of the ignition delay equation, the cylinder pressures are very similar because all tests used the same intake pressure. Thus, the only difference should be the temperature of the unburned charge. Based on the estimates of the end-gas temperature, the correlation for the knock intensity for the dual injection strategy should be higher than for the direct injection only strategy.

5.4.4 Thermal Efficiency and Efficiency Benefit Analysis

Figure 5.10 compares the gross indicated thermal efficiency for the two injection strategies at four identical EGR conditions. The bottom panel shows the thermal efficiency

difference between dual injection and direct injection only with no EGR. The dual injection knock limit occurred at 21.5 CAD combustion phasing (CA50), and the average efficiency difference between the two injection strategies was 0.2% which is within the standard deviation of the data, so the thermal efficiency was considered unchanged by the injection strategy. The upper three panels show identical trends, so the knock limited (KL) or maximum brake torque (MBT) thermal efficiency are considered the same for both injection strategies. Although the knock limit for dual injection is earlier than for direct injection only, the total mass of fuel and air is less than for direct injection only. The gross IMEP of dual injection was improved due to the faster flame speed, and the unchanged efficiency could be the result of the complementary effects of the lower fuel mass and slightly higher IMEP.

The effects of EGR dilution on indicated thermal efficiency are also presented in Figure 5.10. The data show EGR dilution leads to knock limit extension due to the changes in the mixture composition, which dilutes the working fluid and changes the specific heat ratio. To separate the two benefits, the dashed blue line is drawn at a CA50 of 21.5 crank angle degree in Figure 5.10. This CA50 value is from the knock limit of the dual injection strategy for 0% EGR. The yellow circles at crossing points indicate the efficiency at the same phasing, and the red symbol indicates the knock limited point at each dilution condition. These values are presented in Figure 5.11 which is a summary graph of the thermal efficiency benefit analysis. The figure describes the knock limited conditions and the efficiency at the same phasing from Figure 5.10. In addition, the purple star symbol shows the pure gasoline knock limited condition using direct injection only with no EGR. The experimental conditions were exactly the same as the E20 condition (black dashed line). So, the efficiency difference between E0 (purple star) and E20 (black square) is solely the knock limit extension benefit from gasoline to E20.

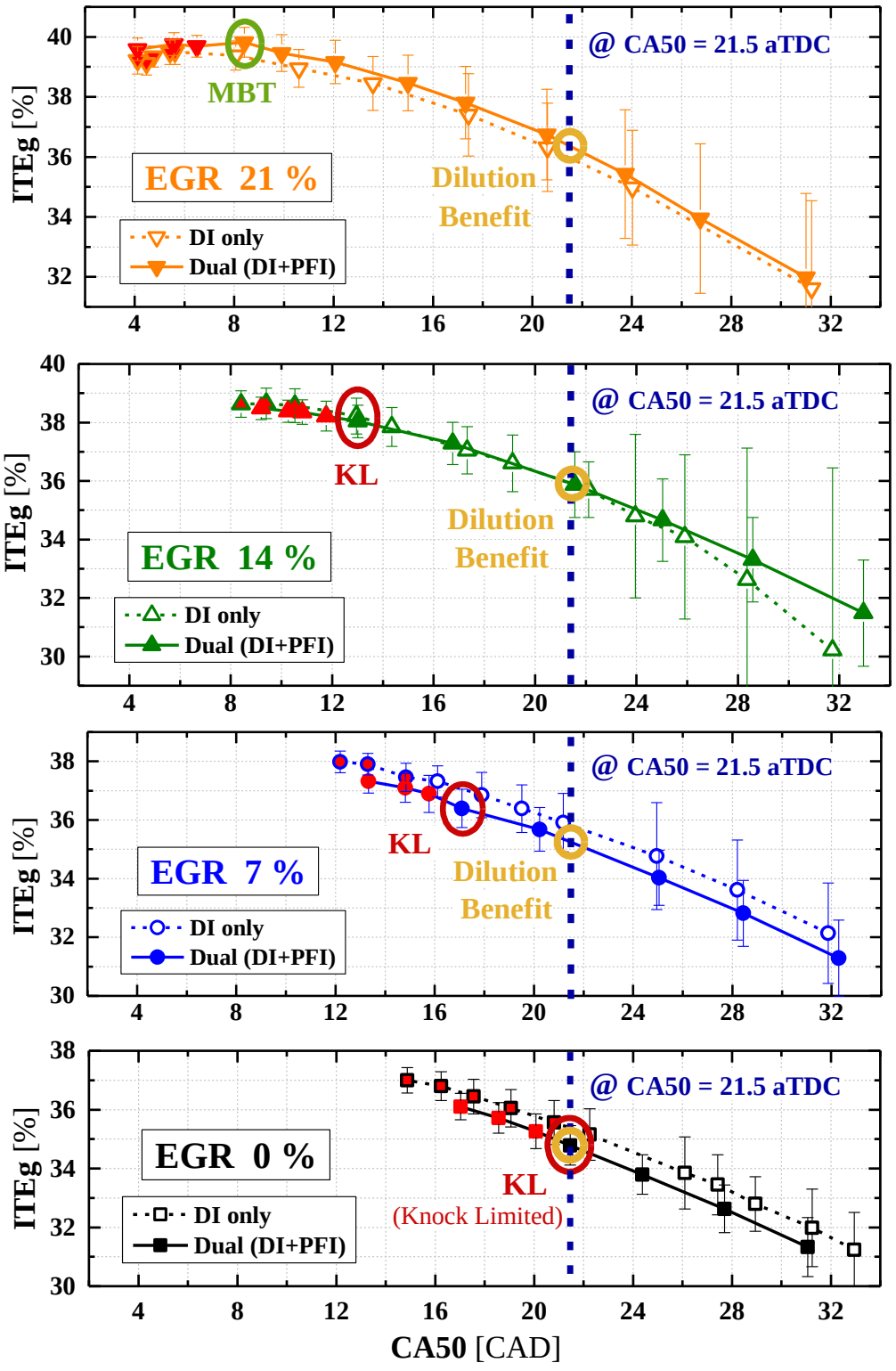

Figure 5.10 Effects of fuel injection strategy and EGR levels on Gross Indicated Thermal Efficiency (ITEg). The dashed blue line is the CA50 at the knock limit for the case of no-EGR dual injection

The yellow line which is from the constant phasing efficiency shows the mixture composition benefit from only EGR dilution, and the difference between the blue and yellow lines indicates the knock limit extension benefit of EGR dilution. As the different slopes of the two lines show, the knock limit extension benefit is roughly twice that of the working fluid mixture benefit.

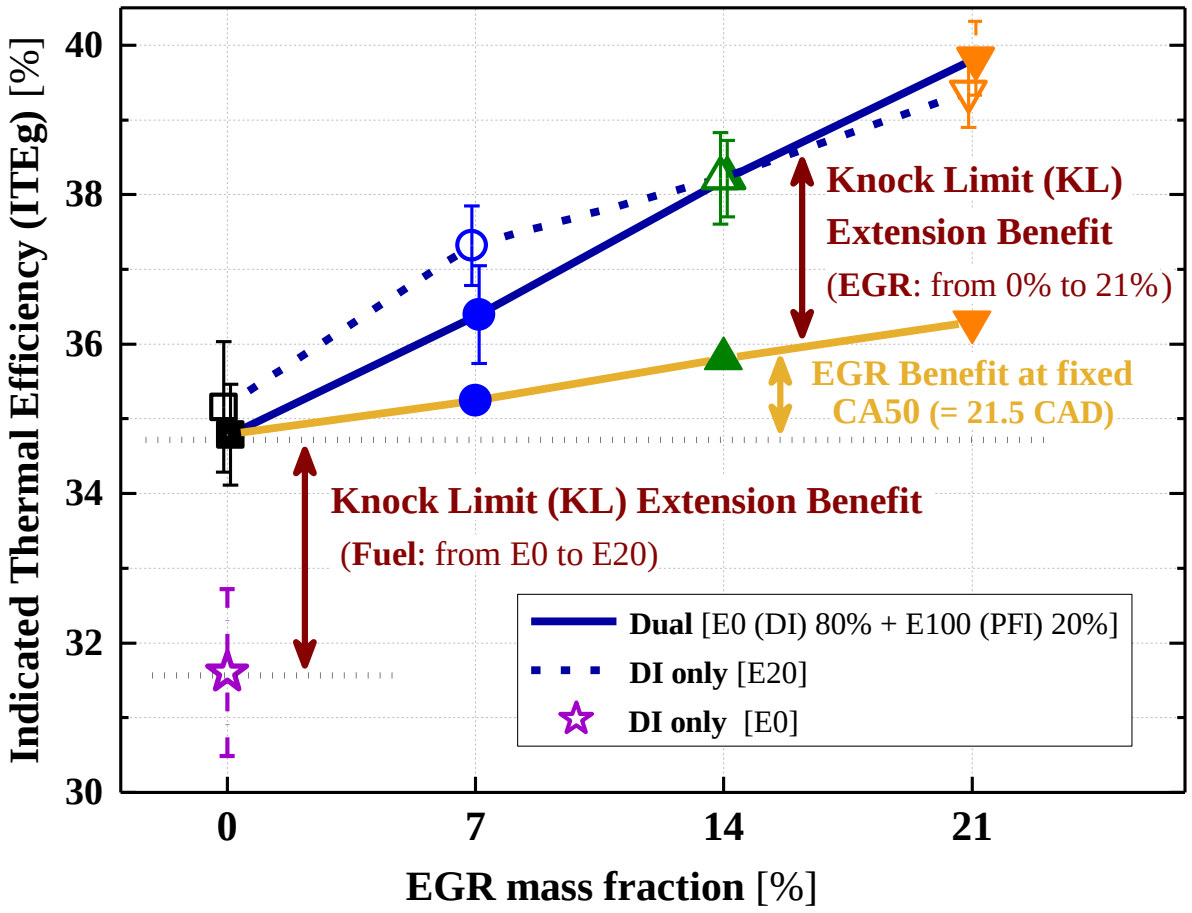

Figure 5.11 Thermal efficiency benefit analysis of EGR dilution and knock limit extension

5.5 EGR Dilution Tolerance

5.5.1 Combustion Stability (CoV of IMEPg)

Another potential benefit of dual injection, aside from knock limit extension, is to improve combustion stability at EGR diluted conditions by formation of a homogeneous ethanol-air mixture near the spark plug. In order to directly compare the combustion stability between the two injection strategies, coefficient of variance (CoV) values of the IMEPg are illustrated with a contour plot in Figure 5.12 as a function of combustion phasing and EGR mass fraction. A threshold CoV of 3% is shown in the figure as the thicker line. In the color scale, red indicates an unstable region and blue indicates a stable region. The CoV results for dual injection show a larger region of stability compared with direct injection only. The effects of the two injection strategies is clear at lower levels of EGR dilution. The slope of the 3% stability threshold is less steep for the dual injection strategy, but the values of the combustion phasing at the 3% CoV threshold for 21% EGR dilution are similar for the different injection strategies. Therefore, the results show dual injection yields a larger stability benefit at lower dilution conditions.

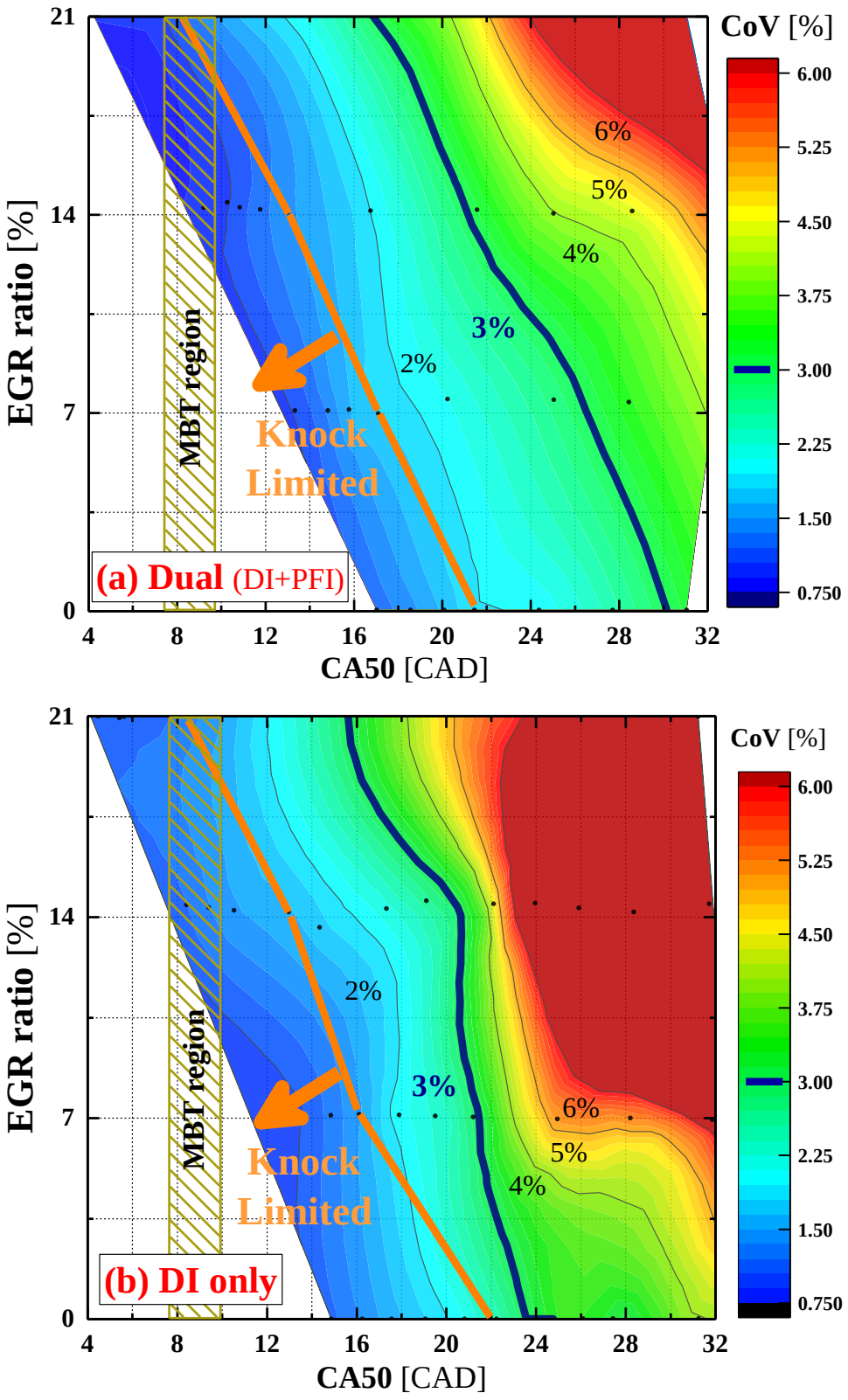

Figure 5.12 CoV of gross IMEP contour plot based on combustion phasing (CA50) and EGR mass fraction; (a) Dual injection and (b) Direct injection.

5.5.2 Combustion Phasing Analysis

In order to investigate the amount of combustion stability improvement, combustion duration data are shown in this section. Szybist et al. [92] determined that the flame speed is one of the most significant factors affecting EGR dilution tolerance. The initial flame kernel correlated with the time of ignition (CA00) to CA05 duration (CA0005) as a highly turbulent flame develops from the spherical flame kernel established by the spark discharge. Figure 5.13 shows the CA0005 duration data for all experimental conditions. With increasing dilution, the time for flame kernel development significantly increased. However, the differences in CA0005 between the two injection strategies are marginal, and only lower dilution cases show that the CA0005 for dual injection has slightly shorter duration from retarded point to knock limited phasing.

Figures 5.14 and 5.15 indicate the combustion duration between 5 and 50 percent (CA0550) and 50 to 90 percent (CA5090) of the total mass of fuel burned. The CA0550 represents the rapid burning phase of turbulent flame propagation from the spark side of the combustion chamber to the near wall region. The CA5090 is the termination phase close to the wall [7]. Both figures clearly show dual injection has shorter durations for all EGR conditions, and the difference is more obvious in the CA0550 graph. Based on the turbulent flame propagation and termination phase information, the PFI ethanol injection helped the turbulent phase in the middle of the cylinder and the end flame termination regions. However, another possibility to explain the faster burn duration is the higher in-cylinder temperature compared with direct injection only case.

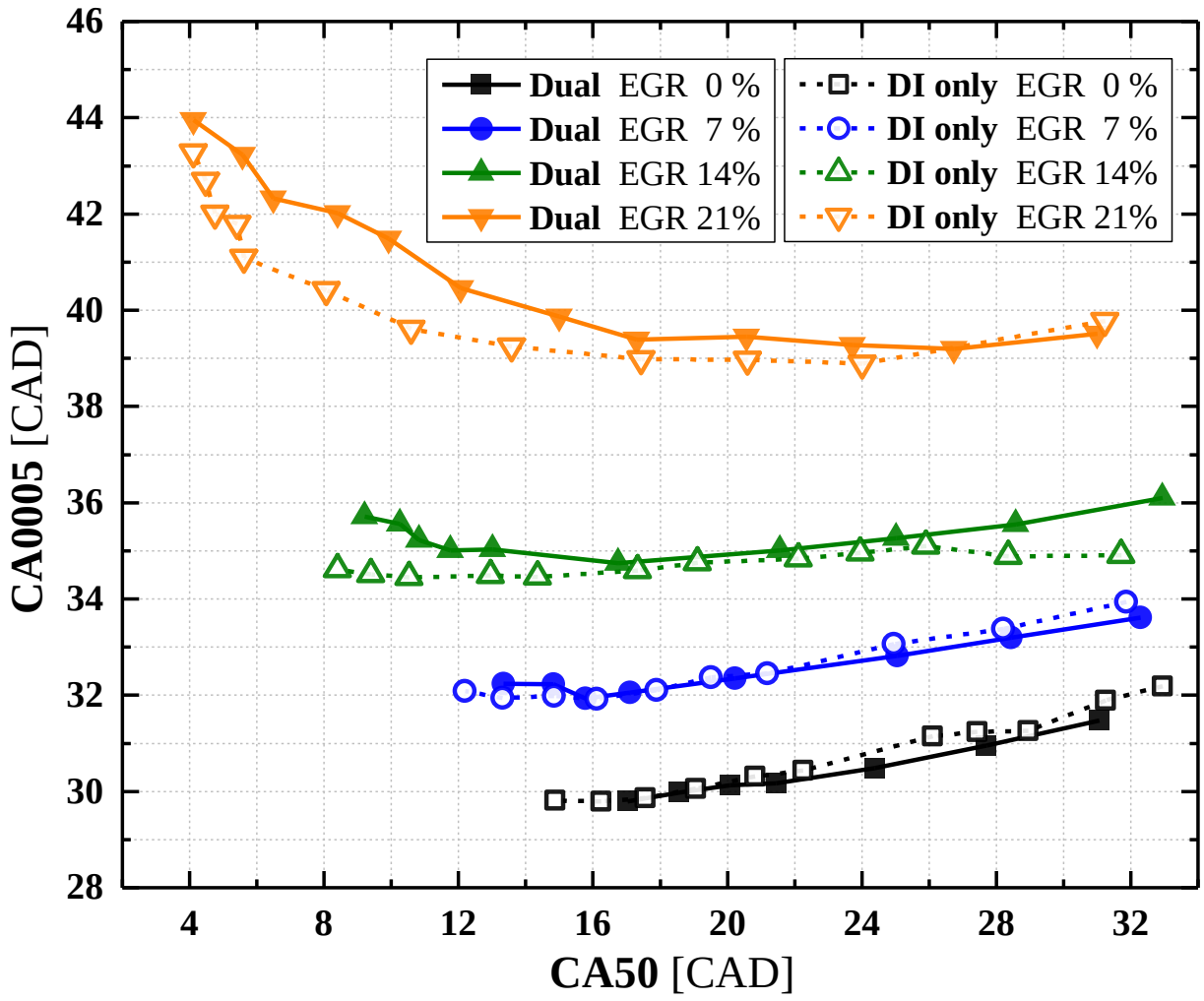

Figure 5.13 Effects of fuel injection strategy and EGR levels on the crank angle degree difference between spark timing and 5% mass fraction burned (CA0005) as a function of combustion phasing

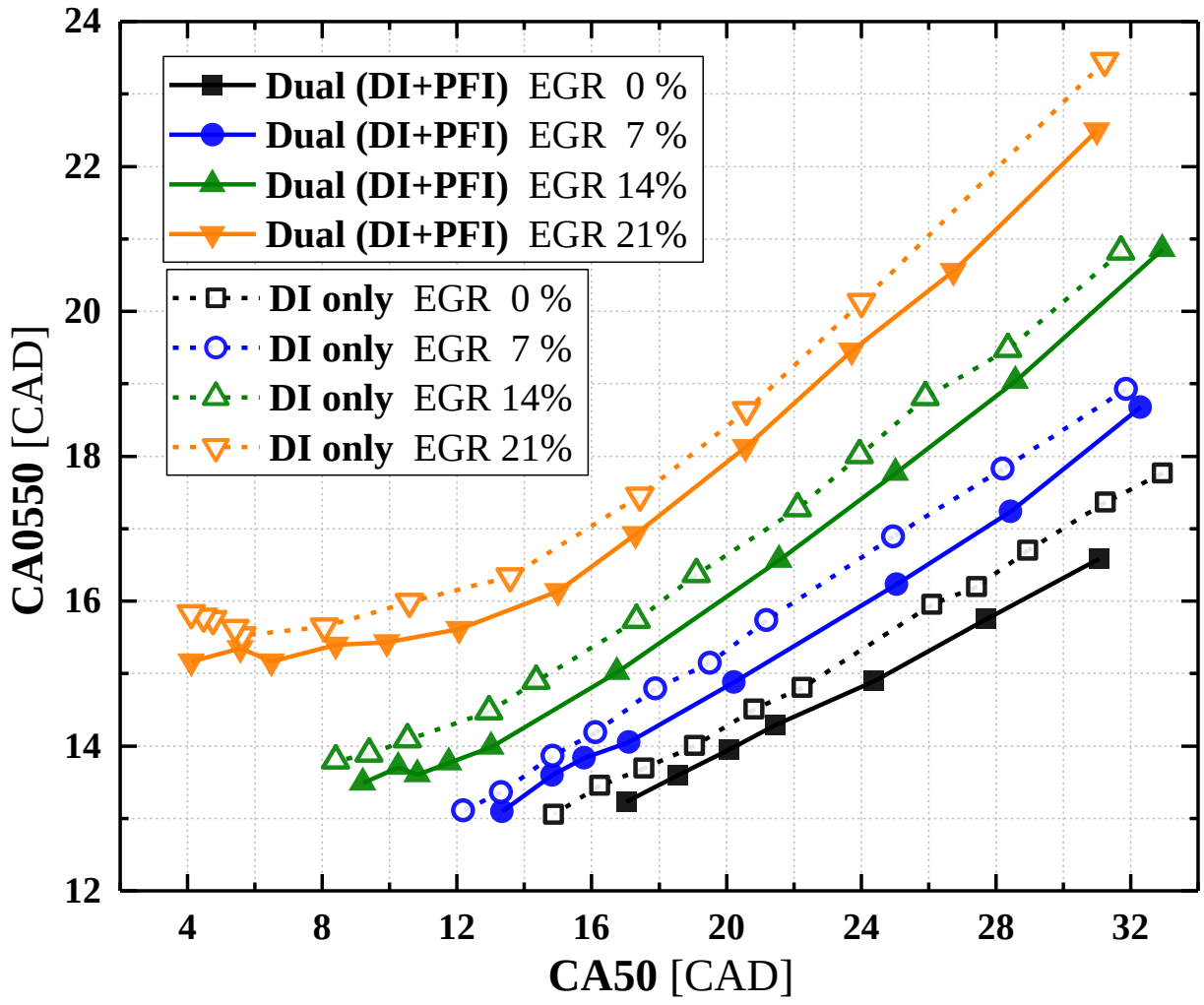

Figure 5.14 Effects of fuel injection strategy and EGR levels on the duration of 5% to 50% mass fraction burned (CA0550) as a function of combustion phasing

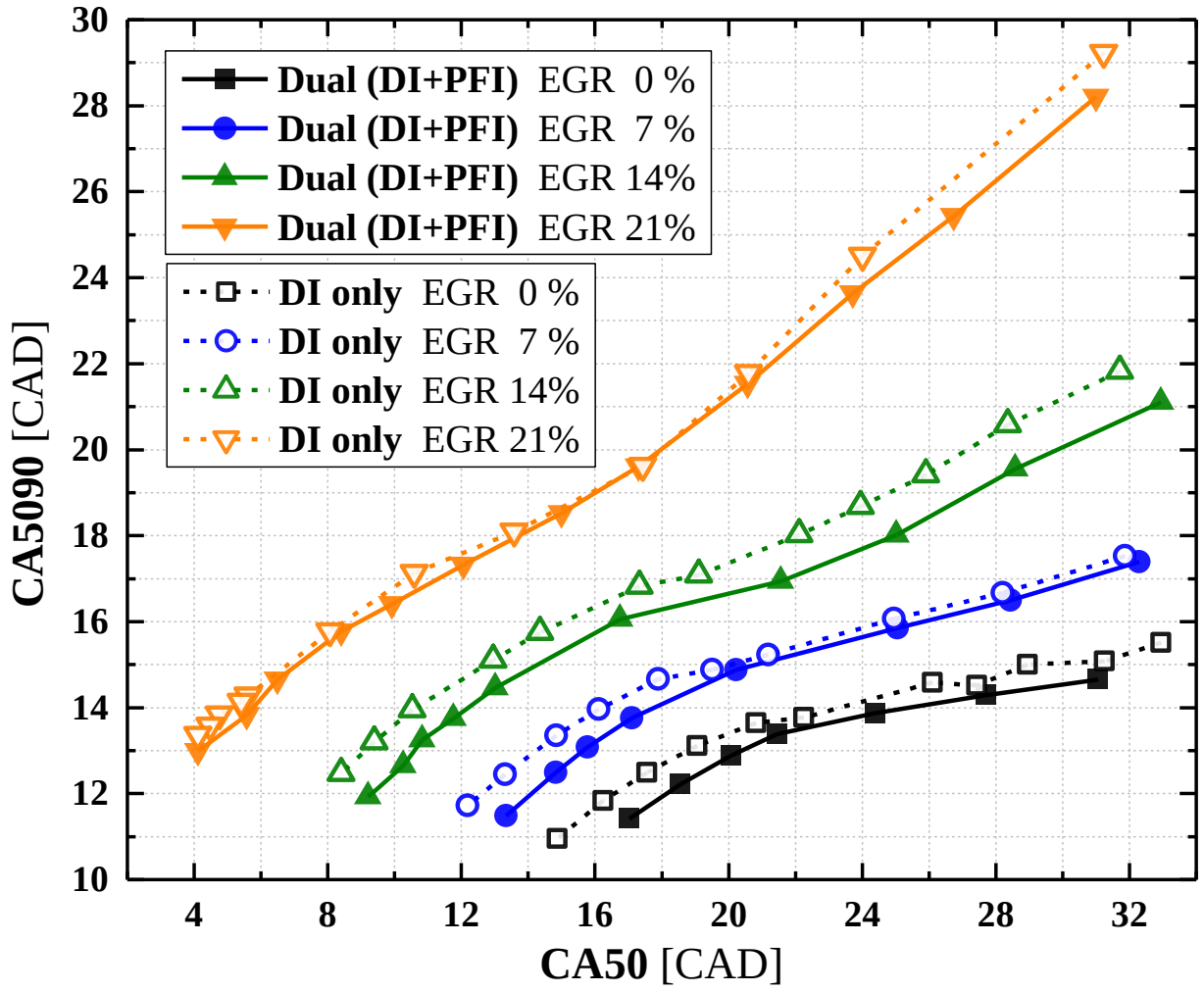

Figure 5.15 Effects of fuel injection strategy and EGR levels on the duration of 50% to 90% mass fraction burned (CA5090) as a function of combustion phasing

5.6 Particulate Matter and Gaseous Emissions

5.6.1 Particulate Matter Emissions

Figures 5.16, 5.17, and 5.18 show the total particulate number and the size distribution results, respectively. In Figure 5.16, the baseline condition with purple star symbol is presented as the DI only results using gasoline with no ethanol and no EGR. Comparison of the gasoline DI only with no EGR results with the E20 data shows the effects of ethanol addition on particulate number emissions. All cases below the knocking limit yielded lower particulate number emissions. In addition, all cases showed that the amount of particulate matter dramatically increased after reaching the knocking limit, and there was no difference in particulate number with EGR dilution before the knock limit. The fuel injection strategy had negligible effect on the total particulate number trends.

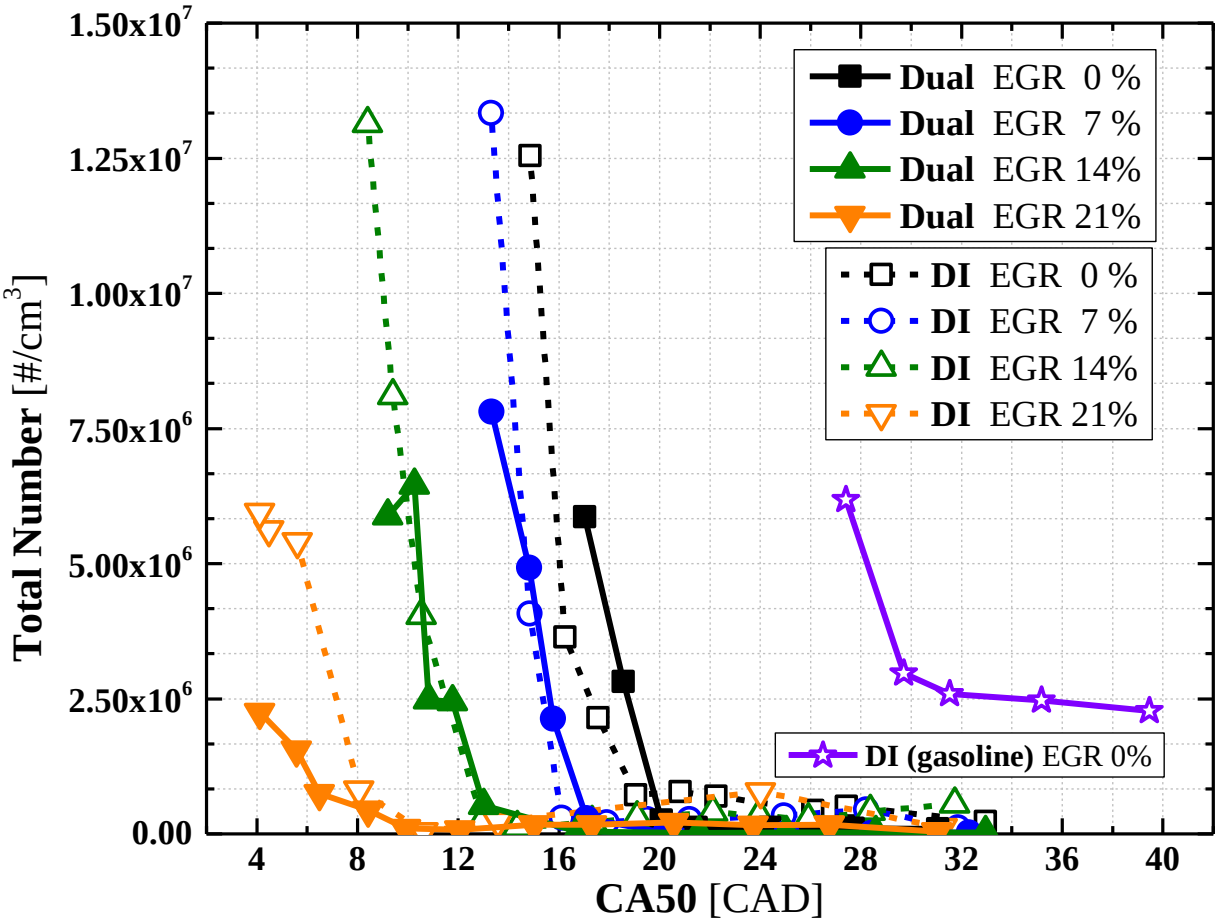

Figure 5.16 Total particulate number emissions based on combustion phasing

Figure 5.17 and 5.18 show the size distribution of the particulate emissions from the two injection strategies and the concentration trends of nucleation and accumulation modes. The smallest group of particulate matter size, with diameters of ≤ 50 nm (or 23 nm [93]), are typically referred to as nucleation mode. Growth of nucleation mode particles leads to accumulation mode, which are normally between 50 nm (23 nm) and 1μm in vehicle measurements [94–96]. The dashed line graphs in the first column are the direct injection only cases with the four levels of EGR dilution, and the second column presents the results for the dual injection cases. The maximum values of the nucleation and accumulation modes are

indicated in the graphs with arrows, and the total number of the nucleation and accumulation modes are presented in the third column. The scale is the same in all graphs to facilitate comparisons. The difference between the first and second columns after knock-limited conditions shows that the particulate matter emissions for dual injection are lower than for direct injection only, regardless of the mode. For knock limited conditions, increasing the EGR ratio, the number of nucleation mode particles, and the number of accumulation mode particles generally decreased. The column of Figure 5.18 highlights this trend. The knock limited values of the accumulation mode (red symbols) are higher than the knock limited nucleation mode values (blue symbols) at 0 and 7% EGR condition. But as EGR increased to 14% the concentration of the two modes were almost identical and then for EGR of 21% the concentration of the nucleation mode exceeded the accumulation mode for knock limited conditions. The nucleation mode particles are mostly comprised of unburned hydrocarbon or liquid droplets [93], so the trends for increased nucleation and total hydrocarbon emissions (presented in the next section) agrees well.

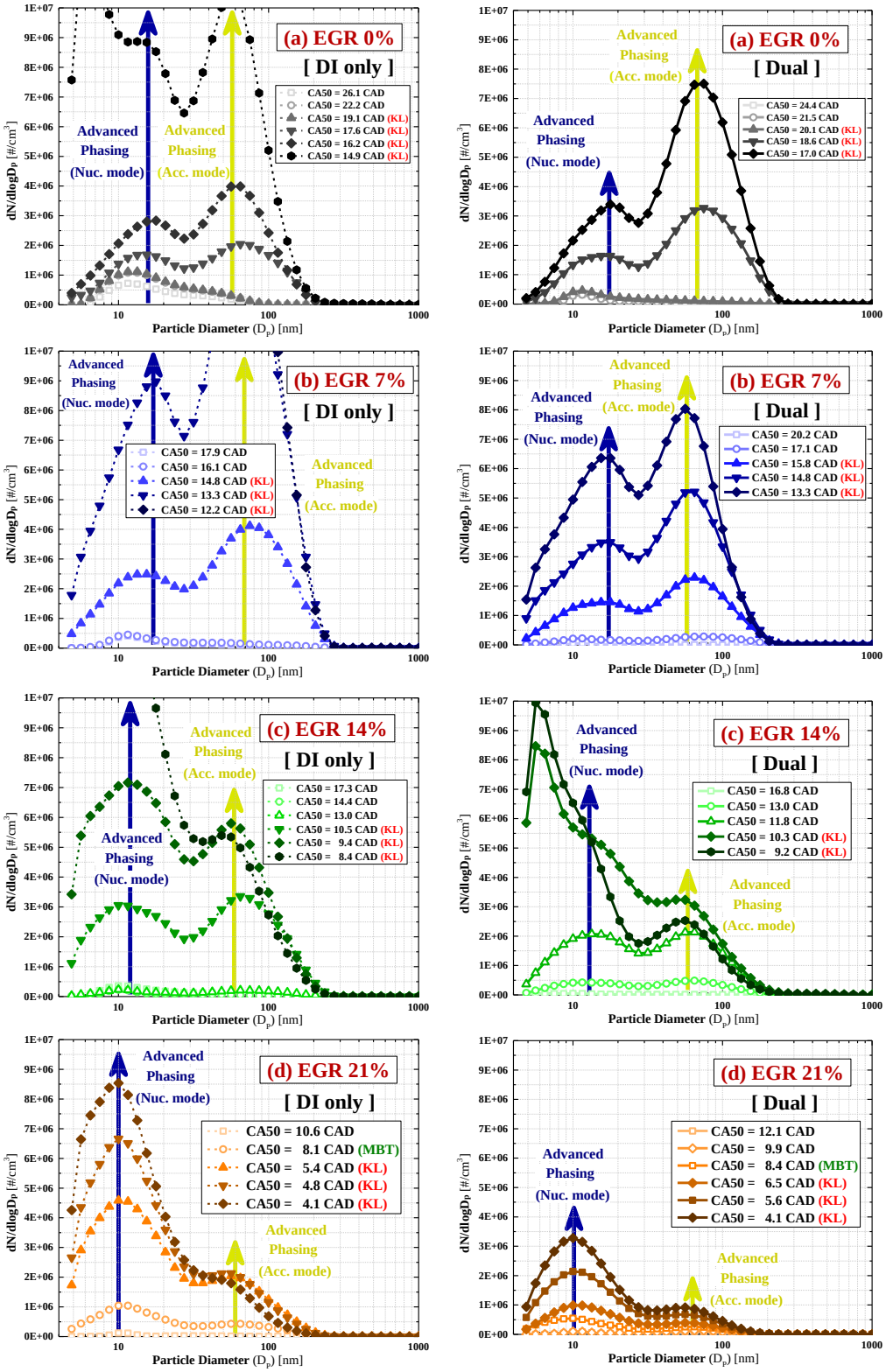

Figure 5.17 Size distributions of the particulate matter emissions where the left column presents the DI only data, the right column presents the dual injection data. For each column, the results for the different EGR levels are presented as: (a) EGR 0%, (b) EGR 7%, (c) EGR 14%, and (d) EGR 21%.

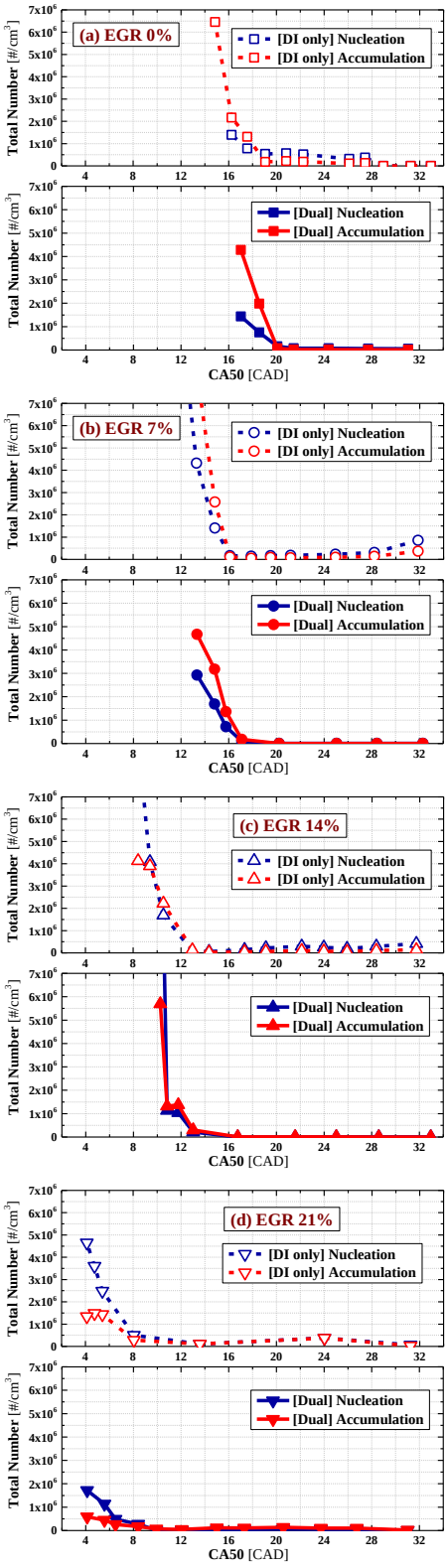

Figure 5.18 Comparisons of Nucleation and Accumulation mode concentrations as a function of combustion phasing (CA50) for both strategies. Each result for the different EGR levels are presented as: (a) EGR 0%, (b) EGR 7%, (c) EGR 14%, and (d) EGR 21%.

5.6.2 Gaseous Emissions

Figures 5.19 and 5.20 show the total hydrocarbon (THC) and nitrogen oxide (NO_x) emissions, respectively. The emissions were recorded 5 times at each test condition at intervals of 5 seconds, and the error bars indicate the standard deviation of the data. THC values increased with increasing EGR dilution, and this trend is consistent with the increased nucleation mode of the particulate matter emissions. Thus, the nucleation mode particles at the higher EGR condition are assumed to be predominantly unburned hydrocarbon droplets. Also, dual injection showed lower total hydrocarbon emissions than direct injection only in all conditions. Faster burn duration and slightly higher cylinder temperatures could help reduce the unburned hydrocarbon emissions.

The nitrogen oxide emissions clearly decreased with increasing EGR dilution ratio, which is attributed to the reduced maximum in-cylinder temperatures associated with dilution. Although the total mass of the fuel with dual injection is lower than with direct injection, the dual injection data showed similar or slightly higher (for the 14% EGR case only) nitrogen oxide emissions than direct injection only. This could be due to the higher unburned cylinder temperature for dual injection, offsetting the similar burned gas temperature.

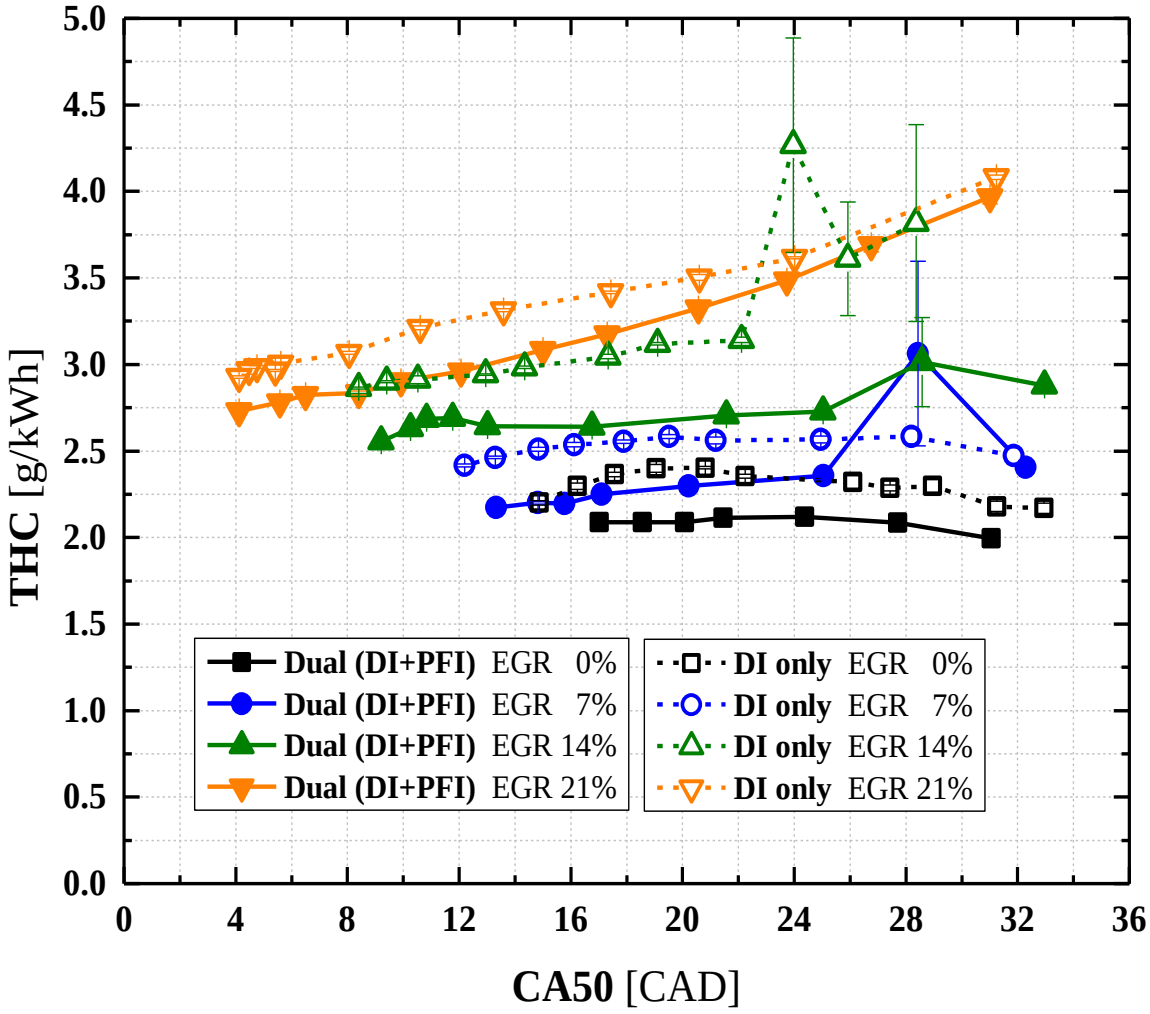

Figure 5.19 Effects of fuel injection strategy and EGR levels on indicated specific total hydrocarbon (THC) emissions

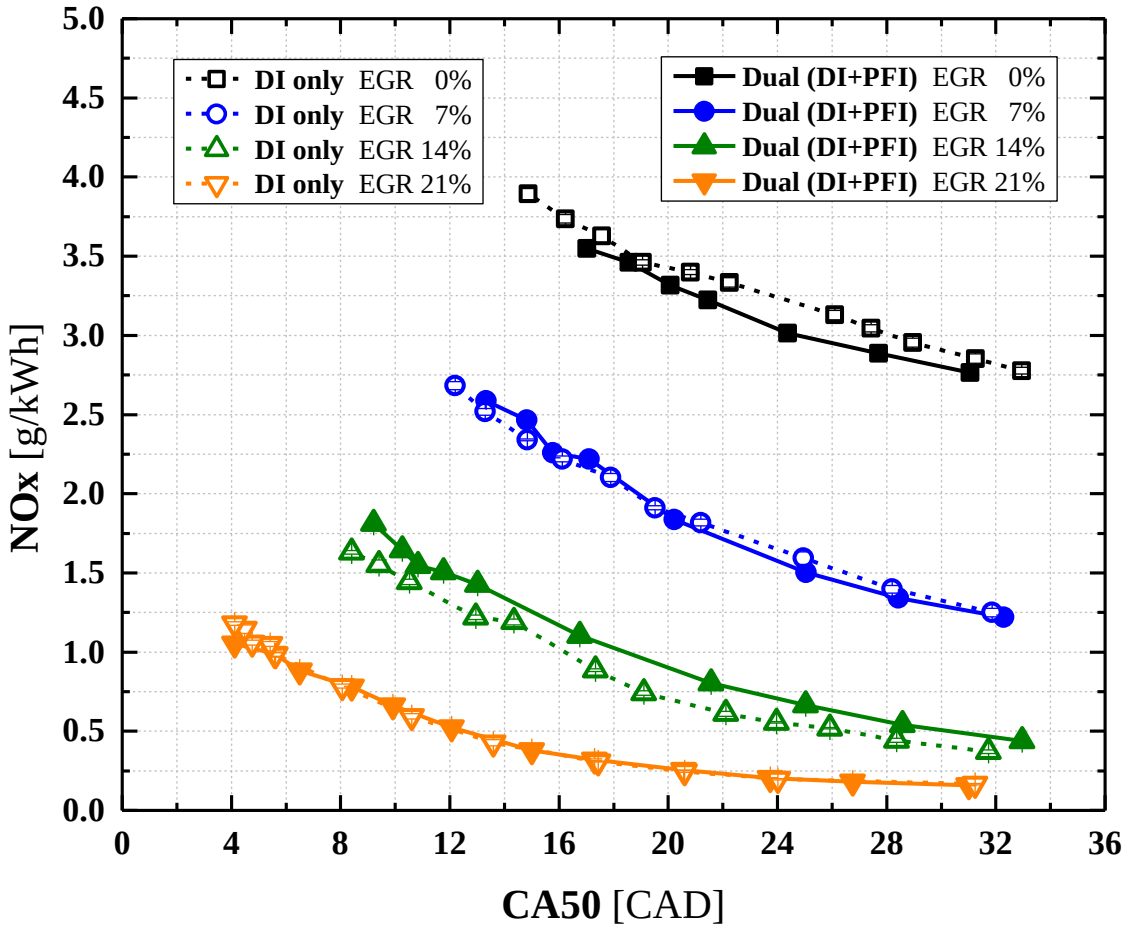

Figure 5.20 Effects of fuel injection strategy and EGR levels on indicated specific nitrogen oxide (NO_x) emissions

5.7 Conclusions and Summary

An experimental study of the effects of dual fuel injection on knock, efficiency, and EGR tolerance was performed and compared with a direct injection fueling strategy at various levels of EGR dilution. The most important conclusions of the study were the demonstration that the

dual fuel injection strategy improved combustion stability but did not extend the knock limit based on combustion phasing, and the overall thermal efficiency was comparable between the two injection strategies at all EGR conditions.

Based on the experimental results and analyses, the following additional conclusions are drawn:

- Dual injection with gasoline DI and ethanol PFI resulted in slightly later knock-limited combustion phasing compared with direct injection with E20 DI only. The knock intensity of dual injection based on identical phasing was higher than the knock intensity of direct injection.
- Dual injection showed lower volumetric efficiency than direct injection, likely caused by the enhanced charge cooling of direct injection and fresh air displacement of evaporated port injected fuel. Consequently, the gross IMEP for dual injection was proportionally lower than for direct injection.
- Burn duration represented by CA1090 for dual injection was slightly shorter than for direct injection. Estimated unburned gas temperature; however, was higher than for direct injection. The higher temperature was presumed to be the major reason for the increased knock vulnerability.
- With increasing EGR mass fraction, knock limited thermal efficiency increased linearly for both injection strategies. The benefit from the knock limit extension by EGR was more than two times higher than the dilution composition benefit.
- Using a 3% of CoV limit, the stability benefit of dual injection was higher at low dilution conditions. Faster burn duration of dual injection was assumed to be the major reason for the improved stability.

- Based on analysis of the combustion analysis, the port injected ethanol was most beneficial to the middle stage (CA0550) of combustion which includes flame propagation from the chamber to the near wall region.
- Particulate matter emissions dramatically increased after the knock limit in all cases. Particulate emissions for dual injection were slightly lower than for direct injection at knock limited conditions. This trend could be caused by less local fuel rich pockets and higher in-cylinder peak temperature.
- With increasing EGR, accumulation mode particulates decreased, and nucleation mode particles increased for both injection strategies.
- Total hydrocarbon emissions increased with increasing EGR for both injection strategies and were lower for dual injection compared with DI only injection.
- Nitrogen oxide emissions for dual injection were similar or slightly higher than for direct injection. NO_x emissions clearly decreased with increasing EGR.

Chapter 6

Multiple Injection for Improving Knock, Gaseous and Particulate Matter Emissions in Direct Injection SI Engines

6.1 Preface

This chapter is about the third strategic parameter about the multiple injection strategy. A conventional E10 fuel is used for investigating the effect of multiple injection on engine combustion and emissions. The abstract for this chapter is attached below.

Advances in fuel injector technology have enabled research and development on a large variety of direct injection spark ignition (DISI) engine fueling strategies targeted to improve engine performance and reduce engine-out emissions. This study explores the effect of multiple injections on knock, engine efficiency and stability, and particulate number and gaseous emissions on a single-cylinder research DISI engine. Work to date on multiple injections in the literature was reviewed, and then two aspects of multiple injection strategies were experimentally investigated: the number of injections (up to five times in a cycle); and the timing of the injections (classified relative to the timing of intake valve opening and closing). A boosted, single-cylinder research engine equipped with a state-of-the-art piezoelectric hollow cone spray direct injector and research grade E10 gasoline was used for the study. The results

show multiple injections maintain torque and combustion stability compared with single injection and increase the knock limits and thermal efficiencies (slightly, maximum 0.7% improvement based on absolute ITEg) due to improved heat release phasing, especially with an additional late injection during the intake valve closed (compression stroke) period. The gaseous pollutant emissions including nitrogen oxides and unburned hydrocarbons were significantly reduced with multiple injections (25% reduction for NOx and unburned hydrocarbons), particularly with injection during the compression stroke. In contrast, carbon monoxide emissions increased with multiple injections for all non-knocking conditions. Increasing the number of injection events significantly reduced particulate number emissions, and the decrease in particulate number was not a sensitive to the injection timing.

6.2 Introduction

The standards for engine efficiency and emissions are becoming more stringent due to rigorous emission regulations and the need for more fuel-efficient vehicles to reduce the carbon intensity of the transportation sector. Engine downsizing and boosting with direct injection in the spark ignition (SI) engine has been shown to be one of the most promising ways to overcome the limitations of traditional port injected, naturally aspirated SI engines, and to achieve the emissions standards [97–99]. By reducing cylinder displacement, the engine can be operated in a more efficient region at higher loads, and the relative friction losses are reduced compared with conventional SI engines. Also, by increasing the boost level, thermal efficiency increases due to the rise in volumetric efficiency and reduction in pumping losses [3,5,6]. With increasing boost level, however, knock propensity is severely increased due to the rise in pressure and

temperature of the mixture, and the increased knock limits the potential gains thermal efficiency, the higher pressure and temperature can also increase some pollutant emissions [7]. In order to mitigate knock and achieve other benefits, a common approach is to use direct injection of the fuel. Direct injection generally decreases knock by maximizing fuel charge cooling, which also improves volumetric efficiency compared with conventional port fuel injection engines [100,101]. Although direct injection in SI engines has been playing a significant role in knock mitigation, there still exists a gap for improving knock limits under boosted conditions. In addition, knock limit extension of direct injection engines has a significant impact on both gaseous and particulate matter emissions [7]. Thus, continuing research on injection strategies is essential to improving both performance and emissions of direct injection SI engines.

To date, a variety of injection strategies have been explored in the literature to improve both performance and emissions of direct injection in SI engines. One of the earliest trials for gasoline direct injection was charge stratification with enhanced flow, such as swirl and tumble. The knock free engine concept called the Texaco Combustion Process (TCP) stratified-charge engine [102–105] explored the operation of the combustion phase of the cycle with a spray guided diffusion flame for eliminating end-gas auto-ignition in the 1960~1970's. The TCP concept showed a noticeable improvement in fuel economy and air-toxic emissions but had critical limitations at cold start and with combustion stability. A decade later, the Programmed Combustion (PROCO) engine concept [106–108], which utilized gasoline fueled stratified charge with lean mixtures in a higher compression ratio engine, was introduced for improving fuel economy and emissions by Ford Motor Company. The PROCO engine concept demonstrated good attributes and was developed into multi-cylinder engines with further enhancements, such as dual spark plug, combustion chamber design, and so on. Around the same

time, several other stratified gasoline direct injection development efforts were undertaken, including work by Klöckner-Humboldt-Deutz [109], General Motors [110], Mitsubishi [111], Maschinenfabrik Augsburg-Nürnberg [112], Ricardo [113], Southwest Research Institute [114], and others [115]. Although all these efforts made noteworthy progress in both efficiency and emissions, the commercialization of direct injection SI engines was not smooth at that time, due to a lack of sufficiently robust fuel injector technology with regard to precise real-time control, nozzle design, proper fuel atomization, durability, and so on. In particular, the mechanically driven direct injectors could not fully overcome the major problems associated with fuel stratification, such as lower stability, higher hydrocarbon emissions, and soot deposition near the injector holes. Thereafter, gasoline direct injection development hit a lull and most of the direct injector studies were focused in the field of diesel engines. In the early 2000's, interest in direct injection strategies for gasoline spark ignition engines re-emerged to replace port fuel injection with direct fuel injectors that were more robust and more durable than their predecessors.

As gasoline direct injectors were being commercialized and injector technologies were developed, more effective solutions for combustion and emission problems became necessary. One of the fuel injection strategies with the greatest potential to optimize direct injection engine performance and emissions is multiple injection (or sometimes called split injection), which injects fuel multiple times in a cycle, and has been applied in recent gasoline direct injection engines. Originally multiple injection was developed for improving soot and nitrogen oxide emissions in diesel engines via pilot or post injections [116,117], and such strategies achieved good results not only in emissions but also in engine combustion quality and noise [118,119]. So, multiple injection strategies have become an important element of engine calibration strategies in compression ignition engines and have led to efficiency improvement, soot reductions,

expansion of the use of alternative fuels, and other developments [120–124]. The application of multiple injection in spark ignition engine, however, has not been as thoroughly studied to date, and the potential of advanced fuel strategies merits further exploration. To date, only partial multiple injections and limited strategic approaches have been implemented in production engines to mitigate as cold start problems [125,126], and most of strategies have been developed for solenoid type injectors with six to eight hole injector designs. Recently, fast piezo-electric type direct injectors with hollow cone sprays have become available with capability for up to five injections per cycle [127]. Piezo-electric injectors offer the opportunity to compare the effects of multiple injection strategies with different fuel spray development characteristics than the solenoid-type sprays.

Hence, the objective of the current work is to summarize the state of understanding of the effects of multiple injections on SI engine performance and to experimentally characterize and compare the effect of multiple injections from a piezo-electric injector on knock limits, engine performance, and gaseous and particulate matter emissions. Specifically, the effects of two primary factors were experimentally analyzed in depth: the number of fuel injections; and the injection timing (relative to the intake valve opening and closing). The information provided here is intended to offer strategic guidelines for operating the multiple injections in direct injection spark ignition engines.

6.3 A Review of Multiple Injection Studies in SI Engines

Various aspects of multiple injection studies for gasoline direct injection engines have been explored over the past decade via both simulation and experiment. However,

comprehensive and strategic studies on multiple injection effects are still lacking for many important hardware configurations, like cone spray injectors. Previous work on multiple injection studies that have been reported to date are summarized here, particularly with respect to learning on spray mixing characteristics and engine performance (e.g., thermal efficiency, engine out emissions, etc.) via physical experiments and computational engine simulations.

6.3.1 Previous Studies of the Benefit of Multiple Injection

6.3.1.1 Improving Charge Composition Homogeneity

In contrast to the fully stratified charge combustion concept, in-cylinder mixture homogeneity is one of the most important factors for stoichiometric spark ignition combustion with regard to pollutant emissions and engine performance. It is generally known that late fuel injection causes more uneven in-cylinder mixtures compared with an early single fuel injection near the intake valve opening event. But using a partial late injection through split injection, homogeneity can be improved for several reasons.

Li et al. [128] studied the effects of multiple injection on the mixture formation process using several laser sheet imaging techniques (laser induced fluorescence (LIF), particle image velocimetry (PIV), and laser absorption scattering (LAS)). They compared single and double injection with varying the dwell time between the first and second injection, and three major findings were determined to explain the improved homogeneity observed with multiple injection. The first observation was reduced high density liquid droplets on the leading edge of the first spray, so the total leading-edge area could be doubled by split injection regardless of the mixture flow. Another observation was the increased radial width of each spray plume due to the interaction between the second spray and the air flow induced by the first spray. The interaction

promoted the second spray edge evaporation and the region of lean mixture (i.e. charge with a fuel-to-air equivalence ratio of $\phi < 0.7$) was significantly reduced. The last observation was the combustible mixture region (where ϕ is between 0.7 and 1.3) was expanded with multiple injection, and this phenomenon was also found in their stratified charge spray observations [129,130].

Imaoka et al. [131] conducted multiple injection experiments using LIF visualization and numerical simulations. A homogeneity index, which uses the ratio of the average to the standard deviation of the equivalence ratio distribution on the piston plane cross section, was introduced in the study, and the results showed that around 4% of the homogeneity index was improved in the triple injection case compared with single injection based on the fixed center of injection timing. Serras-Pereira et al. [132] compared the spray formation between early single injection and split injection using a very late second injection using optical imaging. Although their experimental set up was intended to realize semi-stratification, the flame radius with double injection showed higher growth ratio than single injection due to the elimination of a lean zone (improved homogeneity) near the spark plug.

6.3.1.2 Enhancing Turbulence

Turbulence including swirl and tumble is also a key factor for improving performance, knock, and emissions in spark ignition engines. Kim et al. [133] studied the effect of double injection on in-cylinder turbulence using numerical simulation and optical engine experiments. Two double injection cases were compared using different dwell times between the first and second injections. Both experimental and simulation results agreed that multiple injection improves turbulent intensity, and the short dwell time case showed higher turbulence ratio than the long dwell time case. Their observation, however, showed decreased compositional

homogeneity with maximized turbulence unlike the other studies summarized above. The discrepancy may be because the first injection timing was relatively late (in the middle of intake), and this agrees with a similar study conducted by Song et al. [134]. Thus, optimization of the first injection timing also could be an important factor for improving both turbulence and homogeneity.

6.3.1.3 Lowering Fuel Impingement on Combustion Chamber and Piston Surfaces

Piston and cylinder wall impingement are known as the primary reasons for particulate matter emissions from SI engines due to the formation of a local fuel rich zone or pool fires. Studies on the relationships between multiple injections and fuel surface impingement have been actively conducted to date.

Wang et al. [135,136] studied spray characteristics of split injection under different flash boiling conditions using a high pressure vessel. They observed substantially shortened total spray penetration length as well as reduced spray impingement on the impact wall in the vessel with a double injection strategy. Also, they showed the dwell interval between the first and second injections could affect the rate of fuel film development on the wall, and that a longer dwell interval tends to reduce fuel films from the second injection due to better flash boiling. Similarly, Li et al. [129,137] experimentally observed the reduced penetration length and increased radial width of the spray using multiple injections.

Seo et al. [138] conducted an impingement study of multiple injections using engine computational fluid dynamics simulations. The amount of liquid fuel film on the piston was simulated by varying the second injection mass ratio using fixed injection timing. The results showed that a higher amount of fuel in the second injection (up to 70%) generates less liquid film on the piston, but an overly high amount of second injection mass increases total engine-out

particulate emissions cause by lowering the mixing rate. So, proper mass distribution is recommended for both performance and emissions. Su et al. [139] conducted a similar simulation study, considering up to triple injection, and they also claimed that reducing the first injection mass (down to 40% by mass) is beneficial for lowering particulate emissions for both double and triple injections.

6.3.1.4 Maximizing Charge Cooling Effects

Knocking in SI engines is closely related to the in-cylinder temperature especially near the end-gas region, and the average in-cylinder temperature can be lowered by maximizing charge cooling. Charge cooling effects can be improved by later injection, especially after the intake valve closing time, but it has been difficult to realize the benefit with conventional single injection, due to incomplete combustion with retarded start of injection (SOI). By adopting multiple injections, knock limit extension is possible with partial late injections. Yang and Anderson [140] introduced this concept a couple of decades ago, and they conducted engine experiments by comparing PFI (Port Fuel Injection) and DI (Direct Injection) with single and double injection. Their results showed that multiple injection with an optimized injection mass ratio of 2:1 and timing of 270:150 before top dead center (bTDC) improved indicated mean effective pressure (IMEP) by about 2 ~ 3% compared with single injection, possibly due to the charge cooling. Later, studies on the relationship between multiple injection and knock re-started. Imaoka et al. [131] studied the effects of single, double, and triple injection on charge cooling. The results showed charge cooling efficiency was improved with more injections, possibly due to lowered cylinder temperature and pressure, but pressure oscillations related to instability increased. Wei et al. [141] also conducted engine experiments which showed some potential for extending knock limits with multiple injections, and their results showed improved

engine stability with double injection regardless of the injection timing in contrast with the study of Imaoka et al. [131]. Thus, more research is needed regarding spark knock and multiple injection strategies.

6.3.2 Engine Performance

6.3.2.1 Thermal Efficiency and Fuel Consumption

Few studies have considered the thermal efficiency and fuel consumption benefits of multiple injection. The work that has been reported suggests there is a small efficiency improvement, unless one changes combustion modes, such as via dilution or lean stratification, or changes the hardware, e.g. increase the compression ratio. Based on the literature on this topic, the mechanisms of multiple injections for improving thermal efficiency can be divided into three major categories: combustion quality improvement (e.g., higher combustion efficiency, faster burn duration, and so on); knock limit extension; and combustion mode changes (e.g., lean stratification, etc.)

Duan et al. [141] studied the effect of double injection on engine combustion using six conditions, in which they varied the second injection mass fraction and timing with fixed first injection and spark timing. All cases showed slightly higher thermal efficiency except for late second injection with large fuel mass, and this trend agreed with the combustion efficiency trends. For fixed spark timing, the thermal efficiency benefit is affected by not only combustion efficiency, but also by advanced phasing and slightly shortened burn duration. Singh et al. [127] comprehensively studied multiple injection effects in a multi-cylinder engine, from single to quadruple injection using gasoline piezo-electric injectors. The maximum achievable thermal efficiency also improved slightly under multiple injection conditions due to improved

combustion efficiency, and the effects were more effective under boosted condition. While multiple injections had lower impact on improving thermal efficiency, engine-out emissions were dramatically improved for CO, unburned hydrocarbons, and particulate number. However, NOx emissions increased slightly with multiple injections.

In the work by Wei et al. [142], the authors demonstrated knock limit extension and improved the thermal efficiency (1.2% brake thermal efficiency improvement with optimized double injection), which they attributed to charge cooling. Imaoka et al. [131] showed about 5 g/kWh reduced fuel consumption rate with the triple injection strategy.

Thermal efficiency improvement through different combustion modes is also one of the major benefits of multiple injections. Zeng and Sjöberg [143] explored double injection benefits for stratified charge combustion modes with lean charge and dilution using exhaust gas recirculation (EGR). Higher indicated thermal efficiency was achieved, up to 40%, with optimized injection timing for combustion stability and emissions. Costa et al. [144] and Oh et al. [145] also demonstrated the benefits of a lean stratified engine combustion with improved efficiency and emissions.

6.3.2.2 Fuel Compatibility

A greater choice of gasoline fuels is available worldwide, so fuel compatibility studies in combination with fuel injection strategies have been an important factor in SI engine development. One of the most popular alternative fuels is ethanol, and the effects of multiple injections using ethanol have been explored recently. Turner et al. [146] studied different bio-ethanol blend ratios under multiple injection conditions, and showed the oxygenated fuel benefits are maintained under multiple injection conditions. Singh et al. [127,147] also studied ethanol compatibility for multiple injection strategies varying the ratio of ethanol up to 85 percent, and

the benefits of multiple injections on engine efficiency were consistent at different ethanol blending ratios.

Merola et al. [148] examined the compatibility of pure n-butanol fuel with double injection in an optical engine, and the engine combustion results showed that the multiple injection benefits could be even greater with the alternative fuel compared with conventional gasoline due to better mixture formation and fuel evaporation. Daniel et al. [149] also studied two alternative fuels (2,5-dimethylfuran and ethanol) and compared the results with conventional gasoline. The benefits of multiple injections were obtained for engine combustion and emissions for the alternative fuels with proper optimization of the injection strategy.

6.3.3 Engine-out Emissions

6.3.3.1 Gaseous Emissions

The benefits of multiple injections on regulated gaseous emissions such as nitrogen oxides, carbon monoxide, and unburned hydrocarbon emissions have been reported in several studies. Most of the results showed the potential of multiple injections for reducing nitrogen oxides emissions due to the reduced in-cylinder temperatures [141,150], and for reducing carbon monoxide, and unburned hydrocarbons emissions [127]. One noteworthy observation, however, is that most of the results showed trade-offs with regard to the gaseous pollutant emission, but not all pollutant emission reductions. So, detailed optimization for emissions appears to be necessary to avoid uneven emissions outcomes.

6.3.3.2 Particulate Matter Emissions

One of the major benefits of multiple injections is a reduction of particulate matter emissions. He et al. [151] reported the effect of split injection on particulate matter emissions at different loads. Their results showed total particulate number concentration was reduced by half using double injection under high load conditions, but that the reduction was not as significant under low load conditions. Costa et al. [152] also showed reduced particulate matter emissions for homogeneous stratified lean combustion using an optically-accessible gasoline direct injection (GDI) engine and numerical simulation. They attributed the lower particulate emissions to reduced piston wall films caused by lowered fuel impingement. In contrast, Park et al. [153] showed somewhat increased particulate matter emissions using multiple injections with a direct-injection spark-ignition (DISI) engine and gasoline fuel, although the results could have been due to the higher second injection mass used. The prior work demonstrates that well-designed injection strategies are necessary for particulate matter reduction.

6.4 Experimental Details

6.4.1 Engine and Fuel Specifications

A boosted Ricardo Hydra single-cylinder research engine was used to explore the effect of multiple injections on performance and emissions in this study. The pent-roof design of the cylinder head included a centrally mounted direct injector (Bosch HDEV4) and side-mounted spark plug. The direct injector was a piezoelectric injector and produced a hollow cone spray with a maximum 30 mm penetration length. The fuel supply system for direct injection used a fuel flow meter to calculate the air-fuel equivalence ratio in conjunction with an air mass flow

meter (Fox Instruments FT2). The air to fuel equivalence ratio was confirmed by the measured gaseous emissions using an emissions bench (Horiba MEXA-7100DEGR) and a lambda meter (ETAS LA4) with a lambda sensor (Bosch LSU 4.9) in the exhaust runner.

The compression ratio of the engine was 10.5:1 with 0.5-liter displacement volume. The valve timing was fixed for all experimental conditions, and the valve opening duration was 226 crank angle degrees for both the intake and exhaust valves based on 0.5mm valve lift. Additional specifications are summarized in Table 6.1.

Figure 6.1 shows a schematic diagram of the boosted Hydra single-cylinder research engine and supporting facilities. Intake air was compressed and filtered, and the pressure was regulated using a pneumatic valve downstream of the air filters to maintain the target intake pressure at the intake plenum. The air supply system to the engine intake included a by-pass heater and cooler located upstream of the intake plenum to maintain constant intake air temperature. Engine oil and coolant were conditioned by external systems to maintain constant temperature, and an oil filter was located in the oil conditioning system.

Table 6.1 Engine geometry and specifications for Chapter 6

Parameter	Value
Displaced Volume	500 cm^3
Bore / Stroke	86 mm / 86 mm
Connecting Rod	143 mm
Compression Ratio	10.5 : 1
Intake Valve Timing	IVO 362 / IVC 136 bTDCign
Exhaust Valve Timing	EVO 138 / EVC 364 aTDCign
Head Design	Pent-roof
Number of Valves	4
Spark Plug	Side mounted
Direct Injector	Bosch HDEV4 piezoelectric spray guided injector. Hollow-cone spray (85° ± 5° spray angle)

The engine operating parameters were controlled using an in-house developed National Instruments (NI) Labview field-programmable gate array (FPGA) and real-time programs. The hardware was accompanied by eight digital and analog input and output modules in a compact real-time controller (cRIO). The engine operating program allowed control of spark timing, fuel injection timing, and fuel injection duration for the direct injector. The low-speed data including temperature, pressure, air and fuel flows, etc., were recorded using NI modules and signal conditioning extension for instrumentation (SCXI) systems.

A Horiba MEXA-7100DEGR was used to measure the gaseous emissions. NO_x, CO, CO_2, O_2, and total hydrocarbon (THC) emissions were measured and the air to fuel equivalence ratio (λ) was determined using the gaseous emissions bench. Exhaust gases were sampled from the center of the exhaust plenum through a perforated tube and transferred to the emission analyzers using a heated filter and heated sample line.

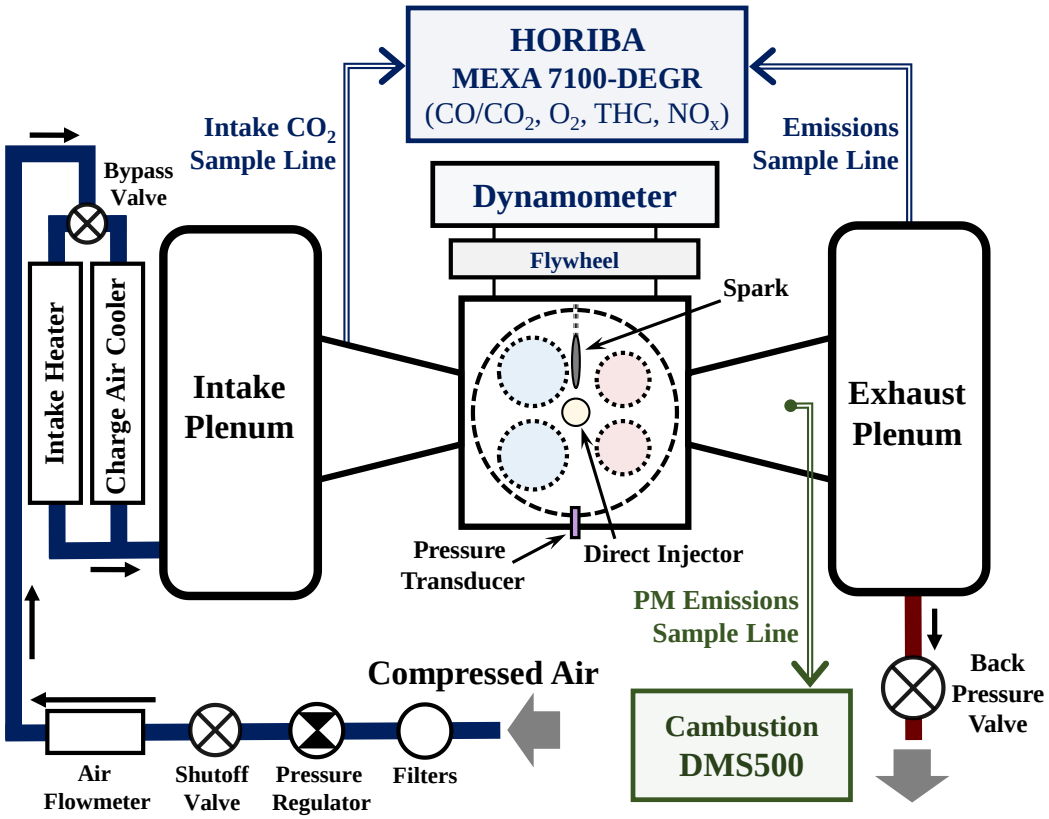

Figure 6.1 Schematic of the boosted Ricardo Hydra single cylinder DISI (Direct Injection Spark Ignition) research engine

Table 6.2 Fuel specification for Chapter 6

Fuel Properties *	**Gasoline (E10)**
Carbon (Wt%) [a]	81.94 % m/m
Hydrogen (Wt%) [a]	14.43 % m/m
Oxygen (Wt%) [b]	3.63 % m/m
Ethanol (C_2H_5OH) Contents [b]	10.46 % m/m (9.66 % v/v)
Research Octane Number [c]	98.7
Motor Octane Number [c]	90.0
Sensitivity (R-M) [c]	8.7
Gross (Higher) Heating Value [d]	45.14 MJ/kg
Net (Lower) Heating Value [d]	42.08 MJ/kg
Density at 60.0°F [e]	0.7329 g/mL

*Analytical results of Paragon Laboratories, Livonia, MI, USA. (2018)

[a] ASTM D5291 [b] ASTM D4815 [c] ASTM D2699/D2700

[d] ASTM D240 [e] ASTM D4052

Particulate matter emissions including particle number (PN) concentration and size distribution were measured using a fast particulate analyzer (Cambustion DMS500 mk2). The measurement range for particle size was from 5 nm to 1000 nm (1 μm) with two-stage dilution. For all engine conditions, the samples were diluted with heated dry air (150 °C) in the first stage with 6:1 dilution ratio to prevent condensation of hydrocarbons and water and to prevent significant particle agglomeration. The samples were diluted with dry air at the second dilution stage with 1:1 dilution ratio. The first stage inlet flow was regulated to 8 liter per minute with a 1.0 mm size orifice and cyclone to capture large particles. Exhaust samples were collected from the exhaust side runner with a 0.25 inch (6.35 mm) diameter insulation stainless steel tube. All

data were collected at a sampling rate of 0.1 Hz for 50 seconds and subsequently averaged, and the standard deviation calculated.

The gasoline fuel used in the study was a research grade E10 gasoline (gasoline with 10 volumetric percent of ethanol). The research octane number was 98.7 and motor octane number was 90.0 (sensitivity of 8.7). The fuel analytical results from Paragon Laboratories are summarized in Table 6.2.

6.4.2 Combustion Analysis and Knock Quantification

High-speed in-cylinder pressure data were sampled for 200 cycles at 0.1 crank angle degree resolution using a pressure transducer (Kistler 6125A piezoelectric) which was located on the side of the cylinder head. The pressure signal was amplified (AVL IFEM) and recorded (AVL Indiset module) with a crank angle encoder signal (AVL 365C01). The high-speed intake and exhaust pressure data were also measured for heat release analysis using piezo-resistive transducers (Kistler 4007 and 7533A water cooled) at the same resolution in the intake and exhaust runner.

A two-zone heat release analysis code for spark ignition engines was used to calculate combustion rates and in-cylinder temperatures with estimated mixture specific heat ratio and residual gas fraction. A detailed analysis description of the code and validation results can be found in Ortiz-Soto et al. [23]. Calculations were performed for all 200 cycles of the cylinder pressure data, and a 3.5 kHz low pass filter was applied to the in-cylinder pressure data prior to conduct analysis. For each cycle, a standard Woschni [154] heat transfer correlation with variable mixture properties was used to calculate the gross heat release rate and mass fraction

burned. Combustion parameters including phasing and burn duration were calculated for each cycle and then the average and standard deviation values were determined for all cycles. The internal residual fraction, defined as the mass of fuel and air charge remaining in the cylinder from the previous cycle relative to the total mass of the initial fuel and air charge was estimated for each cycle using the state equation method under positive valve overlap condition.

Knocking and combustion stability results are sensitive to the surrounding environment, so each set of the experiments was repeated three times on different days. Knock was measured two separate ways for each experiment: the first using audible knock during the experiments with a microphone and speaker in the control room; and the second using knock intensity calculations based on the in-cylinder pressure data from each cycle.

A peak-basis knock intensity calculation method called 'KI peak to peak' was used for knock quantification. The process of calculating the 'KI peak to peak' involves filtering the raw pressure signals using a 3.5 kHz high pass filter and fast Fourier transformation (FFT). After applying the FFT, the difference between the maximum to minimum peak of the filtered pressure using Equation 6.1.

$$\mathbf{KI}_{\mathbf{peak\ to\ peak}} = \left| \left(\boldsymbol{max} \{ \boldsymbol{p(i)} \} \right) - \left(\boldsymbol{min} \{ \boldsymbol{p(i)} \} \right) \right| \qquad (6.1)$$

In Equation 6.1, *p(i)* indicates the filtered pressure and '*i*' is the crank angle degree. The range of '*i*' is set from -20 TDCign to +70 TDCign, to avoid noise from other sources such as intake and exhaust valve closing signals. Signal oscillation caused by the valve closing is occasionally higher than the knocking oscillation in lower knocking cycles. The detailed calculation including FFT filtering guideline and validation with other knock quantification

methods is described in Han et al. [15]. The knock threshold value of 'KI peak to peak' was set at 0.42 bar in this study.

6.4.3 Experimental Conditions

In all tests, the intake and exhaust pressure were set to 1.20 bar (boosted condition) and 1.05 bar, respectively, and the global air-to-fuel equivalence ratio was maintained at 1.00. Spark dwell time was held constant at 2.22 ms which is equivalent to 20-crank angle degree at an engine speed of 1500 rpm with constant ignition energy. The fuel rail pressure was held at 200 bar with an external high-pressure nitrogen cylinder and an accumulator. The fixed operating conditions are summarized in Table 6.3.

Table 6.3 Engine experimental condition

Parameter	Value
Engine Speed	1500 rpm
Fuel Rail Pressure	200 bar
Air/Fuel Equivalence Ratio (λ)	1.00
Spark Dwell Time	2.22 ms (20 CAD at 1500 rpm)
Intake / Exhaust Pressure (abs)	1.20 bar / 1.05 bar
Intake Air Temperature	26.0 °C ± 0.5 °C
Coolant Temperature	85 °C
Oil Temperature	85 °C

6.4.3.1 Start of Injection (SOI) Effects

Prior to the design of the experimental conditions, a start of injection (SOI) study was performed to determine the proper injection timings for multiple injection strategies, with regard to engine combustion and emissions. The SOI timing was changed from 360 bTDC to 80 bTDC in 20 degree increments with the same spark timing (22 bTDCign). Figure 6.2 shows the engine combustion and emissions results, and Figure 6.2 (a) depicts the effect of SOI on the subsequent phasing of 5% mass fraction burned, 10% burned, 50% burned with standard deviation, and 90% burned at the same spark timing. Combustion phasing and burn duration was relatively consistent from the intake valve open (IVO) timing to right before intake valve close (IVC) timing, but increased after ~160 bTDC injection. Combustion stability also decreased after 160 bTDC injection. Figure 6.2 (b) indicates particulate matter (PM) emissions (left vertical axis) and nitrogen oxides emissions (right vertical axis) as a function of single SOI timing. PM emissions were very high for injection before TDC due to significant piston impingement, and PM emissions return to more moderate emissions near 300 bTDC. But the PM emissions showed a small peak between the 260 to 220 bTDC in the IVO range, and this trend consistent with other test conditions. This peak is presumed to be due to valve impingement of the fuel spray plume for this particular engine design. Particle number emissions started to increase from the IVC timing near 140 bTDC. The nitrogen oxide emissions showed similar trends as the PM emissions and decreased after IVC timing due to decreased cylinder peak temperature. Based on these results, the proper SOI timing for multiple injection was set as 280 bTDC for the main injection with additional injections between 200 and 160 bTDC during the intake stroke.

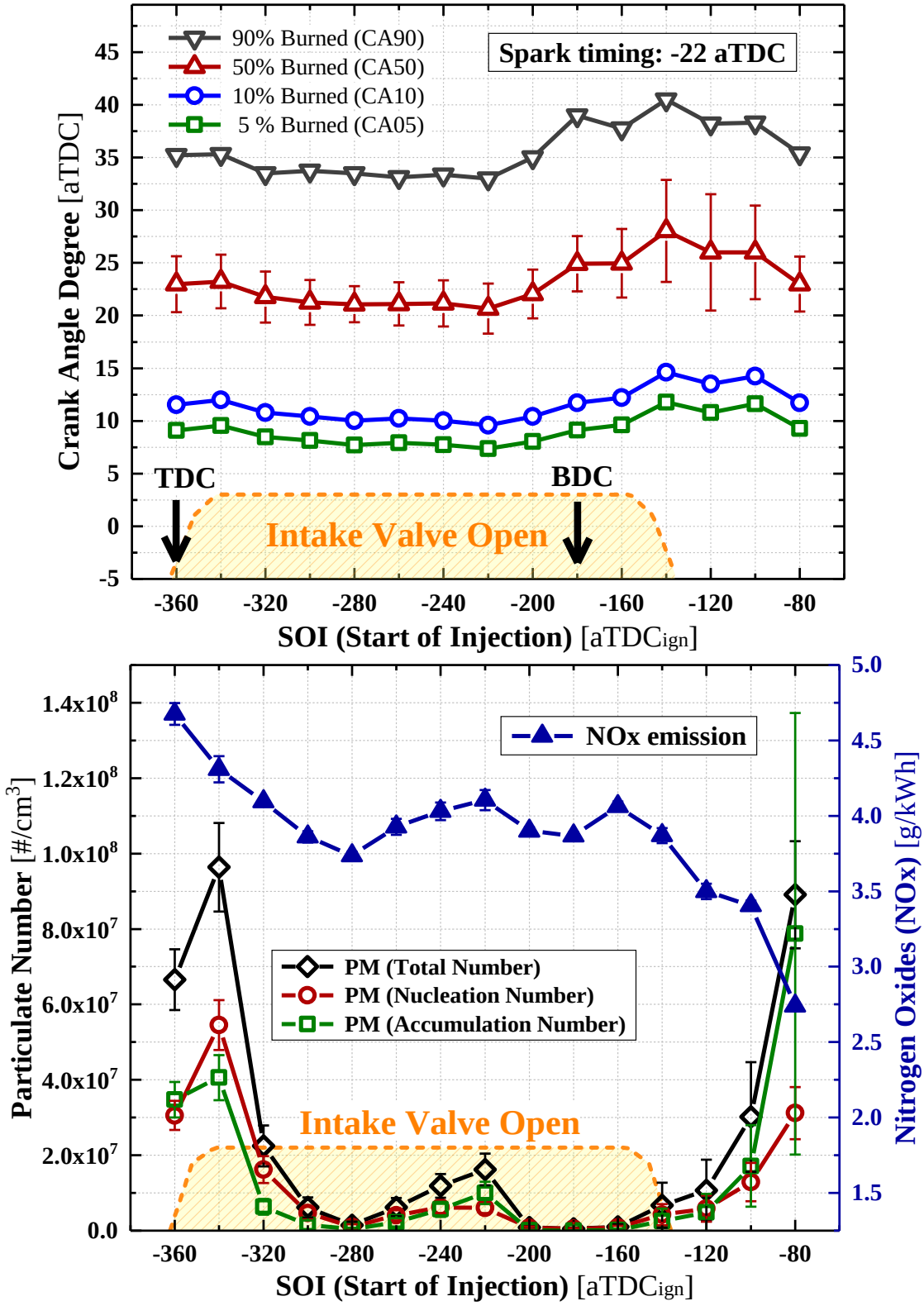

Figure 6.2 Burn durations and emissions results as a function of SOI timing with single injection

6.4.3.2 Experimental Design by Injection Region and Number

In order to investigate the effects of multiple injections on both combustion and emissions, two major variables were considered based on guidance from the literature and the single injection tests. The first variable was the number of injections in a cycle, and the other was the injection timing based on the region. The injection timing was divided into two regions in crank angle space, based on IVC timing. Figure 6.3 shows a schematic of the regions used in the study: 'Region I' which includes the intake stroke region (before IVC) and 'Region II' which includes the compression stroke (after IVC). Three cases varying the number of injections for each region were studied. Specifically, the cases were single, double, and quadruple injections for 'Region I', and double, triple, and quintuple injections for 'Region I + II'. The notation '+1' indicates the 'Region II' injection while holding the injection timing in the 'Region I' constant. The main/first injection timing was set to 280 bTDC, and the second injection timing was set to 180 bTDC, based on the experimental results from the preliminary single-injection timing study. The quadruple injection timing was the same as the double injection timing, but each of the double injections were separated into two injection events each with a 20 crank angle degree separation to the start of the injection events. Specifically, the quadruple injection timing was set to 290, 270, 190, and 170 bTDC. For the 'Region II' injections, the timing was set to 100 bTDC for all compression stroke cases.

The detailed experimental conditions are summarized in the Table 6.4 including the injection fuel mass ratios used. The amount of injected fuel mass was equally distributed in 'Region I', and when the 'Region II' was activated, the 'Region II' injection amount was fixed to 33.3%, and the rest of the fuel mass was equally distributed, as in the 'Region I' cases.

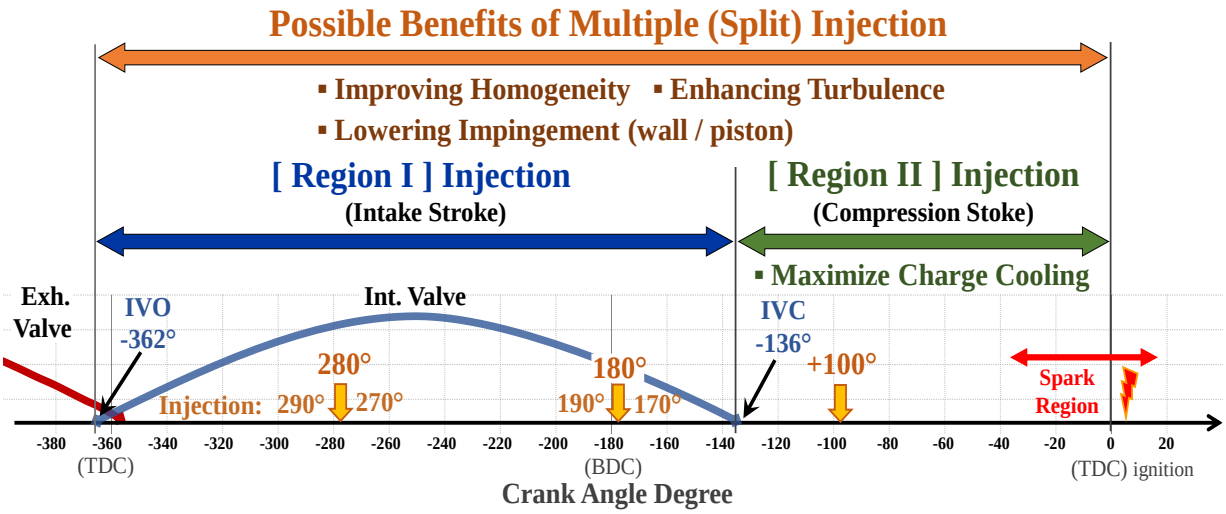

Figure 6.3 Schematic of the regions and potential benefits of different injection strategies as a function of cycle timing [CAD]. Timing of important events such as spark timing and valve events are also provided for reference.

Table 6.4 Experiment conditions for the region-based injection strategies.

Injection Region	**Injection Event** (# of injection)	**SOI** [bTDC]	**Injection Mass Ratio** (Σ = 100 %)
Region I (Intake Stroke)	**1 inj.**	280	100 %
	2 inj.	280 & 180	50 % × 2
	4 inj.	290 + 270 & 190 + 170	25 % × 4
Region I + II (Intake and Compression Stroke)	**1 + 1 inj.**	280 + 100	66.6% × (100 %) + 33.3 %
	2 + 1 inj.	280 & 180 + 100	66.6% × (50 % × 2) + 33.3 %
	4 + 1 inj.	290+270 & 190+170 + 100	66.6% × (25 % × 4) + 33.3 %

6.4.4 Uncertainty Analysis

Uncertainty analysis was performed to determine the precision and repeatability of the experimental results, for example, combustion phasing, efficiencies, and emissions based on the square root of the variance method described by Moffat [24], which is explained in the Equation 6.2.

$$\delta \boldsymbol{R} = \sqrt{\sum_{i=1}^{N} \left(\frac{\partial \boldsymbol{R}}{\partial \boldsymbol{X}_i} \, \delta \boldsymbol{X}_i \right)^2} \qquad (6.2)$$

Each individual term in the parenthesis was combined by a root sum square method, and the result represents the contribution made of the uncertainty in the variable, δX_i, to the overall uncertainty of the result δR. Each term has the same form: the partial derivative of R with respect to X_i multiplied by the uncertainty interval for the variables. The number of samples N was 200 for the high-speed data such as the in-cylinder pressure data, and five for the gaseous emissions with a 5 second sampling interval, and six for the particulate matter emissions with 10 seconds interval.

6.5 Engine Combustion and Knock

6.5.1 Combustion Phasing and Knock Limit

In order to find the maximum brake torque (MBT) or knock limited (KL) conditions for each injection case, spark timing was adjusted from 18 bTDC to 30 bTDC at a boosted intake

air-pressure of 1.2 bar. Figure 6.4 shows the combustion phasing (i.e., CA50) and knock limited data as a function of spark timing. The solid lines with filled symbols are the 'Region I' injections (with 1, 2, and 4 injections), and the dashed lines with open symbols are the 'Region I + II' injections (i.e., using the 'Region I' strategy with an additional 100 bTDC injection in 'Region II' for a total of 2, 3, and 5 injections; see Figure 6.3 and Table 6.4). For the line and symbol colors, single, double, and quadruple injections are black, blue, and green color, respectively, and the red symbols indicate the knocking points. The error bar is the uncertainty for 200 cycles described in Equation 6.2, and all graphs in this study follow the same formatting. To clearly compare the 'Region I' and 'Region I + II' injection strategies, the six relevant cases are separated into the top three panels of Figure 6.4 (a), (b), and (c). The results show that regardless of the use of 'Region II' injection, the combustion phasing was almost identical, except for the knock limits. The amount of extended knock limited spark advance (KLSA) enabled via 'Region II' activation was identical for the different injection strategies except for the quadruple injection case. The exception for quadruple injection is likely because quadruple injection in 'Region I' already extended the knock limit by one CAD. The bottom two panels of Figure 6.4, (d) and (e), compare the number of injections results for 'Region I' and 'Region I + II', respectively. The combustion phasing differences were also within the uncertainty intervals for these cases, and the knock limit differences were negligible, except for slight (1 CAD) extension with the quadruple injection in the 'Region I' case.

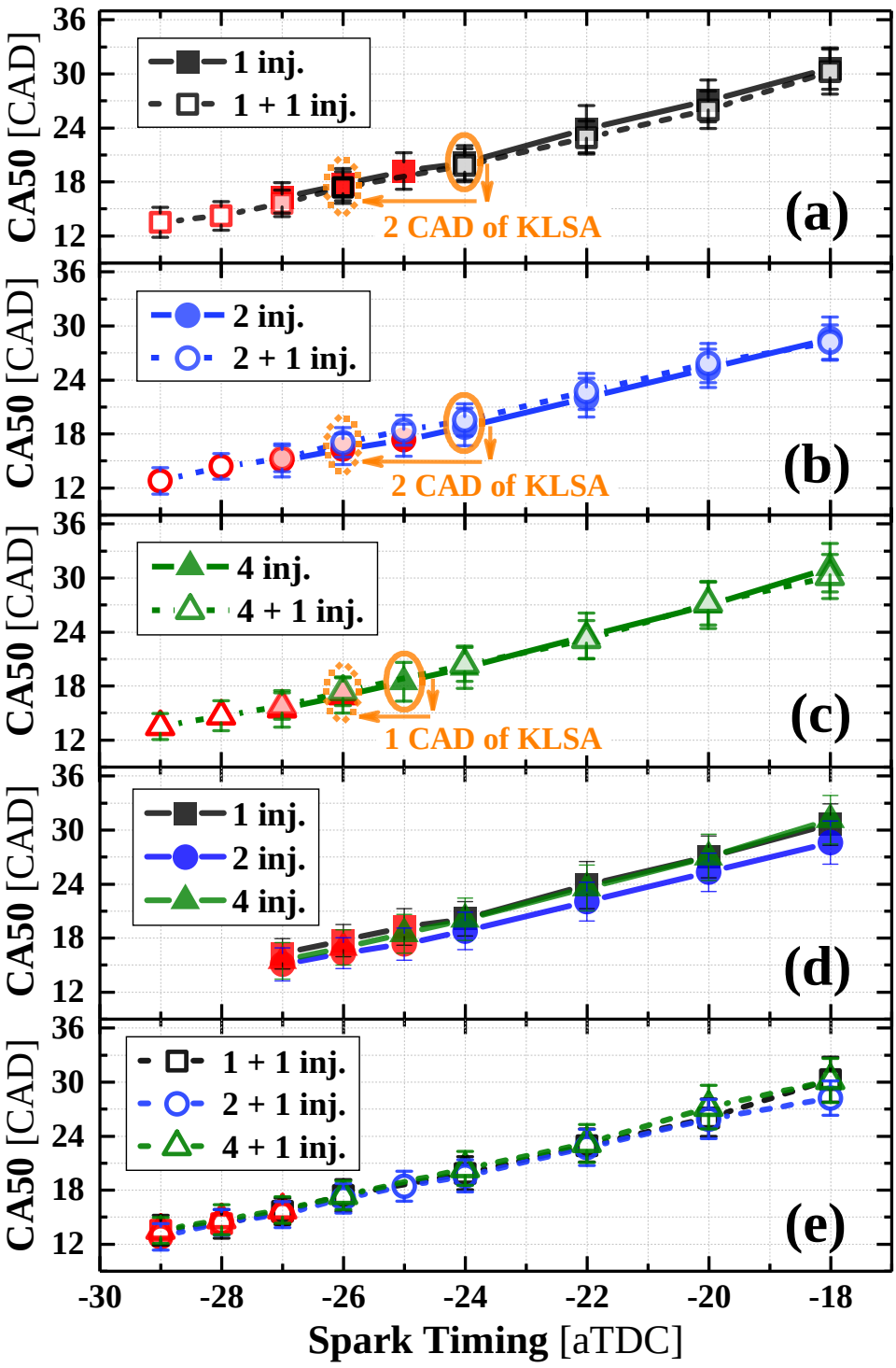

Figure 6.4 Combustion phasing (CA50) as a function of spark timing; (a), (b), and (c): comparison between 'Region I' and 'Region I + II'; (d) and (e): comparisons of 1, 2, and 4 inj. in 'Region I' and Region 'I + II'.

Figure 6.5 shows the knock intensity results for all six injection strategies as a function of combustion phasing (CA50) on a log scale. With advancing the combustion phasing, the knock intensity gradually increased at first and dramatically increased after the onset of knock. The red horizontal line indicates the knock threshold which is set to 0.42 bar based on a 'KI peak to peak' calculation, and the area above the red horizontal line is considered the knocking region. To investigate the effect of the number of injections, the 'Region I' injection cases with solid lines are compared first. The single injection baseline showed the earliest knock onset, and double and quadruple injections in 'Region I' showed the next knock onset, with around 2 crank angle degrees limit extension. Based on this result, it could be concluded that multiple injections improved the knock limit, even if only the intake valve open region ('Region I') was used. A noteworthy observation is that the quadruple injection results show slightly more vulnerability to knock compared with double injection. This could be because the 20 CAD interval of the first two injections and the second two injections was relatively short, so the collision between the first spray tail and the leading edge of the following spray may have resulted in uneven mixtures compared with the double injection case. This trend is apparent in the 'Region I + II' injection cases as well.

To investigate the injection region effect, the 'Region I + II' injection cases are compared with the single injection baseline. All the 'Region II' activation cases showed the largest extension of the knock limit, and the order of the extension was the same as found for the 'Region I' injection cases. To compare the injection region effect, the '2 inj.' (solid blue line) and '1+1 inj.' (dashed black line, total 2 inj.) cases are compared with the single injection baseline (solid black line) results. The '1+1 inj.' resulted in roughly twice the phasing extension compared with the '2 inj.' case, even with less fuel mass in the second injection (recall 50% of

the fuel mass was in '2 inj.' and 33.3% was in '1+1 inj.'). The results indicate multiple injections are effective at extending the knock limits, but the impact of the injection region is more significant than the impact of the number of injections. The impact of the number of injections on the knock limit extension was more effective in the 'Region I' cases compared with the 'Region I + II' cases. This could be because there are diminishing benefits with continuously increasing the number of injections, or because the 'Region I' injection amount is limited to only two thirds of the fuel mass.

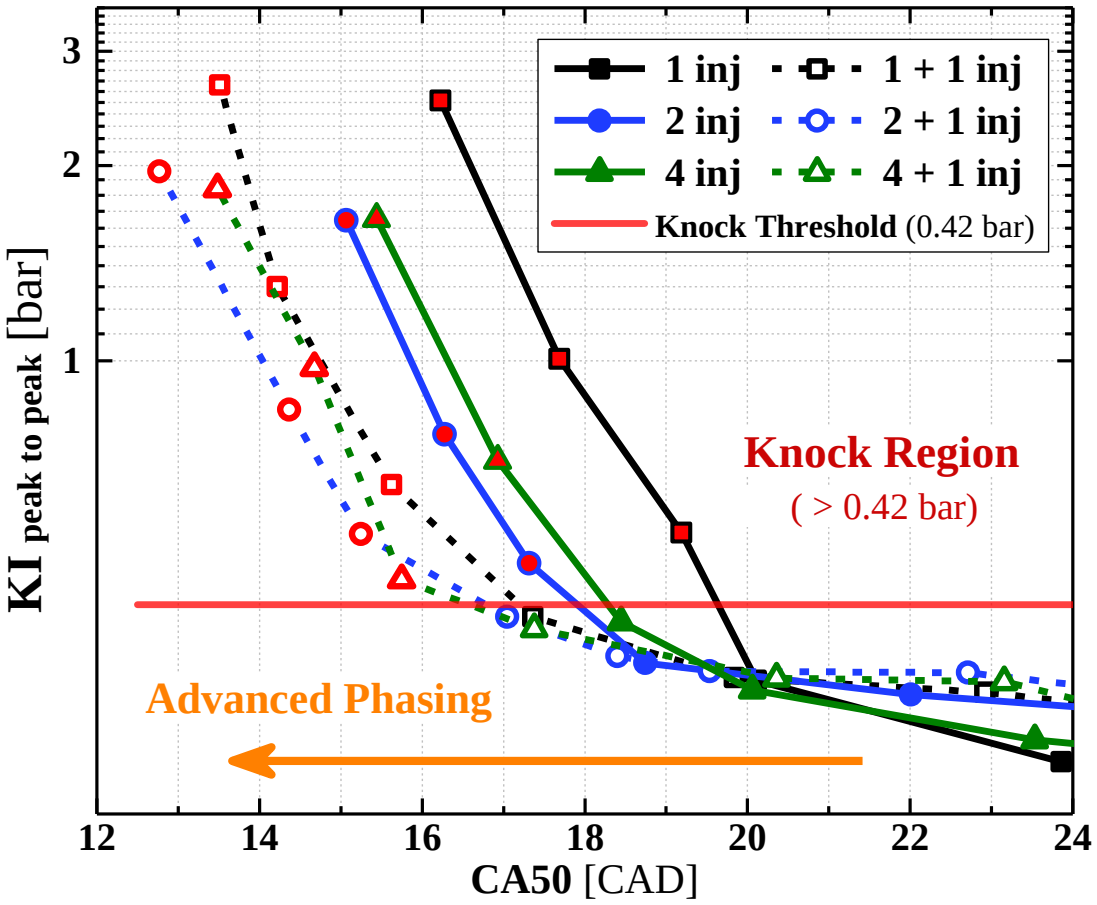

Figure 6.5 Knock intensity as a function of combustion phasing (CA50) and knock limited phasing for each injection strategy (where the knock limit is defined by the intersection of the experimental data with the red horizontal line). The red open and filled symbols denote knocking conditions.

6.5.2 Burn Duration and Knock Limit

Knocking is generally affected by both the burn duration and the auto-ignition time of the mixture in the end-gas region. So, a comparison of the burn duration helps understand the trends of the knocking results. Figure 6.6 shows the burn duration (CA1090) as a function of the combustion phasing, following the format used in Figure 6.4. The top three panels compare the 'Region II' effects on the burn duration, and the bottom two panels compare the number of injections in the two regions. In the top three graphs, the differences between the 'Region I' and 'Region I + II' injections clearly show the use of 'Region II' increases the burn duration. There could be several reasons for the slow burning rates in the 'Region II' closed-valve injection cases. Burn duration is known to be a function of the flow field characteristics, such as turbulence and the unburned mixture state and composition, including flame speed, and the flame speed is a function of temperature, pressure, and fuel-to-air equivalence ratio, as shown in Equation 6.3 [7,155]. Thus, one of the possible reasons for the increased burn duration for a closed intake valve injection strategy is reduced cylinder temperature due to maximized charge cooling effects. Another reason could be due to changes in the distribution of the in-cylinder fuel-to-air equivalence ratio by partial stratification. Although high stratification typically uses very late injection to make the mixture rich near the spark plug with a globally lean condition, the 'Region II' injection at 100 bTDC is between high stratified injection and homogeneous charge injection in 'Region I'. Thus, there could be a different equivalence ratio gradient with activation of fuel injection in 'Region II' due to partial stratification. More thorough comparisons are discussed in the next section with a heat release analysis. The effect of the number of injections on burn duration in each region shows almost identical trends in the bottom two panels

of Figure 6.6. Based on the results, a key conclusion is that the burn duration is predominantly affected by the injection region rather than the number of injections.

$$S_L = S_{L,0} \left(\frac{T_u}{T_0}\right)^{\alpha} \left(\frac{p}{p_0}\right)^{\beta} \tag{6.3}$$

*$S_{L,0}$, α, β = function of ϕ (proportional to the fuel to air equivalence ratio).

- T_0: reference temperature (298.15 K) - p_0: reference pressure (1 atm.)

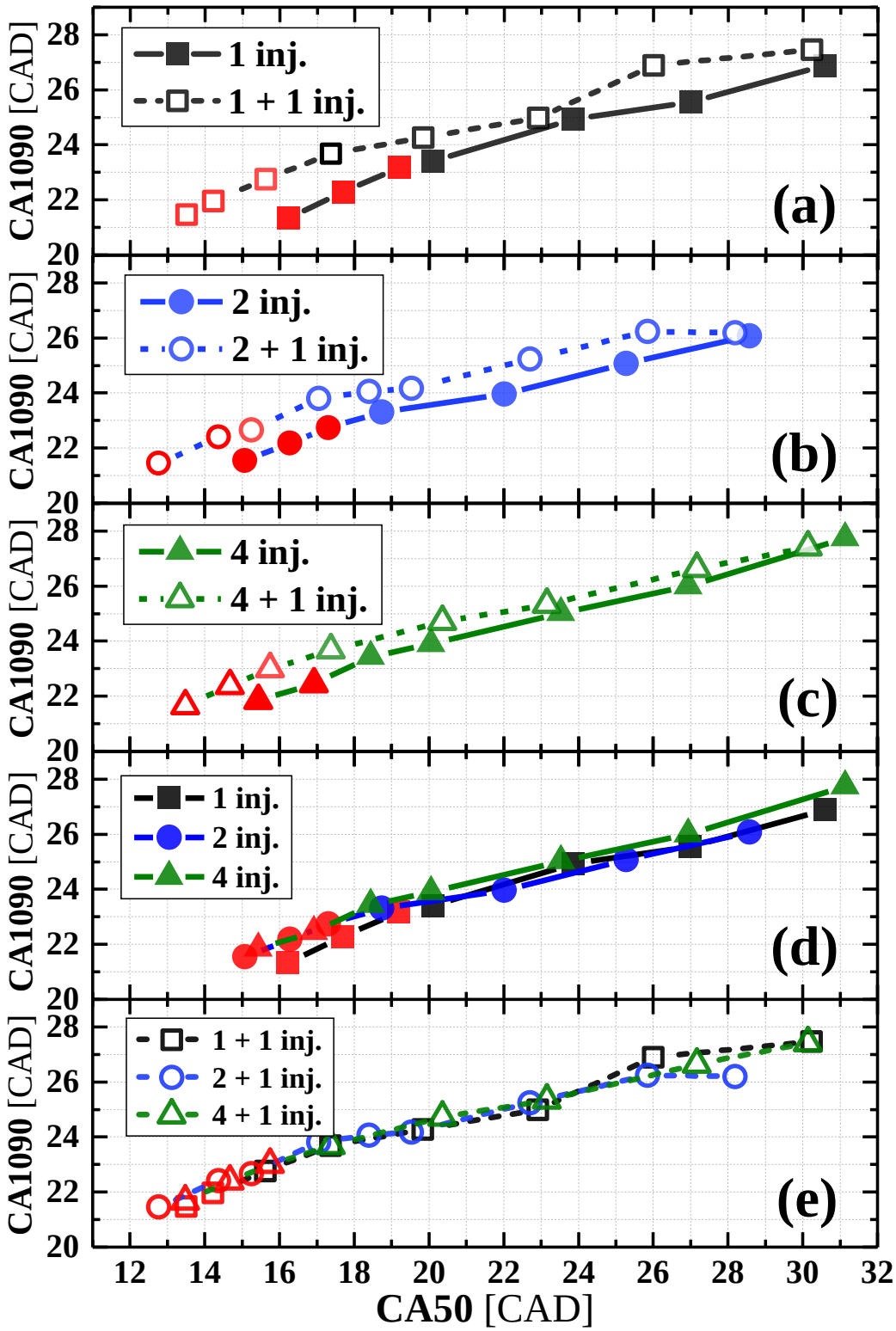

Figure 6.6 Comparison of average burn duration (CA1090) of the different injection strategies as a function of combustion phasing (CA50). The red open and filled symbols denote knocking conditions.

6.5.3 Heat Release Analysis

To evaluate the effects of injection region and number of injections on combustion characteristics, the heat release rate (RoHR) for each case are shown in Figure 6.7. Each rate of heat release curve is a time-history selected from a non-knocking condition with combustion phasing (CA50) of 19.5 CAD with a 0.6 standard deviation (± 0.8 variance), and the curves are averaged heat release values of the 200 cycles. Panels (a) to (c) of Figure 6.7 show the effect of injection region on heat release rate. All three cases show the initial slope of 'Region I + II' is higher than the initial slope of 'Region I', and the decrease in the heat release rate after the maximum RoHR occurs earlier for 'Region I + II' compared with 'Region I'. Additionally, the peak heat release rates for the 'Region I + II' cases are lower than for the 'Region I' injection cases. The difference decreases with an increasing number of injections. Because of these differences in RoHR, the burn duration (CA1090) of 'Region I + II' should be longer than for the 'Region I', as the results in Figure 6.6 showed.

Figure 6.7 (d) and (e) compare the effects of the number of injections on heat release rate. As with the comparison of the effects of injection region, more injections attenuate the changes in the heat release rates and lower the peak heat release rates. One additional noteworthy observation is that the 'Region I' injection in Figure 6.7 (d) shows higher peak RoHR occurs later than with 'Region I + II' injection data shown in Figure 6.7 (e). It could be inferred that the mixture formation characteristics are differentiated by the activation of the closed intake valve injection. When the closed intake valve injection is activated, higher local fuel-to-air equivalence ratio or increased turbulent flow could be generated near the spark plug, compared with the case with only an injection in the open intake valve region. Considering the almost identical gross indicated mean effective pressures (IMEPg) for all six cases and the significantly extended

knock limits for the ‘Region I + II’ injection cases, both the lowered cylinder temperature and improved mixture flow induced by the last injection likely influenced the flame development characteristics, as well as, the end-gas side auto-ignition characteristics.

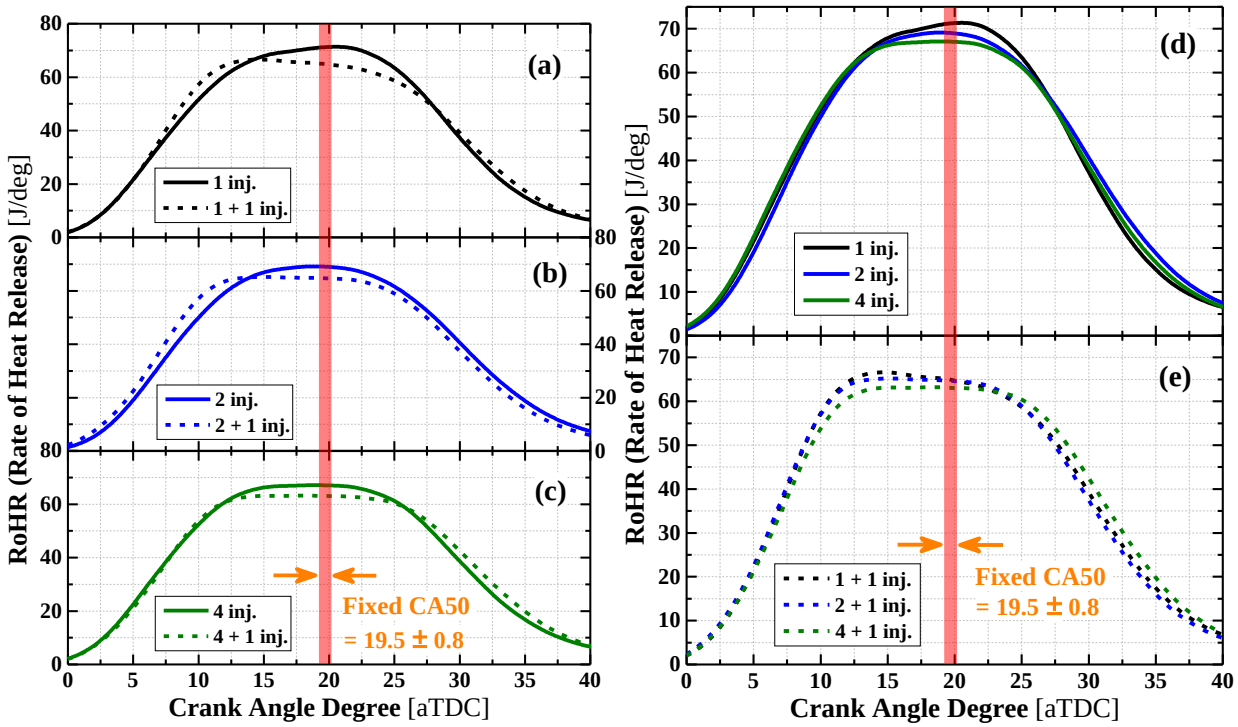

Figure 6.7 Comparison of heat release rate for cycles with the same combustion phasing.

6.5.4 Combustion Efficiency

Combustion efficiency was calculated for the six cases using Equation 6.4 [7]. The calculation was based on the measurements of the mole fractions of the engine exhaust gas species CO, THC, and H_2 shown as x_i in Equation 6.4. The particulate emissions were relatively low, so they were excluded from the calculation, and the hydrogen species were calculated using the unburned hydrocarbon and carbon monoxide values.

$$\eta_c = 1 - \frac{\sum_i x_i \, Q_{LHVi}}{\left(\frac{\dot{m}_f}{\dot{m}_a + \dot{m}_f}\right) Q_{LHVf}} \tag{6.4}$$

Figure 6.8 presents the results for combustion efficiency as a function of phasing for all the injection strategies studied. The differences between the lowest and highest values were relatively small (less than 1%) for identical combustion phasing, but the 'Region I + II' injection cases generally showed lower combustion efficiency compared with 'Region I' injections. This could be due to slightly increased stratification level with a late injection under global stoichiometric conditions. The trend agrees with the multi-cylinder engine experiments using E85 fuel conducted by Singh et al. [127], and the lower of combustion efficiency with E10 fuel compared with higher ethanol percentage blends with gasoline. For the comparisons of the number of injections in the 'Region I', the double- and quadruple-injection cases showed slightly lower combustion efficiency than the single-injection baseline. Some studies reported better combustion efficiency with multiple injections [127,141], but this study showed slightly decreased trends for the intake-stroke injection cases. A possible reason for the slightly lower combustion efficiency seen in the present work is the longer dwell time between the first and second injection events (100 crank angle degrees) compared with the other studies.

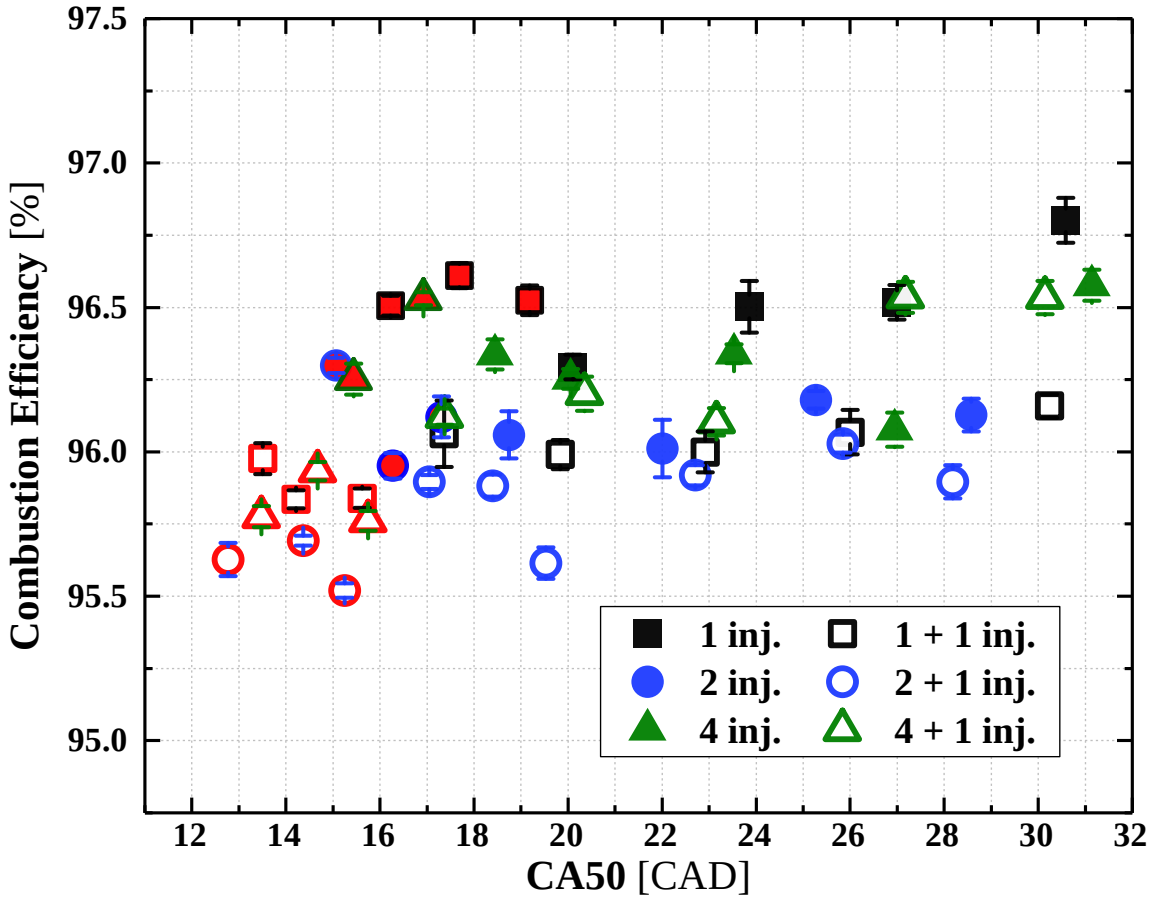

Figure 6.8 Combustion efficiency as a function of combustion phasing (CA50) for the different injection strategies.

6.5.5 Thermal Efficiency and Combustion Stability

The gross indicated thermal efficiency (ITEg) was calculated using Equation 6.5 and plotted in Figure 6.9. Overall, the thermal efficiencies for the six cases were almost identical, and the small differences were within the uncertainty limits. A distinct efficiency improvement from extending the knock limit is seen in the 'Region II' activation cases of the top three panels, and the amount of efficiency improvement was highest with the single injection case (0.7% improvement based on absolute value), followed by double injection (0.4%), and quadruple

injection (0.1%). The increased efficiency, however, was also within the uncertainty range, indicating the effects of multiple injection on efficiency is possible, but not significant. The lower two panels in Figure 6.9 compare the number of injections. Double and quadruple injection strategies extended the knock-limited phasing by around 1 CAD, and the trends were the same as for the different regions of injection.

$$\eta_{t,i} = \frac{W_i}{\dot{m}_f \, Q_{LHV}} \tag{6.5}$$

The effects of the injection strategies on the combustion stability indicated by the coefficient of variation of gross indicated mean effective pressure (CoV of IMEPg) is shown in Figure 6.10. The combustion stability followed almost identical trends as the thermal efficiency. So, multiple injections did not degrade or improve stable engine operation.

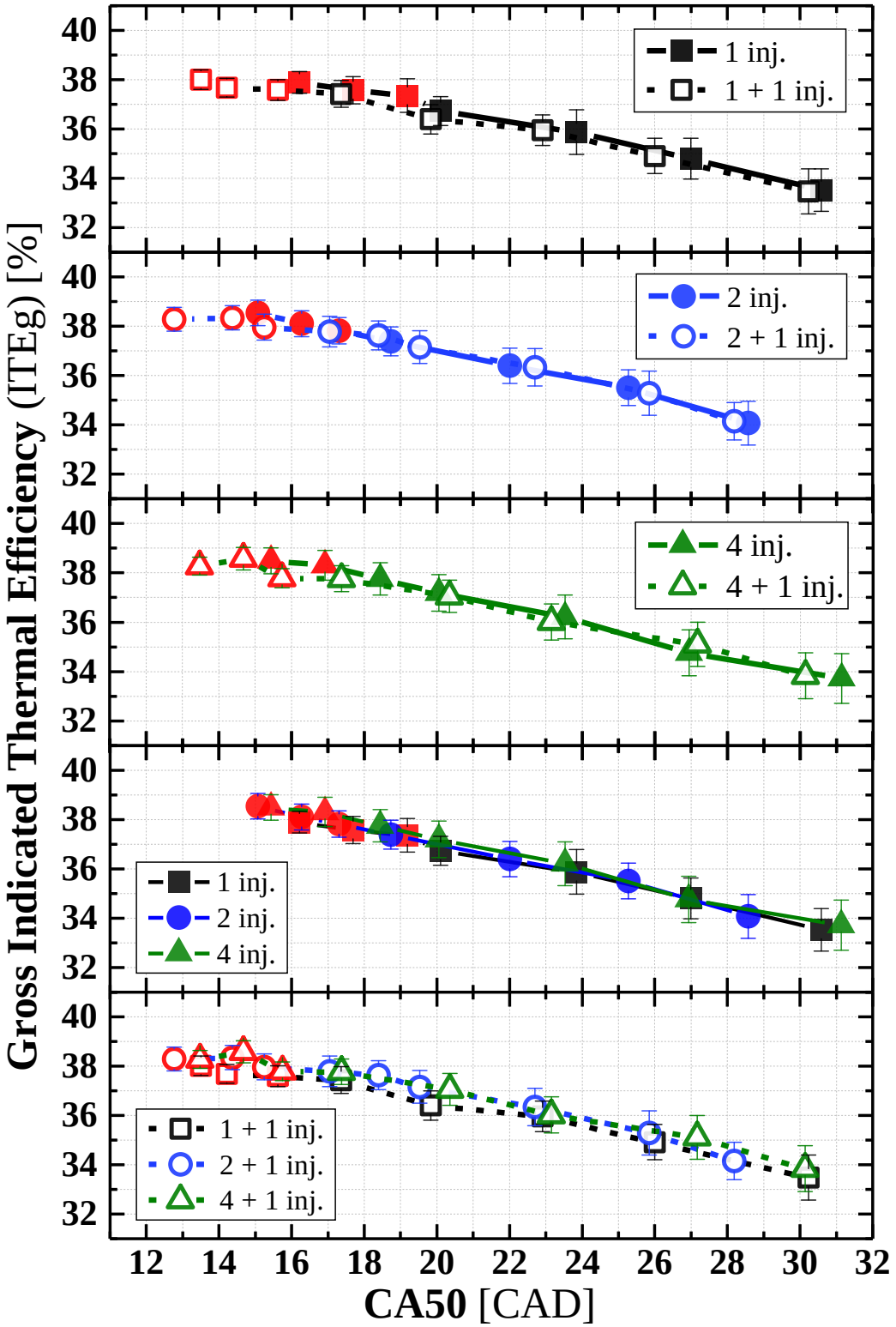

Figure 6.9 Comparisons of gross indicated thermal efficiency (ITEg) for the different injection strategies as function of combustion phasing.

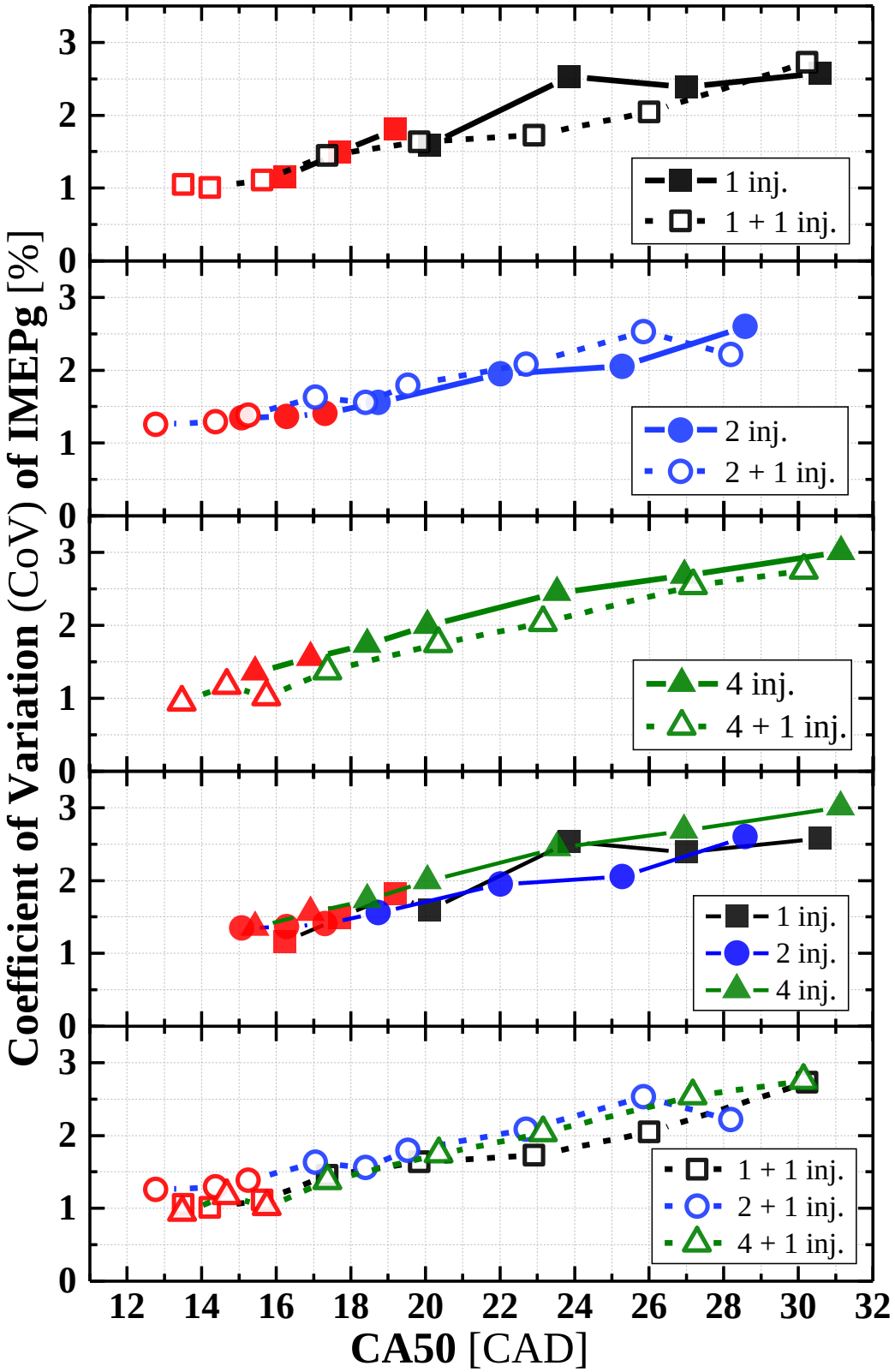

Figure 6.10 Combustion Stability (CoV of IMEPg) comparisons as a function of combustion phasing.

6.6 Gaseous Emissions

6.6.1 Nitrogen Oxides (NO_x) Emissions

The engine-out emissions of nitrogen oxides (NO_x) are presented in Figure 6.11 as a function of combustion phasing on an indicated specific basis. The effects of the number of injections clearly shows reduced NOx emissions for the double and quadruple injections compared with the baseline single injection in 'Region I'. The quadruple injection strategy led to slightly higher NOx emissions than the double injection strategy, similar to the trends observed for knocking. The 'Region I + II' injection cases (dashed lines) showed the same trends as the 'Region I' injection results. The effects of injection region yielded a greater NOx emissions reduction than the effects of the number of injection events. NOx emissions were reduced by 25%, as shown by the differences between the 'Region I' solid lines and 'Region I + II' dashed lines.

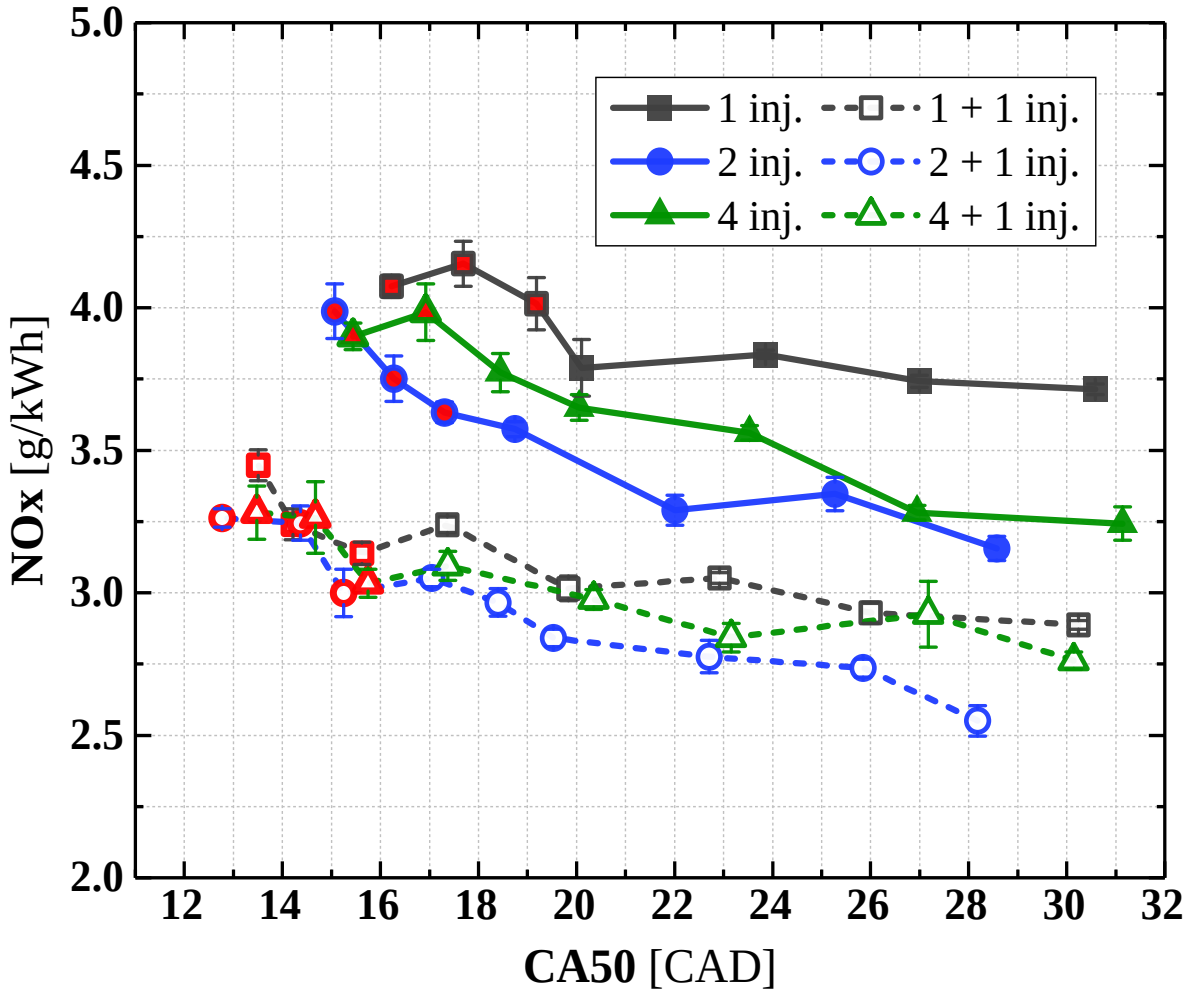

Figure 6.11 Effects of different injection strategies on NOx emissions as a function of combustion phasing. The red open and filled symbols denote knocking conditions.

The possible reasons for the effects of multiple injections on nitrogen oxides emissions could be due to reduced in-cylinder temperatures or changes in mixture stratification. The level of nitrogen oxides emissions is highly correlated with peak in-cylinder temperature [35,36,156], and injection in 'Region II' during the compressions stroke maximizes charge cooling. To understand the temperature differences between injecting in 'Region I' and 'Region I + II', calculated in-cylinder temperature profiles are plotted in Figures 6.12 and 6.13. Double and quadruple injections under the same spark timing at 24 bTDC are compared for both injection

regions. Figure 6.12 shows the starting point of the temperature difference near the compression stroke injection timing (100 bTDC). Before injecting the fuel in the "Region II', the temperatures for all four cases are almost identical, but the temperature profiles gradually begin to change after injection.

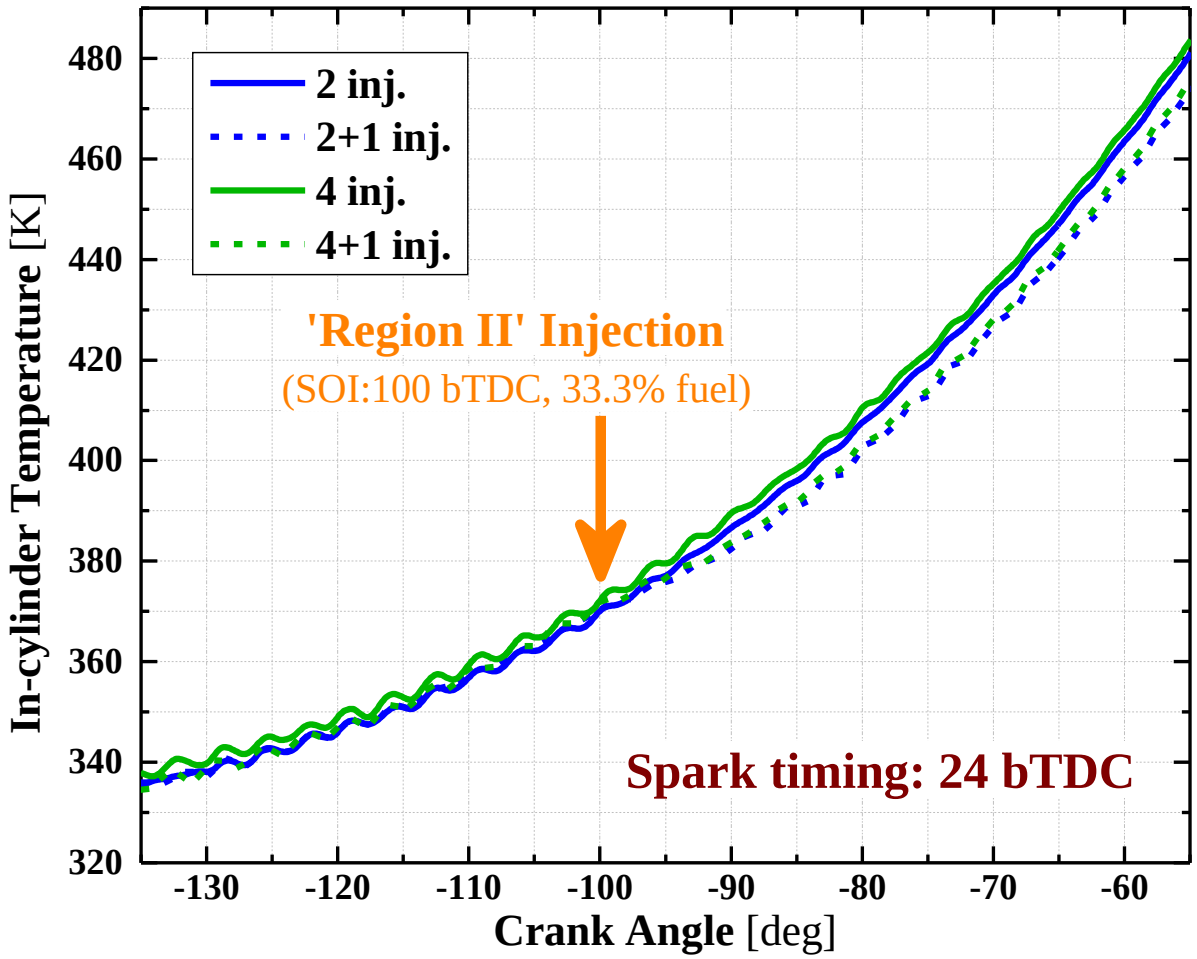

Figure 6.12 Calculated in-cylinder temperature for double and quadruple injection cases near the 'Region II' injection timing (100 bTDC)

Figure 6.13 (a) and (b) show the calculated temperature profiles near TDC and the peak temperature region. The temperature differences between 'Region I' and 'Region I + II' injection

are increased by more than 10 K near TDC, and reach a maximum of around 65 K based on the peak cylinder temperature. The peak cylinder temperature for double injection is slightly higher than for quadruple injection, which could be because the combustion phasing is a bit retarded for the quadruple injection cases, even though the spark timing is identical for both injection regions. The temperature estimates indicate the differences in NOx emissions between the double and quadruple injection cases cannot be explained entirely by changes in for the different injection regions. The temperature differences are relatively small, and the changes are in the opposite direction with respect to the observed changes in the NOx emissions. So, charge cooling effects alone do not explain the decrease in nitrogen oxide emissions.

Lavoie et al. [36,157] studied engine-out nitric oxide emissions under lean and rich conditions with an extended kinetic mechanism, and the findings were applied to develop strategies to reduce NOx emissions, such as stratified charge engine operation [158]. Because NO formation is maximized near stoichiometric conditions, when locally rich and lean zones are formed through mixture stratification, the overall nitric oxide emissions are significantly reduced even when the global fuel-to-air equivalence ratio remains stoichiometric. So, the nitrogen oxides emissions of double and quadruple injection cases may be reduced through higher stratification levels compared with baseline single injection. In addition, higher nitrogen oxides emissions for quadruple injection could be due to reduced stratification by splitting the double injections into four injections with the same center of injection and not providing enough dwell time between the first and second pairs of injections.

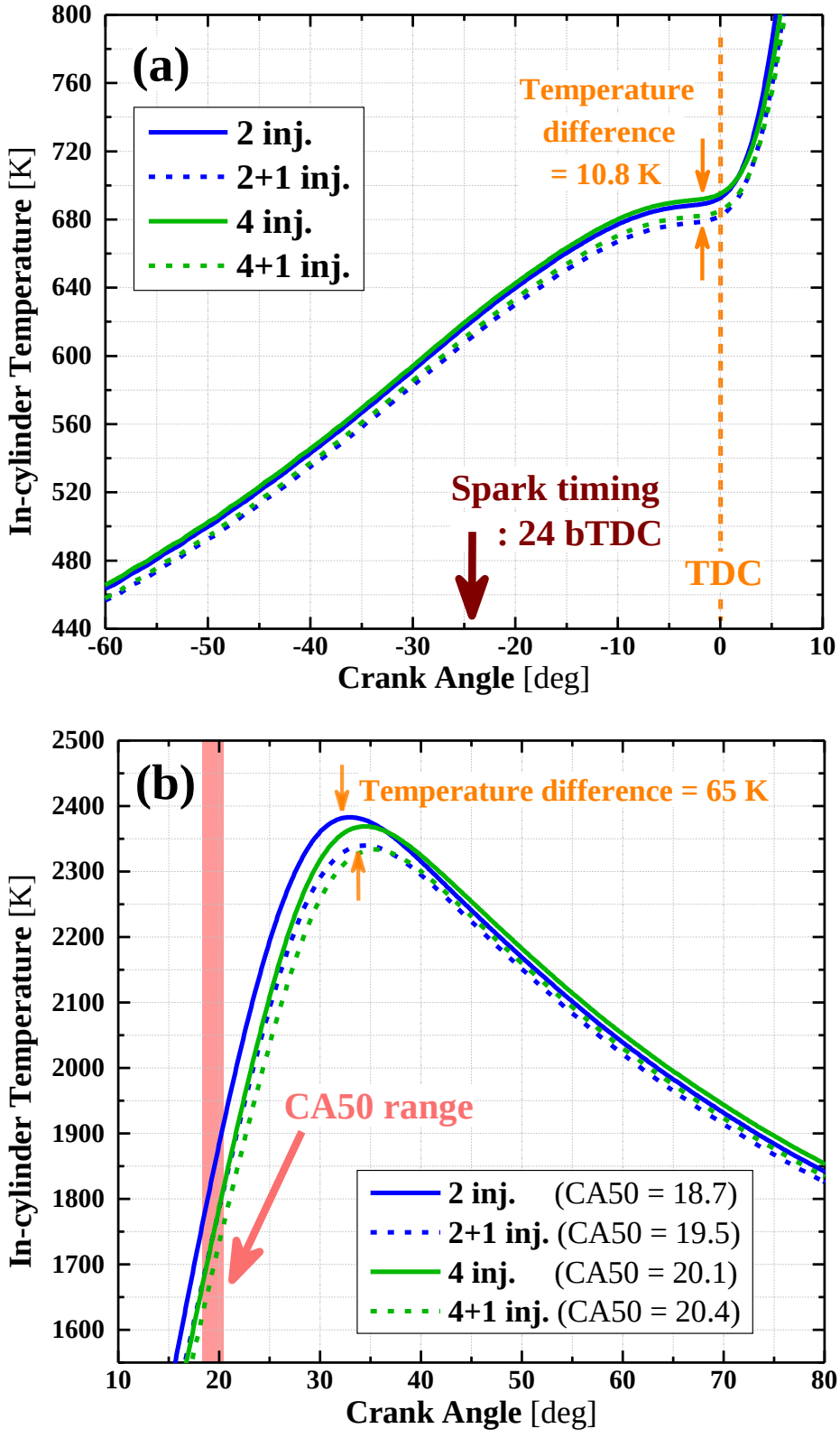

Figure 6.13 Calculated in-cylinder temperature for double and quadruple injection cases: (a) near spark timing and TDC, (b) near the peak temperature after CA50.

6.6.2 Unburned Total Hydrocarbon (THC) Emissions

The measured unburned total hydrocarbon (THC) emissions are presented in Figure 6.14 as a function of combustion phasing. The originally measured values were obtained on a ppm C1 scale and the values were converted to indicated specific basis. Like the NOx emissions, the total unburned hydrocarbon results were also significantly reduced by multiple injection events, and the trends were similar except for the order of the quadruple- and double-injections. The injection region was a dominant factor for nitrogen oxides reduction, but both the injection region and number of injections were effective at reducing the THC emissions. THC emissions are generally affected by flame quenching, fuel filling the crevice volume, fuel absorption into oil layers, incomplete combustions, and so on [7]. The general conditions and global air-to-fuel equivalence ratios were the same for all experiments, so the reasons for the reduced unburned hydrocarbon emissions are likely due to reduced fuel spray impingement on the combustion chamber walls and piston crown.

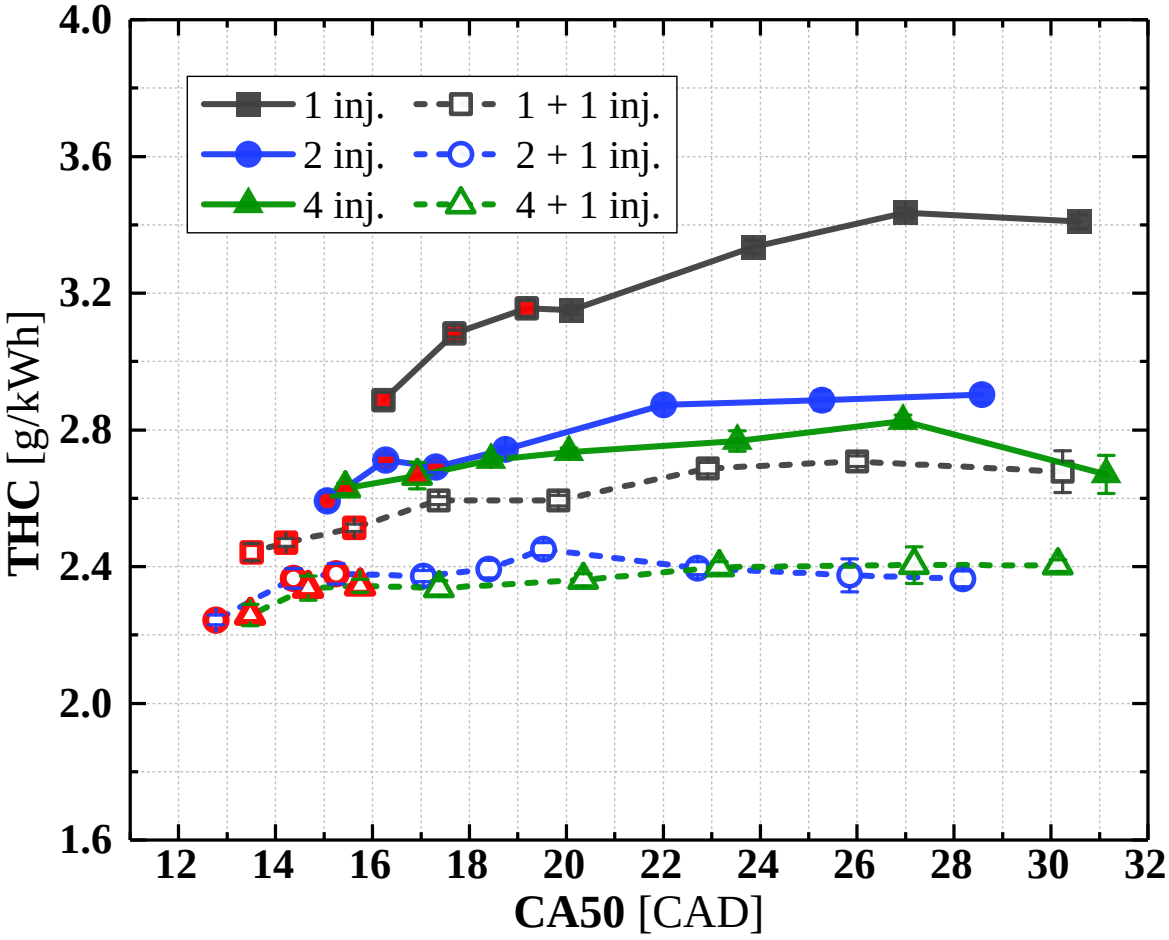

Figure 6.14 Effects of different injection strategies on total unburned hydrocarbon (THC) emissions as a function of combustion phasing. The red open and filled symbols denote knocking conditions.

6.6.3 Carbon Monoxide (CO) Emissions

The engine-out carbon monoxide (CO) emission results are shown in Figure 6.15 as a function of combustion phasing. Unlike the NOx and THC emissions, the CO emissions increased with multiple injections. Carbon monoxide emissions are primarily controlled by the global and local fuel-to-air equivalence ratio. Considering the increased stratification created by

multiple injections, the increased carbon monoxide results are reasonable. The trade-off between CO and NOx and THC emissions also agrees with other studies of multiple injection strategies [127,148,159].

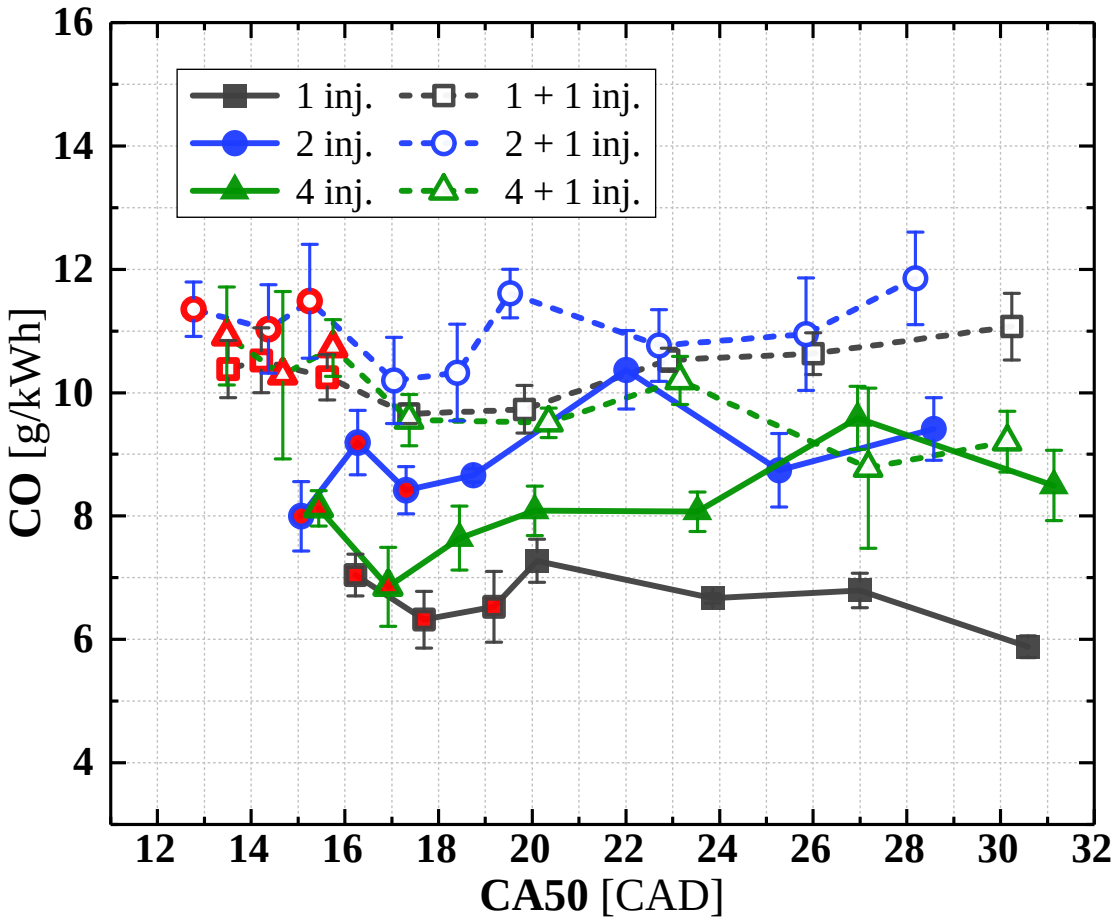

Figure 6.15 Effects of different injection strategies on carbon monoxide (CO) emissions as a function of combustion phasing. The red open and filled symbols denote knocking conditions.

6.7 Particulate Matter Emissions

As introduced in the literature review, several experimental studies have shown that multiple injection reduces the particulate matter emissions, but an in depth understanding of the impact of multiple injections on the size distributions and numbers remains to be developed. So, this section deals with the effect of multiple injections on the particulate number and size distribution on the two bases of comparisons of multiple injection impacts: number of injections and injection region.

6.7.1 Total Particulate Number Emissions

The total particle number (PN) emissions in the nuclei and accumulation modes include particle size/diameters in the range from 5 nm to 1000 nm (= 1 μm) [37,160]. Figure 6.16 shows the total PN results for all six injection cases as a function of combustion phasing. Total PN under non-knocking conditions showed similar trends regardless of the combustion phasing, but the total PN increased significantly after the onset of knock with similar rate of increase for the different strategies. This trend agrees with previous knocking research [67] and the possible reasons could be locally fuel rich regions induced by increased heat transfer or flame quenching near the wall and piston [161–164], knock induced detonation waves near the end-gas [165], and so on. Additional analyses of the relationship between knock and particulate matter are discussed in Chapter 7.

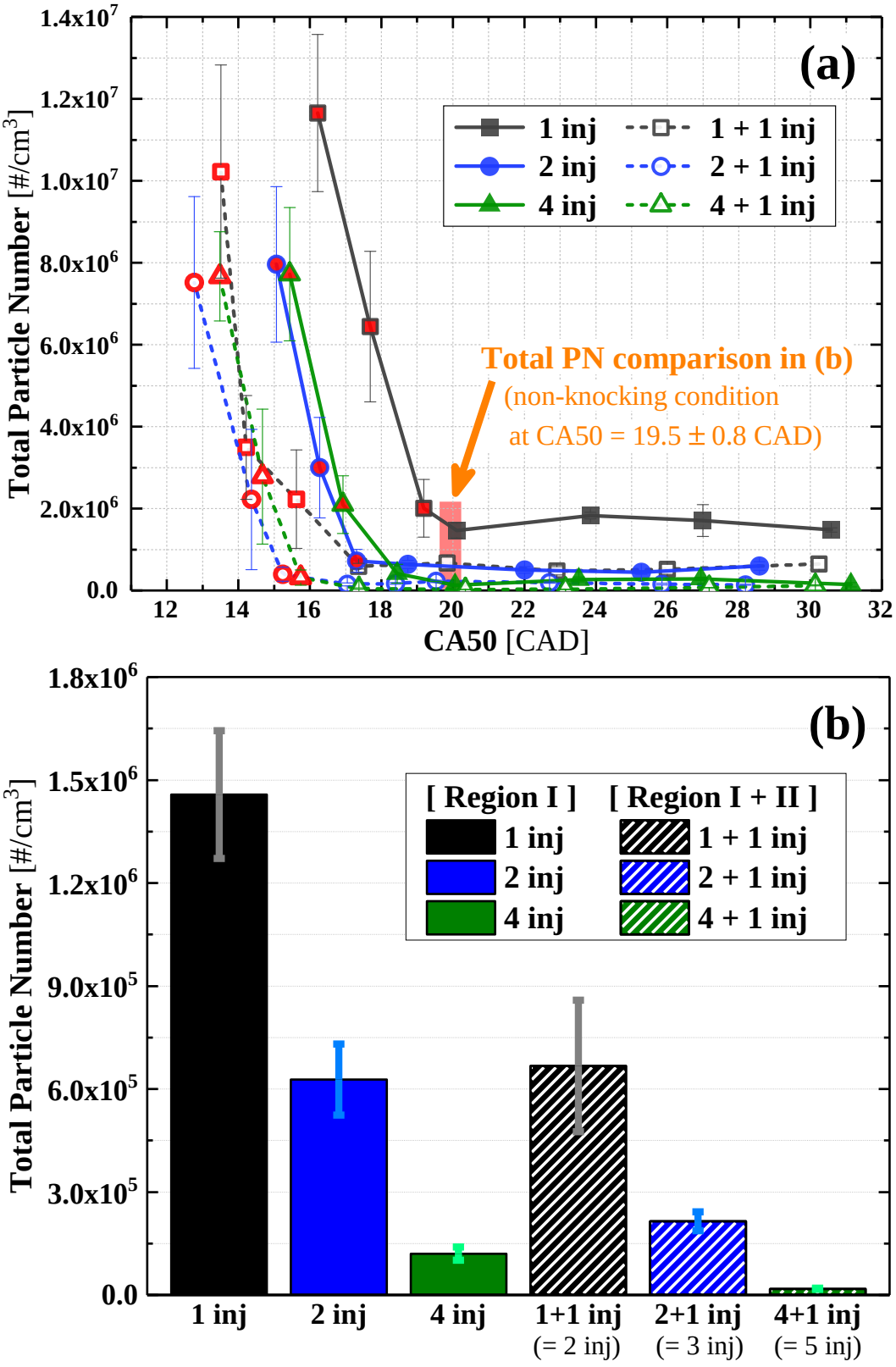

Figure 6.16 Effects of different injection strategies on total PN emissions as a function of a) combustion phasing and b) fixed combustion phasing. The red open and filled symbols denote knocking conditions.

In order to compare the PN data from the multiple injection cases, total PN emissions at the same combustion phasing points (CA50 near 19.5 CAD, i.e., knock-limited point of the baseline) are presented in detail in Figure 6.16. The first three cases are 'Region I' injection and the last three cases are 'Region I + II' injection with one third of the fuel mass injected in the compression stroke. Results for both injection regions show significantly reduced total PN with increasing number of injections, and the level of the PN reduction is around half with each additional injection. The magnitude of PN emissions reduction agrees with the results for single and double injection conducted by He et al. [151]. The last three cases in the 'Region I + II' region showed the same trends as the 'Region I' injection. The two plus one injection (i.e., three injections) results were approximately half the one plus one injection (i.e., two injections), and the four plus one injection (i.e., five injections) were about a quarter of the triple injection results. The total PN did not seem to be affected by the injection region, with comparable total PN for 'Region I' and 'Region I + II'. In summary, the total PN consistently decreased as the number of injections increased, regardless of the region.

6.7.2 Mode Separation of Particulate Emissions

The size distribution of the particulate emissions of six selected cases are plotted in Figure 6.17 as a function of the particle size (D_p), and the horizontal axis has been converted to log scale for better legibility. Engine-out particulate matter results typically show bimodal size distributions. The smallest group of particulates by size (sub-23 nm particles), referred to as nucleation (nuclei) mode particles, is generally comprised of volatile organics (unburned hydrocarbons) and liquid droplets, and the larger particles with diameters between 23 nm and 1000 nm, called accumulation mode particles, are generally soot aggregates [37]. Bimodal

distributions are not very clear in Figure 6.17, especially for the high number of injection cases, possibly due to the higher number of nucleation mode particles. The size distribution trends were almost identical for all six injection cases.

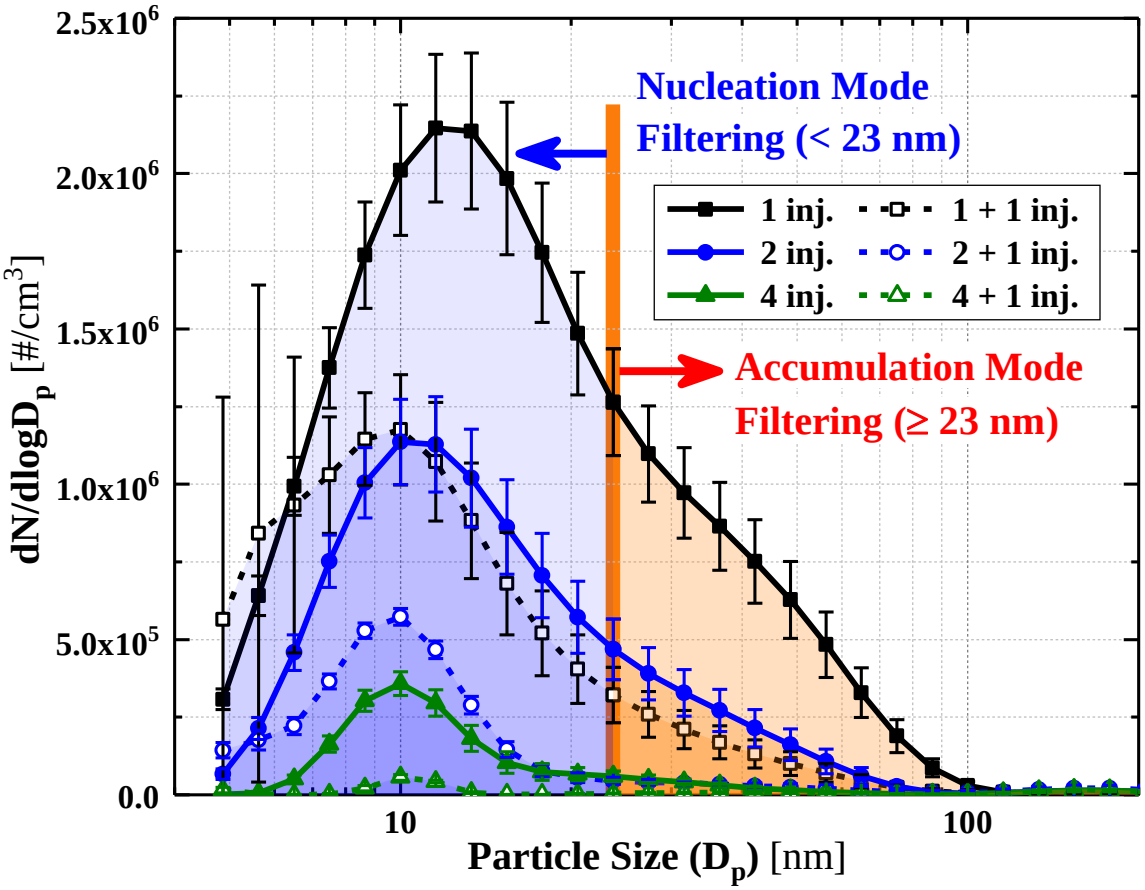

Figure 6.17 Particulate matter emissions size distribution

The number of nucleation and accumulation mode particles, where the mode separation was set as the number of particles smaller than and greater than 23 nm, are plotted in Figure 6.18. The blue column is the total number of nucleation mode particles (i.e., < 23 nm), and the red column is the total number of accumulation mode particles (i.e., > 23 nm). Comparing the data with the single injection baseline case, the nucleation mode particles were around 2.5 times higher than the accumulation mode particles. The difference between nucleation and

accumulation mode numbers increased with more injection events in comparison with the baseline single injection. Seong et al. [166,167] experimentally studied the effects of injection timing on the particulate number emissions for two modes using transmission electron microscopy (TEM) imaging. They found retarded injection timing produced more sub 23 nm nucleation mode particles; consistent with the observations in this work for the two modes, and the differences are greater in the 'Region I + II' injection cases.

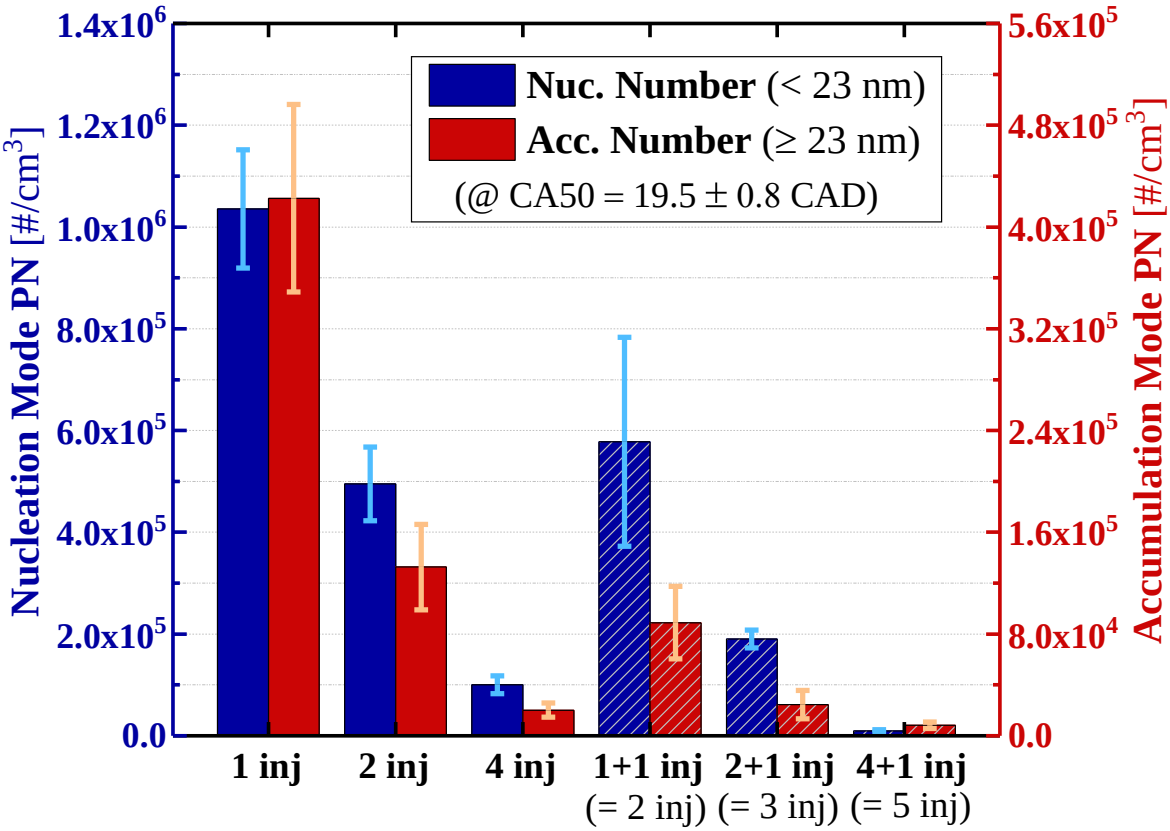

Figure 6.18 Particulate number with mode separation

6.8 Summary and Conclusion

The effects of multiple injections on knock limits and gaseous and particulate matter emissions were experimentally explored with regard to two key parameters: the number of injections and the injection timing and region. The following conclusions are derived from the experimental results and analyses:

(1) Engine Performance and Knock

- Multiple injections were effective at extending the knock limit. In particular, both the number of injections and the injection region were effective for achieving knock limit extension, but the effect of the injection region (when using compression stroke injection) was more significant than increasing the number of injections due to the maximized charge cooling effect.
- Burn duration was extended with compression stroke injection, possibly due to decreased in-cylinder temperature and uneven flow field characteristics induced by the charge stratification.
- Multiple injections gradually decreased the peak heat release rate, and the injection region was more effective than the number of injections on reducing peak heat release rate.
- Combustion efficiency was slightly reduced by compression stroke injection.
- Multiple injections marginally improved thermal efficiency mainly due to the knock limit extension, but the increase was within the uncertainty range of the measurements.
- Combustion stability differences were negligible for all multiple injection conditions considered.

(2) Gaseous Emissions

- Nitrogen oxides emissions were significantly reduced with multiple injections, and the effects of the injection region were more significant than the effects of the number of injections. The decrease was likely due to increased charge stratification and charge cooling effect.
- Unburned hydrocarbon emissions were significantly reduced with multiple injections, and both the injection region and the number of injections were effective for reducing unburned hydrocarbon emissions.
- Carbon monoxide emissions increased with multiple injections. This could be due to increased charge stratification.

(3) Particulate Matter Emissions

- Particulate number emissions were significantly reduced with multiple injections. The decrease was monotonic with the number of fuel injections, and the particulate number emissions decreased by half with each additional injection.
- Particulate number emissions showed no significant sensitivity to the injection region.
- The number of nucleation mode particles was higher than the number of accumulation mode particles, and the differences between the two modes increased with increasing number of injections.

Chapter 7

Knock, as a Source of Particulate Matter Emissions in SI Engines: Phenomenological Analyses and Conceptual Models

7.1 Preface

This chapter is an exploratory study about the relationship between knocking and particulate matter emissions and a phenomenological analysis of this relationship. The phenomenological analyses are described first, and the understanding of this relationship is discussed via three conceptual models compared with the experimental results.

The present study focuses on the understanding of a newly observed relationship between knocking and particulate matter emissions in spark ignition engines. In general, particulate matter emissions rapidly increase after the onset of knock with advancing the spark timing, and the increased amount of particulate matter emissions are proportionate to the knock intensity. This phenomenon is a novel observation, and there is very limited understanding of this phenomenon and this relationship. So, phenomenological analyses are introduced using several experimental data, and three theories are proposed to explain this phenomenon along via conceptual models. The three suggested theories are as follows:

Theory 1. Ring Crevice Mechanism

Theory 2. Insufficient Mixing Mechanism

Theory 3. Shock Wave Mechanism

7.2 Introduction and Background

As discussed in Chapters 3, 5, and 6 regarding particulate matter emissions, an interesting phenomenon about the relationship between knocking and particulate numbers is observed in these experiments. Figures 7.1 to 7.3 present a summary of the results that demonstrate this relationship, which are plotted by total number of particulate matter emissions as a function of combustion phasing (CA50). All three experiments are conducted with the same engine but while operating on different types of fuels or with different types of fuel injection strategies. Figure 7.1 is from operation in port fuel injection mode using four different oxygenated fuel blends in gasoline. The particulate numbers are similar or slightly increased with advancing combustion phasing (empty symbol) but increased right after the onset of knock (filled symbol). Figure 7.2 is from operation in direct injection mode and dual injection mode under different levels of EGR dilution, and all data shows the same trend as seen in Figure 7.1. Figure 7.3 is also from operation in direct injection mode, but with multiple fuel injection strategy (up to 5 injections per cycle). The results of this work also clearly show a dramatic increase of soot formation which begins when knock occurs and is approximately proportional to the knock intensity.

This phenomenon is obvious based on the repeated experiments as shown in previous chapters, but, to date, there is no sound analysis for this phenomenon in the literature.

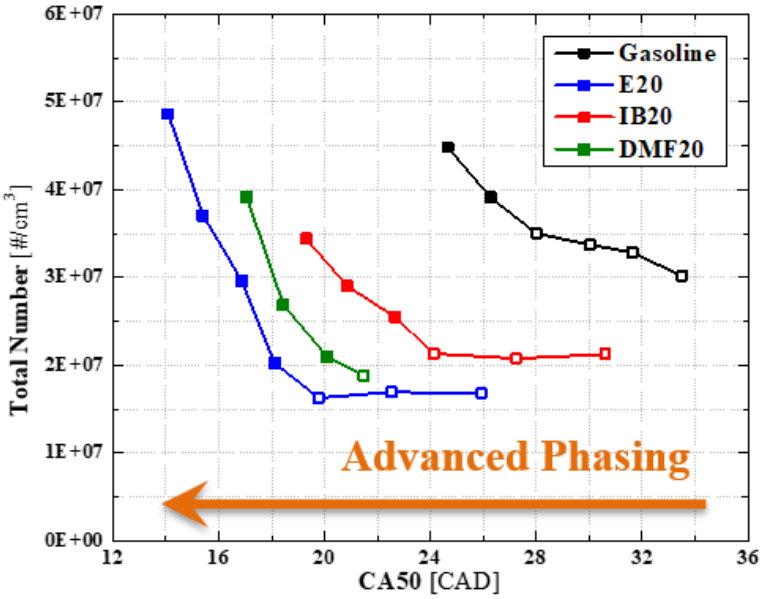

Figure 7.1 Total particulate number of four different fuel sets as a function of combustion phasing. The filled symbols denote knocking conditions. (1500 rpm, 1.4 bar boosted condition, same data as Figure 3.18)

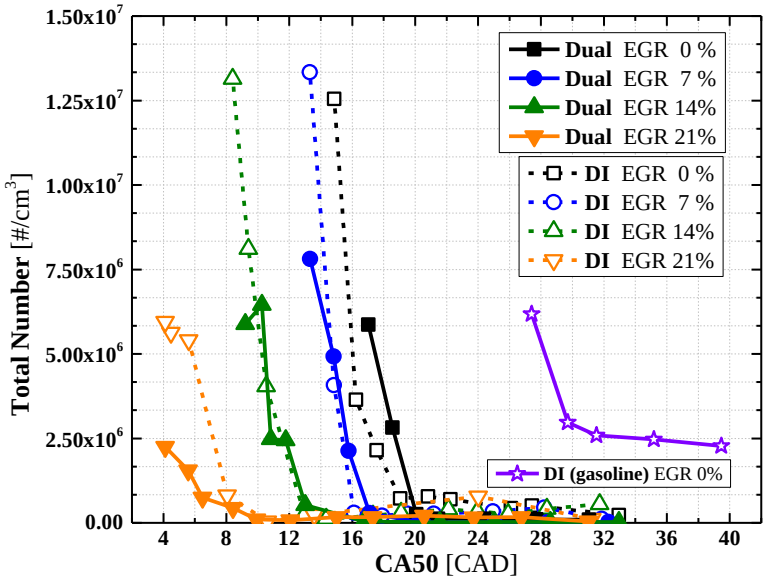

Figure 7.2 Total particulate number of different fueling strategies and EGR dilutions as a function of combustion phasing. Total PN increase after the onset of knocking. (1500 rpm, 1.25 bar boosted condition, same data as Figure 6.16)

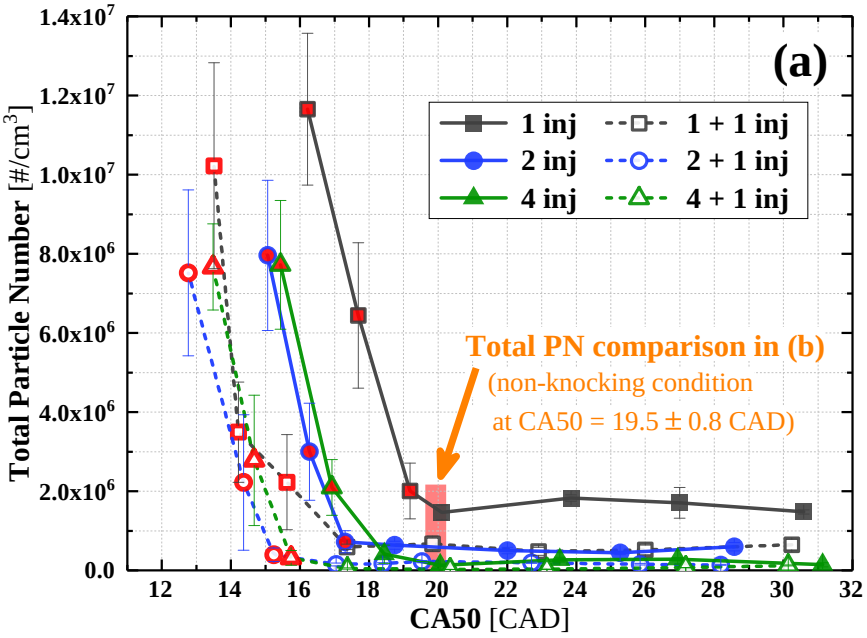

Figure 7.3 Total particulate number of various number of injections as a function of combustion phasing. The red open and filled symbols denote knocking conditions. (1500 rpm, 1.2 bar boosted conditions, same data as Figure 6.16 (a).)

Even though these particulate number results show similar trends, it could be a specific phenomenon caused by a certain characteristics of this boosted Hydra engine, so the same experiments were conducted using a multi-cylinder engine as well. Figure 7.4 shows the particulate number result of a 4-cylinder Ford 1.6L Eco-boost engine using direct injection near knock limited combustion phasing. As Figure 7.4 clearly shows, the particulate number near 16° bTDC spark timing, particulate number emissions are dramatically increased after the onset of knock. In addition, the particulate matter sampling location could be a reason for this phenomenon, so, the sampling port was changed from the exhaust runner to the exhaust plenum in the boosted Hydra engine facility. But the results showed exactly the same trend as the previous experiments.

Based on these experimental results, it looks obvious that knock promotes particulate matter emissions, and there appears to be a relationship between knock intensity and particulate

number emissions. Therefore, an experiment is conducted to better understand this phenomenon in this chapter.

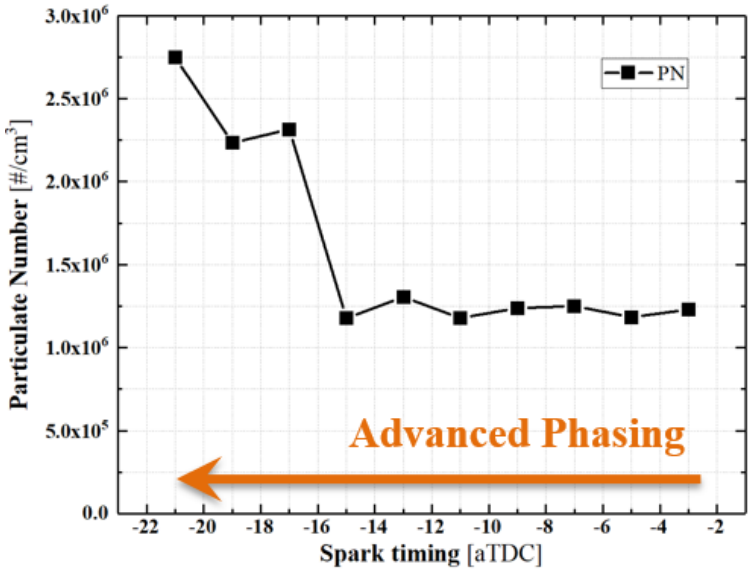

Figure 7.4 Particulate number emissions from 1.6 L Ford Eco-boost engine as a function of spark timing. Total PN increase after the onset of knocking. (Condition: 1500 rpm, 11.0 bar of IMEPn)

7.3 Soot Formation in Internal Combustion Engines

Prior to describing the experimental setup and results, some background on soot formation in internal combustion engines is summarized here for a better understanding of the phenomenon of soot formation leading to the proposed conceptual model.

7.3.1 In-cylinder Local Rich Zone

The formation of soot is a complex process, not entirely understood. However, several key processes have been identified in the past decades that contribute to the process of soot formation, such as locally rich zones ($\phi > 2$), moderate temperatures (~ 1700 K) which

encourage pyrolysis, particle nucleation and growth, followed by condensation and agglomeration [7]. If enough oxygen becomes available due to subsequent mixing with leaner parts of the charge, oxidation of the soot particles will occur. Figure 7.5 shows a schematic of the soot formation process from gas phase fuel to solid particles [168]. The evolution from liquid- or vapor-phase hydrocarbons to solid soot particles and possibly back to gas-phase products involves six commonly identified processes: pyrolysis, nucleation, coalescence, surface growth, agglomeration, and oxidation. This process, however, is only under fuel rich conditions, especially in the surface growth step, or most of soot precursors are burnt with enough oxygen unless the time for oxidation is too short. The local rich zone concept is also described in the studies from Kamimoto et al. [169] and Akihama et al. [170], which is shown in Figure 7.6. As shown by the presence of the soot island surrounded by the soot limit, soot is only produced in the locally rich ($\phi > 2$) conditions and under certain temperature conditions. According to this prerequisite for the soot formation, some relation exists between knocking and the locally rich zone.

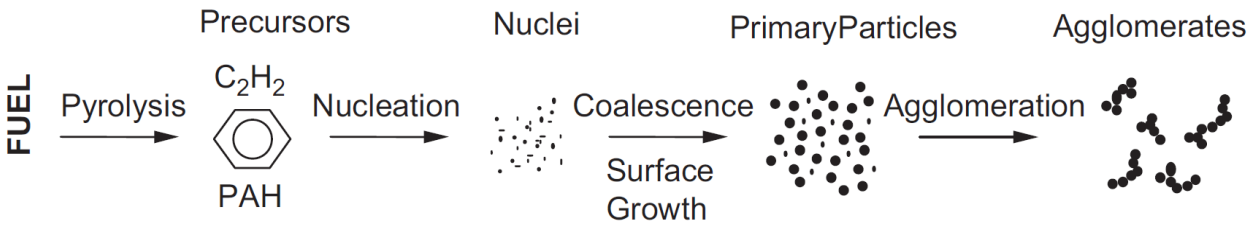

Figure 7.5 Schematic diagram of the steps in the soot formation process from gas phase to solid agglomerated particles [168]

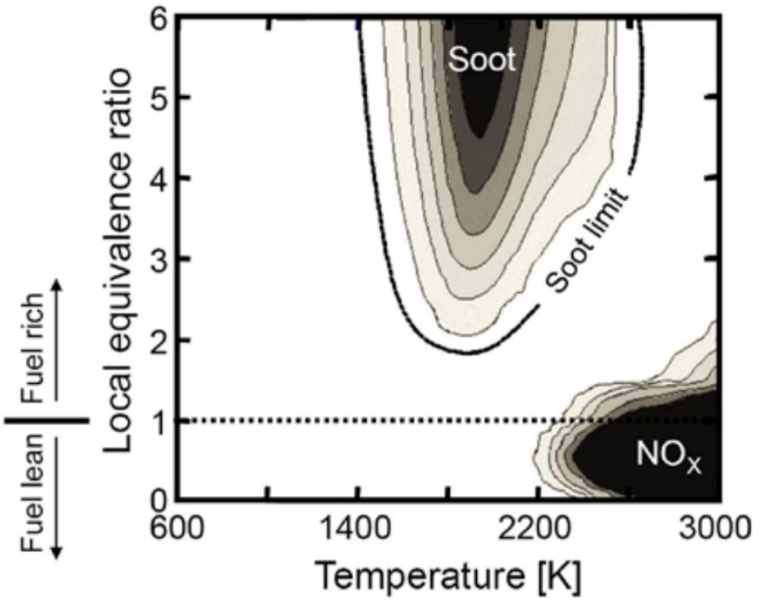

Figure 7.6 Fuel to air equivalence ratio (ϕ) and temperature map for soot and nitrogen oxides (NO_x) emissions [169,170].

7.3.2 Fuel Impingement and Pool Fires

From the viewpoint of the spark ignition engine, the locally rich zone is mostly formed under two conditions, which are fuel impingement on the cylinder walls or the piston crown, and pool fires. Fatouraie et al. [171,172] in direct injection, optical engines observed such impingement, which resulted in visible pool fires at the edge of the piston near the cylinder walls, clearly indicating the formation of particulates. Wooldridge et al., [173] also in an optical engine observed pool fires as well as the associated particulates as revealed by laser scattering images. This agrees with the basic soot formation processes noted above. So, these phenomena could be helpful to understand the relation between knock and soot emissions.

7.4 Phenomenon Investigation: Knock and Particulate Matter Emissions

7.4.1 Experimental Design

In order to experimentally validate the relationship between knock and particulate matter emissions, an experiment is conducted with two main variables: knocking and a locally rich zone. To control the knocking, intake temperature is varied by three different conditions, and the locally rich zone is controlled by two coolant temperatures. As described in Table 7.1, the intake temperature is divided into 30, 60, and 90°C, and the coolant temperature is set to a normal (85°C) and cold (70°C) temperature. The mechanism to control the locally rich zone is described in Figure 7.7, which is similar to high particulate matter emissions under cold starting conditions.

Table 7.1 Engine experimental conditions

Variables		**Knocking**		
		T_{int} = 30°C	T_{int} = 60°C	T_{int} = 90°C
Rich Zone	$T_{coolant}$ = 85°C	●	●	●
	$T_{coolant}$ = 70°C	●	●	●

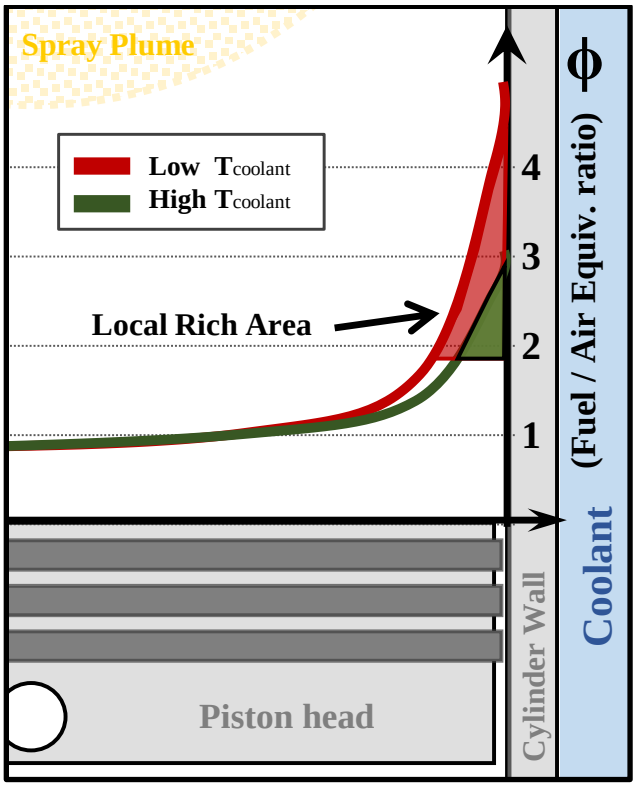

Figure 7.7 A schematic of local rich zone formation by coolant temperature.

7.4.2 Combustion Phasing and Knock Intensity

Figure 7.8 shows knock intensity as a function of combustion phasing for all conditions. Figure 7.8 (a) is the comparison of three intake temperature conditions under normal coolant condition. As expected, the knock limited combustion phasing is moved to a late phasing with increasing intake temperature, and amount of retard varies is consistently. Figure 7.8 (b) depicts the same intake temperature but low coolant temperature. The knock limited combustion is slightly advanced compared to normal coolant temperature, but the amount is negligible.

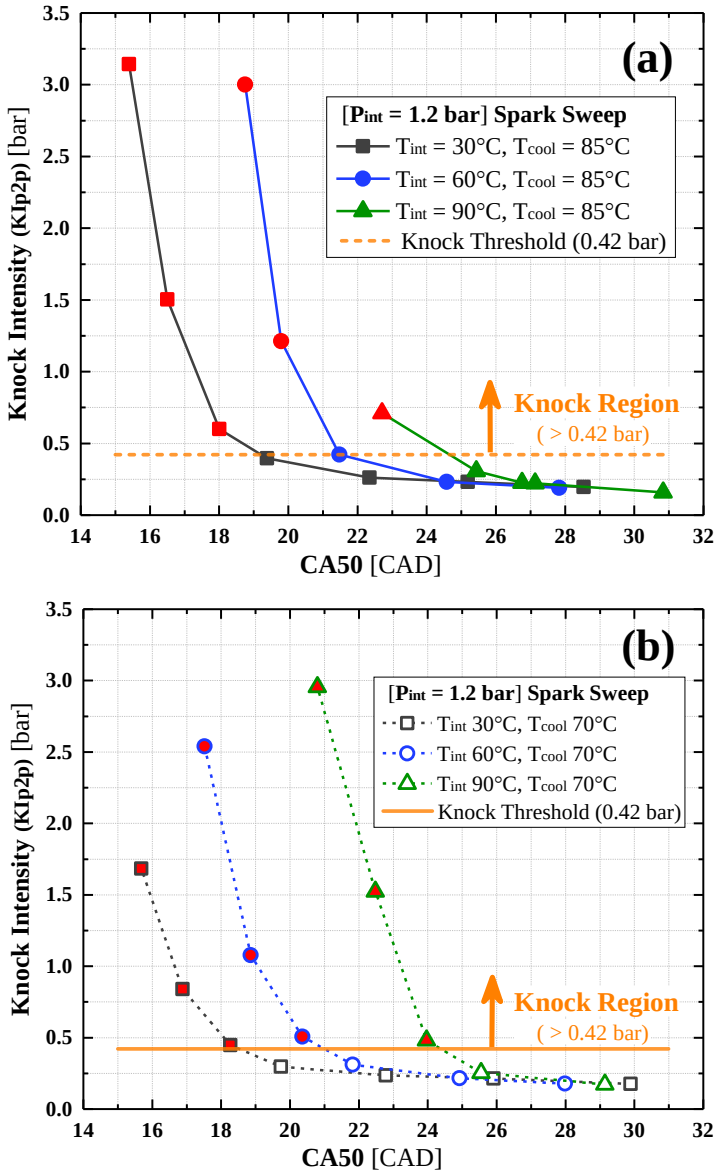

Figure 7.8 Knock intensity of three intake temperature conditions (30, 60, and 90°C) as a function of combustion phasing: (a) T_{cool} = 85°C; (b) T_{cool} = 70°C. The red symbols denote knocking conditions.

7.4.3 Combustion Phasing and Particulate Matter Emissions

Figure 7.9 is the accumulation mode particulate number as a function of combustion phasing. As expected, the particulate number emissions are dramatically increased after the onset of knock for both coolant temperature cases. The lower local rich zone condition in Figure 7.9

(a) shows very low particulate matter emissions under non-knocking conditions, and the higher local rich zone condition in Figure 7.9 (b) shows higher particulate matter emissions under non-knocking condition compared to the high coolant temperature case. But, the particulate matter emissions for the higher local rich zone are affected by the intake temperature, as well. For a better comparison, the differences between different coolant temperatures are shown in Figure 7.10.

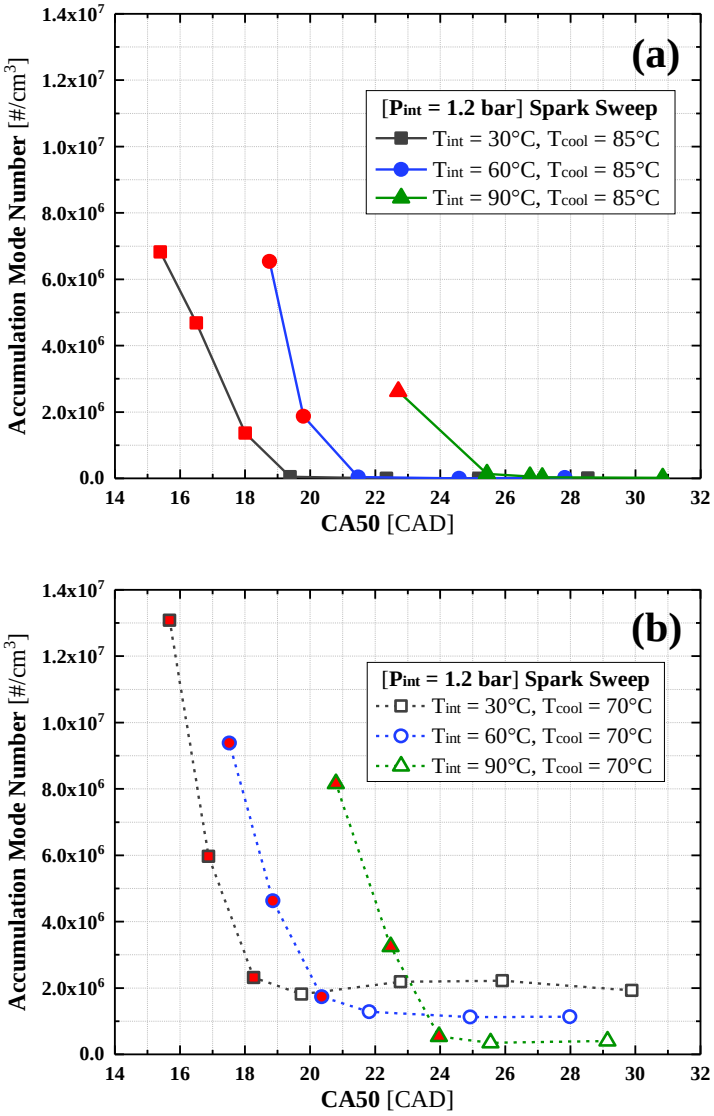

Figure 7.9 Accumulation mode particulate number of three intake temperature conditions (30, 60, and 90°C) as a function of combustion phasing: (a) T_{cool} = 85°C; (b) T_{cool} = 70°C. The red symbols denote knocking conditions.

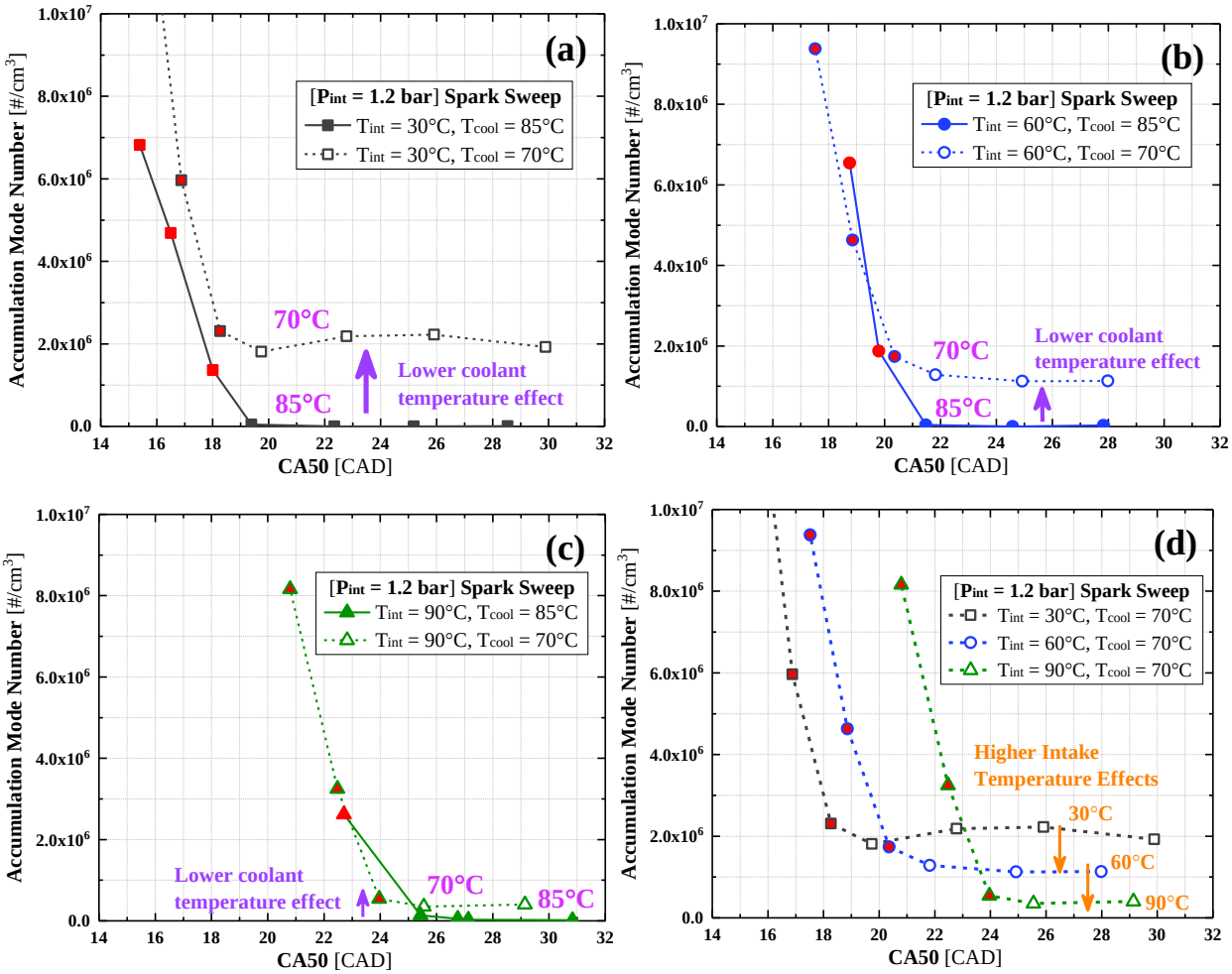

Figure 7.10 Accumulation mode particulate number differences by two temperature effects: (a), (b), and (c) Coolant temperature effect; (d) Intake temperature effect. The red symbols denote knocking conditions.

Figure 7.10 (a) to (c) shows the coolant temperature difference under the same intake temperature. When the intake temperature is lower, the particulate matter emissions differences under non-knocking condition are higher, and the differences are gradually going down. It can be inferred that the in-cylinder temperature, which is differentiated by intake temperature, also affects the area of local rich zone. Figure 7.10 (d) describes the effect of intake temperature on the particulate matter emissions induced by the area of the locally rich zone. The amount of particulate matter decrease is proportional to the intake temperature.

7.4.4 Relation between Knock Intensity and Particulate Matter Emissions

Figure 7.11 shows the relationship between the knock intensity and particulate matter emissions, which is a combined graph of the vertical axes in Figures 7.9 and 7.10. As both coolant conditions show, the particulate matter emissions are generally increased by the knock intensity.

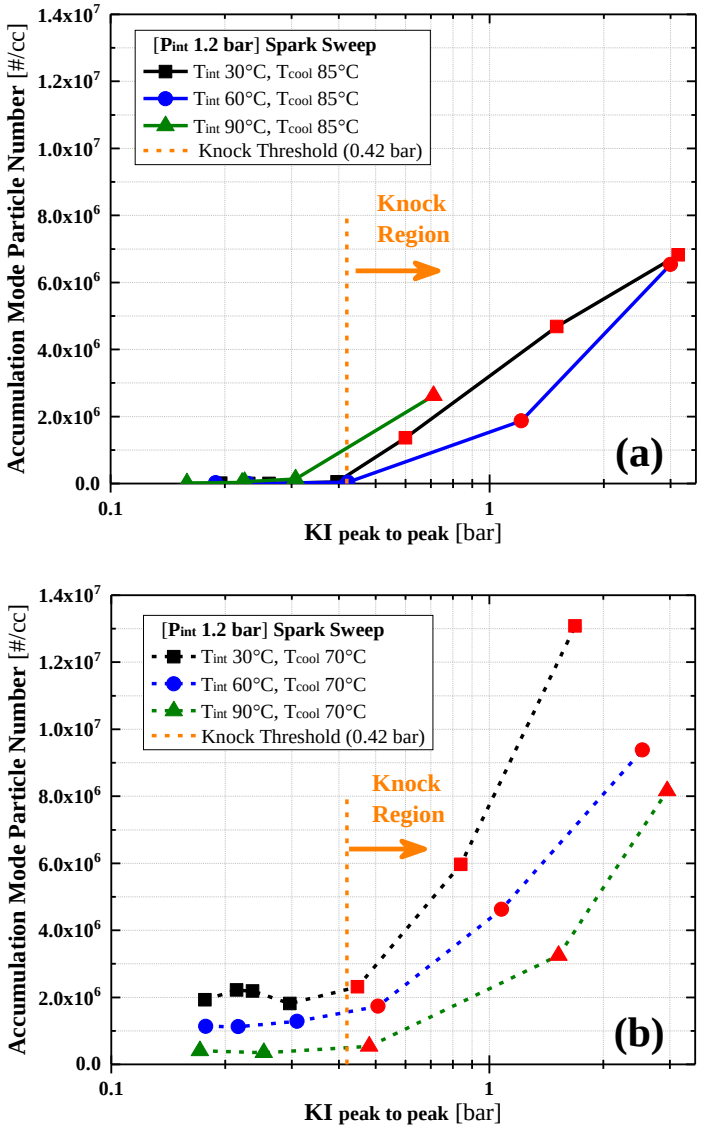

Figure 7.11 Accumulation mode particulate number of three intake temperature conditions (30, 60, and 90°C) as a function of knock intensity in a log scale: (a) T_{cool} = 85°C; (b) T_{cool} = 70°C. The red symbols denote knocking conditions.

7.5 Understanding: Theories and Conceptual Models

In summary of the soot formation under locally rich zones and from the experimental results presented here, three theories are suggested for a better understanding of the phenomenon using conceptual models.

7.5.1 Theory 1. Ring Crevice Mechanism

The sharp increase in particulate emissions with increasing knock intensity described above suggests that the knock event augments the local evaporation process through pressure and local flow oscillations, thus increasing the amount and number of rich pockets near the edge of the cylinder wall. This is consistent with the fact that knock is known to increase heat transfer [161,164,174]. Figure 7.12 depicts the general process of the knocking cycle near the edge of the combustion chamber, from left to right figures, by the time sequence. In general, a thin layer of hydrocarbon and oil is stuck on the cylinder wall in all cycles, and the end-gas auto-ignition creates pressure oscillations. Pressure oscillations induce rapid flow in and out of the top land regions thus releasing additional stored liquid fuel or oil as the second schematic shows. Since knock generally occurs late in the cycle, it will originate near the edge of the cylinder and produce local flow effects that may be more severe than suggested by pressure oscillations measured by a single pressure transducer. The spread-out small hydrocarbon droplets will undergo pyrolysis in the chamber, but the area near the droplet is locally fuel rich condition, so the debris might end up being a soot chunk as described in the last figure.

When viewed from above the engine piston, the cross-sectional view shown in Figure 7.12 will occur only near the end-gas auto-ignition region. With the data observed in this

dissertation, the particulate matter emissions are proportional to the knock intensity. To interpret the relation between knock intensity and particulate matter, the region of end-gas auto-ignition can be drawn as shown in Figure 7.13. The cross-sectional line denoted by "(A – A')" in Figure 7.13 is the same as Figure 7.12. Thus, as increasing the knock intensity, the region of end-gas auto-ignition should be increased, and the cross-sectional area which is drawn with both arrows in Figure 7.13 should be increased as well. Following this ring crevice mechanism (Theory 1), the linearity of the relationship between knock intensity and particulate matter emissions can be understood.

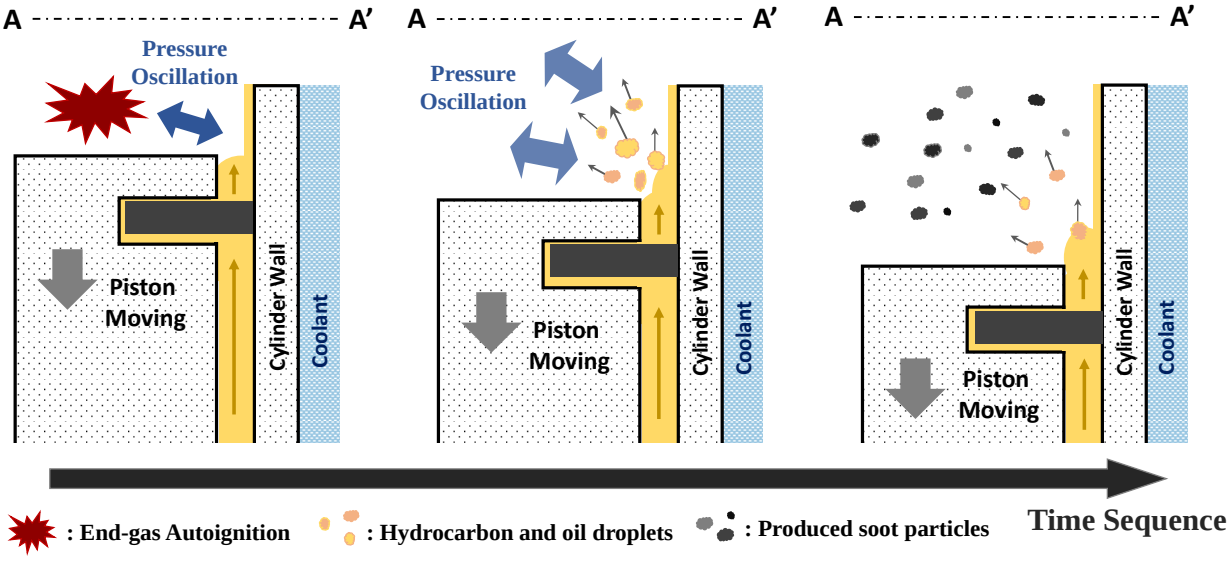

Figure 7.12 Conceptual model of Ring Crevice Mechanism – process (Theory 1)

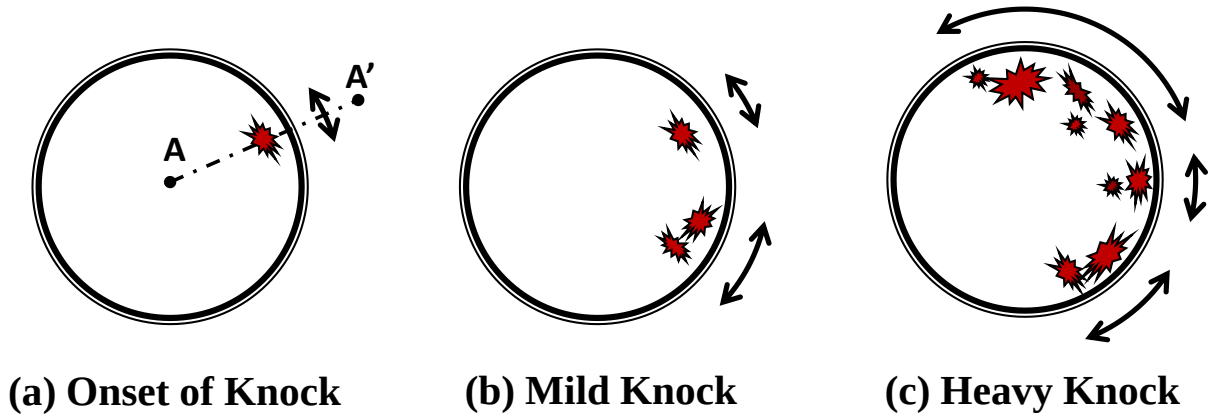

Figure 7.13 Conceptual model of Ring Crevice Mechanism – knock intensity (Theory 1)

7.5.2 Theory 2. Insufficient Mixing Mechanism

The second theory is about the time allotted for mixing of air and fuel. In general, the fuel and air are rapidly mixed as soon as the fuel is injected, but it will need a certain amount of time to be mixed sufficiently ($\phi < 2$), regardless of the injection type, either direct injection or port fuel injection. Figure 7.14 depicts the mixing status of the fuel and air as a function of time. Two parabolic lines denote the fuel (rich – above stoichiometric line $\phi = 1$) and air (lean – below $\phi = 1$) side mixture, and two lines are gradually converging as the mixing time progresses. The yellow area above the soot threshold ($\phi = 2$) stands for the portion of locally rich zones ($\phi > 2$) which generally contribute to formation of particular matter. The normal non-knocking combustion with lower particulate matter emissions is expressed by the dashed green line and an arrow, and the abnormal combustion (i.e., knocking) is indicated by the dashed red lines. When knock occurs, the mixing time is gradually shortened because of the increased auto-ignited regions and the random location of auto-ignition. With increasing knock intensity, such as from

mild to heavy knock, locally rich zones are gradually increased as shown in the yellow area above the soot threshold.

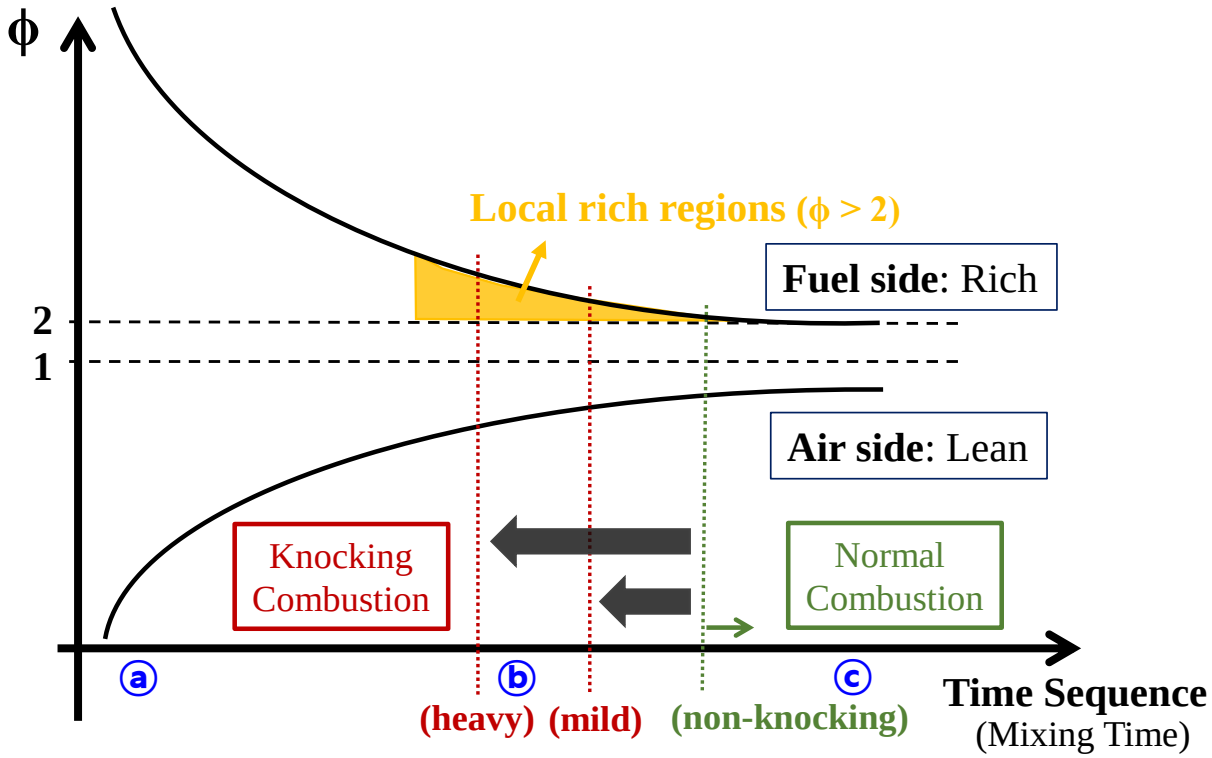

Figure 7.14 Conceptual graph of Insufficient Mixing Mechanism (Theory 2)

To better understand the variation of fuel-to-air equivalence ratio in Figure 7.14, conceptual graphs of air-to-fuel equivalence ratio distributions at three points in this time sequence (i.e., ⓐ, ⓑ, and ⓒ) are shown in Figure 7.15. The time sequence points in Figure 7.14 are (a) initial stage, (b) intermediate stage, and (c) last stage of fuel-air mixing. The initial stage graph in Figure 7.15 (a) is at the time of fuel injection for direct injection (DI). As soon as fuel is injected into the cylinder, fuel-to-air equivalence ratios on each side will be concentrated toward 0 for the air side and high ($\phi >> 2$) for the fuel side. The dashed line in Figure 7.15. (a) is the port fuel injection (PFI) case, which tends to be more highly pre-mixed, so the distributions are less

sharp than in the DI case. As the mixing progresses, areas of high fuel-to-air equivalence ratios are moving toward stoichiometric state as shown in Figure 7.15 (b). At the last stage of the mixing near the normal combustion (i.e., non-knocking condition) in Figure 7.15 (c), the fuel-to-air equivalence ratio have shifted closer to 1.0 as mixing drives the change to be more homogeneous.

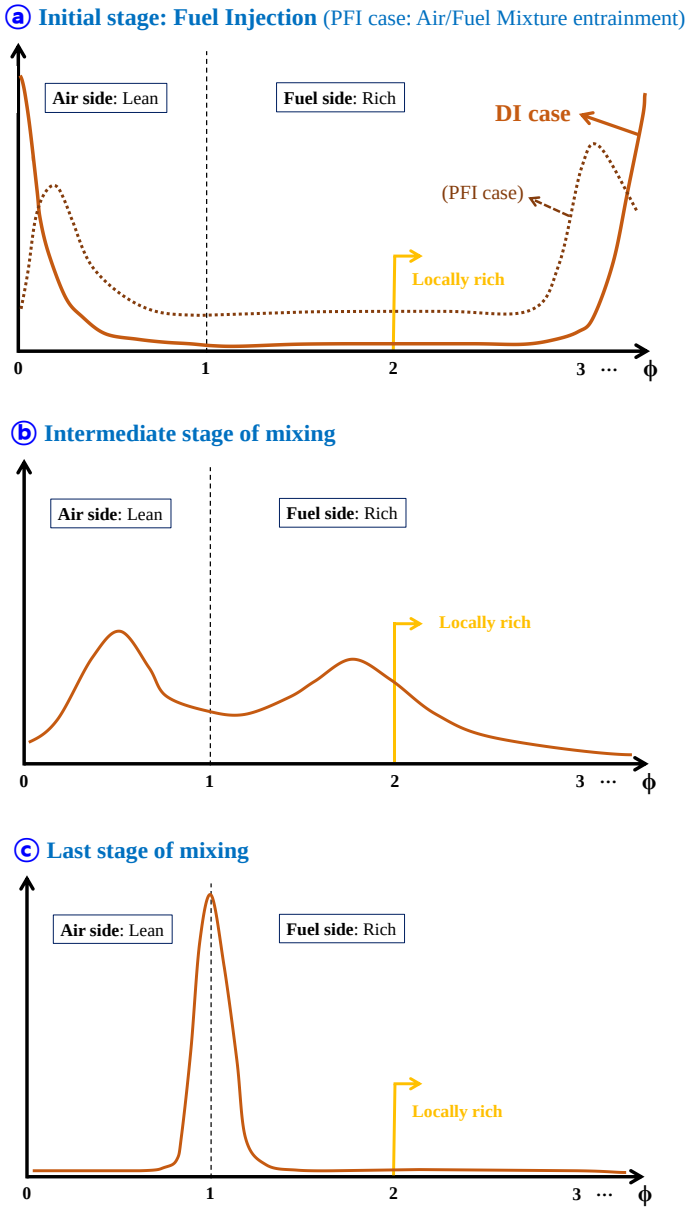

Figure 7.15 Conceptual graph of air-to-fuel equivalence ratio distribution by the mixing stages in Figure 7.14: a) Initial stage, b) Intermediate stage, and c) Last stage of mixing.

7.5.3 Theory 3. Shock Wave Mechanism

It is known that the amount of soot formation is higher under high pressure conditions, even under the same fuel to air equivalence ratio and temperature. Figure 7.16 describes shock-tube soot formation results for iso-octane under different pressure conditions [175]. All conditions are maintained the same, except for pressure, and the results show that high pressure leads to a high soot yield. From this effect of pressure on soot yields, the relationship between knock intensity and particulate matter emissions could be understood. Figure 7.17 shows the detonation region with locally high pressure based on knock intensity. Assuming that all conditions are identical except combustion phasing, the knocking cycle accompanied by detonation will make a higher pressure than a non-knocking cycle. Thus, the shock wave induced detonation region will lead to more particulate matter emissions, and the detonation intensity could be proportional to the increase in the particulate matter emissions.

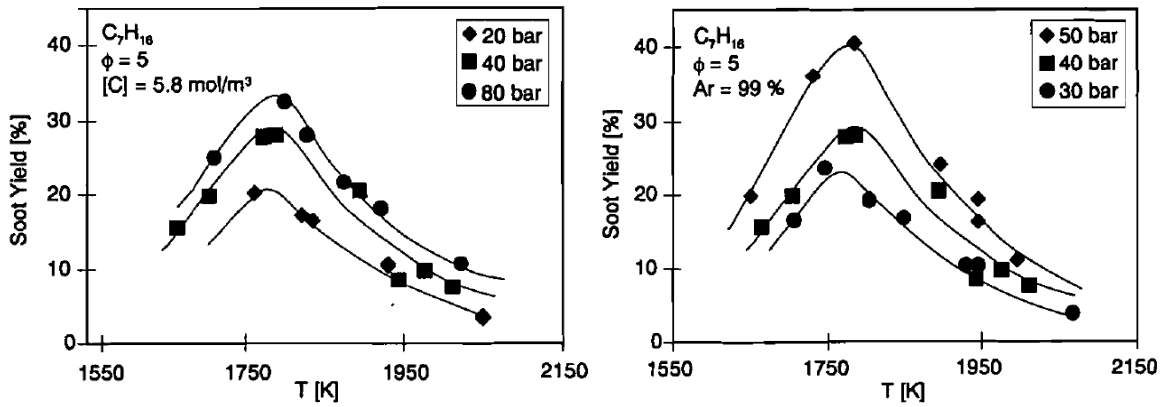

(a) **(b)**

Figure 7.16 (a) Influence of pressure on n-heptane soot yield demonstrated for pressures of 20, 40 and 80 bar at [C] = 5.8 mol/m^3; (b) Soot yield over temperature at constant Ar-concentration of 99% and varied pressures of 30,40 and 50 bar [175]

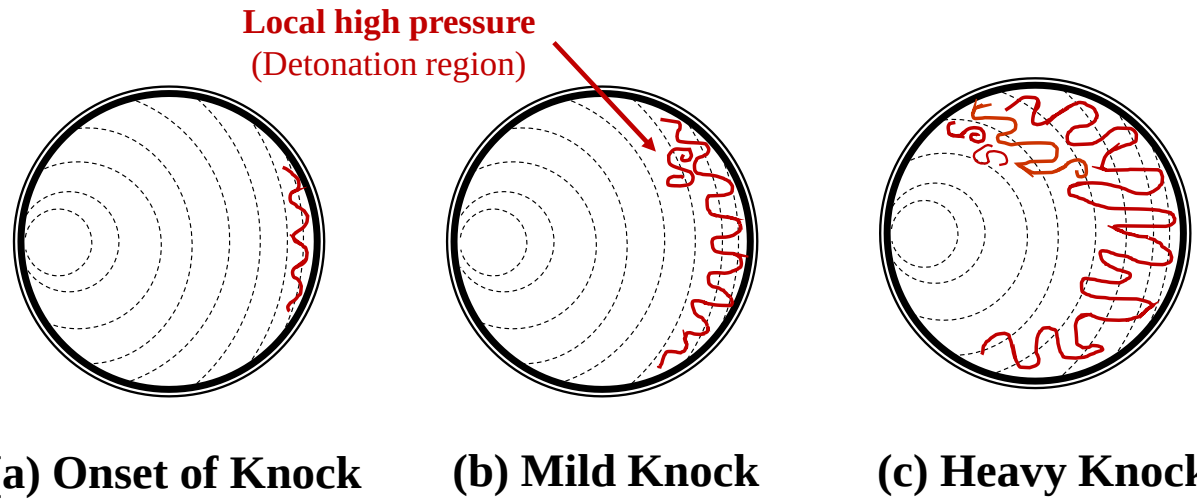

Figure 7.17 Conceptual model of Shock Wave Mechanism - Local high-pressure region (Theory 3)

7.6 Conclusion and Summary

This chapter conducted an exploratory study about the understanding of a newly observed relationship between knocking and particulate matter emissions. The phenomenon is that particulate matter emissions rapidly increase after the onset of knock with advancing the spark timing, and the increased amount of particulate matter emissions are linear to the knock intensity. The results can be divided into two major sections: (1) Phenomenological investigation and (2) Phenomenon understanding with conceptual models.

(1) Phenomenological investigation

Engine experiments were conducted to separate the knocking effect on particulate matter emissions with varied intake temperature and coolant temperature. The results clearly showed that the knock plays a significant role to generate particulate matter emissions, and the knocking effects were even higher than the in-cylinder temperature effect (e.g., cold start condition).

(2) Phenomenon understanding: Conceptual models

To understand the relationship between knocking and particulate matter emissions, three conceptual models were suggested based on the experimental analyses and soot formation process in internal combustion engines. The three suggested theories are as follows:

- Theory 1. Ring Crevice Mechanism

  : augmented release of hydrocarbons from the ring crevice. (Figure 7.12 and Figure 7.13)

- Theory 2. Insufficient Mixing Mechanism

  : increased local rich zones. (Figure 7.14 and Figure 7.15)

- Theory 3. Shock Wave Mechanism

  : increased chemical soot production due to pressure increase. (Figure 7.16 and Figure 7.17)

There is very limited understanding of this phenomenon and relationship, so it is anticipated that this finding will be useful in the engine research fields. Further investigations for the conceptual model validations will be helpful for future work.

1) Ring crevice mechanism (augmented release of hydrocarbons from the ring crevice)

2) Insufficient mixing mechanism (knocking induced increased local rich zone)

3) Shock wave mechanism (increased chemical soot production due to pressure increase)

Chapter 8

Conclusions and Recommendations for Future Work

8.1 Conclusions and Contributions

This dissertation has explored various knock mitigation strategies focusing on fuel characteristics, mixture dilution, and injection strategies for improving efficiency and emissions, and an exploratory study of a novel observation about the relationship between knocking and particulate matter emissions in spark ignition engines. The conclusions and original contributions of the dissertation are summarized as follows.

In Chapter 3, combustion characteristics of three oxygenated fuel (2,5-dimethylfuran, ethanol, and isobutanol) gasoline blends were studied along with different blending ratios and boosting levels. Knock limited combustion phasing, burn duration, and particulate matter emissions results were compared by blend ratio and at 20 volume percent fuel blends, and general engine combustion results such as thermal efficiency, combustion stability, and gaseous emissions were explored as well. The results showed that the effect of 2,5-dimethylfuran addition on knock limit extension is similar to the effect of ethanol addition, and the effect is stronger with increasing boost level. The total particle number emission and particle size distribution of the particulate matter emissions gradually decreased with increasing oxygenated

fuel blend level, and the order was same as the order of knock limit extension. However, 2,5-dimethylfuran addition generally yields a wider soot distribution compared to the alcohol group fuels. This study provides valuable insights for the utilization of oxygenated fuels as gasoline additives, especially for the novel oxygenated fuel candidate, 2,5-dimethylfuran. The novelty of this fuel study is unraveling the anti-knock effect and particulate matter emissions characteristics of 2,5-dimethylfuran and the detailed comparison with two important alcohol group fuels.

In Chapter 4, the impact of syngas (hydrogen and carbon monoxide) addition on engine combustion and knock was experimentally investigated with an intensive comparison between EGR dilution and lean conditions. The amount of syngas was controlled on an energy basis, from 0% to 15%, to compare the difference between EGR and air dilution. Knocking tendencies with respect to the frequency, combustion phasing, and burn duration were analyzed based on observed engine knock. Also, the thermal efficiency and emissions differences were discussed in detail. The results showed that with increasing the syngas addition, knocking is significantly suppressed, and the effect was more beneficial with EGR dilution than with air dilution. Since the use of syngas to support engine combustion is of increasing interest in the advanced spark ignition engine field due to rapidly developing fuel reformation technology, precise engine combustion guidelines are needed, especially for knock resistance and dilution tolerance. In this respect, this study offers important insights for the operation of syngas aided combustion, especially for the highly diluted advanced spark ignition engines.

In Chapter 5, a unique fuel injection concept, dual fuel injection using both a direct injector (DI) and a port fuel injector (PFI), was experimentally explored with regard to the knock and EGR dilution limit extension. Thermal efficiency benefit analysis between EGR dilution and knock limit extension was studied in detail, as well. A baseline for comparison with dual

injection results was made using direct injection fueling only. A splash blended E20 fuel was used for the direct injection only tests, and for the dual fuel injection tests, 80 volume percent of gasoline was injected using DI, and 20 volume percent of ethanol was injected using PFI. EGR mass fraction was varied from 0 to 21 percent in increments of 7 percent. The results showed that dual injection was beneficial to shorten the burn duration and improve combustion stability but was slightly more sensitive to knock than direct injection, due to increased unburned gas temperature. The particulate matter emissions from dual fuel injection showed improved results compared to direct injection only, and the gaseous emissions showed lower unburned hydrocarbons and similar nitrogen oxides compared with direct injection only. In addition, the thermal efficiency benefit analysis results showed that the EGR dilution benefit was two times higher than the knock limit extension benefit. Based upon these results, it can be concluded that the dual fuel injection could be a good strategy for highly diluted spark ignition engines for improving combustion stability and particulate emissions. Also, the thermal efficiency benefit analysis result provides important insight for engine calibration and concept design fields for high efficiency vehicles.

In Chapter 6, multiple injection strategies with a state-of-the-art piezoelectric hollow cone spray direct injector were investigated with respect to the effects on engine combustion characteristics and emissions. Two features of multiple injection strategies were experimentally investigated: the number of injections and the timing of injections. The results from thermodynamic process analyses confirmed that multiple injection maintains torque and combustion stability compared to single injection but extends the knock limit and thermal efficiency due to improved heat release phasing, especially with an additional late injection during the intake valve closed (compression stroke) period. The gaseous pollutant emissions,

including nitrogen oxides and unburned hydrocarbons, were significantly reduced with multiple injection, particularly with compression stroke injection. In contrast, carbon monoxide emissions were increased. Particulate matter emissions were not directly related to the injection period, but the number of injections significantly reduced particulate matter emissions. This study provides important visions for the development of future direct injection spark ignition strategies, especially with advanced fuel injectors. Also, the results contribute to the particulate matter reduction studies through optimized application of state-of-the-art fuel injectors.

In Chapter 7, a novel understanding of a unique phenomenon, which is the relationship between knock and particulate matter emissions, was analyzed and explained with conceptual models for spark ignition engines. In general, particulate matter emissions are rapidly increased after the onset of knock in the process of spark advance, and the increased amount of particulate number emissions are linear to the knock intensity. This phenomenon was analyzed with experimental data under several knocking related conditions, and three theories were proposed along with conceptual models. The proposed theories were as follows:

1) Ring crevice mechanism (augmented release of hydrocarbons from the ring crevice)

2) Insufficient mixing mechanism (knocking induced increased local rich zone)

3) Shock wave mechanism (increased chemical soot production due to pressure increase)

This phenomenon has not been revealed previously, and there is a minimal understanding of this phenomenon and relationship. Therefore, these suggested mechanisms and conceptual models are expected to have significant impacts on the field of engine combustion research.

8.2 Recommendations for Future Work

The present dissertation focused on three major parameters, which are fuel properties, mixture dilution, and injection strategies, and a relationship between knocking and particulate matter emissions. Future work also could be concentrated on these parametric impacts and relationships.

(1) Fuel properties: Two types (oxygenated fuels and syngas) of fuel studies conducted in the present dissertation provided a significant improvement on knock limit extension and emissions. As the knocking results for 2,5-dimethylfuran gasoline blends suggest under boosted condition, octane blending response studies of the furan functional group, which shows a highly non-linear trend, could have a significant impact on advanced fuel research. Besides, other fuel blends, beyond binary blends including ternary or higher-order blends, and optimization studies could also yield highly impactful new information. In addition, this dissertation explored particulate matter emissions from using alternative fuels. From the perspective of particulate matter emissions, studies of the PMIs (Particulate Matter Indices) [176,177] of fuels with furan functional groups will provide valuable insights for future work.

(2) Mixture dilution: Two major dilution strategies were studied in this dissertation: EGR (stoichiometric) and air (lean) dilution. Recently, fuel impacts on advanced combustion modes including gasoline compression ignition (GCI) [178,179], spark assisted compression ignition (SACI) [180–183], reactivity controlled compression ignition (RCCI) [184–186], etc., have been actively being explored. These compression ignition modes also would benefit from the sophisticated study of dilution strategies as pursued in this dissertation. So, studies of these advanced engine mode studies informed by the results from this dissertation will have a considerable impact on the future fuel and engine combustion research. In addition, different

types of dilution such as water injection or water vapor dilution could also provide impactful insights.

(3) Injection strategies: The dual fuel injection strategy studied in this dissertation provided dilution limit extension and reduction of particulate matter emissions. This information also could be applied in advanced spark ignited combustion modes, such as SACI concept under different load [187,188]. Furthermore, with direct injection, port fuel injection, and dual fuel injection, each mode has different advantages based on operating conditions, so optimization studies would be valuable that leverage each benefit using both injectors with respect to improving efficiency and particulate matter emissions. Another future study utilizing this injection concept is water injection using port fuel injectors. Many water injection studies are using custom made water injectors, but using commercial port fuel injectors for water injection could be a cost-effective injection strategy. So, optimization of port injection of water will be an interesting study for future engines. Also, studies of multiple fuel injections showed a considerable benefit for reducing particulate matter emissions. Water injection technology in spark ignition engine has a significant drawback for the particulate matter emissions, so the multiple injection combined with water injection studies could have a significant potential for future spark ignition engines enabling dramatic extension of knock limits.

(4) Relationship between knocking and particulate matter emissions: The present research on the relationship between knock and particulate matter emissions is at an early stage. So, this study can be expanded in many ways, such as to consider the impact on particulate matter emissions using different fuels, dilution levels, novel fuel injection concepts, etc. Also, the three conceptual models in Chapter 7 could be validated through additional experiments. The first theory (Ring crevice mechanism) could be verified by gaseous fuel or carbon-free fuel (e.g.,

hydrogen) engine knocking experiments to change the amount of hydrocarbons in the ring crevice. The second theory (Insufficient mixing mechanism) could be tested by temperature variation at fixed spark and injection timing to identify the mixing threshold. The third theory (Shock wave mechanism) could be verified by using an optically accessible engine under knocking conditions and measuring the soot volume fraction across the cylinder.

Appendices

A. Data Processing (MATLAB Script for Knock Intensity Calculation: 'KI 20' and 'KI peak to peak')

```
%% Knocking Intensity Calculator (KI20 KIp2p Calculator) - 2016.Aug.
%   Contact info: Taehoon Han (taehoonh@umich.edu)
%   This code is made for AL1122 Hydra SCRE.
%   Filtering limit is 3500 Hz (High Pass Filter)
%   KI20 reference: SAE Technical paper # 902135 (Konig et al.)

%% initialization
clear all
close all
clc
tic

%% I. Condition and iFile Loading

% [1] rpm & case setup (!check everytime!)
rpm = 1500;
iFile_start_num = 0000;

% [2] iFile setup (Expand for loop in case of multiple data processing)
for iFn=1:1   % expand for multiple data
iFile_number{iFn} = ['Data.',num2str(iFn+iFile_start_num-1)];

for i=1:length(iFile_number)
    [~, b, ~, ~, ~] = iFileReadMat_v5(iFile_number{i});
% data(i).a = a;
  data(i).b = b;
% data(i).c = c;
% data(i).d = d;
% data(i).e = e;
end

%% II. Cylinder Pressure Extract

% [x-axis] : CAD -> 7200 by 1
Pcyl_x_axis = data(i).b(1,3).x_vek ;
```

```
      % [y-axis] : Cyl Pressure -> 7200 by 200
      for i=1:length(iFile_number)
          for j=1:200
          Pcyl_200_raw(:,j) = data(i).b(1,3).daten(:,j) ;
          end
      end

      % Cylinder Pressure PLOT
      figure(1)
      plot(Pcyl_x_axis,Pcyl_200_raw)
      xlim([-20,50])

      %% III. Knocking Filtering (using FFT)

      [length,width] = size (Pcyl_200_raw) ;
      Pcyl_1_raw =Pcyl_200_raw;  % [bar]

      for k = 1:200

          % (1) Using FFT algorithm in matlab for spectral analysis
          Freq = 50*rpm;  % Frequency rpm to cps(Hz)
          Pcyl_FFT(:,k) = fft(Pcyl_1_raw(:,k));   % Pcyl FFT result (Complex
Number)
          Pcyl_Length = 7200; % Data Length (mostly 7200) %
=length(Pcyl_1_raw);
          Pcyl_FFT_abs(:,k) = abs(Pcyl_FFT(:,k)/Pcyl_Length); % Abs of Pcyl
FFT (Magnitude of Complex)
          Pcyl_FFT_abs_half(:,k) = Pcyl_FFT_abs(1:Pcyl_Length/2+1);    % Half
of Symmetric values.

          % (2) Plot the Frequency Domain
          FreqD_x_axis = Freq*(0:(Pcyl_Length/2))/Pcyl_Length;

      %     % Frequency Domain Plots
      %     figure (2)
      %     plot(FreqD_x_axis,Pcyl_FFT_abs_half,'b')
      %     title('Frequency Domain at 1500rpm')
      %     ylim([0,0.01])
      %     xlim([0,Pcyl_Length*10/2])
      %     xlabel('f[Hz]')
      %     ylabel('|S(f)|')
      %     hold on

          % (3) High Pass Filter using Chebyshev2 function.
              [z,p,kn] = cheby2(50,80,(3500/45000),'high');
                  % call high-pass Chebyshev Type II Filter with given order
and cut-off frequency.
                  % Order = 50 / R value = temporarily 80 (Yu Chen)
                  % Frequency: 1500 rpm = 25 rps = 25*360*10 ps = 90000 1/s
(Hz)
              [sos,g] = zp2sos(z,p,kn); % designs a high-pass filter and
returns its zeros, poles, and gain.
              Filtered_Ringing(:,k) = filtfilt(sos,g,(Pcyl_1_raw(:,k))); %
forward then reverse filter to avoid phase lag on signal.
```

```
            % Filtered Pressure PLOT
            figure (3)
            plot(Filtered_Ringing);
            xlim([0,7200])
        end

        %% IV. Knocking Intensity Calculation

        for k = 1:200
            % % (1) Calculating the KIp2p (Knock Intensity)
            KI_p2p_max(:,k) = max(Filtered_Ringing(3500:5500,k));
            KI_p2p_min(:,k) = min(Filtered_Ringing(3500:5500,k));
            KI_p2p_each = KI_p2p_max(:,k) - KI_p2p_min(:,k) ;
            KI_p2p_table(:,k) = KI_p2p_each ;

            % % (2) Calculating the KI20 (Knock Intensity & Duration)
            KI20_Nsamp = 200;
            knock_peak(:,k) = max(abs(Filtered_Ringing(3500:5500,k)));
            Pcyl_x_axis_positive = Pcyl_x_axis+360;
                % First loop: Knocking Start Point finding
                for KI1 = 1:length
                        if
(Pcyl_x_axis_positive(KI1)>=350)&&(Pcyl_x_axis_positive(KI1)<=550)&&(abs(Filt
ered_Ringing(KI1,k))==knock_peak(:,k))
                        KnockStart_x_axis(:,k) = Pcyl_x_axis_positive(KI1);
                        end
                end
                % Second loop: KI20 of each cycles
                KI20_start(:,k) = floor(KnockStart_x_axis(:,k)*10)+1 ;
                KI20_end(:,k) = floor(KnockStart_x_axis(:,k)*10)+200 ;
                KI20_sum = 0;

                for KI2 = KI20_start(:,k) : KI20_end(:,k) ;
                        KI20_each(KI2-KI20_start(:,k)+1,k) =
Filtered_Ringing(KI2,k) ;
                        KI20_each_sqr(KI2-KI20_start(:,k)+1,k) =
(KI20_each(KI2-KI20_start(:,k)+1,k))^2 ;
                        KI20_sum = KI20_sum + KI20_each_sqr(KI2-
KI20_start(:,k)+1,k) ;
                end
                KI20 = KI20_sum/KI20_Nsamp ;
                KI20__table(:,k) = KI20;
        end
        % % (1) Mean Value of the KIp2p (Knock Intensity)
        KI_p2p__Mean(iFn,:) = mean(KI_p2p_table)
        % % (2) Mean Value of the KI20 (Knock Intensity & Duration)
        KI20__Mean(iFn,:)  = mean(KI20__table)
        end
```

B. Supplemental Material for Combustion Characteristics of Oxygenated Fuel Gasoline Blends (Chapter 3)

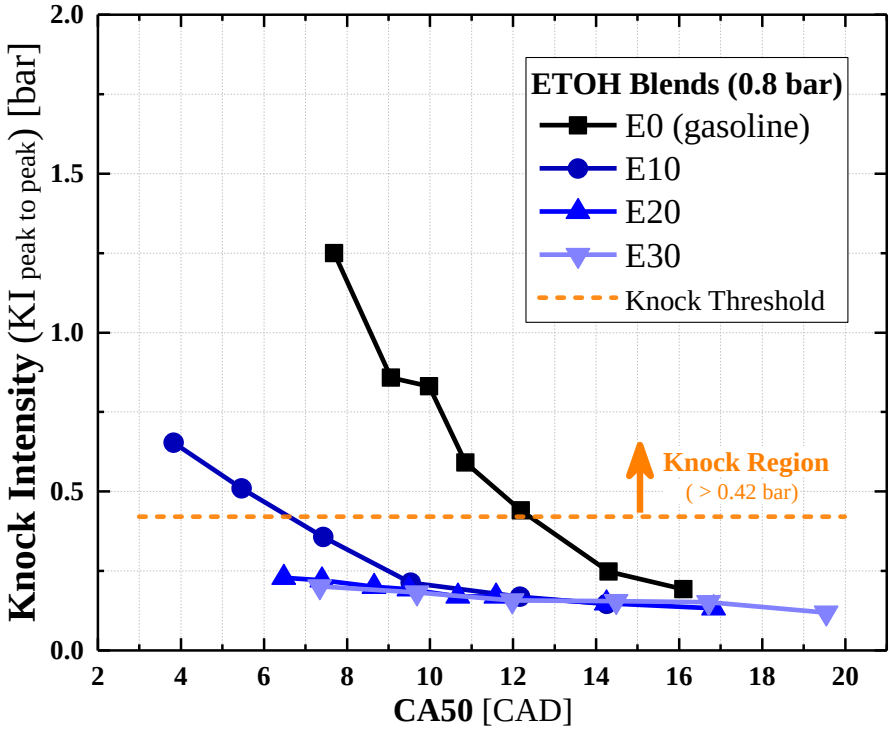

Figure A. 1. Knock intensity for ETOH blends under 0.8 bar intake pressure as a function of combustion phasing (CA50)

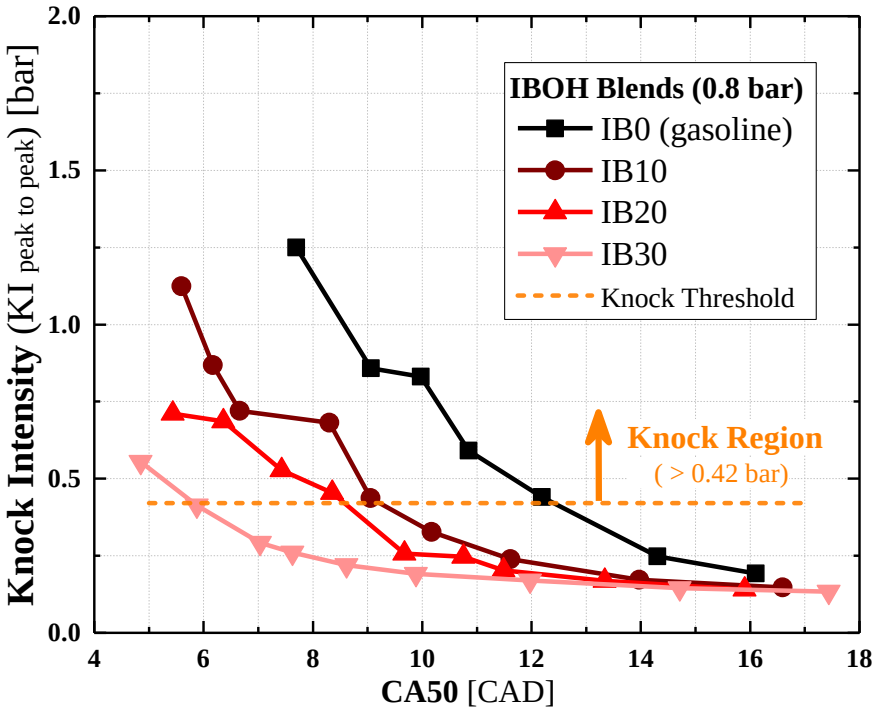

Figure A. 2. Knock intensity for IBOH blends under 0.8 bar intake pressure as a function of combustion phasing (CA50)

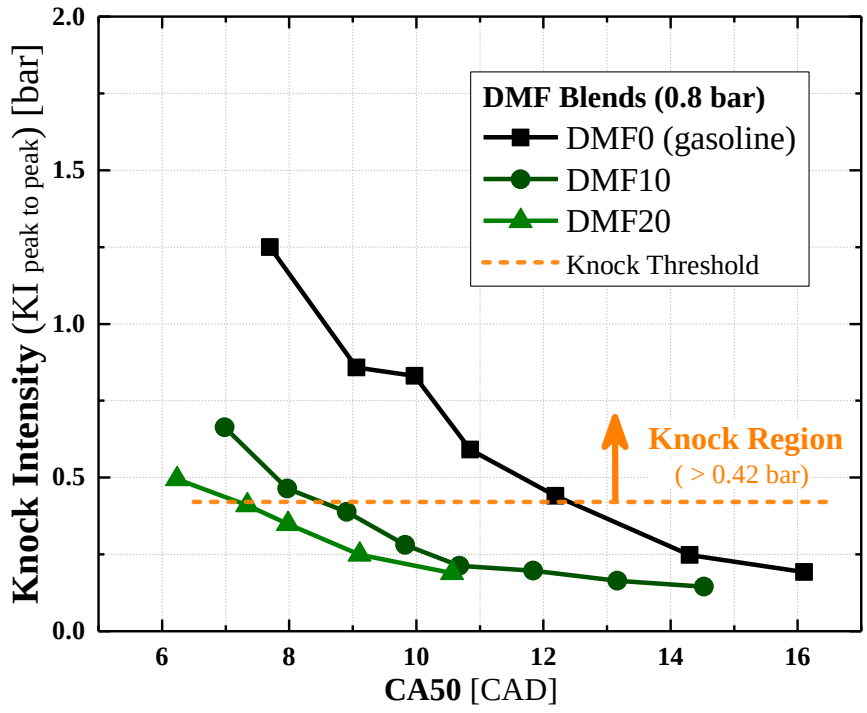

Figure A. 3. Knock intensity for DMF blends under 0.8 bar intake pressure as a function of combustion phasing (CA50)

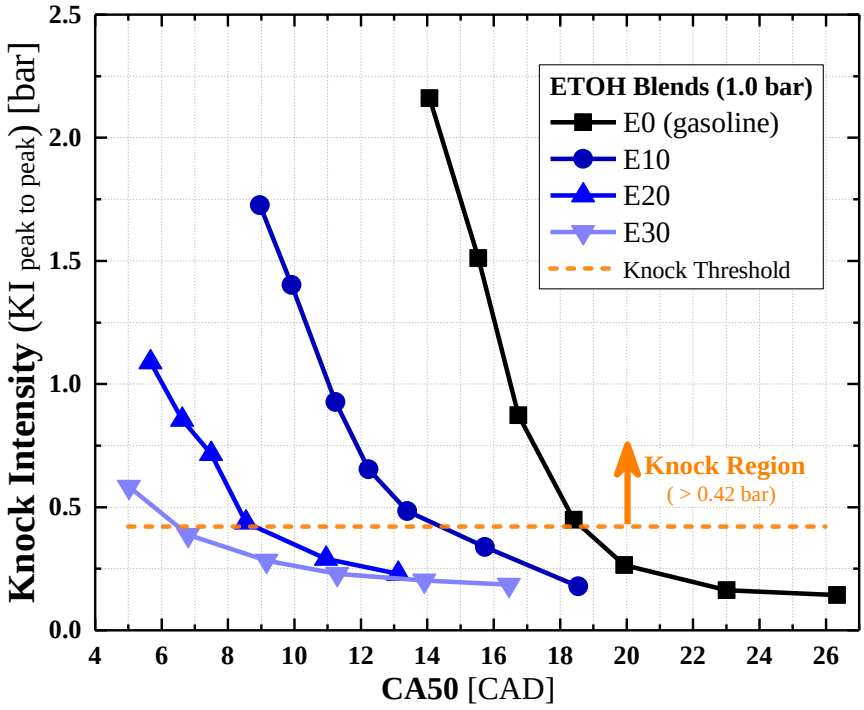

Figure A. 4. Knock intensity for ETOH blends under 1.0 bar intake pressure as a function of combustion phasing (CA50)

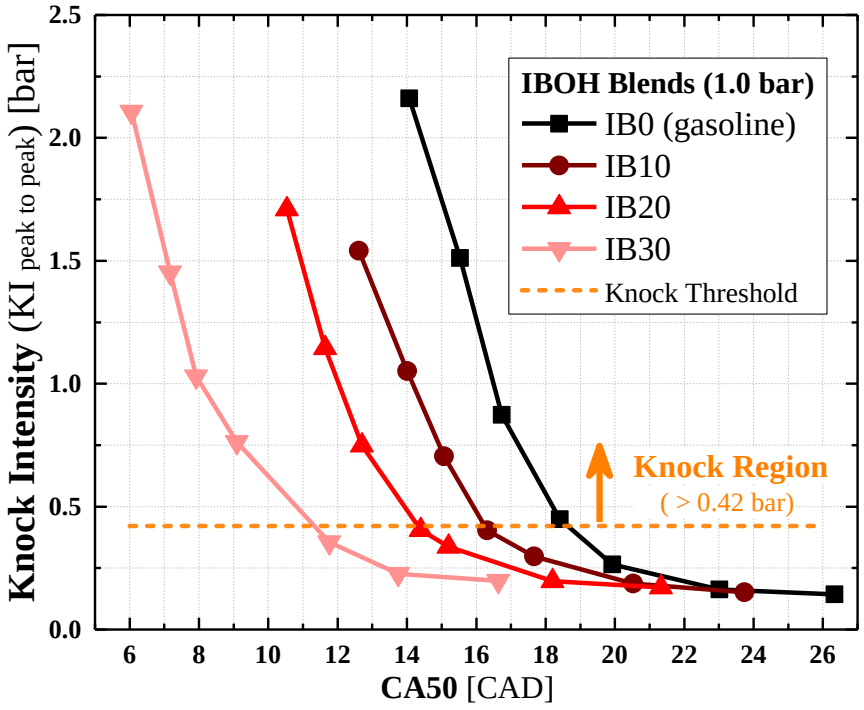

Figure A. 5. Knock intensity for IBOH blends under 1.0 bar intake pressure as a function of combustion phasing (CA50)

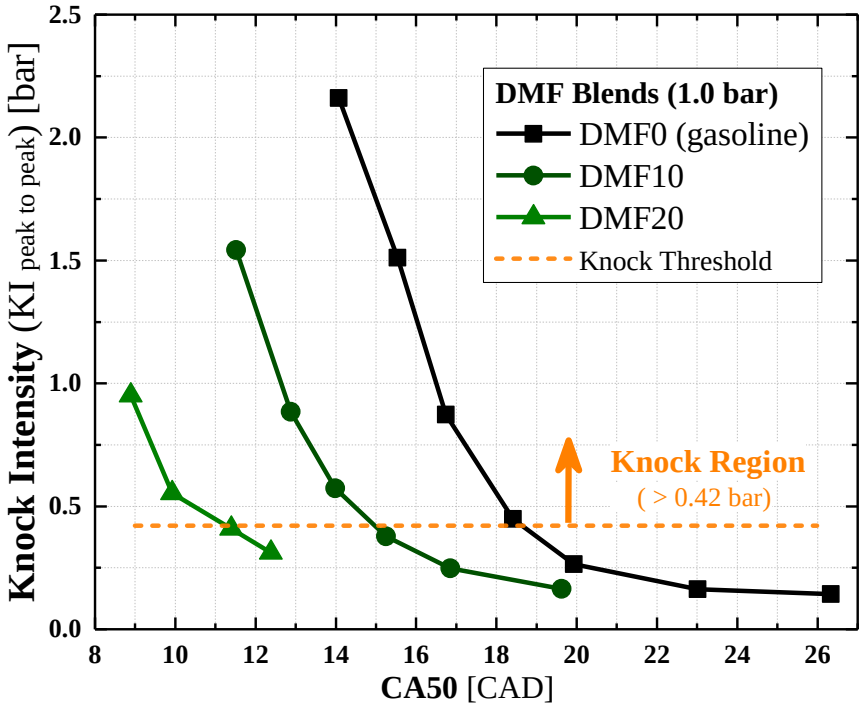

Figure A. 6. Knock intensity for DMF blends under 1.0 bar intake pressure as a function of combustion phasing (CA50)

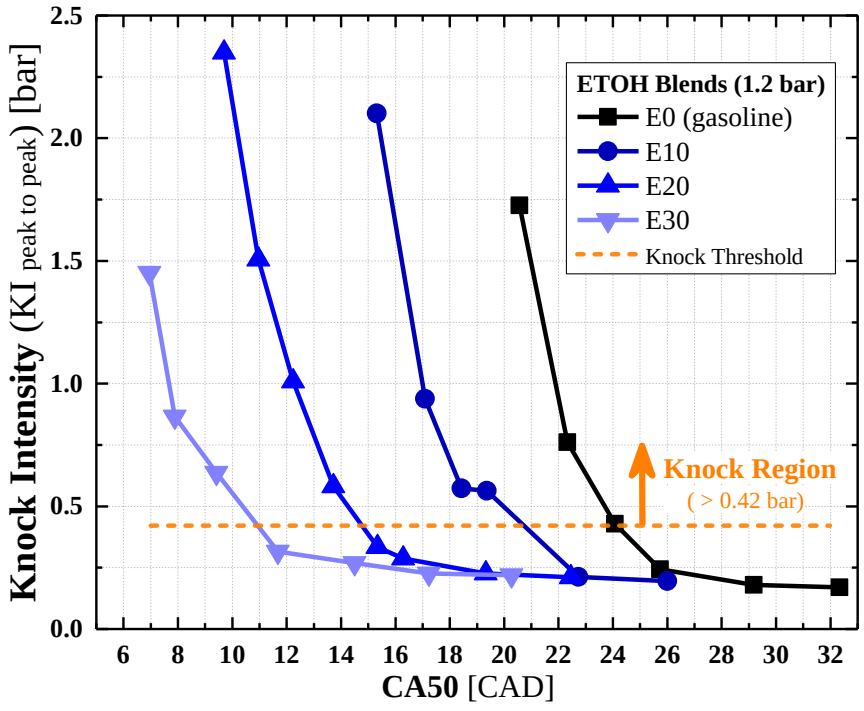

Figure A. 7. Knock intensity for ETOH blends under 1.2 bar intake pressure as a function of combustion phasing (CA50)

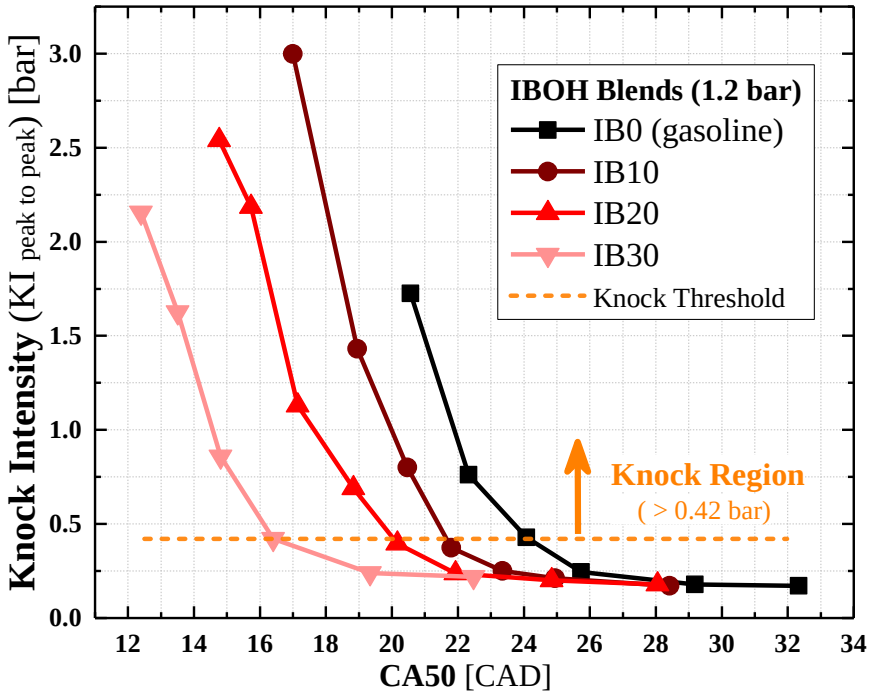

Figure A. 8. Knock intensity for IBOH blends under 1.2 bar intake pressure as a function of combustion phasing (CA50)

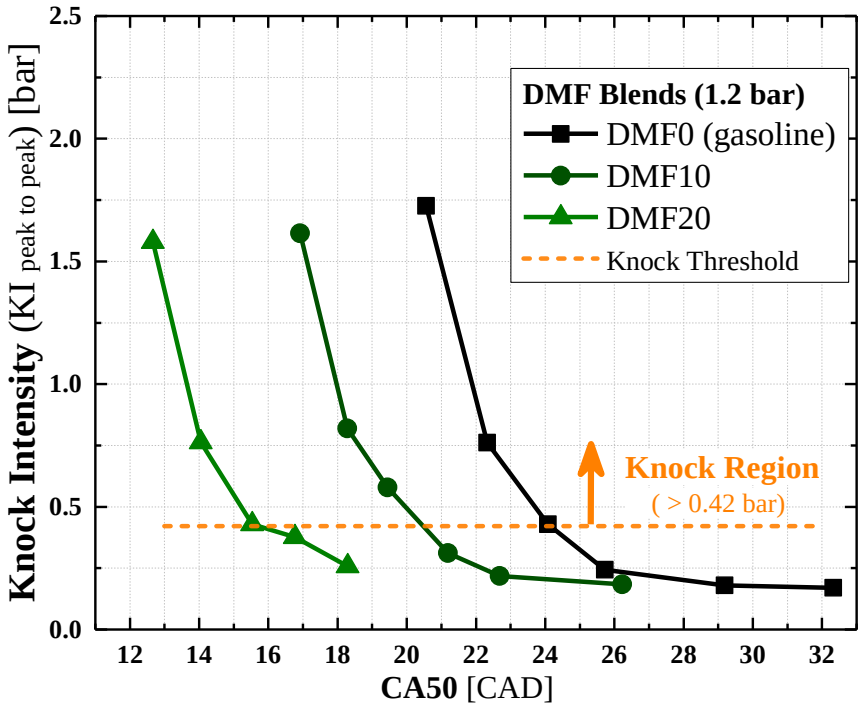

Figure A. 9. Knock intensity for DMF blends under 1.2 bar intake pressure as a function of combustion phasing (CA50)

Bibliography

[1] EURO Emissions Standards, Emissions from light-duty vehicles in the automotive sector. European Commission., (2015). https://ec.europa.eu.

[2] Passenger car miles per gallon, normalized to CAFE, The International Council on Clean Transportation. (2019). https://theicct.org/.

[3] S. Richard, G. Font, F. Le Berr, O. Grasset, M. Fremovici, On the Use of System Simulation to Explore the Potential of Innovative Combustion Systems: Methodology and Application to Highly Downsized SI Engines Running with Ethanol-Gasoline Blends, SAE Technical Paper. (2011). doi:10.4271/2011-01-0408.

[4] D. Han, S.-K. Han, B.-H. Han, W.-T. Kim, Development of 2.0L Turbocharged DISI Engine for Downsizing Application, SAE Technical Paper. (2007). doi:10.4271/2007-01-0259.

[5] G. Lavoie, E. Ortiz-Soto, A. Babajimopoulos, J.B. Martz, D.N. Assanis, Thermodynamic sweet spot for high-efficiency, dilute, boosted gasoline engines, International Journal of Engine Research. 14 (2012) 260–278. doi:10.1177/1468087412455372.

[6] A. Lewis, E. Ortiz-Soto, G. Lavoie, D.N. Assanis, Scaling and dimensional methods to incorporate knock and flammability limits in models of high-efficiency gasoline and ethanol engines, International Journal of Engine Research. 16 (2015) 181–196. doi:10.1177/1468087414530387.

[7] J.B. Heywood, Internal combustion engine fundamentals, McGraw-Hill Higher Education, 1988.

[8] R. Schießl, U. Maas, Analysis of endgas temperature fluctuations in an SI engine by laser-induced fluorescence, Combustion and Flame. 133 (2003) 19–27. doi:10.1016/S0010-2180(02)00538-2.

[9] S. Russ, A Review of the Effect of Engine Operating Conditions on Borderline Knock, SAE Technical Paper. (1996). doi:10.4271/960497.

[10] X. Zhen, Y. Wang, S. Xu, Y. Zhu, C. Tao, T. Xu, M. Song, The engine knock analysis - An overview, Applied Energy. 92 (2012) 628–636. doi:10.1016/j.apenergy.2011.11.079.

[11] J.M. Towers, R.L. Hoekstra, Engine Knock, A Renewed Concern In Motorsports - A Literature Review, SAE Technical Paper. (1998). doi:10.4271/983026.

[12] J. Brettschneider, Berechnung des Liftverhaeltnisses von Luft-Kraftstoff-Gemsichen und des Einflusses on MeBfehlern auf lambda, Bosch Tschnische Berichte, Stuttgart. 6 (1979) 177–186.

[13] R.S. Spindt, Air-Fuel Ratios from Exhaust Gas Analysis, SAE Technical Paper. (1965). doi:10.4271/650507.

[14] Cambustion, DMS500 Instrument Principle, (2002). https://www.cambustion.com/products/dms.

[15] T. Han, G. Lavoie, M. Wooldridge, A. Boehman, Effect of Syngas (H_2/CO) on SI Engine Knock under Boosted EGR and Lean Conditions, SAE International Journal of Engines. 10 (2017). doi:10.4271/2017-01-0670.

[16] A.J. Shahlari, J.B. Ghandhi, A Comparison of Engine Knock Metrics, in: SAE International Technical Paper, 2012. doi:10.4271/2012-32-0007.

[17] G. Brecq, O. Le Corre, Modeling of In-cylinder Pressure Oscillations under Knocking Conditions: Introduction to Pressure Envelope Curve, in: SAE International Technical Paper, 2005. doi:10.4271/2005-01-1126.

[18] N. Cavina, E. Corti, G. Minelli, D. Moro, L. Solieri, Knock Indexes Normalization Methodologies, in: SAE International Technical Paper, 2006. doi:10.4271/2006-01-2998.

[19] K. Burgdorf, I. Denbratt, Comparison of Cylinder Pressure Based Knock Detection Methods, in: SAE International Technical Paper, 1997. doi:10.4271/972932.

[20] R. Worret, S. Bernhardt, F. Schwarz, U. Spicher, Application of Different Cylinder Pressure Based Knock Detection Methods in Spark Ignition Engines, SAE Technical Paper. (2002). doi:10.4271/2002-01-1668.

[21] G. Konig, C.G.W. Sheppard, End Gas Autoignition and Knock in a Spark Ignition Engine, in: SAE International Technical Paper, 1990. doi:10.4271/902135.

[22] AVL, Indipar - Acquisition Parameter Editor AVL Indicom 2011, User's Guide. (2010).

http://www.avl.com.

[23] E. Ortiz-Soto, G. Lavoie, J. Martz, M. Wooldridge, D. Assanis, Enhanced heat release analysis for advanced multi-mode combustion engine experiments, Applied Energy. 136 (2014) 465–479. doi:10.1016/j.apenergy.2014.09.038.

[24] R.J. Moffat, Describing the Uncertainties in Experimental Results, Experimental Thermal and Fluid Science. 1 (1988) 3–17. doi:10.1016/0894-1777(88)90043-X.

[25] E.F. Obert, Internal combustion engines and air pollution, Pearson, 1973.

[26] Y. Román-Leshkov, C.J. Barrett, Z.Y. Liu, J.A. Dumesic, Production of dimethylfuran for liquid fuels from biomass-derived carbohydrates, Nature. 447 (2007) 982–985. doi:10.1038/nature05923.

[27] J. Yanowitz, E. Christensen, R. McCormick, Utilization of renewable oxygenates as gasoline blending components, Contract. 303 (2011) 275–300. doi:10.2172/1024518.

[28] API Research Project 45, Tabulated Knock-Test Data, June 30,. 45 (1956).

[29] J.E. Anderson, T.G. Leone, M.H. Shelby, T.J. Wallington, J.J. Bizub, M. Foster, M.G. Lynskey, D. Polovina, Octane Numbers of Ethanol-Gasoline Blends: Measurements and Novel Estimation Method from Molar Composition, SAE Technical Paper. (2012). doi:10.4271/2012-01-1274.

[30] W.R. Leppard, The Chemical Origin of Fuel Octane Sensitivity, SAE Technical Paper. (1990). doi:10.4271/902137.

[31] J.P. Szybist, D.A. Splitter, Pressure and temperature effects on fuels with varying octane sensitivity at high load in SI engines, Combustion and Flame. 177 (2017) 49–66. doi:10.1016/j.combustflame.2016.12.002.

[32] C.K. Westbrook, M. Mehl, W.J. Pitz, M. Sjöberg, Chemical kinetics of octane sensitivity in a spark-ignition engine, Combustion and Flame. 175 (2017) 2–15. doi:10.1016/j.combustflame.2016.05.022.

[33] S. Wu, D. Kang, H. Zhang, R. Xiao, A.L. Boehman, The oxidation characteristics of furan derivatives and binary TPGME blends under engine relevant conditions, Proceedings of the Combustion Institute. 37 (2019) 4635–4643. doi:10.1016/j.proci.2018.08.060.

[34] N. Xu, Y. Wu, C. Tang, P. Zhang, X. He, Z. Wang, Z. Huang, Experimental study of 2,5-dimethylfuran and 2-methylfuran in a rapid compression machine: Comparison of the ignition delay times and reactivity at low to intermediate temperature, Combustion and

Flame. 168 (2016) 216–227. doi:10.1016/j.combustflame.2016.03.016.

[35] Y.B. Zeldovich, The Oxidation of Nitrogen in Combustion Explosions, Acta Physicochimica U.S.S.R. 21 (1946) 577–628.

[36] G.A. Lavoie, J.B. Heywood, J.C. Keck, Experimental and theoretical study of nitric oxide formation in internal combustion engines, Combustion Science and Technology. 1 (1970) 313–326. doi:10.1080/00102206908952211.

[37] D.B. Kittelson, Engines and nanoparticles: A review, Journal of Aerosol Science. 29 (1998) 575–588. doi:10.1016/S0021-8502(97)10037-4.

[38] S. Zhong, R. Daniel, H. Xu, J. Zhang, D. Turner, M.L. Wyszynski, P. Richards, Combustion and emissions of 2,5-dimethylfuran in a direct-injection spark-ignition engine, Energy and Fuels. 24 (2010) 2891–2899. doi:10.1021/ef901575a.

[39] G.D.J. Guerrero Peña, Y.A. Hammid, A. Raj, S. Stephen, T. Anjana, V. Balasubramanian, On the characteristics and reactivity of soot particles from ethanol-gasoline and 2,5-dimethylfuran-gasoline blends, Fuel. 222 (2018) 42–55. doi:10.1016/j.fuel.2018.02.147.

[40] E. Christensen, G.M. Fioroni, S. Kim, L. Fouts, E. Gjersing, R.S. Paton, R.L. McCormick, Experimental and theoretical study of oxidative stability of alkylated furans used as gasoline blend components, Fuel. 212 (2018) 576–585. doi:10.1016/j.fuel.2017.10.066.

[41] J. Song, K. Cheenkachorn, J. Wang, J. Perez, A.L. Boehman, P.J. Young, F.J. Waller, Effect of oxygenated fuel on combustion and emissions in a light-duty turbo diesel engine, Energy and Fuels. 16 (2002) 294–301. doi:10.1021/ef010167t.

[42] J. Stokes, T.H. Lake, R.J. Osborne, A Gasoline Engine Concept for Improved Fuel Economy – The Lean Boost System, SAE Technical Paper. (2000). doi:10.4271/2000-01-2902.

[43] T. Lieuwen, V. Yang, R. Yetter, Synthesis Gas Combustion: Fundamentals and Applications, CRC Press, 2009.

[44] A.L. Boehman, O. Le Corre, Combustion of Syngas in Internal Combustion Engines, Combustion Science and Technology. 180 (2008) 1193–1206. doi:10.1080/00102200801963417.

[45] J.A. Topinka, M.D. Gerty, J.B. Heywood, J.C. Keck, Knock Behavior of a Lean-Burn , H2 and CO Enhanced, SI Gasoline Engine Concept, SAE Technical Paper. (2004). doi:10.4271/2004-01-0975.

[46] D. Fennell, J. Herreros, A. Tsolakis, K. Cockle, J. Pignon, P. Millington, Thermochemical recovery technology for improved modern engine fuel economy – part 1: analysis of a prototype exhaust gas fuel reformer, RSC Adv. 5 (2015) 35252–35261. doi:10.1039/C5RA03111G.

[47] T. Alger, B. Mangold, Dedicated EGR: A New Concept in High Efficiency Engines, SAE International Journal of Engines. 2 (2009) 2009-01–0694. doi:10.4271/2009-01-0694.

[48] Y. Chang, J.P. Szybist, J.A. Pihl, D.W. Brookshear, Catalytic Exhaust Gas Recirculation-Loop Reforming for High Efficiency in a Stoichiometric Spark-Ignited Engine through Thermochemical Recuperation and Dilution Limit Extension, Part 1: Catalyst Performance, Energy and Fuels. 32 (2018) 2245–2256. doi:10.1021/acs.energyfuels.7b02564.

[49] Y. Chang, J.P. Szybist, J.A. Pihl, D.W. Brookshear, Catalytic Exhaust Gas Recirculation-Loop Reforming for High Efficiency in a Stoichiometric Spark-Ignited Engine through Thermochemical Recuperation and Dilution Limit Extension, Part 2: Engine Performance, Energy and Fuels. 32 (2018) 2257–2266. doi:10.1021/acs.energyfuels.7b02565.

[50] L. Bromberg, D.R. Cohn, A. Rabinovich, J.E. Surma, J. Virden, Compact plasmatron-boosted hydrogen generation technology for vehicular applications, International Journal of Hydrogen Energy. 24 (1999) 341–350. doi:10.1016/S0360-3199(98)00013-5.

[51] J. Mulot, M. Niethammer, S. Mukerjee, K. Haltiner, S. Shaffer, Development update on Delphi's solid oxide fuel cell systems, in: Fundamentals and Developments of Fuel Cells Conference, 2008.

[52] K. Ashida, H. Maeda, T. Araki, M. Hoshino, K. Hiraya, T. Izumi, Study of an On-board Fuel Reformer and Hydrogen-Added EGR Combustion in a Gasoline Engine, SAE International Journal of Fuels and Lubricants. 8 (2015) 358–366. doi:10.4271/2015-01-0902.

[53] C.S. Daw, J.P. Szybist, J.A. Pihl, Y. Chang, G.B. Fisher, Stretch Efficiency for Combustion Engines: Exploiting New Combustion Regimes, DOE Vehicle Technologies Office and Hydrogen and Fuel Cells Program Annual Merit Review, 2016. http://energy.gov/sites/prod/files/2014/03/f11/ace015_daw_2010_o.pdf.

[54] T. Alger, J. Gingrich, B. Mangold, The Effect of Hydrogen Enrichment on EGR Tolerance in Spark Ignited Engines, in: SAE International Technical Paper, 2007.

doi:10.4271/2007-01-0475.

[55] T. D'Andrea, P.F. Henshaw, D.S.K. Ting, The addition of hydrogen to a gasoline-fuelled SI engine, International Journal of Hydrogen Energy. 29 (2004) 1541–1552. doi:10.1016/j.ijhydene.2004.02.002.

[56] J.A. Goldwitz, J.B. Heywood, Combustion Optimization in a Hydrogen- Enhanced Lean-Burn SI Engine, SAE International Technical Paper. (2005). doi:10.4271/2005-01-0251.

[57] T. Shinagawa, T. Okumura, S. Furuno, K.-O. Kim, Effects of Hydrogen Addition to SI Engine on Knock Behavior, SAE Technical Paper. (2004). doi:10.4271/2004-01-1851.

[58] M.D. Gerty, J.B. Heywood, An Investigation of Gasoline Engine Knock Limited Performance and the Effects of Hydrogen Enhancement, SAE Technical Paper. (2006) 1–21. doi:10.4271/2006-01-0228.

[59] Y. Chen, R. Raine, Engine Knock in an SI Engine with Hydrogen Supplementation under Stoichiometric and Lean Conditions, SAE Int. J. Engines. 7(2) (2014) 595–605. doi:10.4271/2014-01-1220.

[60] Y. Chen, Effect of Hydrogen Supplementation on Performance, Knock Behaviour, and Emissions of an SI Engine Operating at Lean Air-fuel Ratios, University of Auckland, 2015.

[61] W.F. Stockhausen, R.J. Natkin, D.M. Kabat, L. Reams, X. Tang, S. Hashemi, S.J. Szwabowski, V.P. Zanardelli, Ford P2000 Hydrogen Engine Design and Vehicle Development Program Reprinted From : SI Combustion and Flow Diagnostics, (2002).

[62] S. Szwaja, K. Bhandary, J. Naber, Comparisons of hydrogen and gasoline combustion knock in a spark ignition engine, International Journal of Hydrogen Energy. 32 (2007) 5076–5087. doi:10.1016/j.ijhydene.2007.07.063.

[63] K.M. Chun, K.W. Kim, Measurement and Analysis of Knock in a SI Engine Using the Cylinder Pressure and Block Vibration Signals, in: SAE International Technical Paper, 1994. doi:10.4271/940146.

[64] X. He, M.T. Donovan, B.T. Zigler, T.R. Palmer, S.M. Walton, M.S. Wooldridge, a. Atreya, An experimental and modeling study of iso-octane ignition delay times under homogeneous charge compression ignition conditions, Combustion and Flame. 142 (2005) 266–275. doi:10.1016/j.combustflame.2005.02.014.

[65] S.M. Walton, X. He, B.T. Zigler, M.S. Wooldridge, An experimental investigation of the

ignition properties of hydrogen and carbon monoxide mixtures for syngas turbine applications, Proceedings of the Combustion Institute. 31 II (2007) 3147–3154. doi:10.1016/j.proci.2006.08.059.

[66] Ž. Ivanič, F. Ayala, J. Goldwitz, J.B. Heywood, Effects of Hydrogen Enhancement on Efficiency and NOx Emissions of Lean and EGR-Diluted Mixtures in a SI Engine, in: SAE International Technical Paper, 2005. doi:10.4271/2005-01-0253.

[67] T. Han, G. Lavoie, M. Wooldridge, A. Boehman, Dual Fuel Injection (DI + PFI) for Knock and EGR Dilution Limit Extension in a Boosted SI Engine, SAE Technical Paper. (2018). doi:10.4271/2018-01-1735.

[68] Y. Iwamoto, K. Noma, O. Nakayama, T. Yamauchi, H. Ando, Development of Gasoline Direct Injection Engine, SAE Technical Paper. (1997). doi:10.4271/970541.

[69] N.S. Jackson, J. Stokes, P.A. Whitaker, T.H. Lake, Stratified and Homogeneous Charge Operation for the Direct Injection Gasoline Engine - High Power with Low Fuel Consumption and Emissions, SAE Technical Paper. (1997). doi:10.4271/970543.

[70] C. Park, S. Kim, H. Kim, Y. Moriyoshi, Stratified lean combustion characteristics of a spray-guided combustion system in a gasoline direct injection engine, Energy. 41 (2012) 401–407. doi:10.1016/j.energy.2012.02.060.

[71] G. Zhu, T. Stuecken, H. Schock, X. Yang, D.L.S. Hung, A. Fedewa, Combustion Characteristics of a Single-Cylinder Engine Equipped with Gasoline and Ethanol Dual-Fuel Systems, SAE Technical Paper. (2008). doi:10.4271/2008-01-1767.

[72] G. Zhu, D. Hung, H. Schock, Combustion characteristics of a single-cylinder spark ignition gasoline and ethanol dual-fuelled engine, Proceedings of the Institution of Mechanical Engineers Part D-Journal of Automobile Engineering. 224 (2010) 387–403. doi:10.1243/09544070jauto1236.

[73] R. Daniel, C. Wang, H. Xu, G. Tian, D. Richardson, Dual-Injection as a Knock Mitigation Strategy Using Pure Ethanol and Methanol, SAE International Journal of Fuels and Lubricants. 5 (2012) 2012-01–1152. doi:10.4271/2012-01-1152.

[74] X. Wu, R. Daniel, G. Tian, H. Xu, Z. Huang, D. Richardson, Dual-injection: The flexible, bi-fuel concept for spark-ignition engines fuelled with various gasoline and biofuel blends, Applied Energy. 88 (2011) 2305–2314. doi:10.1016/j.apenergy.2011.01.025.

[75] R. Daniel, H. Xu, C. Wang, D. Richardson, S. Shuai, Combustion performance of 2,5-

dimethylfuran blends using dual-injection compared to direct-injection in a SI engine, Applied Energy. 98 (2012) 59–68. doi:10.1016/j.apenergy.2012.02.073.

[76] R. Daniel, H. Xu, C. Wang, D. Richardson, S. Shuai, Gaseous and particulate matter emissions of biofuel blends in dual-injection compared to direct-injection and port injection, Applied Energy. 105 (2013) 252–261. doi:10.1016/j.apenergy.2012.11.020.

[77] Y. Zhuang, G. Hong, Investigation to Leveraging Effect of Ethanol Direct Injection (EDI) in a Gasoline Port Injection (GPI) Engine, SAE Technical Paper. (2013). doi:10.4271/2013-01-1322.

[78] Y. Zhuang, G. Hong, The Effect of Direct Injection Timing and Pressure on Engine Performance in an Ethanol Direct Injection Plus Gasoline Port Injection (EDI+GPI) SI Engine, SAE Technical Paper. (2013). doi:10.4271/2013-01-0892.

[79] Y. Zhuang, G. Hong, Effects of direct injection timing of ethanol fuel on engine knock and lean burn in a port injection gasoline engine, Fuel. 135 (2014) 27–37. doi:10.1016/j.fuel.2014.06.028.

[80] Y. Zhuang, Y. Qian, G. Hong, The effect of ethanol direct injection on knock mitigation in a gasoline port injection engine, Fuel. 210 (2017) 187–197. doi:10.1016/j.fuel.2017.08.060.

[81] S. Cho, N. Kim, J. Chung, K. Min, The Effect of Ethanol Injection Strategy on Knock Suppression of the Gasoline/Ethanol Dual Fuel Combustion in a Spark-Ignited Engine, SAE Technical Paper. (2015). doi:10.4271/2015-01-0764.

[82] N. Kim, S. Cho, H. Choi, H.H. Song, K. Min, The Efficiency and Emission Characteristics of Dual Fuel Combustion Using Gasoline Direct Injection and Ethanol Port Injection in an SI Engine, SAE Technical Paper. (2014). doi:10.4271/2014-01-1208.

[83] Z. Wang, H. Liu, Y. Long, J. Wang, X. He, Comparative study on alcohols e gasoline and gasoline e alcohols dual-fuel spark ignition (DFSI) combustion for high load extension and high fuel ef fi ciency, Energy. 82 (2015) 1–11. doi:10.1016/j.energy.2015.01.049.

[84] H. Liu, Z. Wang, Y. Long, S. Xiang, J. Wang, S.W. Wagnon, Methanol-gasoline Dual-fuel Spark Ignition (DFSI) combustion with dual-injection for engine particle number (PN) reduction and fuel economy improvement, Energy. 89 (2015) 1010–1017. doi:10.1016/j.energy.2015.06.051.

[85] H. Liu, Z. Wang, J. Wang, Methanol-gasoline DFSI (dual-fuel spark ignition) combustion

with dual-injection for engine knock suppression, Energy. 73 (2014) 686–693. doi:10.1016/j.energy.2014.06.072.

[86] F. Catapano, S. Di Iorio, P. Sementa, B.M. Vaglieco, Investigation of Ethanol-Gasoline Dual Fuel Combustion on the Performance and Exhaust Emissions of a Small SI Engine, SAE Technical Paper. (2014). doi:10.4271/2014-01-2620.

[87] F. Catapano, S. Di Iorio, P. Sementa, B.M. Vaglieco, Effects of Ethanol and Gasoline Blending and Dual Fueling on Engine Performance and Emissions., SAE Technical Paper. (2015). doi:10.4271/2015-24-2490.

[88] I. Hunwartzen, Modification of CFR Test Engine Unit to Determine Octane Numbers of Pure Alcohols and Gasoline-Alcohol blends, SAE Technical Paper. (1982). doi:10.4271/820002.

[89] R.J. Middleton, J.B. Martz, G.A. Lavoie, A. Babajimopoulos, D.N. Assanis, A computational study and correlation of premixed isooctane air laminar reaction fronts diluted with EGR, Combustion and Flame. 159 (2012) 3146–3157. doi:10.1016/j.combustflame.2012.04.014.

[90] J. McKenzie, W.K. Cheng, The anatomy of knock, SAE Technical Paper. (2016). doi:10.4271/2016-01-0704.

[91] J. McKenzie, W.K. Cheng, Ignition Delay Correlation for Engine Operating with Lean and with Rich Fuel-Air Mixtures, SAE Technical Paper. (2016). doi:10.4271/2016-01-0699.

[92] J.P. Szybist, D. Splitter, Effects of Fuel Composition on EGR Dilution Tolerance in Spark Ignited Engines, SAE International Journal of Engines. 9 (2016) 2016-01–0715. doi:10.4271/2016-01-0715.

[93] B. Giechaskiel, M. Maricq, L. Ntziachristos, C. Dardiotis, X. Wang, H. Axmann, A. Bergmann, W. Schindler, Review of motor vehicle particulate emissions sampling and measurement: From smoke and filter mass to particle number, Journal of Aerosol Science. 67 (2014) 48–86. doi:10.1016/j.jaerosci.2013.09.003.

[94] J.H. Seinfeld, S. Pandis, Atmospheric Chemistry and Physics From Air Pollution to Climate Change, Third Edition (Wiley), 2006.

[95] M.M. Maricq, R.E. Chase, D.H. Podsiadlik, R. Vogt, Vehicle Exhaust Particle Size Distributions: A Comparison of Tailpipe and Dilution Tunnel Measurements, SAE

Technical Paper. (1999). doi:10.4271/1999-01-1461.

[96] DEFRA, Particulate Matter in the United Kingdom, (n.d.). https://uk-air.defra.gov.uk/.

[97] P. Leduc, B. Dubar, A. Ranini, G. Monnier, Downsizing of Gasoline Engine: An Efficient Way to Reduce CO2 Emissions, Oil & Gas Science and Technology. 58 (2003) 115–127. doi:10.2516/ogst:2003008.

[98] T. Lake, J. Stokes, R. Murphy, R. Osborne, A. Schamel, Turbocharging Concepts for Downsized DI Gasoline Engines, SAE Technical Paper. (2004). doi:10.4271/2004-01-0036.

[99] O. Lang, J. Geiger, K. Habermann, M. Wittler, Boosting and Direct Injection -Synergies for Future Gasoline Engines, SAE Technical Paper. (2005). doi:10.4271/2005-01-1144.

[100] W. Anderson, J. Yang, D.D. Brehob, J.K. Vallance, R.M. Whiteaker, Understanding the Thermodynamics of Direct Injection Spark Ignition (DISI) Combustion Systems: An Analytical and Experimental Investigation, SAE Technical Paper. (1996). doi:10.4271/962018.

[101] E. Kasseris, J.B. Heywood, Charge Cooling Effects on Knock Limits in SI DI Engines Using Gasoline/Ethanol Blends: Part 1-Quantifying Charge Cooling, SAE Technical Paper. (2012). doi:10.4271/2012-01-1275.

[102] E.M. Barber, B. Reynolds, W.T. Tierney, Elimination of Combustion Knock - TEXACO Combustion Process, SAE Technical Paper. (1951). doi:10.4271/510173.

[103] C.W. Davis, E.M. Barber, E. Mitchell, Fuel Injection and Positive Ignition A Basis for Improved Efficiency and Economy, SAE Technical Paper. (1961). doi:10.4271/610012.

[104] B.C. Jain, J.M. Rife, J.C. Keck, A Performance Model for the Texaco Controlled Combustion, Stratified Charge Engine, SAE Technical Paper. (1976). doi:10.4271/760116.

[105] R.E. Canup, The Texaco Ignition System-A New Concept for Automotive Engines, SAE Technical Paper. (1975). doi:10.4271/750347.

[106] A.J. Scussel, A.O. Simko, W.R. Wade, The Ford PROCO Engine Update, SAE Technical Paper. (1978) 2706–2725. doi:10.4271/780699.

[107] A. Simko, M.A. Choma, L.L. Repko, Exhaust Emission Control by the Ford Programmed Combustion Process - PROCO, SAE Technical Paper. (1972) 249–264. doi:10.4271/720052.

[108] B.J. Hillyer, W.R. Wade, Single-Cylinder Proco Engine Studies - Fuel and Engine Calibration Effects on Emissions, Fuel Economy and Octane Number Requirements, SAE Technical Paper. (1978). doi:10.4271/780593.

[109] G. Finsterwalder, A New Deutz Multifuel System, SAE Technical Paper. (1972). doi:10.4271/720103.

[110] D.R. Lancaster, Diagnostic Investigation of Hydrocarbon Emissions from a Direct Injection Stratified Charge Engine with Early Injection, Institution of Mechanical Engineers. C397-80 (1980).

[111] M. Miyake, S. Okada, Y. Kawahara, K. Asai, A New Stratified Charge Combustion System (MCP) for Reducing Exhaust Emissions, Combustion Science and Technology. 12 (1976) 29–46. doi:10.1080/00102207608946706.

[112] A.G. Urlaub, F.G. Chmela, High-Speed , Multifuel Engine : L9204 FMV, SAE Technical Paper. (1974). doi:10.4271/740122.

[113] S.R. Norris-Jones, J.T. Russell, "FM" - A High Efficiency Combustion System for the Future Light Duty Engine?, SAE Technical Paper. (1982). doi:10.4271/820760.

[114] R.G. Phatak, K. Komiyama, Investigation of a Spark - Assisted Diesel Engine, SAE Technical Paper. (1983). doi:10.4271/830588.

[115] E.G. Groff, Automotive Direct-Injection Stratified-Charge Engine Development in the 1970-1980's, SAE Technical Paper. (2016). doi:10.4271/2016-01-0175.

[116] D.A. Nehmer, R.D. Reitz, Measurement of the Effect of Injection Rate and Split Injections on Diesel Engine Soot and NOx Emissions, SAE Technical Paper. (1994). doi:10.4271/940668.

[117] Z. Han, A. Uludogan, G.J. Hampson, R.D. Reitz, Mechanism of Soot and NOx Emission Reduction Using Multiple-injection in a Diesel Engine, SAE Technical Paper. (1996). doi:10.4271/960633.

[118] M. Badami, F. Mallamo, F. Millo, E.E. Rossi, Influence of Multiple Injection Strategies on Emissions, Combustion Noise and BSFC of a DI Common Rail Diesel Engine, SAE Technical Paper. (2002). doi:10.4271/2002-01-0503.

[119] J. O'Connor, M. Musculus, Post Injections for Soot Reduction in Diesel Engines: A Review of Current Understanding, SAE International Journal of Engines. 6 (2013) 400–421. doi:10.4271/2013-01-0917.

[120] J. Martin, C. Sun, A. Boehman, J. O'Connor, Experimental Study of Post Injection Scheduling for Soot Reduction in a Light-Duty Turbodiesel Engine, SAE Technical Paper. (2016). doi:10.4271/2016-01-0726.

[121] H.K. Suh, Investigations of multiple injection strategies for the improvement of combustion and exhaust emissions characteristics in a low compression ratio (CR) engine, Applied Energy. 88 (2011) 5013–5019. doi:10.1016/j.apenergy.2011.06.048.

[122] C. Sun, J. Martin, A.L. Boehman, Nanostructure and reactivity of soot produced from a turbodiesel engine using post injection, Proceedings of the Combustion Institute. 37 (2019) 1169–1176. doi:10.1016/j.proci.2018.06.101.

[123] J. O'Connor, M. Musculus, In-Cylinder Mechanisms of Soot Reduction by Close-Coupled Post-Injections as Revealed by Imaging of Soot Luminosity and Planar Laser-Induced Soot Incandescence in a Heavy-Duty Diesel Engine, SAE International Journal of Engines. 7 (2014) 673–693. doi:10.4271/2014-01-1255.

[124] K. Yehliu, A.L. Boehman, O. Armas, Emissions from different alternative diesel fuels operating with single and split fuel injection, Fuel. 89 (2010) 423–437. doi:10.1016/j.fuel.2009.08.025.

[125] P.E. Kapus, A. Fuerhapter, H. Fuchs, G.K. Fraidl, Ethanol Direct Injection on Turbocharged SI Engines - Potential and Challenges, SAE Technical Paper. (2007). doi:10.4271/2007-01-1408.

[126] D.B. Reiche, S.T. Wooldridge, P.C. Moilanen, G.C. Davis, Experimental Optimization of the Cold Start for the EcoBoost Engine, SAE Technical Paper. (2009). doi:10.4271/2009-01-1491.

[127] R. Singh, T. Han, M. Fatouraie, A. Mansfield, M. Wooldridge, A. Boehman, Influence of fuel injection strategies on efficiency and particulate emissions of gasoline and ethanol blends in a turbocharged multi-cylinder direct injection engine, International Journal of Engine Research. (2019). doi:10.1177/1468087419838393.

[128] T. Li, K. Nishida, Y. Zhang, M. Yamakawa, H. Hiroyasu, An Insight Into Effect of Split Injection on Mixture Formation and Combustion of DI Gasoline Engines, SAE Technical Paper. (2004). doi:10.4271/2004-01-1949.

[129] T. Li, K. Nishida, Y. Zhang, H. Hiroyasu, Effect of split injection on stratified charge formation of direct injection spark ignition engines, International Journal of Engine

Research. 8 (2007) 205–219. doi:10.1243/14680874JER02106.

[130] T. Li, K. Nishida, Y. Zhang, T. Onoe, H. Hiroyasu, Enhancement of stratified charge for DISI engines through split injection (Effect and its mechanism), JSME International Journal, Series B: Fluids and Thermal Engineering. 48 (2005) 687–694. doi:10.1299/jsmeb.48.687.

[131] Y. Imaoka, K. Shouji, T. Inoue, T. Noda, A Study of a Multistage Injection Mechanism for Improving the Combustion of Direct-Injection Gasoline Engines, SAE International Journal of Engines. 8 (2015) 1080–1087. doi:10.4271/2015-01-0883.

[132] J. Serras-Pereira, P.G. Aleiferis, D. Richardson, An experimental database on the effects of single- and split injection strategies on spray formation and spark discharge in an optical direct-injection spark-ignition engine fuelled with gasoline, iso-octane and alcohols, International Journal of Engine Research. 16 (2015) 851–896. doi:10.1177/1468087414554936.

[133] T. Kim, J. Song, S. Park, Effects of turbulence enhancement on combustion process using a double injection strategy in direct-injection spark-ignition (DISI) gasoline engines, International Journal of Heat and Fluid Flow. 56 (2015) 124–136. doi:10.1016/j.ijheatfluidflow.2015.07.013.

[134] J. Song, T. Kim, J. Jang, S. Park, Effects of the injection strategy on the mixture formation and combustion characteristics in a DISI (direct injection spark ignition) optical engine, Energy. 93 (2015) 1758–1768. doi:10.1016/j.energy.2015.10.058.

[135] Z. Wang, C. Jiang, H. Xu, T. Badawy, B. Wang, Y. Jiang, The influence of flash boiling conditions on spray characteristics with closely coupled split injection strategy, Applied Energy. 187 (2017) 523–533. doi:10.1016/j.apenergy.2016.11.089.

[136] Z. Wang, Y. Li, H. Guo, C. Wang, H. Xu, Microscopic and macroscopic characterization of spray impingement under flash boiling conditions with the application of split injection strategy, Fuel. 212 (2018) 315–325. doi:10.1016/j.fuel.2017.10.028.

[137] T. Li, M. Yamakawa, D. Takaki, K. Nishida, Y. Zhang, H. Hiroyasu, Characterization of Mixture Formation Processes in DI Gasoline Engine Sprays with Split Injection Strategy via Laser Absorption and Scattering (LAS) Technique, SAE Technical Paper. (2003). doi:10.4271/2003-01-3161.

[138] J. Seo, J.S. Lee, K.H. Choi, H.Y. Kim, S.S. Yoon, Numerical investigation of the

combustion characteristics and wall impingement with dependence on split-injection strategies from a gasoline direct-injection spark ignition engine, Proceedings of the Institution of Mechanical Engineers, Part D: Journal of Automobile Engineering. 227 (2013) 1518–1535. doi:10.1177/0954407013491216.

[139] J. Su, M. Xu, P. Yin, Y. Gao, D. Hung, Particle Number Emissions Reduction Using Multiple Injection Strategies in a Boosted Spark-Ignition Direct-Injection (SIDI) Gasoline Engine, SAE International Journal of Engines. 8 (2014) 2014-01–2845. doi:10.4271/2014-01-2845.

[140] J. Yang, R.W. Anderson, Fuel Injection Strategies to Increase Full-Load Torque Output of a Direct-Injection SI Engine, SAE Technical Paper. (1998). doi:10.4271/980495.

[141] X. Duan, J. Liu, Y. Tan, B. Luo, G. Guo, Z. Wu, W. Liu, Y. Li, Influence of single injection and two-stagnation injection strategy on thermodynamic process and performance of a turbocharged direct-injection spark-ignition engine fuelled with ethanol and gasoline blend, Applied Energy. 228 (2018) 942–953. doi:10.1016/j.apenergy.2018.06.090.

[142] H. Wei, J. Yu, A. Shao, L. Zhou, J. Hua, D. Feng, Influence of injection strategies on knock resistance and combustion characteristics in a DISI engine, Institution of Mechanical Engineers, Part D: Journal of Automobile Engineering. (2018) 1–13. doi:10.1177/0954407018804118.

[143] W. Zeng, M. Sjöberg, Utilizing boost and double injections for enhanced stratified-charge direct-injection spark-ignition engine operation with gasoline and E30 fuels, International Journal of Engine Research. 18 (2017) 131–142. doi:10.1177/1468087416685512.

[144] M. Costa, U. Sorge, L. Allocca, Increasing energy efficiency of a gasoline direct injection engine through optimal synchronization of single or double injection strategies, Energy Conversion and Management. 60 (2012) 77–86. doi:10.1016/j.enconman.2011.12.025.

[145] H. Oh, C. Bae, J. Park, J. Jeon, Effect of the Multiple Injection on Stratified Combustion Characteristics in a Spray-Guided DISI Engine, SAE Technical Paper. (2011). doi:10.4271/2011-24-0059.

[146] D. Turner, H. Xu, R.F. Cracknell, V. Natarajan, X. Chen, Combustion performance of bio-ethanol at various blend ratios in a gasoline direct injection engine, Fuel. 90 (2011) 1999–2006. doi:10.1016/j.fuel.2010.12.025.

[147] R. Singh, T. Burch, G. Lavoie, M. Wooldridge, M. Fatouraie, Effects of Fuel Injection Events of Ethanol and Gasoline Blends on Boosted Direct-Injection Engine Performance, SAE Technical Paper. (2017). doi:10.4271/2017-01-2238.

[148] S.S. Merola, A. Irimescu, C. Tornatore, L. Marchitto, G. Valentino, Split Injection in a DISI Engine Fuelled with Butanol and Gasoline Analyzed through Integrated Methodologies, SAE International Journal of Engines. 8 (2015). doi:10.4271/2015-01-0748.

[149] R. Daniel, C. Wang, H. Xu, G. Tian, Split-Injection Strategies under Full-Load Using DMF, A New Biofuel Candidate, Compared to Ethanol in a GDI Engine, SAE Technical Paper. (2012). doi:10.4271/2012-01-0403.

[150] G. Stiesch, G.P. Merker, Z. Tan, R.D. Reitz, Modeling the Effect of Split Injections on DISI Engine Performance, 2001 (2001). doi:10.4271/2001-01-0965.

[151] X. He, M.A. Ratcliff, B.T. Zigler, Effects of Gasoline Direct Injection Engine Operating Parameters on Particle Number Emissions, Energy & Fuels. 26 (2012) 2014−2027. doi:10.1021/ef201917p.

[152] M. Costa, U. Sorge, S. Merola, A. Irimescu, M. La Villetta, V. Rocco, Split injection in a homogeneous stratified gasoline direct injection engine for high combustion efficiency and low pollutants emission, Energy. 117 (2016) 405–415. doi:10.1016/j.energy.2016.03.065.

[153] C. Park, S. Kim, H. Kim, S. Lee, C. Kim, Y. Moriyoshi, Effect of a split-injection strategy on the performance of stratified lean combustion for a gasoline direct-injection engine, 225 (2011) 1415–1426. doi:10.1177/0954407011406469.

[154] G. Woschni, A Universally Applicable Equation for the Instantaneous Heat Transfer Coefficient in the Internal Combustion Engine, SAE Technical Paper. (1967) 3065–3083. doi:10.4271/670931.

[155] L.C. Lichty, Internal-Combustion Engines, Sixth Edition, McGraw-Hill Book Company, 1951.

[156] P. Blumberg, J.T. Kummer, Prediction of NO Formation in Spark-Ignited Engines - An Analysis of Methods of Control, Combustion Science and Technology. 4 (1971) 73–95. doi:10.1080/00102207108952474.

[157] G.A. Lavoie, Spectroscopic Measurements of Spark Ignition Engimes, Combustion and

Flame. 15 (1970) 97–108.

[158] G.A. Lavoie, P.N. Blumberg, Measurements of NO Emissions from a Stratified Charge Engine: Comparison of Theory and Experiment, Combustion Science and Technology. 8 (1973) 25–37. doi:10.1080/00102207308946628.

[159] S.H. Mansouri, Y. Bakhshan, Studies of NOx, CO, soot formation and oxidation from a direct injection stratified-charge engine using the k-ε turbulence model, Proceedings of the Institution of Mechanical Engineers, Part D: Journal of Automobile Engineering. 215 (2001) 95–104. doi:10.1243/0954407011525485.

[160] M.M. Maricq, Examining the relationship between black carbon and soot in flames and engine exhaust, Aerosol Science and Technology. 48 (2014) 620–629. doi:10.1080/02786826.2014.904961.

[161] M. Syrimis, K. Shigahara, D.N. Assanis, Correlation Between Knock Intensity and Heat Transfer Under Light and Heavy Knocking Conditions in a Spark Ignition Engine, SAE Technical Paper. (1996). doi:10.4271/960495.

[162] O.A. Eekoye, Heat transfer modeling during knock and flame quenching in an engine chamber, Twenty-Sixth Symposium (International) on Combustion / The Combustion Institute. (1996) 2661–2668. doi:10.1016/S0082-0784(96)80101-9.

[163] M. Syrimis, D.N. Assanis, Piston Heat Transfer Measurements Under Varying Knock Intensity in a Spark-Ignition Engine, SAE Technical Paper. (1997). doi:10.4271/971667.

[164] B. Grandin, I. Denbratt, J. Bood, C. Brackmann, P.-E. Bengtsson, The Effect of Knock on the Heat Transfer in an SI Engine: Thermal Boundary Layer Investigation using CARS Temperature Measurements and Heat Flux Measurements, SAE Technical Paper. (2000). doi:10.4271/2000-01-2831.

[165] Z. Wang, Y. Qi, X. He, J. Wang, S. Shuai, C.K. Law, Analysis of pre-ignition to super-knock: Hotspot-induced deflagration to detonation, Fuel. 144 (2015) 222–227. doi:10.1016/j.fuel.2014.12.061.

[166] H. Seong, K. Lee, S. Choi, Effects of Engine Operating Parameters on Morphology of Particulates from a Gasoline Direct Injection (GDI) Engine, SAE Technical Paper. (2013). doi:10.4271/2013-01-2574.

[167] H. Seong, S. Choi, K. Lee, Examination of Nanoparticles from Gasoline Direct-Injection (GDI) Engines Using Transmission Electron Microscopy (TEM), International Journal of

Automotive Technology. 15 (2014) 175–181. doi:10.1007/s12239−014−0019−5.

[168] D.R. Tree, K.I. Svensson, Soot processes in compression ignition engines, Progress in Energy and Combustion Science. 33 (2007) 272–309. doi:10.1016/j.pecs.2006.03.002.

[169] T. Kamimoto, M. Bae, High Combustion Temperature for the Reduction of Particulate in Diesel Engines, SAE Technical Paper. (1988). doi:10.4271/880423.

[170] K. Akihama, Y. Takatori, K. Inagaki, S. Sasaki, A.M. Dean, Mechanism of the Smokeless Rich Diesel Combustion by Reducing Temperature, SAE Technical Paper. (2001). doi:10.4271/2001-01-0655.

[171] M. Fatouraie, M.S. Wooldridge, S.T. Wooldridge, B.R. Petersen, Effects of Ethanol on In-Cylinder and Exhaust Gas Particulate Emissions of a Gasoline Direct Injection Spark Ignition Engine, Energy & Fuels. 29 (2015) 3399–3412. doi:10.1021/ef502758y.

[172] M. Fatouraie, The Effects of Ethanol / Gasoline Blends on Advanced Combustion Strategies in Internal Combustion Engines, Ph.D. Thesis, University of Michigan, 2014.

[173] S.T. Wooldridge, G.A. Lavoie, C.E. Weaver, Convection Path for Soot and HC Emissions from the Piston Bowl of a Stratified Charge Direct Injection Engine, 3rd Joint Meeting of the U.S. Sections of the Combustion Institute, University of Illinois at Chicago,March 16-19. (2003).

[174] M. Syrimis, D.N. Assanis, Knocking Cylinder Pressure Data Characteristics in a Spark-Ignition Engine, Journal of Engineering for Gas Turbines and Power. 125 (2003) 494–499. doi:10.1115/1.1560709.

[175] H. Kellerer, A. Müller, H.J. Bauer, S. Wittig, Soot formation in a shock tube under elevated pressure conditions, Combustion Science and Technology. 113–114 (1996) 67–80. doi:10.1080/00102209608935488.

[176] E.J. Barrientos, J.E. Anderson, M.M. Maricq, A.L. Boehman, Particulate matter indices using fuel smoke point for vehicle emissions with gasoline, ethanol blends, and butanol blends, Combustion and Flame. 167 (2016) 308–319. doi:10.1016/j.combustflame.2016.01.034.

[177] K. Aikawa, T. Sakurai, J.J. Jetter, Development of a predictive model for gasoline vehicle particulate matter emissions, SAE International Journal of Fuels and Lubricants. 3 (2010) 610–622. doi:10.4271/2010-01-2115.

[178] C. Kolodziej, J. Kodavasal, S. Ciatti, S. Som, N. Shidore, J. Delhom, Achieving Stable

Engine Operation of Gasoline Compression Ignition Using 87 AKI Gasoline Down to Idle, SAE Technical Paper. (2015). doi:10.4271/2015-01-0832.

[179] K.D. Rose, J. Ariztegui, R.F. Cracknell, T. Dubois, H.D.C. Hamje, L. Pellegrini, D.J. Rickeard, B. Heuser, T. Schnorbus, A. Kolbeck, Exploring a Gasoline Compression Ignition (GCI) Engine Concept Analysis of Critical Parameters, SAE Technical Paper. (2013). doi:10.4271/2013-01-0911.

[180] G.A. Lavoie, J. Martz, M. Wooldridge, D. Assanis, A multi-mode combustion diagram for spark assisted compression ignition, Combustion and Flame. 157 (2010) 1106–1110. doi:10.1016/j.combustflame.2010.02.009.

[181] L. Manofsky, J. Vavra, D. Assanis, A. Babajimopoulos, Bridging the gap between HCCI and SI: Spark-assisted compression ignition, SAE Technical Paper. (2011). doi:10.4271/2011-01-1179.

[182] V. Triantopoulos, Experimental and Computational Investigation of Spark Assisted Compression Ignition Combustion under Boosted, Ultra-EGR Dilute Conditions, Ph.D. Thesis, Department of Mechanical Engineering, University of Michigan, Ann Arbor, 2018.

[183] V. Triantopoulos, J. Martz, B, J. Sterniak, G. Lavoie, D. Assanis, S. Bohac, Operating Limits of Spark-Assisted Compression Ignition Combustion under Boosted Ultra-EGR Dilute Conditions in a Negative Valve Overlap Engine, ASME ICEF 2019. (2019).

[184] S.L. Kokjohn, R.M. Hanson, D. a. Splitter, R.D. Reitz, Fuel reactivity controlled compression ignition (RCCI): a pathway to controlled high-efficiency clean combustion, International Journal of Engine Research. 12 (2011) 209–226. doi:10.1177/1468087411401548.

[185] D. A. Splitter, R.D. Reitz, R. Hanson, High Efficiency , Low Emissions RCCI Combustion by Use of a Fuel Additive, SAE International Journal of Fuels and Lubricants. 3 (2010). doi:10.4271/2010-01-2167.

[186] J. Martin, A. Boehman, R. Topkar, S. Chopra, U. Subramaniam, H. Chen, Intermediate Combustion Modes between Conventional Diesel and RCCI, SAE International Journal of Engines. 11 (2018) 835–860. doi:10.4271/2018-01-0249.

[187] P.S. Shingne, M.S. Gerow, V. Triantopoulos, S. V. Bohac, J.B. Martz, A Comparison of Valving Strategies Appropriate for Multimode Combustion Within a Downsized Boosted

Automotive Engine—Part I: High load operation within the spark ignition combustion regime, Journal of Engineering for Gas Turbines and Power. 136 (2014). doi:10.1115/1.4027359.

[188] M.S. Gerow, P.S. Shingne, V. Triantopoulos, S. V. Bohac, J.B. Martz, A Comparison of Valving Strategies Appropriate for Multimode Combustion Within a Downsized Boosted Automotive Engine—Part II: Mid Load Operation Within the SACI Combustion Regime, Journal of Engineering for Gas Turbines and Power. 136 (2014). doi:10.1115/1.4027360.